

STATUS OF THESIS

Title of thesis

MECHANISTIC AND KINETIC STUDIES OF
MICROBIOLOGICALLY INFLUENCED CORROSION
(MIC) IN THE PRESENCE OF DOMINANT SULPHATE
REDUCING BACTERIA (SRB) METABOLIC SPECIES

I MARTIN CHOIRUL FATAH

hereby allow my thesis to be placed at the Information Resource Center (IRC) of Universiti Teknologi PETRONAS (UTP) with the following conditions:

1. The thesis becomes the property of UTP
2. The IRC of UTP may make copies of the thesis for academic purposes only.
3. This thesis is classified as

Confidential

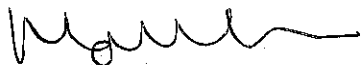
Non-confidential

If this thesis is confidential, please state the reason:

The contents of the thesis will remain confidential for _____ years.

Remarks on disclosure:

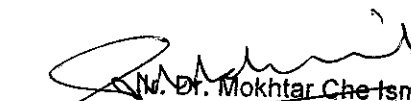
Endorsed by



Signature of Author
Permanent address:

Komplek LAPAN B11, No. 30
Pekayon, Jakarta, Indonesia

Date: 02/01/2013



AP. Ir. Dr. Mokhtar Che Ismail
Associate Professor
Signature of Supervisor
Name of Supervisor
Engineering Department
Universiti Teknologi PETRONAS
Bandar Seri Iskandar, 31750 Tronoh
Perak Darul Ridzuan, Malaysia.

AP. Ir. Dr. Mokhtar Che Ismail

Date: 02/01/2013

UNIVERSITI TEKNOLOGI PETRONAS
MECHANISTIC AND KINETIC STUDIES OF MICROBIOLOGICALLY
INFLUENCED CORROSION (MIC) IN THE PRESENCE OF DOMINANT
SULPHATE REDUCING BACTERIA (SRB) METABOLIC SPECIES

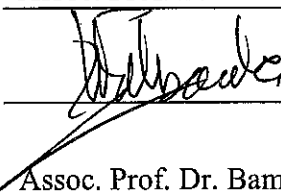
by

MARTIN CHOIRUL FATAH

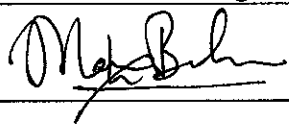
The undersigned certify that they have read, and recommend to the Postgraduate Studies Programme for acceptance this thesis for the fulfilment of the requirements for the degree stated.

Signature:  Ir. Dr. Mokhtar Che Ismail
Associate Professor
Mechanical Engineering Department
Universiti Teknologi PETRONAS
Bandar Seri Iskandar, 31750 Tronoh
Perak Darul Ridzuan, Malaysia.

Main Supervisor: Assoc. Prof. Ir. Dr. Mokhtar Che Ismail

Signature:  DR BAMBANG ARIWAHJOEDI
Associate Professor
Fundamental & Applied Sciences Department
Universiti Teknologi PETRONAS, PERAK

Co-Supervisor: Assoc. Prof. Dr. Bambang Ari Wahjoedi

Signature:  Ir. Dr. Masri Baharom
Head of Department/Senior Lect
Department of Mechanical Engin
Universiti Teknologi PETRONAS
Bandar Seri Iskandar 31750 Tronoh
Perak Darul Ridzuan, Malaysia

Head of Department: Ir. Dr. Masri Baharom

Date: 02/01/2013

MECHANISTIC AND KINETIC STUDIES OF MICROBIOLOGICALLY
INFLUENCED CORROSION (MIC) IN THE PRESENCE OF DOMINANT
SULPHATE REDUCING BACTERIA (SRB) METABOLIC SPECIES

by

MARTIN CHOIRUL FATAH

A Thesis

Submitted to the Postgraduate Studies Programme

as a Requirement for the Degree of

DOCTOR OF PHILOSOPHY

DEPARTMENT OF MECHANICAL ENGINEERING

UNIVERSITI TEKNOLOGI PETRONAS

BANDAR SERI ISKANDAR

PERAK

JANUARY 2013

DECLARATION OF THESIS

Title of thesis

MECHANISTIC AND KINETIC STUDIES OF
MICROBIOLOGICALLY INFLUENCED CORROSION (MIC) IN
THE PRESENCE OF SULPHATE REDUCING BACTERIA (SRB)
DOMINANT METABOLIC SPECIES

I MARTIN CHOIRUL FATAH

hereby declare that the thesis is based on my original work except for quotations and citations which have been duly acknowledged. I also declare that it has not been previously or concurrently submitted for any other degree at UTP or other institutions.

Witnessed by

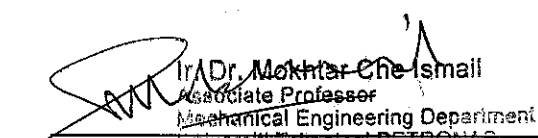


Signature of Author

Permanent address:

Komplek LAPAN B11, No. 30
Pekayon, Jakarta, Indonesia

Date: 02/01/2013



Ir. Dr. Mokhtar Che Ismail
Associate Professor
Mechanical Engineering Department
Universiti Teknologi PETRONAS
Bandar Seri Iskandar, 31750 Tronoh
Perak Darul Ridzuan, Malaysia.

Signature of Supervisor

AP. Ir. Dr. Mokhtar Che Ismail

Date: 02/01/2013

DEDICATION

Above all I want to dedicate this work to:

My parents for their loving care

My wife for her caring love

My Children the symbol of love

ACKNOWLEDGMENTS

I would like to express my sincere appreciation to my supervisor AP. Ir. Dr. Mokhtar Che Ismail, who has never given up correcting the mistakes I made, has encouraged me to broaden my viewpoint, and taught me the meaning of the life. His patience and dedication in directing us students on the way to success, and his goal of providing a reliable research working environment encouraged me to keep going. Under his supervision, I grew professionally and he helped me prepare for the new challenges in my career.

Great thanks go to my co-supervisor, AP. Dr. Bambang Ari Wahjoedi, who was always very confident in me and gave me full support and direction both in my daily life and academic work.

Furthermore I would like also to give a special word of appreciation, to all the mechanical engineering lecturers, all the mechanical engineering technologists, especially Mr. Anuar, Mr. Omar and Mr. Faisal, and all postgraduate officers, especially Pn. Hajjah Kamaliah.

I would like to acknowledge my colleagues at centre for corrosion research, especially Dr. Yuli Panca Asmara and Ms. Syahrini for their invaluable advice, critiques and true friendship. Special thanks also given to Indonesia Community in Bandar-U, PPI UTP. I feel living in my homeland with their presence.

I am very grateful to my parents, who taught me the meaning of struggle in this life. Additionally, I would like to express my deep indebtedness to my wife and my children (Azahra Zeita Zavira, Indana Zulfa and Hasby Asad Bil Fathi) for their true love and support. Their loves is the power in my life and always make my life more colorful.

Finally, I would like to acknowledge the asisstantship granted by Universiti Teknologi PETRONAS.

ABSTRACT

Microbiologically influenced corrosion (MIC) is a serious problem in the oil and gas industry. The most common microorganism responsible for MIC is sulphate reducing bacteria (SRB) which produces detrimental sulphide ions into the environment. Therefore, many studies have been conducted to study the effect of sulphide ions on the corrosion rate of mild steel using inorganic solution chemistry but ignored the possible effects of other SRB metabolic species which are produced along with sulphide such as sulphite, lactate, acetate, pyruvate and thiosulphate. The exclusion of other metabolic species implies some deficiency of the current understanding of MIC problem. Thus, the objective of this work is to elucidate the mechanistic and kinetic of MIC with the presence of dominant SRB metabolic species by which a better MIC prediction could be formulated. The work was conducted in simulated solution containing dominant SRB metabolic species of sulphide, sulphite, lactate, acetate, pyruvate and thiosulphate. Three electrochemical measurement methods were used in this work *i.e.* linear polarization resistance (LPR) test, Tafel polarization (TP) and electrochemical impedance spectroscopy (EIS). Three surface characterization techniques *i.e.* field emission scanning electron microscopy (FESEM), energy dispersive X-rays analysis (EDAX) and X-rays photoelectron spectroscopy (XPS) were used to study the corrosion product morphology on the surface. The pre-screening study showed that the corrosion behaviour of individual species differed in the presence of other metabolic species. The interaction among metabolic species created a more aggressive environment and increased the corrosion rate. In addition, the formation of FeS film and nature of corrosion are dependent on the presence of sulphide. With sulphide concentration around 50 ppm, a thin and porous FeS film was formed which enabled corrosive species to diffuse to the steel surface and increased the corrosion rate. In high concentration of sulphide (more than 200 ppm), FeS film thickness increased substantially, resulted in lower corrosion rate and protected the steel from pitting corrosion.

The FeS formation was observed to be influenced by the presence of other metabolic species, particularly sulphite. The presence of sulphite thins the FeS film which allowed the corrosive species to diffuse to the steel surface, increased the corrosion rate and also resulted in pitting corrosion. Additionally, compared to the sole effect of sulphide on the X52 corrosion, the presence of other species changed the kinetics of sulphide corrosion and affected the formation of FeS film. The corrosion data from this study showed comparable results to the corrosion data obtained from SRB experiments as reported in the open literatures. A predictive equation that considers the SRB metabolic products was developed to predict the SRB corrosion at temperature of 25°C. Statistical analyses showed that the predictive equation has 95% level of confidence

Keywords: Sulphate reducing bacteria (SRB), metabolic products, abiotic chemistry.

ABSTRAK

Pengkakisan yang dipengaruhi oleh kehidupan mikrobiologi (Microbiologically influenced corrosion - MIC) adalah satu masalah yang serius dalam industri minyak dan gas. Mikroorganisme yang biasa ditemui dalam menyebabkan MIC ialah *Sulphate Reducing Bacteria* (SRB) kerana ia menghasilkan ion sulfat ke kawasan sekitarnya. Oleh sebab itu, banyak kajian telah dibuat untuk mengkaji kesan ion sulfat kepada kadar pengakisan besi (mengandungi komposisi karbon yang rendah) dengan menggunakan bahan kimia tidak organik yang tetapi mengabaikan kesan dari hasil metabolisme SRB yang lain seperti sulfida, laktat, asetat, piruvat dan thiosulfat. Pengabaian spesies metabolik ini menyebabkan kurangnya pemahaman tentang masalah MIC hari ini. Jadi, objektif kajian ini adalah untuk menjelaskan mekanisme dan kinetik MIC dengan kehadiran spesies metabolik SRB utama yang mana ramalan MIC yang lebih baik boleh di formulasi. Kajian telah dibuat dalam simulasi larutan yang mengandungi spesies tersebut sulfida, laktat, asetat, sulphate, sulfite, piruvat dan thiosulfat. Tiga (3) cara elektrokimia digunakan dalam kajian ini; ujian LPR, TP dan EIS. Teknik mengkaji keadaan permukaan iaitu FESEM, EDAX dan XPS telah digunakan untuk mengamati morfologi pengakisan pada permukaan besi tersebut. Keputusan awal kajian menunjukkan bahawa terdapat perbezaan yang tersendiri pada setiap kelakuan pengakisan. Interaksi antara spesies metabolik menyebabkan keadaan sekeliling yang lebih agresif dan memangkinkan kadar pengakisan. Tambahan pula, pembentukan lapisan filem FeS dan proses pengakisan adalah bergantung kepada kehadiran sulfat. Lapisan filem FeS yang nipis dan berongga terbentuk dalam larutan yang mengandungi sulfida dengan kadar kepekatan 50 ppm, yang mana membolehkan pemangkin pengakisan untuk menyelinap dan menempel pada permukaan besi dan menaikkan kadar pengakisan.

Dalam larutan yang mengandung sulfida dengan kepekatan tinggi (200 ppm), ketebalan lapisan filem FeS bertambah lalu menyebabkan kurangnya kadar pengakisan dan melindungi permukaan besi dari pengakisan pitting. Pembentukan lapisan filem FeS didapati terpengaruh dengan kehadiran spesies metabolik lain, iaitu sulfite. Kehadirannya menipiskan lapisan filem lalu menyebabkan kesan seperti 50 ppm sulfida di atas. Selain itu, perbandingannya dengan kesan sulfida tersendiri terhadap pengakisan X52, kehadiran species yang lain telah mengubah kinetik pengakisan sulfida juga mempengaruhi pembentukan lapisan filem FeS. Kajian ini menunjukkan hasil yang boleh dibandingkan dengan eksperimen SRB lain yang dilaporkan dari sumber terbuka tentang kadar pengakisan dan lapisan filem yang tipikal. Satu persamaan ramalan yang berkaitan dengan hasil metabolisme SRB telah dibina untuk meramalkan pengakisan SRB pada suhu 25°C. Analisis secara statistik menunjukkan persamaan tersebut mempunyai 95% tahap penerimaan.

Kata kunci: Sulphate reducing bacteria, produk metabolik, bahan kimia abiotik

In compliance with the terms of the Copyright Act 1987 and the IP policy of the university, the copyright of this thesis has been reassigned by the author to the legal entity of the university,
Institute of Technology PETRONAS Sdn Bhd.

Due acknowledgment shall always be made of the use of any material contained in, or derived from, this thesis.

© Martin Choirul Fatah, 2013
Institute of Technology PETRONAS Sdn Bhd
All rights reserved.

TABLE OF CONTENTS

	Page
STATUS OF THESIS	i
APPROVAL PAGE	ii
TITLE PAGE	iii
DECLARATION	iv
DEDICATION	v
ACKNOWLEDGMENTS	vi
ABSTRACT	viii
ABSTRAK	x
TABLE OF CONTENTS	xiii
LIST OF TABLES	xvi
LIST OF FIGURES	xviii
LIST OF ABBREVIATIONS	xxvii
LIST OF SYMBOLS	xxviii
CHAPTER 1: INTRODUCTION.....	1
1.1 Background.....	1
1.2 Problem Statement.....	3
1.3 Research Objectives.....	3
1.4 Scope of Study.....	4
1.5 Organization of Thesis.....	4
CHAPTER 2: LITERATURE REVIEW.....	6
2.1 Microbiologically Influenced Corrosion.....	6
2.1.1 Sulphate reducing bacteria.....	7
2.1.2 Corrosion mechanism by SRB.....	10
2.1.3 MIC related to hydrotesting.....	16
2.1.4 Failure cases caused by SRB.....	17
2.2 SRB experiments.....	19
2.3 Abiotic sulphide experiments compare to SRB experiments.....	24
2.4 Abiotic H ₂ S corrosion.....	26
2.5 Corrosion prediction model.....	35
2.6 Summary.....	37
CHAPTER 3: RESEARCH METHODOLOGY.....	38
3.1 Research test matrix.....	38
3.2. Experimental setting.....	40

3.2.1	Solution preparation.....	42
3.2.2	Material and preparation.....	44
3.3.	Electrochemical corrosion measurements.....	45
3.3.1	Linear polarization resistance (LPR).....	45
3.3.2	Tafel polarization (TP).....	46
3.3.3	Electrochemical impedance spectroscopy (EIS).....	47
3.3	Surface morphology observation and corrosion product analysis	47
3.4.1	Field emission scanning microscope (FESEM).....	48
3.4.2	X-ray photoelectron spectroscopy (XPS) analysis.....	48
3.4.3	Corrosion prediction.....	49
CHAPTER 4: RESULTS AND DISCUSSION.....		50
4.1.	Corrosion kinetic and mechanism.....	50
4.1.1	Pre-screening study: Identification of main metabolic species.....	50
4.1.2	Detailed analyses.....	53
4.1.2.1	LPR test.....	53
a.	Effect of sulphide on the corrosion rate of X52 steel with various sulphite and lactate concentrations in the simulated solution.....	53
b.	Effect of sulphite on the corrosion rate of X52 steel with various sulphide and lactate concentrations in the simulated solution.....	56
4.1.2.2	EIS.....	59
a.	Effect of sulphide.....	59
a.1.	Effect of sulphide without the presence of lactate in various sulphide concentrations in the simulated solution.....	59
a.2.	Effect of sulphide with the presence of 50 ppm lactate and various sulphite concentrations in the simulated solution.....	63
a.3.	Effect of sulphide with the presence of 200 ppm lactate and various sulphite concentrations in the simulated solution.....	65
a.4.	Effect of sulphide with the presence of 400 ppm lactate and various sulphite concentrations in the simulated solution.....	68
b.	Effect of sulphite.....	73
b.1.	Effect of sulphite without the presence of lactate in various sulphide concentrations in the simulated solution.....	73
b.2.	Effect of sulphite with the presence of 50 ppm lactate and various sulphide concentrations in the simulated solution.....	77
b.3.	Effect of sulphite with the presence of 200 ppm lactate and various sulphide concentrations in the simulated solution.....	79

b.4. Effect of sulphite with the presence of 400 ppm lactate and various sulphide concentrations in the simulated solution.....	83
4.1.2.3. Tafel polarization.....	88
4.2. Surface morphology and corrosion prediction.....	90
4.2.1. FESEM and EDAX analysis.....	91
4.2.1.1. X52 steel.....	91
4.2.1.2. Effect of sulphide.....	92
4.2.1.3. Effect of sulphite.....	101
4.2.2. Effect of immersion time.....	110
4.2.2.1. Effect of sulphide.....	110
4.2.2.2. Effect of sulphite.....	118
4.2.3. XPS analysis.....	127
4.3. Discussion.....	137
4.3.1. A possible physical mechanism of corrosion by SRB produced metabolism.....	140
4.3.2. Comparison with SRB experiments.....	141
4.3.2.1. Uniform corrosion.....	141
4.3.2.2. Pitting corrosion.....	143
4.3.3. An empirical equation to predict SRB corrosion rate in temperature 25°C.....	146
4.3.3.1. Equation validation with the data of SRB experiment.....	149
CHAPTER 5: CONCLUSIONS AND RECOMMENDATIONS.....	151
5.1. Conclusions.....	151
5.2. Recommendations.....	152

LIST OF TABLES

Table 2.1	Described Desulfovibrio genera of sulphate reducing bacteria.....	9
Table 2.2	Average concentrations of SRB metabolic products	10
Table 2.3	Concentration of bacteria in neutral water.....	17
Table 2.4	Properties of the iron sulphide.....	29
Table 2.5	Brief description of various SRB corrosion prediction models.....	36
Table 3.1	Test matrix of the preliminary study.....	39
Table 3.2	Test matrix of the detail analyses.....	40
Table 3.3	List of chemicals used.....	41
Table 3.4	Species with concentrations added to the test solution.....	43
Table 4.1	Corrosion rate comparison of species in solution containing other species (mix) and in solution without other solution (sole) in various concentrations.....	52
Table 4.2	Electrochemical impedance parameters fitted from the measured EIS data.....	62
Table 4.3	Electrochemical impedance parameters fitted from the measured EIS data.....	65
Table 4.4	Electrochemical impedance parameters fitted from the measured EIS data.....	68
Table 4.5	Electrochemical impedance parameters fitted from the measured EIS data.....	71
Table 4.6	Electrochemical impedance parameters fitted from the measured EIS data.....	76
Table 4.7	Electrochemical impedance parameters fitted from the measured EIS data.....	79
Table 4.8	Electrochemical impedance parameters fitted from the measured EIS data.....	82
Table 4.9	Electrochemical impedance parameters fitted from the measured EIS data.....	86

Table 4.10 Electrochemical parameters fitted from polarization curves.....	89
Table 4.11 Electrochemical parameters fitted from polarization curves.....	89
Table 4.12 Elemental composition of X52 steel (in wt%).....	92
Table 4.13 Summary of carbon steel corrosion caused by SRB.....	142
Table 4.14 Analysis of variance	146
Table 4.15 Analysis of coefficients results.....	147
Table 4.16 Sum of square.....	147

LIST OF FIGURES

Figure 2.1	SEM micrographs of bacteria cells: (a) spherical; (b) rod shape and filamentous; (c) helical.....	8
Figure 2.2	Proposed reaction of anaerobic corrosion in the presence of an iron surface.....	11
Figure 2.3	Anaerobic corrosion process of mild steel on a precoated iron sulphide film followed by biofilm accumulation up to 21 days.....	13
Figure 2.4	The mechanism of SRB action in MIC based on sulphide corrosion and iron sulphide corrosion products.....	15
Figure 2.5	Corrosion sequence for carbon steel in aqueous H ₂ S solution.....	28
Figure 2.6	Two mechanisms for H ₂ S corrosion. After the initial adsorption of H ₂ S on the steel surface, mackinawite can be from amorphous FeS either by path 1 or path 2.....	30
Figure 3.1	Experimental setting.....	41
Figure 3.2	Glass cell set-up.....	42
Figure 3.3	Sample of electrochemical test: (a) side view; (b) front view.....	44
Figure 3.4	An equivalent circuit used to simulate EIS diagram.....	47
Figure 3.5	FESEM apparatus.....	48
Figure 3.6	XPS apparatus.....	49
Figure 4.1	Effects of individual species on the X52 corrosion rate without the presence of other species in the 3% NaCl solution.....	51
Figure 4.2	Effects of individual species on the X52 corrosion rate with the presence of other species in the 3% NaCl solution.....	52
Figure 4.3	Effect of sulphide concentration on the corrosion rate of X52 steel in various sulphite concentrations without the presence of lactate in the simulated solution.....	54

Figure 4.4	Effect of sulphide concentration on the corrosion rate of X52 steel in various sulphite concentrations with the presence of 50 ppm lactate in the simulated solution.....	54
Figure 4.5	Effect of sulphide concentration on the corrosion rate of X52 steel in various sulphite concentrations with the presence of 200 ppm lactate in the simulated solution.....	55
Figure 4.6	Effect of sulphide concentration on the corrosion rate of X52 steel in various sulphite concentrations with the presence of 400 ppm lactate in the solution.....	55
Figure 4.7	Effect of sulphite concentration on the corrosion rate of X52 steel in various sulphide concentrations without the presence of lactate in the simulated solution.....	57
Figure 4.8	Effect of sulphite concentration on the corrosion rate of X52 steel in various sulphide concentrations with the presence of 50 ppm lactate in the simulated solution.....	57
Figure 4.9	Effect of sulphite concentration on the corrosion rate of X52 steel in various sulphide concentrations with the presence of 200 ppm lactate in the simulated solution.....	58
Figure 4.10	Effect of sulphite concentration on the corrosion rate of X52 steel in various sulphide concentrations with the presence of 400 ppm lactate in the simulated solution.....	58
Figure 4.11	Impedance spectra, presented as Nyquist plot, showed the effect of sulphide concentration without the presence of sulphite in the simulated solution.....	60
Figure 4.12	Impedance spectra, presented as Nyquist plot, showed the effect of sulphide concentration with the presence of 50 ppm sulphite in the simulated solution.....	60
Figure 4.13	Impedance spectra, presented as Nyquist plot, showed the effect of sulphide concentration with the presence of 200 ppm sulphite in the simulated solution.....	61

Figure 4.14	Impedance spectra, presented as Nyquist plot, showed the effect of sulphide concentration with the presence of 400 ppm sulphite in the simulated solution.....	61
Figure 4.15	Impedance spectra, presented as Nyquist plot, showed the effect of sulphide concentration without the presence of sulphite in the simulated solution.....	63
Figure 4.16	Impedance spectra, presented as Nyquist plot, showed the effect of sulphide concentration with the presence of 50 ppm sulphite in the simulated solution.....	63
Figure 4.17	Impedance spectra, presented as Nyquist plot, showed the effect of sulphide concentration with the presence of 200 ppm sulphite in the simulated solution.....	64
Figure 4.18	Impedance spectra, presented as Nyquist plot, showed the effect of sulphide concentration with the presence of 400 ppm sulphite in the simulated solution.....	64
Figure 4.19	Impedance spectra, presented as Nyquist plot, showed the effect of sulphide concentration without the presence of sulphite in the simulated solution.....	66
Figure 4.20	Impedance spectra, presented as Nyquist plot, showed the effect of sulphide concentration with the presence of 50 ppm sulphite in the simulated solution.....	66
Figure 4.21	Impedance spectra, presented as Nyquist plot, showed the effect of sulphide concentration with the presence of 200 ppm sulphite in the simulated solution.....	67
Figure 4.22	Impedance spectra, presented as Nyquist plot, showed the effect of sulphide concentration with the presence of 400 ppm sulphite in the solution.....	67
Figure 4.23	Impedance spectra, presented as Nyquist plot, showed the effect of sulphide concentration without the presence of sulphite in the simulated solution.....	69
Figure 4.24	Impedance spectra, presented as Nyquist plot, showed the effect of sulphide concentration with the presence of 50 ppm sulphite in the simulated solution.....	69

Figure 4.25	Impedance spectra, presented as Nyquist plot, showed the effect of sulphide concentration with the presence of 200 ppm sulphite in the simulated solution.....	70
Figure 4.26	Impedance spectra, presented as Nyquist plot, showed the effect of sulphide concentration with the presence of 400 ppm sulphite in the simulated solution.....	70
Figure 4.27	Nyquist diagrams (a) and Bode plot (b) of X52 steel with the addition of 200 ppm sulphite (0 ppm lactate and 0 ppm sulphide) in the simulated solution. Comparison of experimental data with the fitted results.....	72
Figure 4.28	Impedance spectra, presented as Nyquist plot, showed the effect of sulphite concentration without the presence of sulphide in the simulated solution.....	73
Figure 4.29	Impedance spectra, presented as Nyquist plot, showed the effect of sulphite concentration with the presence of 50 ppm sulphide in the simulated solution.....	74
Figure 4.30	Impedance spectra, presented as Nyquist plot, showed the effect of sulphide concentration with the presence of 200 ppm sulphite in the simulated solution.....	74
Figure 4.31	Impedance spectra, presented as Nyquist plot, showed the effect of sulphide concentration with the presence of 400 ppm sulphite in the simulated solution.....	75
Figure 4.32	Impedance spectra, presented as Nyquist plot, showed the effect of sulphite concentration without the presence of sulphide in the simulated solution.....	77
Figure 4.33	Impedance spectra, presented as Nyquist plot, showed the effect of sulphite concentration with the presence of 50 ppm sulphide in the simulated solution.....	77
Figure 4.34	Impedance spectra, presented as Nyquist plot, showed the effect of sulphite concentration with the presence of 200 ppm sulphide in the simulated solution.....	78

Figure 4.35	Impedance spectra, presented as Nyquist plot, showed the effect of sulphite concentration with the presence of 400 ppm sulphide in the simulated solution.....	78
Figure 4.36	Impedance spectra, presented as Nyquist plot, showed the effect of sulphite concentration without the presence of sulphide in the simulated solution.....	80
Figure 4.37	Impedance spectra, presented as Nyquist plot, showed the effect of sulphite concentration with the presence of 50 ppm sulphide in the simulated solution.....	80
Figure 4.38	Impedance spectra, presented as Nyquist plot, showed the effect of sulphite concentration with the presence of 200 ppm sulphide in the simulated solution.....	81
Figure 4.39	Impedance spectra, presented as Nyquist plot, showed the effect of sulphite concentration with the presence of 400 ppm sulphide in the simulated solution.....	81
Figure 4.40	Impedance spectra, presented as Nyquist plot, showed the effect of sulphite concentration without the presence of sulphide in the simulated solution.....	83
Figure 4.41	Impedance spectra, presented as Nyquist plot, showed the effect of sulphite concentration with the presence of 50 ppm sulphide in the solution.....	84
Figure 4.42	Impedance spectra, presented as Nyquist plot, showed the effect of sulphite concentration with the presence of 200 ppm sulphide in the simulated solution.....	84
Figure 4.43	Impedance spectra, presented as Nyquist plot, showed the effect of sulphite concentration with the presence of 400 ppm sulphide in the simulated solution.....	85
Figure 4.44	Nyquist diagrams (a) and Bode plot (b) of X52 steel with the addition of 50 ppm lactate and 50 ppm sulphide (0 ppm sulphite) in the simulated solution. Comparison of experimental data with the fitted results.....	87

Figure 4.45	Polarization curve of X52 steel with various sulphide concentrations in the presence of 50 ppm lactate and 200 ppm sulphite in the simulated solution.....	88
Figure 4.46	Polarization curve of X52 steel with various sulphite concentrations in the presence of 50 ppm lactate and 200 ppm sulphide in the simulated solution.....	90
Figure 4.47	(a) Surface morphology of bare X52 steel; (b) EDX results.....	92
Figure 4.48	(a) Surface morphology (face view) of X52 steel in the simulated solution with the addition of 200 ppm sulphite and 50 ppm lactate without the presence of sulphide (0 ppm); (b) EDAX results.....	93
Figure 4.49	(a) Surface morphology (face view) of X52 steel in the simulated solution with the addition of 50 ppm sulphide, 200 ppm sulphite and 50 ppm lactate; (b) EDAX results.....	94
Figure 4.50	(a) Surface morphology (face view) of X52 steel in the simulated solution with the addition of 200 ppm sulphide, 200 ppm sulphite and 50 ppm lactate; (b) EDAX results.....	95
Figure 4.51	Elemental film analysis by EDX (a) C element on the grain (b) S element on the film scale.....	96
Figure 4.52	(a) Surface morphology (face view) of X52 steel in the simulated solution with the addition of 400 ppm sulphide, 200 ppm sulphite and 50 ppm lactate; (b) EDAX results.....	97
Figure 4.53	Surface morphology of X52 steel after corrosion product removal in the simulated solution with the addition of 200 ppm sulphite and 50 ppm lactate in various sulphide concentrations (a) 0 ppm; (b) 50 ppm; (c) 200 ppm (d) 400 ppm.....	99
Figure 4.54	Surface morphology (cross view) of X52 steel in the simulated solution with the addition of 200 ppm sulphite and 50 ppm lactate in various sulphide concentrations (a) 0 ppm; (b) 50 ppm; (c) 200 ppm.....	100
Figure 4.55	(a) Surface morphology (face view) of X52 steel in the simulated solution with the addition of 200 ppm sulphide and 50 ppm lactate	

	without the presence of sulphite (0 ppm); (b) EDAX results.....	102
Figure 4.56	(a) Surface morphology (face view) of X52 steel in the simulated solution with the addition of 50 ppm sulphite, 200 ppm sulphide and 50 ppm lactate; (b) EDAX results.....	103
Figure 4.57	(a) Surface morphology (face view) of X52 steel in the simulated solution with the addition of 200 ppm sulphite, 200 ppm sulphide and 50 ppm lactate; (b) EDAX results.....	104
Figure 4.58	(a) Surface morphology (face view) of X52 steel in the simulated solution with the addition of 400 ppm sulphite, 200 ppm sulphide and 50 ppm lactate; (b) EDAX results.....	105
Figure 4.59	Surface morphology of X52 steel after corrosion product removal in the simulated solution with the addition of 200 ppm sulphide and 50 ppm lactate in various sulphite concentrations (a) 0 ppm; (b) 50 ppm; (c) 200 ppm (d) 400 ppm.....	107
Figure 4.60	Surface morphology (cross view) of X52 steel in the simulated solution with the addition of 200 ppm sulphite and 50 ppm lactate in various sulphide concentrations (a) 0 ppm; (b) 50 ppm; (c) 200 ppm.....	108
Figure 4.61	Effects of immersion time on the corrosion rate of X52 steel in various sulphide concentrations in the simulated solution.....	110
Figure 4.62	(a) Surface morphology (face view) of X52 steel in the simulated solution with the addition of 200 ppm sulphite and 50 ppm lactate without the presence of sulphide (0 ppm); (b) EDAX results.....	111
Figure 4.63	(a) Surface morphology (face view) of X52 steel in the simulated solution with the addition of 50 ppm sulphide, 200 ppm sulphite and 50 ppm lactate; (b) EDAX results.....	112
Figure 4.64	(a) Surface morphology (face view) of X52 steel in the simulated solution with the addition of 200 ppm sulphide, 200 ppm sulphite and 50 ppm lactate; (b) EDAX results.....	113

Figure 4.65	(a) Surface morphology (face view) of X52 steel in the simulated solution with the addition of 400 ppm sulphide, 200 ppm sulphite and 50 ppm lactate; (b) EDAX results.....	114
Figure 4.66	Surface morphology of X52 steel after corrosion product removal in the simulated solution with the addition of 200 ppm sulphite and 50 ppm lactate in various sulphide concentrations (a) 0 ppm; (b) 50 ppm; (c) 200 ppm (d) 400 ppm.....	116
Figure 4.67	Surface morphology (cross view) of X52 steel in the simulated solution with the addition of 200 ppm sulphite and 50 ppm lactate in various sulphide concentrations (a) 0 ppm; (b) 50 ppm; (c) 200 ppm.....	117
Figure 4.68	Effects of immersion time on the corrosion rate of X52 steel in various sulphide concentrations in the simulated solution.....	119
Figure 4.69	(a) Surface morphology (face view) of X52 steel in the simulated solution with the addition of 200 ppm sulphide and 50 ppm lactate without the presence of sulphite (0 ppm); (b) EDAX results.....	120
Figure 4.70	(a) Surface morphology (face view) of X52 steel in the simulated solution with the addition of 50 ppm sulphite, 200 ppm sulphide and 50 ppm lactate; (b) EDAX results.....	121
Figure 4.71	(a) Surface morphology (face view) of X52 steel in the simulated solution with the addition of 200 ppm sulphite, 200 ppm sulphide and 50 ppm lactate; (b) EDAX results.....	122
Figure 4.72	(a) Surface morphology (face view) of X52 steel in the simulated solution with the addition of 400 ppm sulphite, 200 ppm sulphide and 50 ppm lactate; (b) EDAX results.....	123
Figure 4.73	Surface morphology of X52 steel after corrosion product removal in the simulated solution with the addition of 200 ppm sulphide and 50 ppm lactate in various sulphite concentrations (a) 0 ppm; (b) 50 ppm; (c) 200 ppm (d) 400 ppm.....	125
Figure 4.74	Surface morphology (cross view) of X52 steel in the simulated solution with the addition of 200 ppm sulphite and 50 ppm lactate	

	in various sulphide concentrations (a) 0 ppm; (b) 50 ppm; (c) 200 ppm.....	126
Figure 4.75	XPS spectra of X52 steel in the presence of 200 ppm sulphite and 50 ppm lactate in the solution (no sulphide): (a) S2p; (b) O1s; (c) Fe2p; (d) C1s.....	129
Figure 4.76	XPS spectra of X52 steel in the presence of 400 ppm sulphide, 200 ppm sulphite and 50 ppm lactate in the solution: (a) S2p; (b) O1s; (c) Fe2p; (d) C1s.....	133
Figure 4.77	XPS spectra of X52 steel in the presence of 200 ppm sulphide and 50 ppm lactate in the solution (no sulphide): (a) S2p; (b) O1s; (c) Fe2p; (d) C1s.....	135
Figure 4.78	Sequence of possible mechanism that might occur in SRB corrosion.....	140
Figure 4.79	Comparison of pitting depth equivalent calculation with SRB experiments/field in cylindrical geometry.....	145
Figure 4.80	Comparison of pitting depth equivalent calculation with SRB experiments/field in hemispherical geometry.....	145
Figure 4.81	Plot of residuals vs fitted value.....	148
Figure 4.82	Normal plot of residuals.....	149
Figure 4.83	Comparison of the empirical equation with SRB experimental data.....	150

LIST OF ABBREVIATIONS

MIC	microbiologically influenced corrosion
SRB	sulphate reducing bacteria
CDT	cathodic depolarization theory
LPR	linear polarization resistance
TP	Tafel polarization
EIS	electrochemical impedance spectroscopy
FESEM	field emission scanning electron microscopy
EDX	energy dispersive X-rays analysis
XPS	X-rays photoelectron spectroscopy
MRB	metal reducing bacteria
MDB	metal depositing bacteria
IOB	iron oxidizing bacteria
APB	acid producing bacteria
SOB	sulphur oxidizing bacteria
BCSR	biocatalytic sulphate reduction
API	American Petroleum Institute
ATCC	American Type Culture Collection
DSM	deutsche samlung von milroorganismen
APS	adenosine phosphosulphate
SCE	saturated calomel electrode
OCP	open circuit potential
R_s	solution resistance in ohm
R_t	charge transfer resistance in ohm
CPE	constant phase element
Ppm	part per million

LIST OF SYMBOLS

P	pressure in MPa
[sulphite]	sulphite concentration in ppm
[sulphide]	sulphide concentration in ppm
[lactate]	lactate concentration in ppm
A	surface are of the steel in m^2
b_a	anodic curve tafel slope
b_c	cathodic curve tafel slope
B	Stern geary constant
CR	corrosion rate in mm/yr
F	Faraday constant, 96.500 C/mole
i_{corr}	corrosion current density in A/cm^2
n	number of electron
R	universal gas constant, $R=8.314 J/(mol K)$
R_p	resistance polarization in ohm
T	temperature
Z	atomic weight in g/mol

CHAPTER 1

INTRODUCTION

1.1 Background

Microbiologically influenced corrosion (MIC) is the deterioration of material caused or accelerated by the presence of bacteria and other microorganisms and their metabolic activities. MIC was reported to account for 20% of the damage caused by corrosion [1]. In oil and gas industry, the overall loss caused by MIC could be over US\$ 100 million per annum [2]. Sulphate-reducing bacteria (SRB) has been the most commonly studied group because of their detrimental effects and can exist in a variety of industrial environments. Failure caused by MIC could occur after hydrotesting test, whereby the hydrotesting fluid is leaving in a pipeline system for many months [3]. The presence of bacteria in the fluid is the source of MIC. It could initiate or accelerate MIC once the appropriate environments e.g. temperature, pH and nutrient are met [4]. Other examples of failure due to SRB were given by Abedi *et al.* and Tiller [5-6].

Due to the nature of MIC which involves the activities and metabolism of microbes, the main challenge faced by engineer is in the understanding of the corrosion mechanism related to the effect of metabolic products. Clearer understanding of the corrosion process leads to a better corrosion prediction and prevention of MIC. Previously, many theories had been proposed to explain MIC mechanism such as cathodic depolarization theory (CDT).

The CDT was proposed by von Wolzogen Kuhr and van der Vlugt in 1923 [7]. According to the CDT, SRB accelerates corrosion of iron due to the removal of atomic hydrogen by the bacterial enzyme hydrogenase. The removed hydrogen reacts with sulphide produced by the SRB, forming H₂S gas which is known to be toxic and corrosive. However, the CDT receives many criticisms such as by Dominique [8]. The main reason is that it does not capture other effects of SRB metabolic products that might contribute to the corrosion kinetics and mechanism.

Therefore, some studies have been conducted to investigate the behaviour of abiotic sulphide representing SRB corrosion. In 1992, Newman *et al.* [9] conducted an experiment using abiotic sulphide on the corrosion of mild steel simulating the corrosion caused by SRB. The results showed that the corrosion rates obtained by abiotic sulphide and SRB experiments had striking similarity. However, one difference was related to the possible massive deposition of FeS as observed when SRB grew in the culture containing Fe²⁺; whereas in abiotic experiment, FeS could only be formed as a result of corrosion.

Recently in 2007, Kuang *et al.* [10] also showed that the electrochemical behaviour of SRB experiment had consistent results with the electrochemical behaviour of abiotic sulphide. They concluded that the electrochemical corrosion behaviour of carbon steel was dependent on the concentration of sulphide generated by the SRB metabolism and is hardly related to the biological activity of SRB and the SRB itself. Sherar *et al.* [11] concluded that the abiotic sulphide experiment is sufficient enough to develop prediction of steel corrosion rate. However, this simplistic approach does not account for the heterogeneity that exists in bacterial system.

On the basis that the abiotic sulphide corrosion rate is comparable to that by SRB experiments, the approach provides an avenue to evaluate other metabolic species that exist and involve in the corrosion process. The multiple effects of dominant metabolic species provide closer resemblance to actual MIC process and hence lead to a more accurate prediction. To our knowledge, there is no published literature that considers other SRB metabolic products in MIC process.

1.2 Problem Statement

Currently-accepted MIC theory based on CDT could not fully explain the corrosion mechanism caused by SRB since the theory is based on sole effect of sulphide. The presence of other metabolic species has important roles as it could alter the corrosion mechanism by changing the environmental conditions primarily the pH value that strongly influences the nature of iron sulphide film formation which dictates the nature of metal loss. Additionally, failures of MIC were reported occur at the oil and gas pipeline [12]. X52 steel is the common carbon steel piping grades for oil and gas transport pipeline [13-14]. Therefore, it is important to investigate the effect of other SRB metabolic products on the corrosion mechanism and kinetics on the X52 steel.

1.3 Research Objectives

The main objective of this research is to evaluate the effect of various SRB metabolic products on the corrosion behaviour of X52 steel, using abiotic chemistry. The work has been carried out to meet the following specific objectives:

- To analyse which SRB metabolic products species that has significant effect in increasing X52 steel corrosion rate.
- To investigate those dominant species on the corrosion rate and mechanism of X52 steel with the presence of other species in the test environment.
- To propose a possible physical mechanism of MIC caused by various SRB metabolic products.
- To develop empirical equation for MIC by SRB based on their metabolic product concentrations.

1.4 Scope of Study

The research investigated the effect of various SRB metabolic product species on the corrosion behaviour of steel using abiotic chemistry. There were six different species used in the tests. However, only three species were used in various variables in this study, while the others were used in a constant value. The linear polarization resistance (LPR) technique was used to measure the polarization resistance (R_p) and calculate corrosion rate. The corrosion mechanism was determined using Tafel polarization (TP) and electrochemical impedance spectroscopy (EIS) techniques. Surface and film morphology were analyzed by FESEM, EDX and XPS techniques. The tests were conducted in static conditions at a room temperature of about 25 °C (± 3 °C). Published SRB experimental data were used as comparison to the results of this study.

1.5 Organization of the Thesis

This thesis consists of five chapters. Chapter 1 describes the research background related to corrosion caused by bacteria. It gives an overview of CDT and its weakness, abiotic sulphide study related to corrosion caused by SRB, problem statement, research objectives, and scope of study.

Chapter 2 contains literature reviews on microbiologically influenced corrosion (MIC), SRB and its environment, SRB metabolic products, SRB experiment, sulphide corrosion, and H₂S corrosion.

Chapter 3 describes research test matrix, experimental setup and methodology, consists of sample preparations, solution preparation. This chapter also describes procedure of each experiment and goals that will be achieved.

Chapter 4 presents the results of corrosion kinetic and mechanism of X52 steel in the simulated solution containing SRB metabolic products. LPR measurements were

used to calculate the corrosion rate, while TP and EIS were used to observed the corrosion mechanism

Chapter 5 presents the results of surface morphology and film characterization of X52 steel in the simulated solution containing SRB metabolic products. Additionally, this chapter also describes the corrosion mechanism that developed based on LPR, TP, EIS and surface morphology results observation. A development of prediction equation was also described in this chapter

Finally, in chapter 6, conclusions and recommendations as result of analysis are presented. This chapter contains summarize of experiment's finding, goals achieved and recommendation for future work which might still be possible for development.

CHAPTER 2

LITERATURE REVIEW

2.1 Microbiologically Influenced Corrosion

Microbiologically influenced corrosion (MIC) is one type of corrosion affecting almost all engineering materials. The term MIC has been defined in many ways that are more or less similar. Some of the definitions for MIC are as follows:

- MIC is an electrochemical process whereby micro-organisms may be able to initiate, facilitate or promote corrosion reactions through the interaction of the three components that make up this system: metal, solution and micro-organisms [15].
- MIC refers to the influence of micro-organisms on the kinetics of corrosion processes of metals, caused by micro-organisms adhering to the interfaces. A prerequisite for MIC is the presence of micro-organisms. If the corrosion is influenced by their activity, other requirements are: an energy source, a carbon source, an electron donor, an electron acceptor and water [15].
- MIC is taking place whenever the reactants or products of the microbial metabolic reactions interact with the reactants or products of electrochemical reactions occurring between the metal surface and the environment in such way that these interferences affect the thermodynamics and/or kinetics of anodic dissolution of metal [16].

Bacterial microbes associated with MIC are ubiquitous. In the environment, it can be found in the form of metal reducing bacteria (MRB), metal-depositing bacteria (MDB), slime-producing bacteria, acid-producing bacteria (APB), iron oxidizing bacteria (IOB) and sulphate reducing bacteria (SRB).

From those types of bacteria, SRB have been recognized as the major culprit in MIC [17]. It is due to their characteristic which can thrive easily, live in anareroic and sulphate environment and produced hydrogen sulphide (H₂S) which is known as a toxic and corrosive gas. A brief information of SRB is given below.

2.1.1 Sulphate reducing bacteria (SRB)

SRB are a diverse group of obligate anaerobic, heterotrophic and mixotrophic bacteria, typified by *Desulfobacter* and *Desulfovibrio* [18]. SRB are bacterial species that can cause dissimilarity reduction of sulfur compounds, such as sulfate, thiosulfate, sulfite and even sulfur to sulfide, using sulfate as the terminal electron acceptor [19]. Javaherdasty [20] narrowed the SRB definition to include any organism that metabolically capable of reducing sulphate to sulphides.

The most common cell morphologies of SRB are curved and oval to rod-shaped. Their diameters usually range from 0.5 to 2 µm. Many SRB are actively motile by flagella. Other forms are spheres and long multicellular filaments. Several types of SRB tend to grow in clumps or cell aggregates and stick to surfaces.

SRB can be found everywhere. They are widespread in soil, seawater, fresh water and muddy sediments. The most common genera of SRB is *Desulfovibrio*, belonging to the the *Desulfovibrionaceae* family in the big group gram-negative mesophilic bacteria. *Desulfovibrio* is also the most frequently found species in anaerobic regions of soil, seawater, fresh water and muddy sediments. It can grow well within the temperature range between 5°C and 50°C, and the pH range from 5 to 10. The micrographs of bacteria cells are shown in Figure 2.1.

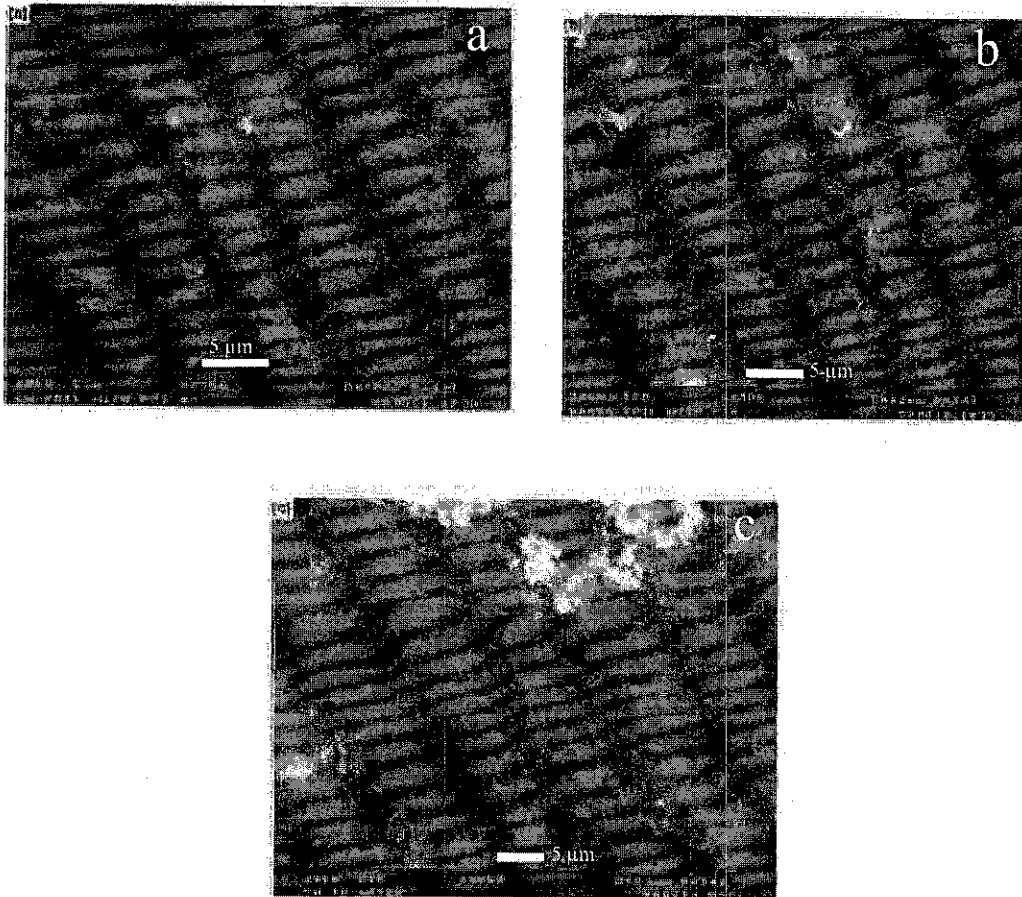


Figure 2.1 SEM micrographs of bacterial cells: (a) spherical; (b) rod shaped and filamentous; (c) helical [21].

SRB used hydrogen or a few simple organic compounds such as lactate or pyruvate as electron donors for sulphate reduction. However, SRB species are now known that oxidize carbon compounds, ranging from acetate to long-chain fatty acids. A list of *Desulfovibrio* genera with their metabolic products is presented in Table 2.1. The average concentration of the metabolic products is listed in Table 2.2.

Table 2.1. Desulfovibrio genera of sulphate reducing bacteria [22].

Organism	Shape	Thermophilic	Salt requirement	Electron donor and acceptors (metabolic products)
Desulfovibrio thermophilus	Rod	Yes	No	Lactate and pyruvate oxidized; Sulphate, sulphite and thiosulphate reduced
Desulfovibrio aculatus	Rod	No	No	Lactate, pyruvate, malate oxidized; Sulphate, sulphite and thiosulphate reduced.
Desulfovibrio sapovorans	Curved rod	No	No	Butyrate, 2-methylbutyrate, higher fatty acids to 18 carbons, lactate, pyruvate oxidized to acetate; sulphate, sulphite reduced
Desulfovibrio baarsif	Curved	No	No	Formate, acetate, propionate, butyrate, isobutyrate, 2-methylbutyrate, higher fatty acids to 18 carbons oxidized to CO ₂ ; sulphate, sulphite, thiosulphate reduced.

The metabolic products of bacteria are determined by their enzymes. Several factors influence the activity of an enzyme. Among the more important are temperature, pH, substrate concentration and the presence or absence of inhibitors [23]. Additionally, the metabolic products of bacteria are also influenced by their growth phase [10]. Factors that influence bacteria growth phase are summarized below [23-24]:

1. Physical requirements: temperature, oxygen and pH.
2. Nutritional requirements: energy source, carbon source, nitrogen source, minerals, water and growth factors.

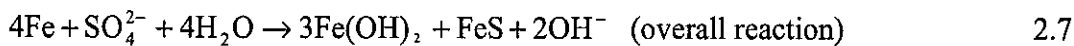
Table 2.2. Average concentrations of SRB metabolic products.

No	Metabolic products	Concentrations (ppm)	Remarks
1.	Sulphide	50	Optimum value of sulphide produced by SRB. Number of SRB detected is 1×10^6 /mL [10].
2.	Sulphate	50	Typical amount of sulphate found in water cooling system [25]. It is noted that the number of sessile SRB found is 5.4×10^3 (CFU/gr) .
3.	Sulphite	100	Number of SO_3^{2-} found in urban environment [26].
4.	Pyruvate	600	It is a maximum value of pyruvate produced by SRB [27].
5.	Lactate	0 - 3200	Range amount of lactate produced by SRB after 23 days inoculation. The Number of SRB detected is 1.1×10^7 /ml [28].
6.	Acetate	95	Maximum acetate concentration produced by SRB with the pyruvate as their energy source [29].
7.	Thiosulphate	> 15	Number of thiosulphate produced by SRB [30].

2.1.2 Corrosion mechanism by SRB

In principle, MIC occurs at the material interface where sessile cells influence the corrosion kinetics of anodic and/or cathodic reactions. MIC does not invoke any new electrochemical reactions, but the involvement of microorganism does change the physiochemical environment at the interface. Example of this includes concentration of nutrition, pH, redox potential and water chemistry. A number of MIC mechanisms of metal corrosion by SRB has been proposed since the first cathodic depolarization theory (CDT) von Wolzogen Kuhr and van der Vlugt [7] and confirmed by Bryant *et al.* [28]. The early work of von Wolzogen Kuhr and van der Vlugt suggested the following electrochemical reactions:

$4\text{Fe} \rightarrow 4\text{Fe}^{2+} + 8\text{e}^-$	(anodic reaction)	2.1
$8\text{H}_2\text{O} \rightarrow 8\text{H}^+ + 8\text{OH}^-$	(water dissociation)	2.2
$8\text{H}^+ + 8\text{e}^- \rightarrow 8\text{H}_{\text{ads}}$	(cathodic reaction)	2.3
$\text{SO}_4^{2-} + 8\text{H} \rightarrow \text{S}^{2-} + 4\text{H}_2\text{O}$	(bacterial consumption)	2.4
$\text{Fe}^{2+} + \text{S}^{2-} \rightarrow \text{FeS}$	(corrosion products)	2.5
$3\text{Fe}^{2+} + 6\text{OH}^- \rightarrow 3\text{Fe}(\text{OH})_2$	(corrosion products)	2.6



The process shown in reaction 2.4 was described as “depolarization” based on theory that these bacteria remove hydrogen that accumulates on the iron surface. The electron removal as a result of hydrogen utilization results in cathodic depolarization forcing more iron to be dissolved at the anode. The direct removal of hydrogen from the surface is equivalent to lowering the activation energy for hydrogen removal by providing a “depolarization” reaction as shown in Figure 2.2 [31]. The enzyme, hydrogenase, synthesized by many species of *Desulfovibrio*, may be involved in this specific depolarization process.

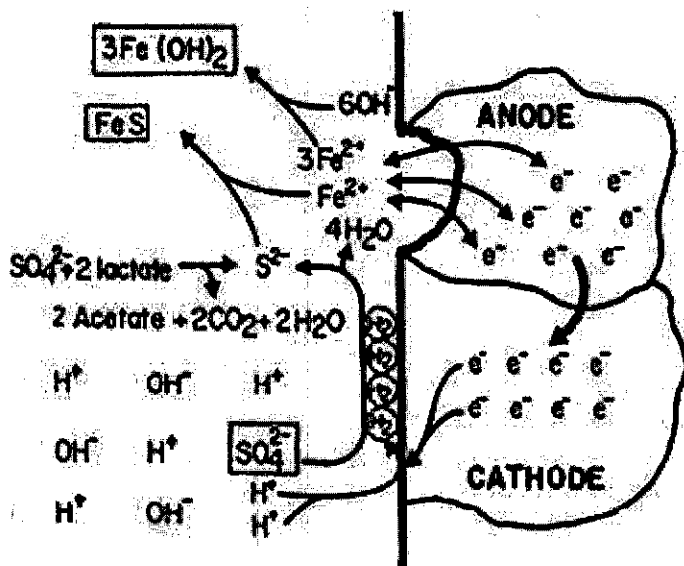


Figure 2.2 Proposed reaction of anaerobic corrosion in the presence of SRB on an iron surface [31].

King and Miller [32] concluded that accelerated corrosion of mild steel in the presence of SRB was due principally to the formation of iron sulphide. Because iron sulphide is not a permanent cathodic depolarizer, sustained corrosion rates were found to be dependent on the removal of the bound hydrogen by the action of bacterial hydrogenase. In contrast, Costello [33] proposed that dissolved H_2S produced by SRB is responsible for the cathodic depolarization.

Lee [31] concluded that corrosion of mild steel in the SRB environment was mainly determined by the nature of metal and environmental conditions such as dissolved iron species. When formation of iron sulphide film on mild steel was prevented before biofilm accumulated, the metal surface retained its scratch lines. However, when iron sulphide was formed before the accumulation of biofilm, visible localized corrosion appeared after 14 days and increased up to 21 days. Intergranular and pitting attacks were found in the localized corrosion area. The hypothesized localized corrosion process is illustrated schematically in Figure 2.3.

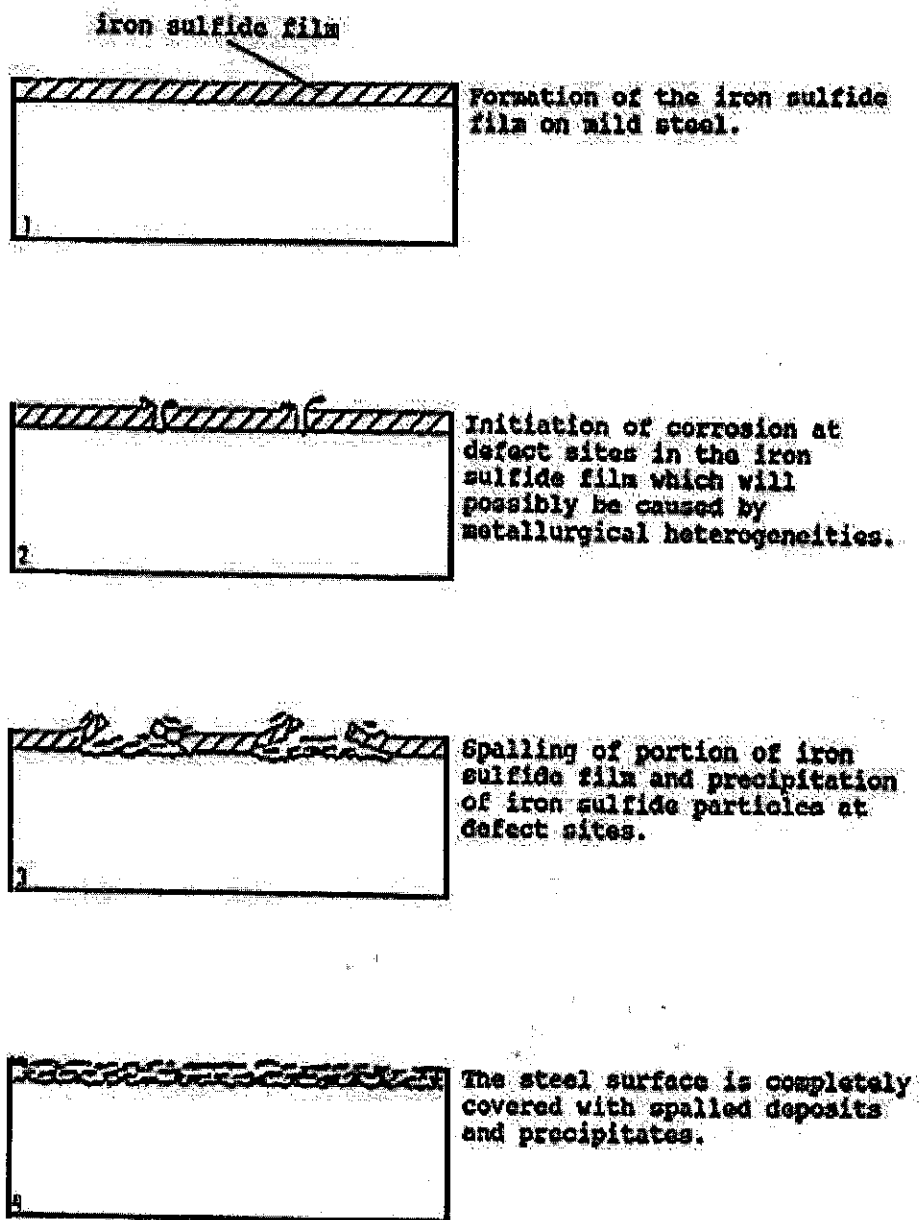
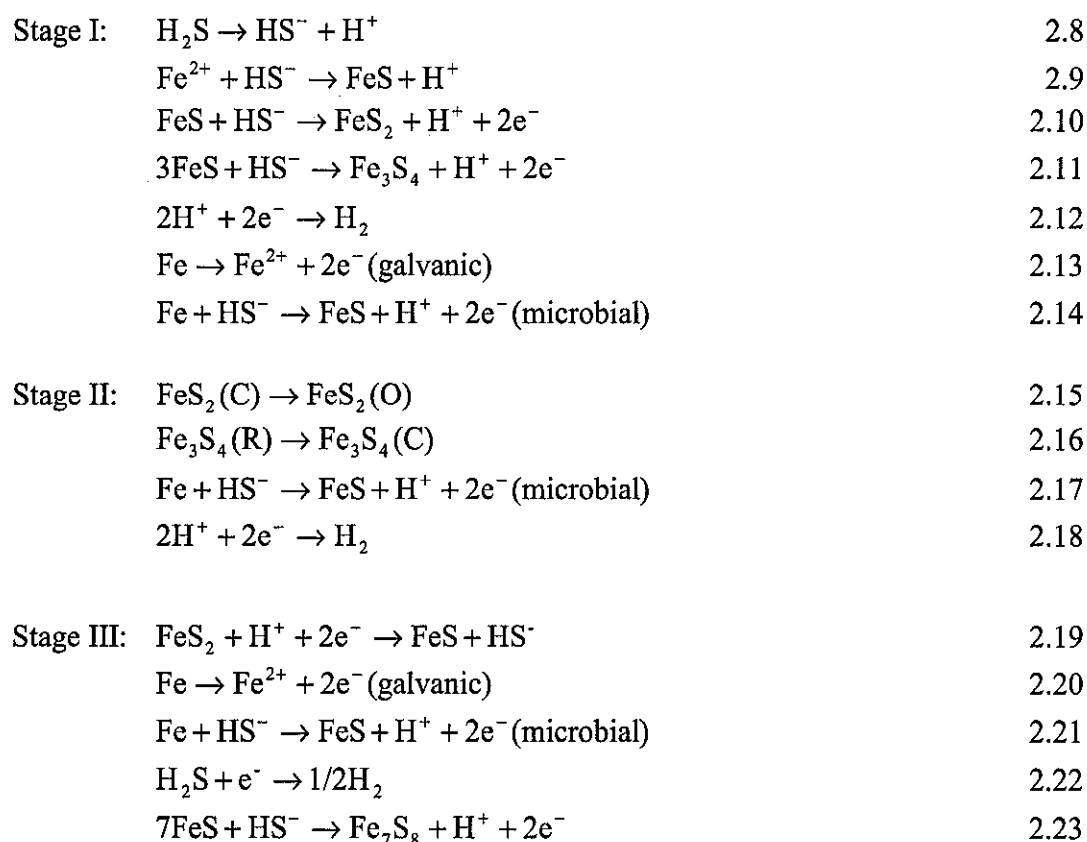


Figure 2.3 Anaerobic corrosion process of mild steel on a pre-coated iron sulphide film followed by biofilm accumulation up to 21 days [31].

Silva [34] proposed that hydrogenase play a key role in the initiation of corrosion caused by SRB. Its involvement in cathodic depolarization should be considered as the catalyst of a reduction reaction, instead of the consumption of a reduction product.

Romero [35-36] proposed a corrosion mechanism by SRB correlating the corrosive species with other factors such as time and open circuit potential, corrosion

products, sessile bacterial growth and attack morphology. He divided the mechanism of SRB corrosion into three stages. The first was controlled by the adsorption of bacterial cells and iron sulphide products, principally *mackinawite* and *pyrite*, over the metallic surface, activating it through the formation of micro galvanic corrosion cells which generated a hydrogen permeation peak. The second stage involved bacterial and inorganic equilibrium, in which the metal was slightly ennobled by the formation of a more compact iron sulphide film mixed with polymers generated planktonically by the bacteria. The third stage was controlled by a severe, localized corrosive process configured into groups of deep, rounded holes, produced mainly by local reduction of pyrite to mackinawite, due to the acidity generated by bacterial corrosion, and its subsequent detachment, leaving the base metal active facing a very large cathode made up of different iron sulphide products adhering to the metal: *mackinawite*, *pyrite*, *esmitite*, *marcasite*, *troilite* and *pyrrhotite*. The corrosion process is illustrated schematically in Figure 2.3 and the reactions are shown in reactions 2.8 to 2.23.



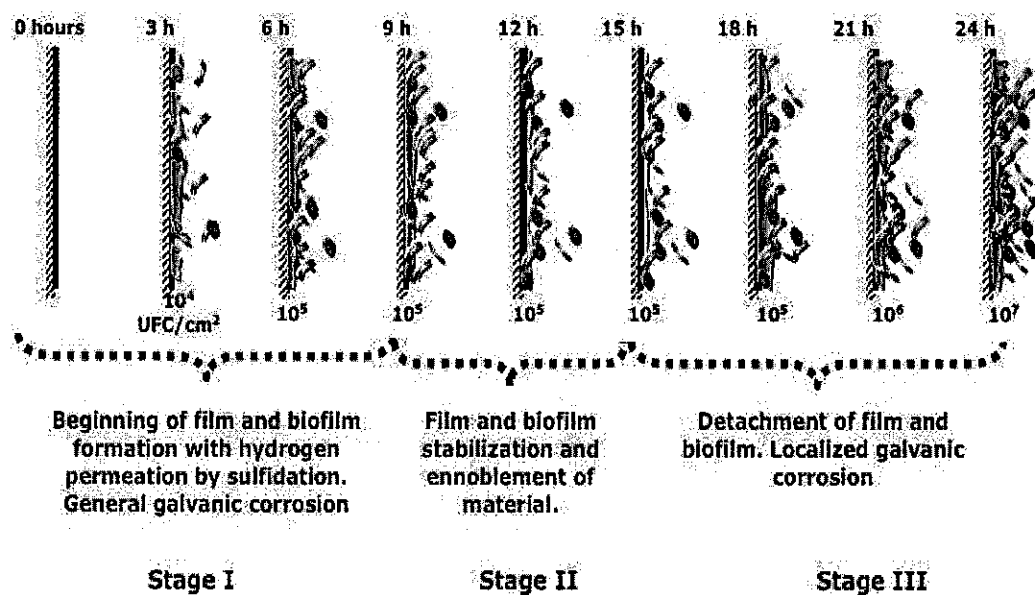


Figure 2.4 The mechanism of SRB action in MIC based on sulphide corrosion and iron sulphide corrosion products [35].

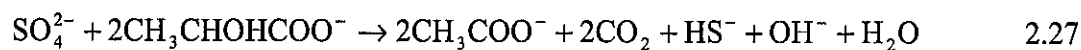
Recent SRB mechanism was proposed by Gu *et al.* [3, 37-38] known as biocatalytic cathodic sulphate reduction (BCSR) theory. The mechanism assumes that MIC occurs because the electrons released by iron dissolution at the anode are utilized in the sulphate reduction at the cathode. The actual cathodic reactions are more complex, but this theory considers only the overall effect as shown in reaction 2.25.



Reaction 2.25 occurs at a negligible rate without biocatalysis from biofilms. The reaction is catalyzed by the hydrogenase enzyme system of hydrogenase positive SRB cells that is responsible for accelerate sulphate reduction. Some hydrogen sulphide ion will convert to hydrogen sulphide, especially in acidic pH as shown in reaction 2.26.



In the presence of carbon source *e.g.* lactate, the sulphate reduction uses electrons donated by oxidation of lactate as shown below:



In summary, most of SRB mechanism focused on the effect of sole sulphide species. To our knowledge, there is no existing theory that considers other SRB metabolic products to explain its corrosion mechanism. The understanding of other SRB metabolic products is important in order to seek a better prediction and prevention of MIC.

2.1.3 MIC related to hydrotesting

MIC is a potential threat related to hydrotesting. Hydrotesting is a common method conducted to assess pipeline integrity (leaks and strength) before service. To conduct hydrotesting, a pipeline is filled with a liquid and pressurized to 125% of its maximum allowable operating pressure (MAOP) and holding the pressure for a period of four to eight hour [39-40]. Seawater, produced water and local river/well water is typically used as the flush fluid. In hydrotesting test, it is often the case that water is left in the system for many months before the systems actually commissioned. The microorganisms *e.g.* SRB, IOB, SOB and APB in the fluid can be initiated or facilitated MIC when meet with its appropriate conditions *i.e* temperature, pH and energy source. The two types of bacteria most likely to cause corrosion in a pipeline exposed to hydrotesting are SRB and APB [39]. Table 2.3 shows the concentration of bacteria in neutral waters [39-40]. Additionally, the fluid temperature used is affected by a variety of factors such as weather, pipe location and water sources. However, it is found that the fluid temperatures during a hydrotesting for marine facility piping vary from 15-30°C and it was reported that MIC can be significant for pilines operating in 15 to 45°C [40].

Table 2.3 Concentration of bacteria in neutral water

Location		Concentration (cells/ml)
Sea water	Continental Shelf & upper 200 m of open ocean	5×10^5
	Deep water (below 200m)	5×10^4
	Deep water (below 320m)	10^2
Fresh waters and saline leaks		10^6
Potable water		10^5

The serious threat of MIC related to hydrotesting is the biofilm left in the pipeline once the pipeline commissioned and used for many years. The biofilm could flourish by using nutrients that naturally available in the fluid.

2.1.4 Failure cases caused by SRB

MIC failures due to SRB have been reported for piping and equipment in marine environment, oil refining industry, fossil fuel, nuclear power plants, and process industries [12]. From open literature, some examples of the failures are summarized below:

- A rotating cylinder board mould (stainless steel type 303 EN 58 M) used for the manufacture of paper and board failed in the crevice regions formed between the axial rods and the outer face of the external spirally wound stainless steel mesh. The failures occurred three years after the mould had been commissioned. Examination revealed pit depths of 3-4 mm occurred in grain boundaries rich in manganese sulphide. It is also found that most of the corrosion had penetrated longitudinally inside the rod creating a hollow section covered only by a thin skin of metal [6].
- Pitting, having an etched and granular morphology, had been found on the parts of vertical axial suction pumps *e.g.* impeller, wear ring and bell house. Sulphide was detected in both the pitted regions and the corrosion products taken from several locations. The corrosion products, the slime films present

on the surface of the various components and the river water all contained a large population of bacteria with SRB as the predominant species [6].

- Severe internal corrosion, with over 50% thickness loss in many locations, was encountered in a 610 mm diameter, API 5L Grade-B Sch-20 carbon steel pipeline used for carrying light crude oil. The design life of such a pipeline is typically more than 30 years. However, the severe corrosion damage occurred after about 7 years of service. A high H₂S content was detected and it was an indication of SRB activity [41].

- A transmission oil products API 5L X52 pipeline in northern part of Iran cracked in 2004. Failure occurred in a portion of the pipeline that was placed at the top of a forest zone hill. The cracked zone was at 9 o'clock position. Field observation showed loosening, overlap-opening and disbanding of the applied polyethylene tape coating on the external surface of the pipeline in corroded section. High intensity of sulphur component and the observation of black corrosion product on the external surface of the pipe indicate SRB activity. A number of NDE and microbial activity test confirmed that SRB have been created and intensified pitting corrosion and have had important roles in crack development [5].

- A carbon steel heat-exchanger was installed along a fresh water line at the reverse osmosis unit at the refinery plant. After 1 1/2 years from start-up the heat exchanger failed as a result of rust-colored deposits formation that clogged tubes, leads, tube sheets and connecting pipes. The heat exchanger was operated in temperature 15 to 25°C. Microbiological analysis conducted in water and in corrosion products revealed the existence of SRB which are 52 (CFU^a/ml) and 5.x10³ (CFU/g) for planktonic and sessile bacteria respectively. The SRB is suspected causing pitting corrosion under rust slime layers on the parts of heat exchanger (tube, sheets, etc) [25].

2.2 SRB experiments

SRB have been extensively studied in order to seek better understanding on its influence on the corrosion kinetic and mechanism with the aim to improve prevention and mitigation techniques.

Ocando *et al.* [36] studied the effect of ferrous ions on the pH and H₂S on biofilms generated by SRB. A SRB pure culture of *Desulfovibrio desulfuricans*, grown in modified ATCC 1249 medium, was used in this study. They concluded that in the absence of ferrous ions, the pH on the iron surface decreased sharply to very low values due to a complex biofilm formation, which protected the material and impeded the hydrogen ions consumption by the corrosion process. However, in the presence of ferrous ions, the pH at metal interface remained almost constant and near to neutral values, due to the severity of the corrosion process, where the HS⁻ and H⁺ are consumed and massive sulphides precipitation occurred. In addition, they found that the bacteria and corrosion products were mixed and formed a complex biofilm structure that covered the iron surface, being in some cases protective depending mainly on the ferrous ions presence.

Rainha *et al.* [42] studied the influence of SRB, grown in a lactate/sulphate medium, on the anaerobic corrosion of mild steel. The bacteria used were *Desulfovibrio desulfuricans* ATCC 27774. Higher corrosion rates as well as the transpassive dissolution of Fe(0) or Fe(II) compounds to Fe(III) were observed. These effects were most probably due to high quantities of sulphide and/or to other alterations in the sulphate/lactate medium produced by the microbial activity of the SRB. In addition, they confirmed that the presence of SRB induces changes in the kinetics and mechanism of the anodic dissolution of iron in the lactate/sulphate media.

Amaya and Perez [43] studied SRB influence on the corrosion behaviour of API-XL70 steel. They indicated that the presence of microorganisms is controlled through the diffusion of the reaction at the cathode. Their studied also showed that SRB induced localized corrosion.

Benetton and Castaneda [44] observed SRB biofilm growth and its influence in corrosion monitoring. The bacteria used was *Desulfovibrio gabonensis* (DSM 10636) and *Desulfovibrio capillatus* (DSM 14982) grown in supplemented artificial seawater. The results showed that bio film formation induced diffusion controlled corrosion, where biofilm combined with corrosion products is acting as an infinite diffusion layer. Furthermore, they stated that cathodic depolarization mechanism is limited to the activation controlled (no biofilm). Once biofilm is established, the rate limiting step is diffusion controlled.

Miranda *et al.* [45] studied the role of *Desulfovibrio capillatus* on the corrosion behaviour of carbon steels under anaerobic conditions. Different concentrations of thiosulphate as electron acceptor for bacterial growth were employed. Their study showed that the corrosion activity of carbon steel notably increased, due to high concentration of bacterial metabolites. It is also noted that thiosulphate is used by SRB as the principal factor in the corrosion process.

Duan *et al.* [46] studied corrosion behaviour of carbon steel influenced by anaerobic biofilm in natural seawater. The bacteria used were sulphate reducing bacteria (SRB), *Desulfovibrio caledoniensis* and iron oxidising bacteria (IOB) *Clostridium sp.* They found that single species (SRB only) produced iron sulphide and accelerated corrosion, but mixed species (SRB and IOB) produced sulphate green rust and inhibited corrosion. In addition, they stated that the biotic sulphide produced by SRB, could only temporarily accelerated carbon steel corrosion. The continued existence of SRB was the key to the accelerated corrosion, implying that steel and bacteria should make direct or indirect contact through conducting FeS or possibly through electron shuttles.

Dzierzewicz *et al.* [47] investigated the relationship between microbial metabolic activity (expressed by generation time, rate of H₂S production and the activity of hydrooxygenase and adenosine phosphosulphate (APS) reductase enzymes) and biocorrosion of carbon steel. The bacteria used was *Desulfovibrio desulfuricans*, isolated from soil and mud samples. The bacteria were incubated for 6 days in the lactate/sulphate liquid medium under anaerobic conditions. It is noted that the rate of

H₂S production was approximately directly proportional to the specific activities of the investigated enzymes. These activities were inversely proportional to the generation time. The carbon steel MIC rate was strongly affected by bacterial resistance to metal ions. On contrast, it is observed weaker correlation between the MIC rate and the activity of enzymes.

Kuang *et al.* [10] studied the effects of SRB on the corrosion behaviour of carbon steel. Their results showed that SRB growing process consisted of three different stages, namely: exponential, death and residual phases. The corrosion behaviour of carbon steel in the system containing SRB hardly related on the active SRB number, but it depends on the accumulation of the metabolism products of SRB. Moreover, the anode process and the corrosion rate are accelerated during the exponential phase and stable during the death and residual phase.

Gayosso *et al.* [48-49] evaluated the corrosion rate of X52 steel, induced by a microbial consortium, isolated from the Atasta Nohoch gas transporting pipeline in Mexico. The major species identified was *Desulfovibrio viatnamensis*. They recorded the corrosion rate of X52 steel was about 0.3 mm/yr. Their study also indicated that the damage observed on the metal surface depends upon the sessile microorganism's population.

Frank *et al.* [50] investigated the effect of CO₂ introduction on the corrosion behaviour of carbon steel in bacteria environment. It was observed that SRB growth was stimulated probably due to the creation of an anaerobic environment, yielding a highly corrosive environment.

Mendoza *et al.* [51] observed the corrosion kinetics X52 steel caused by SRB. The bacteria were isolated from the inner deposits of a pipeline that transports sour gas in the marine region of Mexico. The bacteria were identified as *Desulfovibrio sp.* By weight loss method, they recorded that the corrosion rate of X52 steel was 0.15 mm/yr.

Li *et al.* [52] studied the corrosion behaviour of carbon steel influenced by SRB in soil environments. They concluded that the existence of SRB greatly influences the corrosion behaviour of carbon steel. The potential in control case (biocide added) was around -600 mV and always more positive than that in SRB cases. However, in the presence of SRB, the potential increased slightly for the first 6 days and then maintained around -740 mV/SCE, but the potential fluctuated -600 mV to -800 mV/SCE after 50 days until the experiment ended. In control case, the corrosion rate observed was stable around 0.02 mm/yr. However, with the presence of SRB, the corrosion rate was fluctuating with the maximum value of 0.4 mm/yr. Moreover, they concluded that the corrosion behaviour of carbon steel in anaerobic conditions was divided into three categories, *i.e.*, (1) anaerobic inorganic corrosion which depends on the ability to utilize the cathodic reactants, *e.g.* water or hydrogen ion. (2) the precipitation of protective film caused no decrease of electrical resistance (no start of corrosion). (3) MIC induced by SRB; this corrosion starts after the protective film ruptured, caused developing of localized corrosion.

Romero and Urdaneta [15] studied the correlation between *Desulfovibrio* sessile growth and OCP, hydrogen permeation, corrosion products and morphological attack on iron. The bacteria used was *Desulfovibrio desulfuricans*. Some conclusions have been made from their study:

- H₂S generated by SRB is the precursor for bacterial corrosion of steel.
- In the presence of ferrous ions, the genus *Desulfovibrio* severely corrodes iron approximately 0.43 mm/yr in the form of groups of deep holes.
- In the presence of SRB and ferrous ions, the iron sulphide products formed starting with mackinawite, could be: *pyrite*, *esmitite*, *marcasite*, *greigite*, *pyrrhotite* and *troilite*. However, pyrite is the most protective principally when it is mixed with extracellular polymeric membrane generated by the bacteria.
- Bacterial corrosion diminishes pH locally favoring the reduction of pyrite to mackinawite and severe localized steel corrosion where the bacteria are formed in colonies.

- The mackinawite formed does not have protective characteristics due to its hydrophilic character and its sizeable volume which causes it to detach leaving the base metal bare and exposed to the corrosive fluid.

Gramp *et al.* [53] observed the formation of Fe sulphides in cultures of SRB and in abiotic sulphide. Their results showed that mackinawite and greigite were dominant iron sulphide phases found in SRB cultures. Meanwhile, *mackinawite*, *greigite* and *pyrite* were found in abiotic sulphide with *greigite* as the more prevalent one.

Herbert *et al.* [54] characterized the surface chemistry and morphology of crystalline iron sulphides precipitated in media containing SRB. Their study showed that the iron sulphide produced were composed of both ferric and ferrous iron coordinate with monosulphide, with lesser amounts of disulphide and polysulphides also present. In addition, they concluded that the precipitates possessed a surface composition similar to greigite, with the remaining composed of disordered *mackinawite*.

Zhao *et al.* [55] studied the effect of SRB on carbon steel corrosion in sea mud. It is observed that the presence of SRB increased the carbon steel corrosion rate by 182% compared with that in sterile sea mud. With the excess of dissolved H₂S, they observed the transformation of protective FeS film to FeS₂ or other non stoichiometric polysulphide. Such transformation changes the state of former layer and accelerated the corrosion process.

The growth behaviour of SRB was investigated by Hu [56]. Her study showed that both SRB growth rate and the protective iron sulphide film were affected by the ferrous iron concentration. Increasing ferrous ion concentrations increased the SRB growth rate and corrosion rate. In addition, it is observed that the increase of SO₄²⁻ concentration within the range of 1.93 g/l to 6.5 g/l decreased the planktonic growth and the corrosion rate of mild steel.

Jobalia [57] studied the role of a biofilm and its characteristics in MIC. His study showed that the corrosion by SRB is also influenced by temperature. At lower temperature (5 °C and 25 °C), the corrosion rate observed is lower than those at 37 °C. This is due to the corrosion by SRB is influenced by the number of SRB cell, and the cell growth rate is strongly affected by temperature. He also found that the presence of iron concentrations influenced the corrosion type. With the presence of 5 ppm and 50 ppm iron concentrations, there was no localized attack observed. However, with the presence of 25 ppm, where the super saturation occurred, localized attack was observed.

In summary, H₂S produced by SRB and FeS film formed, have significant role in corrosion caused by SRB. However, the similar role of biotic sulphide and abiotic sulphide in the presence of other SRB metabolism products on the corrosion mechanism and kinetic of carbon steel is still unclear and need further investigation. Therefore, it becomes a challenge to characterize and compare the abiotic and biotic sulphide role on carbon steel.

2.3 Comparison between abiotic sulphide experiments and SRB experiments (biotic)

Based on the review above, the corrosion caused by SRB is mainly related to the sulphide ion produced and FeS film formed. A number of experiments have been conducted to investigate the behaviour of abiotic sulphide compared to biotic sulphide.

Newman *et al.* [9] studied the effect of abiotic sulphide on the corrosion rate of steel in neutral solution. The corrosion rate measured in abiotic sulphide is a few times lower than those achievable in SRB experiment, however the similarity is striking. They underlined that the difference is probably related to the aspect of SRB corrosion which had not been simulated, namely the massive deposition of FeS that occurred when SRB grow in culture media containing Fe²⁺. In the abiotic experiments, FeS could only form as a result of corrosion. Furthermore, they highlighted the

importance of biofilm formation including extracellular protein produced by SRB which help to cement the particulate FeS together. In an abiotic experiment, the FeS film formed can be fragile and may create crevice condition on the metal surface.

Videla *et al.* [58-59] compared the corrosion products formed in biotic and abiotic media. From their study, the chemical and structural analyses of sulphide films formed under abiotic and biotic solutions have the following characteristics:

- In biotic and abiotic sulphide films, the outer layers are formed by both FeS and FeS₂. However, in a biogenic sulphide film, FeS is the major species whereas in an abiotic sulphide film FeS₂ is predominant.
- The chemical composition of tubercles formed in abiotic and biotic solutions is different. The main contrast is that the corroded metal surface underneath a biogenic film is made up of iron sulphide whereas in a non biogenic film corresponds to an iron hydroxide or oxide.
- The films formed under biogenic conditions are more adherent to the surface of the metal than those formed in abiotic media, which are flaky and loosely adherent.
- The inner shell contained more sulphur in biotic films than those formed in abiotic media.
- Biogenic sulphide solution is less aggressive compared to abiotic sulphide.
- The previous history of the sulphide film may play a relevant role in the corrosion behaviour of carbon steel. According to sulphide concentration, and to the presence or absence a biofilm, the protective characteristics of the sulphide corrosion product layer may change. During the different stages of the biofilm growth, biogenic layers of corrosion products can offer some protection to the metal by improving the adherence of the sulphide film but can also enhance corrosion by inducing the presence of heterogeneities at the metal surface.
- The type of FeS formed (either as a compact film, or as a soft precipitate, or in suspension) conditions the sulphide effect on iron dissolution.

Kuang *et al.* [10] concluded that the corrosion rate caused by SRB is hardly related to the active SRB number, but it depends on the accumulation of the metabolism SRB products, *i.e.* sulphide. Their results also showed that the potentiodynamic polarization curves in the presence of SRB showed consistency results with potentiodynamic polarization curves in the medium containing different concentrations of Na₂S.

Sherar *et al.* [11] characterized the corrosion morphology of carbon steel induced by abiotic sulphide and biotic sulphide. It is concluded that biofilm formation and corrosion product morphology are highly nutrient dependent. Reducing the carbon content in solution appears to favour abiotic corrosion leading the formation of crystalline FeS. It is also confirmed that the dominant iron phase formed was *mackinawite* under both abiotic and biotic conditions. In addition, they claimed that the use of abiotic sulphide is sufficient enough to develop steel rate prediction. However, this simplistic approach does not account for the heterogeneity that exists in bacterial system.

From the review above, it is proposed that the use of abiotic sulphide could be used to simulate the SRB corrosion. However, in the real SRB corrosion, the corrosive species is not only limited to the sulphide. In their metabolic activities, SRB also produce other species that could harmful the steel, *e.g.* CO₂, acetate, sulphite, pyruvate, sulphate and lactate. The presence of these species could alter the role of sulphide on the corrosion kinetic and mechanism. Therefore, the remaining challenge is to investigate the effect of sulphide in the presence of other species as relevance to MIC caused by SRB.

2.4 Abiotic H₂S Corrosion

The role of corrosion by SRB is related to the formation of sulphide product. The sulphide may react with hydrogen to form H₂S. Therefore, a brief review of hydrogen sulphide is given below.

The dissociation of hydrogen sulphide in water involves a series of chemical reactions as described from Equations 2.28 to 2.32. The proposed chemical reactions steps are [60]:

i. H₂S dissolution



ii. H₂S dissociation



iii. HS⁻ dissociation



iv. H₂S Reduction



v. FeS formation by precipitation



The reactions of H₂S in aqueous vary with pH. In acidic solutions, the dominant sulphide species is molecular H₂S. At pH of about 6, the solution will contain bisulphide ions. The higher pH will result in the formation of bisulphide. At pH of around 7, the amount of H₂S molecular and bisulphide forms is similar [61].

In H₂S corrosion system, there are different possibilities of iron sulphide formation in aqueous solution [62]. The formation of solid film on the surface is due to anodic dissolution of iron. Ferrous ions dissolve into solution and react with sulphide ions in the solution, hence no film of corrosion product on the surface. The formation of sulphide can also be by mixing reaction between ferrous ions that react on the surface and in solution. Those film formations bring different film porosities of iron sulphides. The porous surface facilitates the cathodic reaction and creates anodic dissolution of iron that affects to the corrosion rate [62]. The types of FeS are influenced by temperature and H₂S activity [61]. Based on kinetics theories, several

types of FeS are commonly found in oil field corrosion are *pyrite* (FeS_2), *pyrrhotite*, *troilite*, *amorphous iron sulphide*, *cubic iron sulphide* and *mackinawite*.

Figure 2.5 shows corrosion sequence for carbon steel in aqueous H_2S solution [63-64]. Table 2.3 shows properties of the iron sulphide.

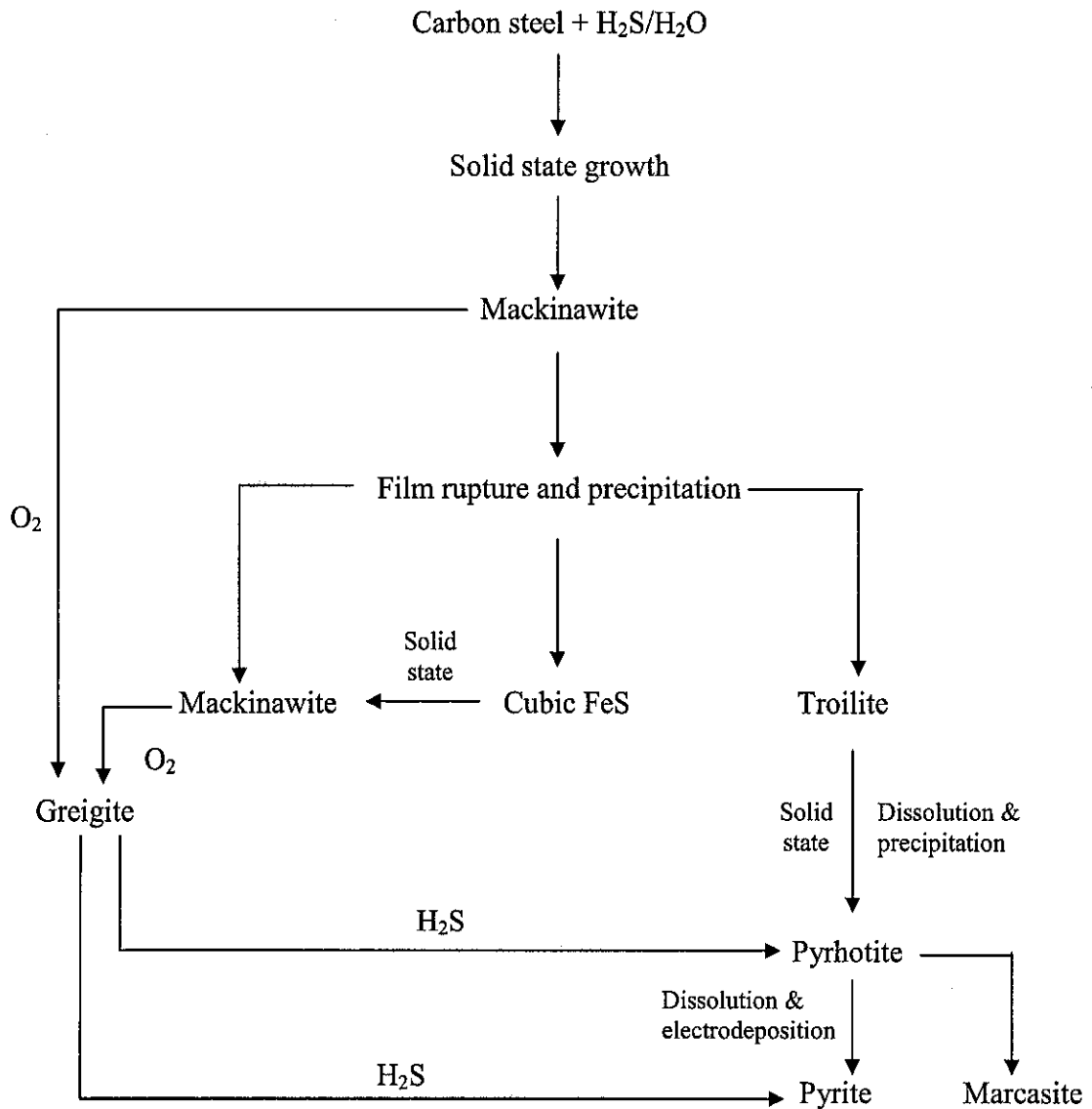


Figure 2.5 Corrosion sequence for carbon steel in aqueous H_2S solution [65-66].

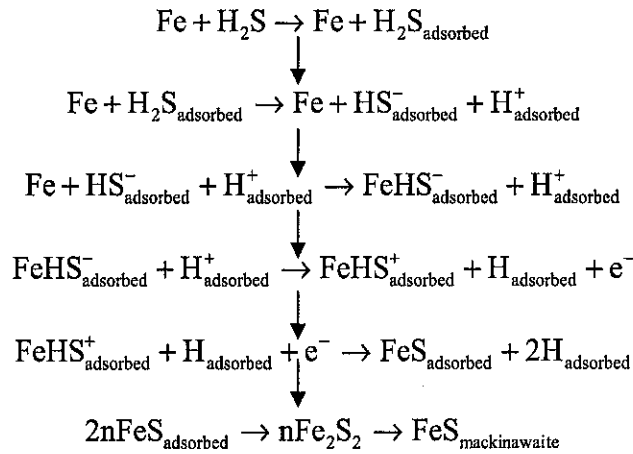
Table 2.4 Properties of the iron sulphide [67]

	Mineral Type					
	Mackinawite	Pyrrhotite	Greigite	Marcasite	Pyrite	Smythit
Formula	$\text{Fe}_{(1-x)}\text{S}$	$\text{Fe}_{(1-x)}\text{S}$	$\text{Fe}_{(1-x)}\text{S}$	$\text{Fe}_{(1-x)}\text{S}$	$\text{Fe}_{(1-x)}\text{S}$	$\text{Fe}_{(1-x)}\text{S}$
Value of x	0.057-0.064	0.00-0.14	0.25	0.5	0.5	0.00-0.18
Crystal structure	Tetragonal	NiAs type	Cubic	Orthorhombic	Cubic	Rhombohedral

Smith *et al.* [65-66] proposed two mechanisms of H_2S as shown in Figure 2.6.. The second path is more preferable and could be described as follows:

- H_2S diffuses to the steel surface.
- H_2S reacts with the steel to form *mackinawite* scale on the surface.
- *Mackinawite* scale dissolves to $\text{Fe}(\text{HS})^+$ and HS^- .
- $\text{Fe}(\text{HS})^+$ diffuses away from the steel surface, and
- More H_2S diffuses to react with the exposed steel.

Path 1:



Path 2

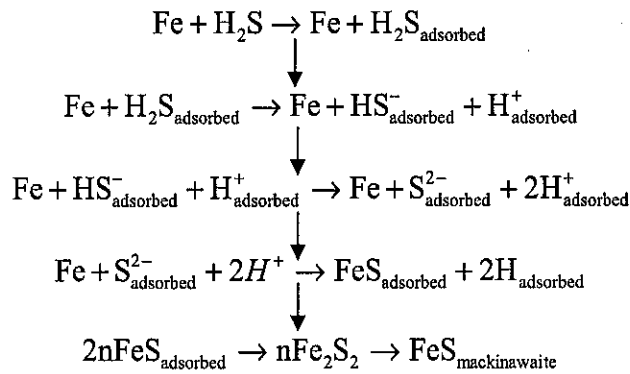


Figure 2.6 Two mechanisms for H₂S corrosion. After the initial adsorption of H₂S on the steel surface, mackinawite can be formed from amorphous FeS either by path 1 or path 2 [65-66].

Besides increasing the corrosion rate, the presence of H₂S could inhibit the rate of corrosion. Ma *et al.* [68] proposed a probable mechanism of the inhibitive effect of H₂S as follows:





The species FeSH^+ may be incorporated directly into a growing layer of *mackinawite* via Eq. (2.36).



Or it may be hydrolyzed to yield Fe^{2+} via Eq. (2.37)



Ma *et al.* [68] stated, if reaction (2.36) dominated the electrode surface, then the nucleation and growth of one or more of the iron sulphides, *i.e.* *mackinawite*, *cubic ferrous sulphide* or *troilite* occurs. However, the role of H_2S accelerates or inhibits the rate of corrosion, depending on the pH value. At lower pH values (<2), ferrous ion dissolves through reaction (2.37). As a result, there will be less iron sulphide film due to its high solubility at low pH. Meanwhile, at the pH values of 3-5, H_2S begins to exhibit its inhibiting effect as FeSH^+ species may form partially *mackinawite* through reaction (2.36). The *mackinawite* can convert into *troilite* which is more stable and protective. At a pH of more than 5, *mackinawite* was the only observed product of corrosion. As *mackinawite* has less protective ability than *troilite*, the inhibiting effect of H_2S decreases.

Tang *et al.* [69] studied the effect of H_2S concentration (59 – 409 ppm) on the corrosion behaviour of carbon steel at 90°C. The results showed that the corrosion rate increased with the increase of H_2S concentrations. H_2S showed strong acceleration effect on the cathodic hydrogen evolution of carbon steel, causing carbon steel to be seriously corroded. The corrosion products formed on carbon steel surface were composed of *mackinawite*, which was loose and did not show any protective properties. Severe localized corrosion on the steel surface was also observed, which may be attributed to cementites stripped off from the grain boundary.

When H_2S gas presents with CO_2 gas, there will be a growth competition between FeCO_3 and FeS films which affects to the corrosion rate. Nesic *et al.* [70] constructed a model that identified the growth of film formation containing $\text{H}_2\text{S}/\text{CO}_2$ gas. The

initial film formed is started by FeS film formation. Then, the FeCO₃ film becomes thicker and denser at the metal/film interface due to an increase in pH and Fe²⁺ concentration.

Brown [60] found that the corrosion rate in CO₂ environment increased in the presence of small H₂S concentration of less than 30 ppm. However, he also observed a decreasing of corrosion rate in the presence of 100 ppm H₂S. The scale produced was adherent and protective enough to retard corrosion attack. The scale was more protective when temperature was increased to 80°C.

The findings by Brown was supported by Lee [71]. Lee concluded that small amount of H₂S (10 ppm) lead to rapid reduction of the corrosion rate. Based on the SEM observation, they found that the scale formed on the surface that inhibited corrosion rate has a mackinawite structure.

Agrawal *et al.* [72] observed that the phenomena of accelerated corrosion in a CO₂ and H₂S environment occurs at low H₂S concentration. They found that there was a strong correlation between the corrosion rates and the temperature. In the range of H₂S concentration studied, the corrosion rate showed a polynomial curve with increasing the temperature.

Kvarekval *et al.* [73] studied the effect of H₂S concentrations ranging from 150 – 450 ppm in a CO₂ environment. The results showed that higher corrosion rates were obtained in the presence of H₂S compared to experiments without H₂S. The corrosion rates were in the range of 0.1-2 mm/yr.

Singer *et al.* [74] observed that trace amounts of H₂S greatly retards the CO₂ corrosion with general corrosion rates usually 10 to 100 times lower than their pure CO₂ equivalent. The most protective conditions were observed at the lowest partial pressure of H₂S. However, corrosion rate increased when more H₂S was added. The presence of trace amounts of H₂S (0.004 bar) in the CO₂ environment sharply decreases the corrosion rate by two orders of magnitude. As the partial pressure of H₂S is increased to 0.13 bar, the tendency is reversed and the general corrosion rate increased by an order of magnitude.

Carew *et al.* [75] observed a rapid and significant reduction in the CO₂ corrosion rate both in single and multiphase flow in the presence of 10 ppm H₂S. At higher H₂S concentrations (up to 250 ppm) the trend was reversed and a mild increase of the corrosion rate was observed.

Schmitt *et al.* [76] stated that a change in pH from 4 to 6 had only little effect on the corrosion rate, and at pH 6, 60 °C and 25 ppm H₂S, protective corrosion films were formed and no localized corrosion were observed [77]. The effect seems to vanish at higher pH values (5.5-7) and higher temperatures (>80°C), when a protective film is formed. They concluded that an increase of the CO₂ partial pressure in the same flow system from 3.8 to 10.6 bar reduces the maximum corrosion rates from about 15 to 0.2 mm/y under conditions when semi-protective films are formed, e.g. in the pH range below 5.2 [78].

In combination with CO₂, corrosion rate of H₂S showed different phenomena compared to without CO₂ as reported by Makarenko *et al.* [79]. With CO₂, the corrosion process is accelerated by cathodic reaction of hydrogen ion reduction. It has been proven that CO₂ corrosion of carbon steel increases by 1.5–2 times with increase of H₂S content in the mixture (p H₂S<0.5 MPa) in the temperature range 20–80°C. Further increasing in H₂S content (p H₂S≥0.5–1.5 MPa), the corrosion rate will decrease, especially in the temperature range 100–250°C, because of the influence of FeS and FeCO₃ on corrosion. It may relate to formation of protective film [79].

Choi *et al.* [80] studied the effect of H₂S on the CO₂ corrosion of carbon steel in acidic solutions. The results showed that the addition of 100 ppm H₂S to CO₂ induced rapid reduction in the corrosion rate at both pHs 3 and 4. The inhibition effect is attributed to the formation of thin FeS film on the steel surface that suppressed the anodic dissolution reaction.

Abelev *et al.* [81] examined the effect of H₂S on iron corrosion in 3 wt% NaCl solution saturated with CO₂ in temperature range of 25-85 °C. Small H₂S concentrations (5 ppm) have an inhibiting effect on corrosion in the presence of CO₂ at temperatures from 25 to 55 °C. However, 50 ppm H₂S is needed to provide significant corrosion inhibition. At higher H₂S concentrations, the corrosion rate increases rapidly, while still remaining below the rate for the H₂S free solution.

Corrosion protection in the temperature range 25 to 55 °C is attributed to adsorption of sulphur on the native iron oxide, and this layer provides significant corrosion inhibition. The main species responsible for inhibition included Fe(II) bonded to S and O. Meanwhile, at higher H₂S concentrations a thicker layer of iron corrosion products forms on the surface by a dissolution precipitation mechanism. However, this layer is porous and inhomogeneous, having voids and irregularities yielding less protective characteristic to the steel.

Sun [64] showed that mackinawite is the dominant scale formed on the steel surface, which protects the steel from corroding in CO₂/H₂S corrosion. She also highlighted that the makeup of the surface scale not only depends on the water chemistry and the respective solubility of iron carbonate and iron sulphides, but also on the competitiveness of the two scale formation mechanisms. Only at very high supersaturation of iron carbonate are both iron carbonate and *mackinawite* scale are found on the steel surface, with iron carbonate in the outer portion of the *mackinawite* scale.

Based on the review above, H₂S could increase or decrease the corrosion rate of mild steel. However, the roles of H₂S in increasing or decreasing the corrosion rate were influenced by other factors, such as: its concentrations and pH.

2.5 Corrosion prediction model

Predictive models are developed as an engineering design tool in project development and subsequent operation and maintenance of the plant [82]. Although there are many different models available, basically they were developed from two approaches:

1. Worst case or maximum risk approach, which is based solely on laboratory test data; and
2. Most probable risk approach that is partly based on field data.

Nesic *et al.* [83] presented a good review of the models and categorized them into three groups:

1. Mechanistic models – utilizing from theoretical background to describe the mechanism of underlying reaction;
2. semi-empirical models – partly based on firm theoretical background and partly based on empirical functions; and
3. Empirical models – based mostly on best-fit parameters from exponential results, hence, relying on minimal theoretical background.

In MIC field, prediction models have been developed by some authors to predict corrosion caused by SRB. The models are summarized in Table 2.5 below.

Table 2.5 Brief description of various SRB corrosion prediction models

Author	Brief description	Comments on metabolic species
Peng <i>et al.</i> [84]	A mathematical model that was developed based on the sulphate utilization kinetics by SRB. The models most sensitive to the sulphate diffusion coefficient and maximum sulphate utilization rate.	The model only considers sulphate as the parameter input. No other metabolic species take into account.
Darbi <i>et al.</i> [85]	A numerical model that solved using finite different technique. To develop the model, CDT was adopted as the MIC mechanism. Effect of sulphate and SRB kinetic growth rate were taken into account in this model.	The model only considers sulphate as the parameter input
Garber <i>et al.</i> [86]	A mathematical model that measured CO ₂ corrosion pitting in the presence of SRB. The existence of SRB is assumed by the presence of sulphate ions in the system.	SRB metabolic species represented by sulphate and acetate concentrations were used as the parameter input.
Gu <i>et al.</i> [38]	A mechanistic model that was developed based on biocatalytic sulphate reduction theory. The model considers both mass transfer resistance (when there is a pit) and charge transfer resistance (when the biofilm thickness is small).	This model was developed based on the use of electron released in anodic process to the sulphate reduction at the cathode. The model considers organic acid and sulphate as the parameter input

Based on the review above, it is seen that there is no empirical model developed that consider SRB main metabolic species as the parameter input. Most of the existing models are mathematical and mechanistic model that consider sulphate as the parameter input.

2.6 Summary

Currently-accepted MIC theory based on CDT could not fully explain the corrosion mechanism caused by SRB since the theory is based on sole effect of sulphide. In addition, recent studies have shown that abiotic chemistry could be used to simulate SRB corrosion. However, most of the studies are limited to the use of sole sulphide. In the real SRB corrosion, the corrosive species is not only limited to the sulphide. In their metabolic activities, SRB also produce other species *e.g.* CO₂, acetate, sulphite, pyruvate, sulphate and lactate. The presence of other metabolic species has important roles as it could alter the corrosion kinetic and mechanism of steel.

CHAPTER 3

RESEARCH METHODOLOGY

In this study, electrochemical experiments and surface characterization analysis were conducted. Electrochemical experiments were performed to study the effects of SRB metabolic products on the kinetic and corrosion mechanism of X52 steel. The electrochemical techniques used were linear polarization resistance (LPR), electrochemical impedance spectroscopy (EIS) and Tafel polarization (TP). Surface characterization analyses were performed to investigate the film morphology formed from corrosion process by using FESEM, EDAX and XPS.

3.1 Research Test Matrix

The test matrices were constructed to achieve the objective stated. The work on this study basically is divided into two stages *i.e.* pre-screening and detail analysis.

The pre-screening study was conducted in two steps. The first step was aimed to study the effect of individual species on the corrosion rate of X52 steel. The second step was conducted to study the effect of individual species with the addition of other species (in constant value for each species, 200 ppm) in the solution. The species used were sulphide, sulphate, sulphite, acetate, lactate, pyruvate and thiosulphate. These species were used as there were generated in the SRB metabolic process [22]. Table 3.1 shows test matrix of the pre-screening study.

Table 3.1 Test matrix of the pre-screening study

Parameter	Description
Steel Type	X52 steel
Solution	3 % NaCl
De-oxygenation gas	CO ₂
Species added	Sulphide, sulphate, sulphite, acetate, lactate and thiosulphate
Concentrations (ppm by weight)	0, 50, 200, 400
Temperature (°C)	25
Technique	LPR
Objective	<ul style="list-style-type: none"> • To observe the behaviour of individual species on the X52 steel corrosion rate with and without the addition of the other species in the solution. • To define which species that have more significant effect on the X52 steel corrosion rate.

The results from pre-screening study were used to define the parameters that used in detail analysis. The test matrix for detail analysis is shown in Table 3.2 below.

Table 3.2 Test matrix of the detail analyses

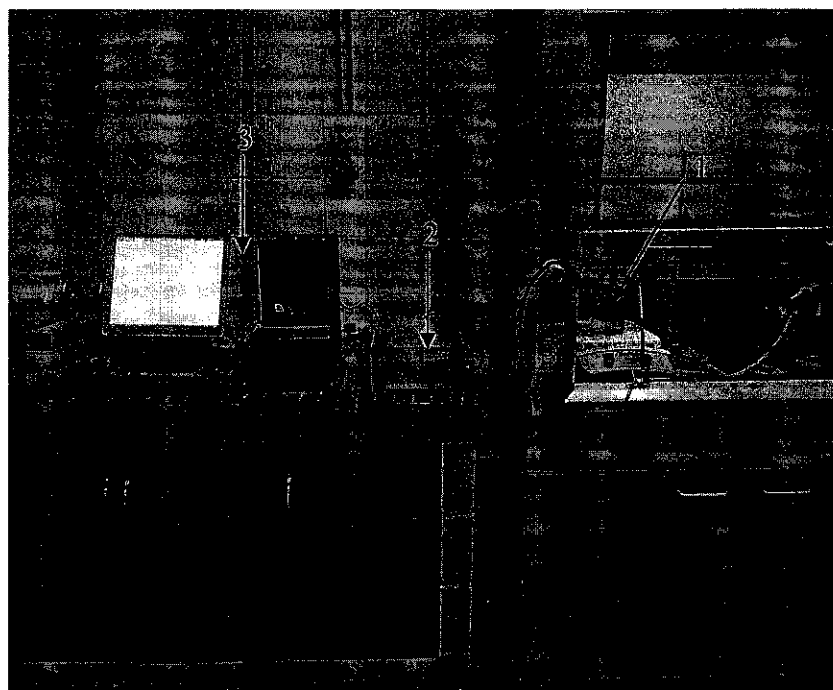
Parameter	Description
Steel Type	X52 steel
Solution	3 % NaCl
De-oxygenation gas	CO ₂
Species added in various concentrations	Three most significant species
Concentrations (ppm by weight)	0, 50, 200, 400
Temperature (°C)	25
Technique	LPR, EIS, TP, FESEM/EDAX and XPS
Objective	<ul style="list-style-type: none"> • To observe the significant species on the corrosion kinetics, mechanism and morphology of X52 steel. • To propose a possible corrosion mechanism caused by SRB metabolic products on X52 steel. • To develop an empirical equation to predict corrosion by SRB at temperature 25°C.

3.2 Experimental Setting

The test assembly consisted of a standard one-litre glass cell of solution saturated with CO₂ for 1 hour prior to the exposure of an electrode. CO₂ purging was maintained throughout the test to minimize the ingress of air. The tests were conducted at atmospheric pressure and temperature of around 25°C. The chemicals used were listed in Table 3.3 and the picture of experimental setting is shown in Figure 3.1. For the detail of glass cell set-up, it is shown in Figure 3.2.

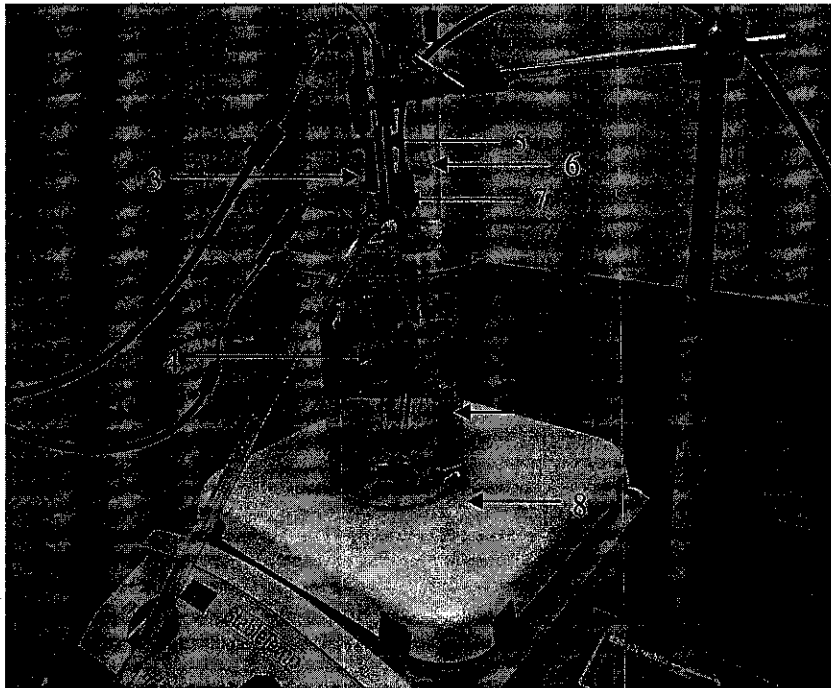
Table 3.3 List of chemicals used

Species	Chemical compound	Purity (%)	Source
Sodium chloride	NaCl	≥ 99	Merck
Sulphite	Na ₂ SO ₃	≥ 97.5-110.5	Merck
Sulphate	Na ₂ SO ₄	≥ 99%	Merck
Sulphide	Na ₂ S·9H ₂ O	≥ 95%	R&M Chemicals
Thiosulphate	Na ₂ S ₂ O ₃ ·5H ₂ O	≥ 99.5-101%	Merck
Pyruvate	C ₃ H ₃ NaO ₃	≥ 99%	Merck
Acetate	CH ₃ COONa	≥ 99%	Merck
Lactate	(S)-Lactic acid	90%	Merck



1. Glass cell set-up; 2. Potentiostat; 3. Computer

Figure 3.1 Experimental setting



1. Glass cell; 2. CO₂ bubbler; 3. Reference electrode; 4. Working electrode;
5. Counter electrode; 6. Thermometer; 7. pH meter; 8. Heater

Figure 3.2 Glass cell set-up

The electrochemical measurements were based on a three-electrode system, using computer controlled, ACM Gill 12 Weldtester. The reference electrode used was an Ag/AgCl (3 M KCl) and the auxiliary electrode was a graphite. The electrochemical techniques used in this study were linear polarization resistance (LPR), Tafel polarization (TP) and electrochemical impedance spectroscopy (EIS). Electrochemical measurements data were taken approximately after 90 minutes of immersion time.

3.2.1 Solution preparation

The solution was made based on a standard of solution preparation as mentioned by Jeffery *et al* [87] and Furniss *et al* [88]. In the preliminary study, a 3% NaCl solution

was used as the solution. It was reported that the *Desulfovibrio* genera growth optimum at 3 % NaCl concentrations, suggesting its marine origin [45]. Initially the glass cell was assembled; a salt solution was prepared by filling 500 ml-de-ionized water into 1-litre beaker, and then 30 grams of NaCl was added to the cell. The water was then stirred with magnetic stirrer bar until the NaCl dissolved in the solution. After that, the species under study was added based on the desired concentrations. The water was then stirred again until the species added mixed well. Lastly, the beaker was filled up to 1 litre with de-ionized water.

In the detailed analyses study, test solution was prepared to simulate water containing SRB metabolic products species. To prepare the solution, similar method was used as in the preliminary study. The difference is relying on the concentrations of species added. Three species *e.g.* sulphide, sulphite and lactate, were used in various concentrations which are 0, 50, 200 and 400 ppm. For other species, the concentration was setting in constant value as listed in Table 3.4. In this study, the 3% NaCl solution added with species listed in Table 3.4 is called simulated solution and the concentration used is in ppm by weight.

The selected species concentrations are based on their concentrations ranges observed in the SRB experiment or in the environment [10, 25-30]. However, the concentrations selected are in the minimum value of the range. This selection is related to SRB growth phase which is an exponential phase, whereby the corrosion process is in an active condition [10].

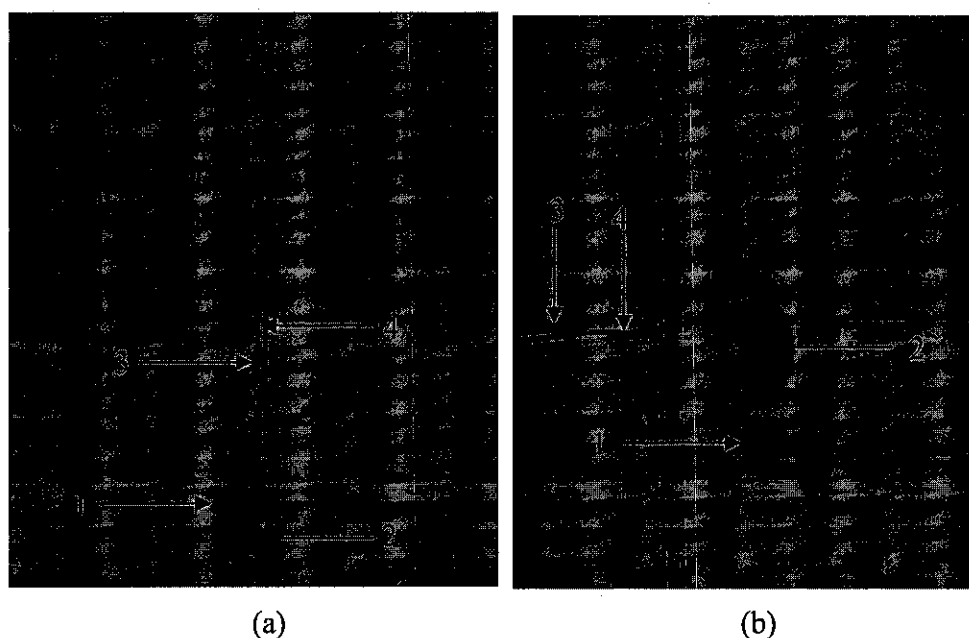
Table 3.4 Species with constant concentrations added to the 3% NaCl solution

Species	Concentrations (ppm by weight)
Pyruvate	100
Sulphate	50
Acetate	50
Thiosulphate	200

3.2.2 Material and preparation

The working electrode of this study was taken from X52 steel pipeline. The pipeline was cut and machined to cylindrical rod with an exposed area of 0.5 cm^2 .

For the electrochemical test, sample was made by cutting the steel rod 8 mm height each. Then the sample was connected with 20-cm-long copper wire to deliver current during test. Small diameter plastic hose covers copper wire to avoid interference or contact with solution during test. Next step was mounting the sample with epoxy resin and leaving one open lateral side as primary object of this research. The sample is shown in Figure 3.3. Prior to immersion, the specimen surface was ground to 600 SiC paper, rinsed with deionised water and degreased with acetone.



1. Epoxy; 2. Working electrode; 3. Plastic hose cover; 4. Copper wire.

Figure 3.3 Sample of electrochemical test: (a) side view; (b) front view.

For the surface morphology (face view taken by FESEM) and corrosion product analysis (XPS) tests, sample was made by cutting the steel rod 8 mm height each. The sample was then mounting with epoxy resin and leaving one open lateral side as

primary object for the observation. Prior to immersion, the specimen surface was ground to 600 SiC paper, rinsed with deionised water and degreased with acetone.

Different method was used to prepare sample for cross sectional view. The sample was prepared in the following way. A bare of X52 steel (in rectangular form) was prepared. One side of the specimen was polish up to 1micron grade (while the other sides were coated, so that the film was formed only in one side), rinsed with deionised water, degreased in acetone and dried in a compressed hot air flow. The specimen was then immersed in the simulated solution. After 90 minutes of immersion times, the specimen was taken out, rinsed with deionised water, degreased in ethanol, dried in a compressed hot air flow and put in the epoxy resin holder with the position of the sample side that containing film is perpendicular to the holder base. After the sample covered with epoxy resin, the sample was polish-up again up to 1 micron, rinsed with deionised water, degreased in ethanol and dried in a compressed hot air flow. The sample then was put under the FESEM apparatus to observe the film thickness.

3.3 Electrochemical Corrosion Measurements

Corrosion measurement was performed using linear polarization resistance (LPR), Tafel polarization (TP) and electrochemical impedance spectroscopy (EIS). LPR test was performed to obtain corrosion rate data, while TP and EIS were performed to obtain information on the corrosion mechanism.

3.3.1 Linear polarization resistance (LPR)

The LPR tests were conducted with a scan rate of 10 mV/min, and a scan range of -10 to +10 mV from the corrosion potential and repeated at least twice for each case. This method is based on ASTM standard G 102-89 [89].

The polarization resistance (R_p) was given by Stern and Geary's equation [90]

$$R_p = \frac{\Delta E}{\Delta I} = \frac{B}{i_{corr}} \quad 3.1$$

$$\text{where } B = \frac{b_a b_c}{2.303(b_a + b_c)} \quad 3.2$$

b_a and b_c = Tafel slopes for anodic and cathodic curves respectively.

The Stern-Geary constant, B , was calculated using cathodic and anodic Tafel slope based on Tafel analysis of the polarization curve. A value of 26 mV decade⁻¹ is considered.

The corrosion current density can be related directly to the corrosion rate (CR) from Faraday's law :

$$\text{Corrosion rate (mm year}^{-1}\text{)} = \frac{315Zi_{corr}}{\rho nF} \quad 3.3$$

where,

- i_{corr} = corrosion current density in $\mu\text{A cm}^{-2}$
- ρ = density of iron, 7.8 g cm^{-3}
- F = Faraday's constant, $96500 \text{ C mole}^{-1}$
- Z = atomic weight in g mol^{-1}
- n = number of exchanged electron

3.3.2 Tafel polarization (TP)

Tafel polarization were performed on individual coupons in freshly prepared solutions. The sample was polarized either in the anodic or cathodic direction with the scan - 300 mV to + 200 mV from E_{corr} . The sweep rate was 60 mV/min.

3.3.3 Electrochemical impedance spectroscopy (EIS)

EIS was measured under a sinusoidal excitation potential of 10 mV in the frequency range of 0.5 mHz to 10 kHz. The EIS curves were fitted using an open available software, namely EIS spectrum analyser® Beta version [91] .

An equivalent circuit, as shown in Figure 3.4, was used to fit all the measured impedance data, where R_s is the electrolyte resistance, R_t is the charge transfer resistance and CPE is a constant phase element. The equivalent circuit above has been used to fit the impedance data in solution containing sulphide [92].

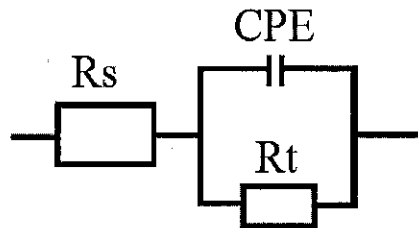


Figure 3.4 An equivalent circuit used to simulate the EIS diagram.

3.4 Surface morphology observation and corrosion product analysis

After the experiment, the specimen was used for additional *ex situ* analyses. The morphology and composition of each product were analyzed using field emission scanning electron microscope (FESEM), energy-dispersive x-ray spectroscopy (EDAX) and x-ray photoelectron spectroscopy (XPS) analysis. To observe the corrosion morphology under the corrosion products, the corrosion products were removed using the chemical products-cleanup method as mentioned by Finnegan [93].

3.4.1 Field emission scanning electron microscope (FESEM)

FESEM and EDAX examination was performed only on selected LPR conditions. The magnifications were ranged from 300 X to 5000 X. During FESEM test, surface and film profile (size of film, distribution) was captured to obtain information about morphology of corrosion product. EDAX examination was performed directly after image capturing to determine chemical composition of film formed. FESEM and EDAX examination was performed using Supra® 55 VP ZEISS Instruments, with the maximum voltage of 30 kV. The FESEM apparatus is shown in Figure 3.5.

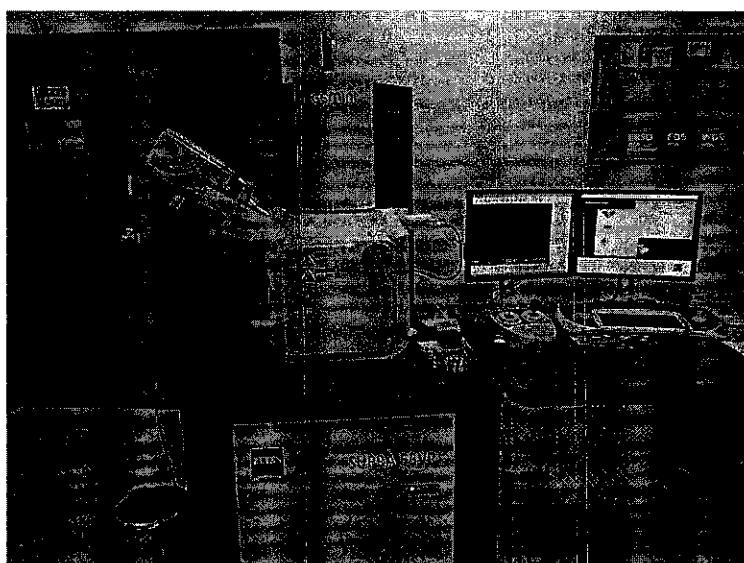


Figure 3.5 FESEM apparatus

3.4.2 X-ray photoelectron spectroscopy (XPS) analysis.

To ascertain the elements identified by the EDAX, the corrosion product was analyzed using XPS. XPS is very sensitive characterization technique for thin surface [92, 94]. Therefore, it could be suitable for examining the chemical state of the elements formed on the corrosion product. XPS analysis was performed using Thermo scientific K-Alpha equipment with the maximum ion gun energy of 4000 eV. The XPS apparatus is shown in Figure 3.6

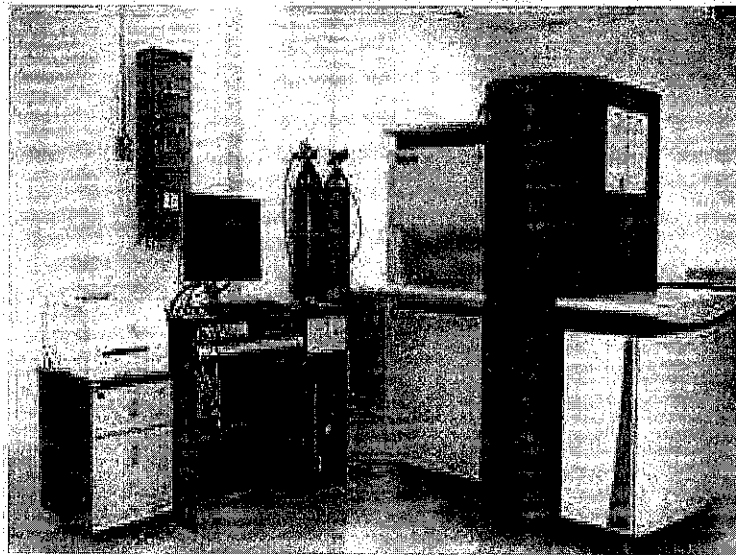


Figure 3.6 XPS apparatus

3.4.3 Corrosion prediction

Corrosion prediction equation was developed based on the graph fitting of LPR measurements. Minitab® software was used to fit the graph of LPR measurements. The equation developed was then validated using statistical analysis.

CHAPTER 4

RESULTS AND DISCUSSION

This chapter presents the results and discussions of corrosion kinetics, corrosion mechanism and surface morphology of X52 steel in the simulated solution containing SRB metabolic products. This chapter also presents the physical mechanism of corrosion by dominant SRB metabolic species and a development of corrosion prediction.

4.1 Corrosion kinetics and mechanism

4.1.1 Pre-screening study: Identification of main metabolic species

The pre-screening study was conducted using the LPR method to determine the corrosion rate of X52 steel under various abiotic conditions. The conditions were simulated based on SRB metabolic products found in the real SRB environment. The main metabolic products of SRB consist of seven various species representing seven independent variables in this study and requiring a large number of experiments. To reduce the number of experiment, pre-screening study was performed to determine three species that have more significant effect on the corrosion rate of X52 steel.

Initially, the individual effect of each metabolic species on the corrosion rate of X52 steel was evaluated. It is observed, as shown in Figure 4.1 , that only the addition of sulphite resulted in significant increase of the corrosion rate. The corrosion rate increases with the increasing of its concentrations. For example, the addition of 600 ppm sulphite increased the corrosion rate from 2 to 8 mm/yr, which was 3-fold higher compared to X52 steel in sulphite-free solution.

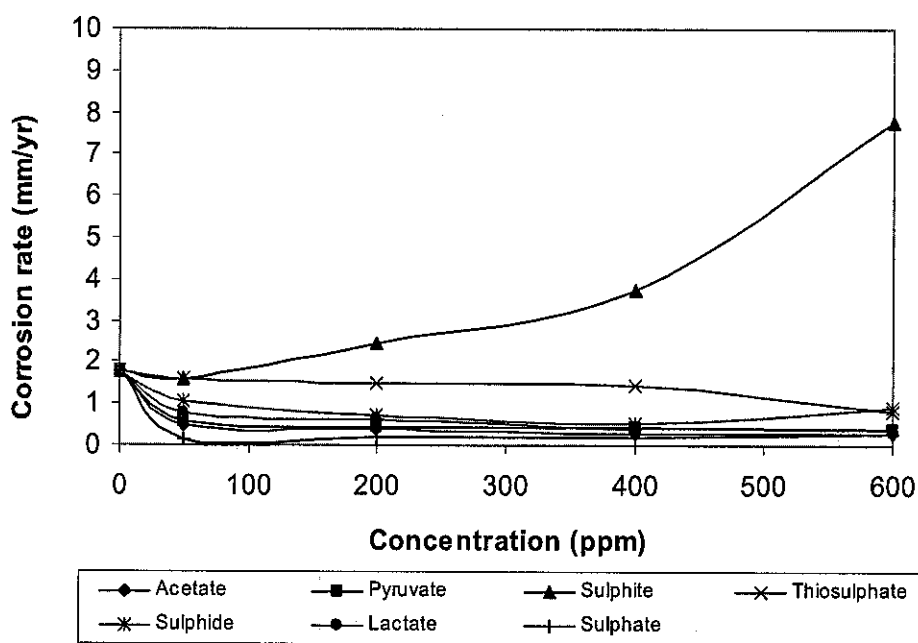


Figure 4.1 Effects of individual species on the X52 corrosion rate in the 3% NaCl solution.

In the subsequent test, the effects of individual species were analyzed with the presence of constant concentrations (200 ppm) of other species. It is seen from Figure 4.2 that the corrosion rate of most species decreased with the concentration above 400 ppm. Therefore, 400 ppm is taken as the maximum concentration for the detailed analyses study as the corrosion rate in this concentration is in active condition. Additionally, it is observed that the corrosion behaviour of individual species was changed with the presence of other species. Sulphide, sulphite and lactate became having a significant effect on the X52 corrosion rate. Furthermore, it is observed that the presence of other species caused the corrosion of individual species were higher than that without the presence of other species in the solution.

Table 4.1 shows the comparison of X52 corrosion rate with and without the presence of other species. It is observed that the corrosion rates of individual species between with and without the presence of other species are different. Without the presence of other species, the corrosion rate tends to increase with the addition of more concentrations. However, with the presence of other species, a decreasing of

corrosion rate is observed. It is believed that the synergistic effect among the species caused the corrosion rate increased or decreased.

Table 4.1 Corrosion rate comparison of species in solution containing other species (mix) and in solution without other species (sole) in various concentrations.

Species	Corrosion rate (mm/yr)									
	0 ppm		50 ppm		200 ppm		400 ppm		600 ppm	
	Sole	Mix	Sole	Mix	Sole	Mix	Sole	Mix	Sole	Mix
Sulphide	5.61	2.6	6.65	3.6	6.31	4.9	6.15	7.8	6.5	2.3
Sulphite	3.86	5.03	5.43	6.1	6.31	6.8	7.6	8.9	11.6	4.8
Lactate	5.68	3.7	6.46	4.3	6.81	4.8	6.08	5.7	6.08	3.2

From the pre-screening study, there are main findings that can be concluded as summarized below:

1. The presence of other species influences the corrosion rate of X52 steel caused by individual species.
2. In the presence of other species, sulphide, sulphite and lactate have significant effects in increasing X52 steel corrosion rate.

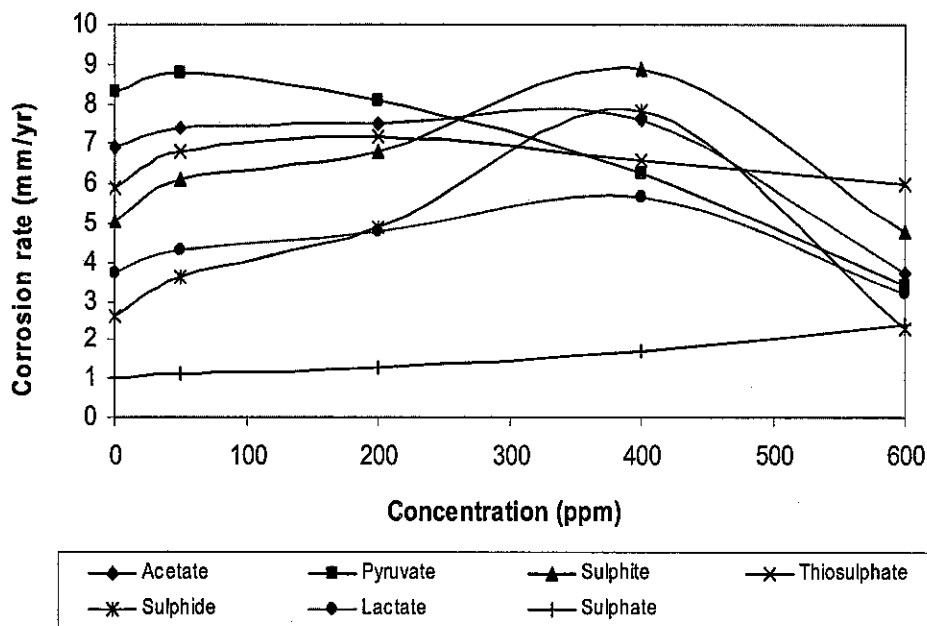


Figure 4.2 Effects of individual species on the X52 corrosion rate with the presence of other species in the 3% NaCl solution.

Therefore, in the detailed analyses study, the tests were conducted in various concentrations of sulphide, sulphite and lactate. Meanwhile, the concentrations of other species *i.e.* acetate, pyruvate, sulphate and thiosulphate, were in the constant value based on their concentration found in the nature.

4.1.2 Detailed analyses

The results of the pre-screening study were further investigated in the detailed analyses study using electrochemical techniques (LPR, EIS and TP) and surface morphology analysis.

4.1.2.1 LPR test

The LPR tests were conducted to observe the effects of various concentrations of sulphide and sulphite with the addition of various lactate concentrations represent the simulated solution containing SRB metabolic products.

a. Effect of Sulphide on the corrosion rate of X52 steel with various sulphite and lactate concentrations in the simulated solution

The effects of sulphide on the X52 corrosion rate were studied in various concentrations of sulphite and lactate in the simulated solution. The results are shown in Figure 4.3 to Figure 4.6.

In Figure 4.3, the effects of sulphide concentrations on the X52 corrosion rate were studied in various sulphite concentrations. It is observed that the addition of 50 ppm sulphide increased the corrosion rate. However, with the addition of 200 and 400 ppm sulphide, the corrosion rate decreased. This trend is true in all sulphite concentrations.

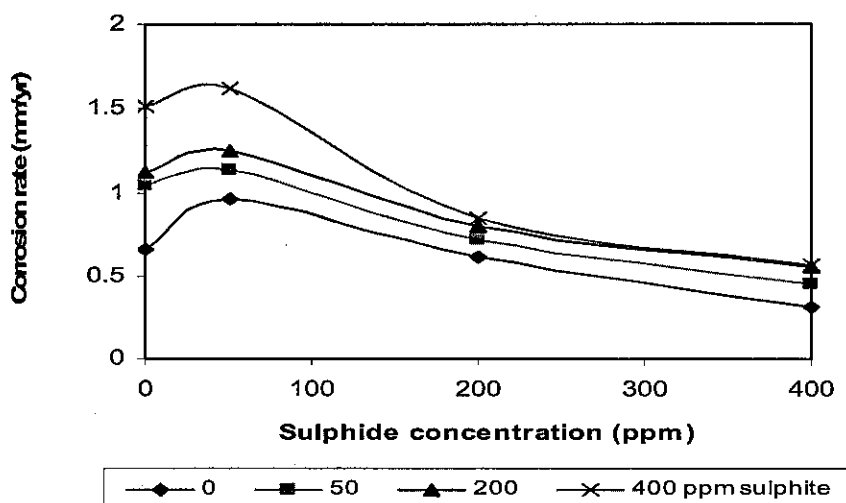


Figure 4.3 The effect of sulphide concentration on the corrosion rate of X52 steel in various sulphite concentrations without the presence of lactate in the simulated solution.

Figure 4.4 shows the effects of sulphide concentrations on the X52 corrosion rate in various sulphite concentrations with the addition of 50 ppm lactate in the simulated solution. It is observed that the addition of 50 ppm sulphide increased the corrosion rate. However, with the addition of 200 and 400 ppm sulphide, the corrosion rate decreased. This trend is true in all sulphite concentrations.

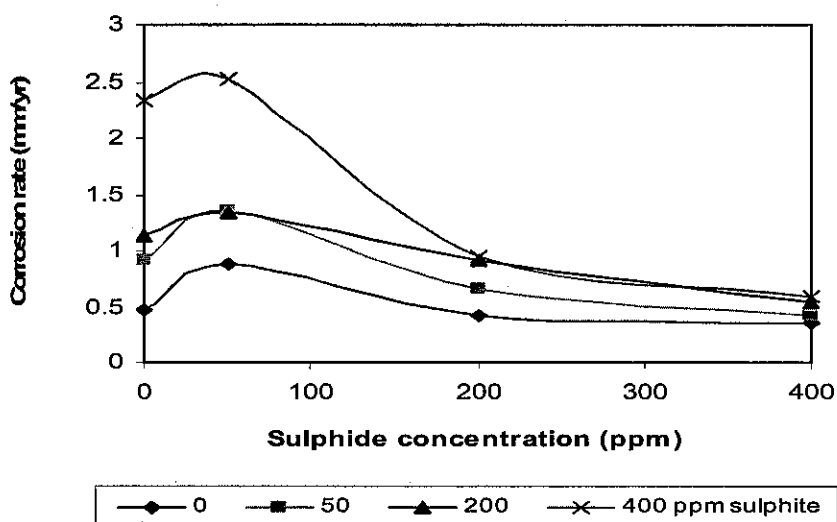


Figure 4.4 The effect of sulphide concentration on the corrosion rate of X52 steel in various sulphite concentrations with the presence of 50 ppm lactate in the simulated solution.

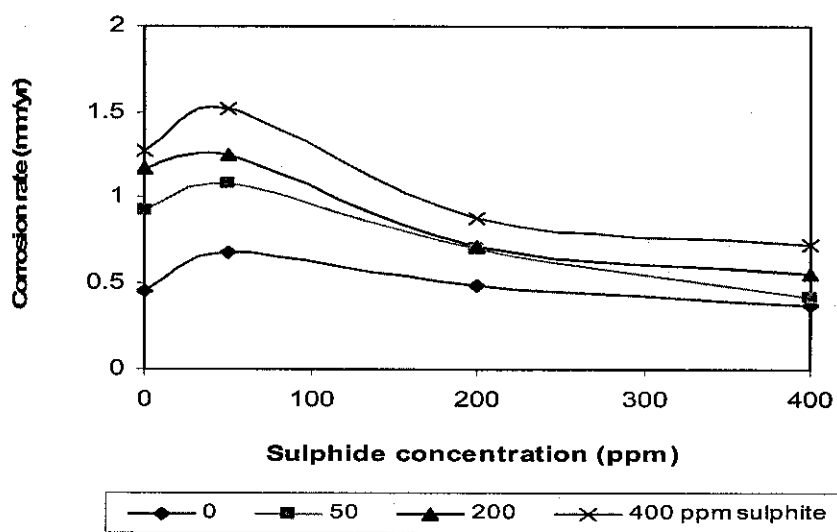


Figure 4.5 The effect of sulphide concentration on the corrosion rate of X52 steel in various sulphite concentrations with the presence of 200 ppm lactate in the simulated solution.

Figure 4.5 shows the effects of sulphide concentrations on the X52 corrosion rate in various sulphite concentrations with the addition of 200 ppm lactate in the simulated solution. A similar trend was observed with 50 ppm lactate in the solution, whereby the corrosion rate increased with the addition of 50 ppm sulphide and decreased with the addition of 200 and 400 ppm sulphide.

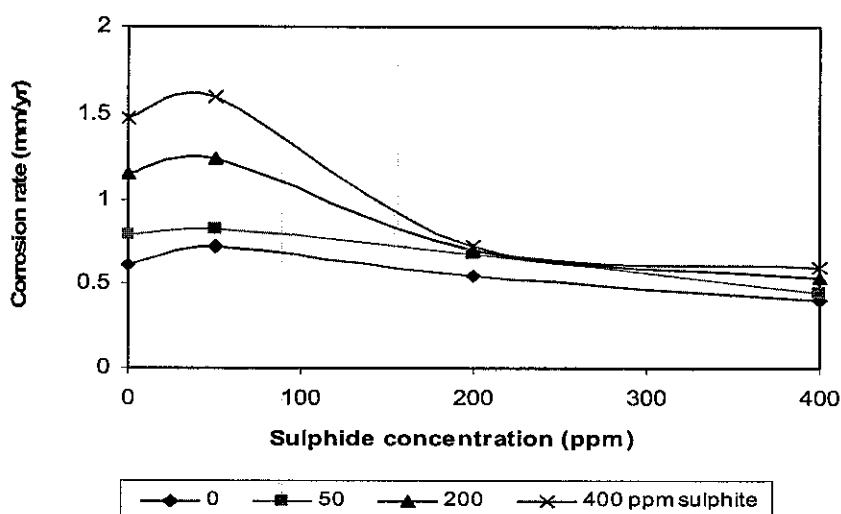


Figure 4.6 The effect of sulphide concentration on the corrosion rate of X52 steel in various sulphite concentrations with the presence of 400 ppm lactate in the simulated solution.

The effects of sulphide concentrations on the X52 corrosion rate in various sulphite concentrations with the addition of 400 ppm lactate in the simulated solution is shown in Figure 4.6. It is observed that the addition of 400 ppm lactate did not change the trend of sulphide concentrations on the X52 corrosion rate.

In general, the corrosion rate of X52 steel increased with the presence of 50 ppm sulphide and decreased with 200 and 400 ppm sulphide concentrations. This trend is observed in all sulphite and lactate concentrations.

b. Effect of Sulphite on the corrosion rate of X52 steel with various sulphide and lactate concentrations in the simulated solution

The effects of sulphite on the X52 corrosion rate were studied in various concentrations of sulphide and lactate. The results are shown in Figure 4.7 to Figure 4.10.

In Figure 4.7, the effects of sulphite concentrations on the X52 corrosion rate were studied in various sulphide concentrations. It is observed that the X52 corrosion rate increased with increasing sulphite concentrations. This trend is true in all sulphide concentrations.

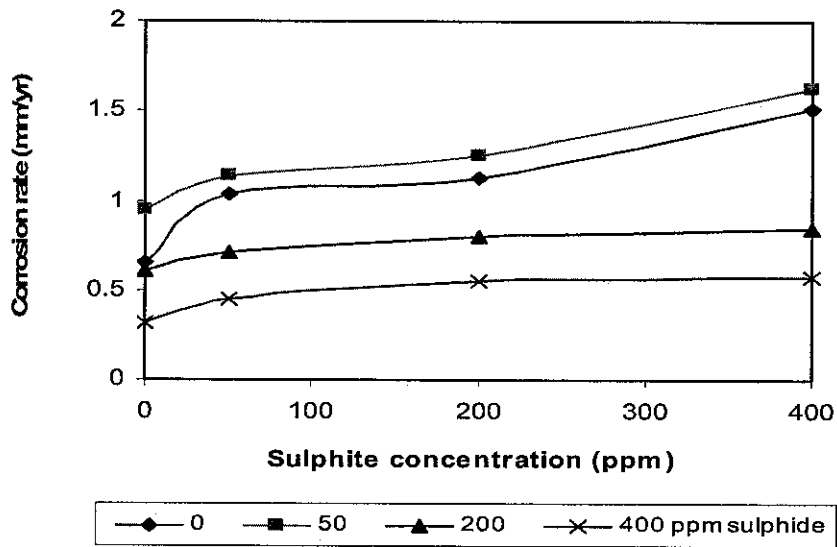


Figure 4.7 The effect of sulphite concentration on the corrosion rate of X52 steel in various sulphide concentrations without the presence of lactate in the simulated solution.

Figure 4.8 shows the effects of sulphite concentrations on the X52 corrosion rate in various sulphide concentrations with the addition of 50 ppm lactate in the simulated solution. It is observed that the addition of sulphite concentrations increased the corrosion rate. This trend is observed in all sulphide concentrations.

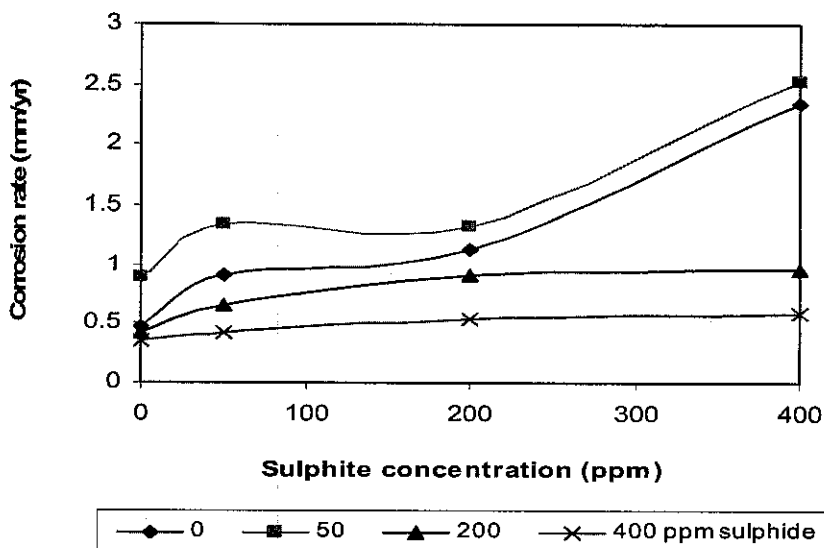


Figure 4.8 The effect of sulphite concentration on the corrosion rate of X52 steel in various sulphide concentrations with the presence of 50 ppm lactate in the simulated solution.

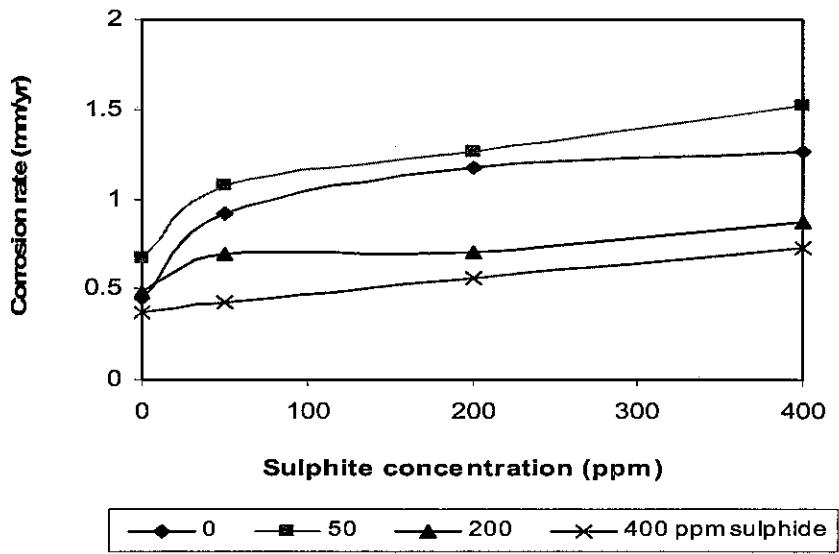


Figure 4.9 The effect of sulphite concentration on the corrosion rate of X52 steel in various sulphide concentrations with the presence of 200 ppm lactate in the simulated solution.

Figure 4.9 shows the effects of sulphite concentrations on the X52 corrosion rate in various sulphide concentrations with the addition of 200 ppm lactate in the simulated solution. A similar trend was observed with 50 ppm lactate in the solution, whereby the corrosion rate increased with the increasing of sulphite concentrations.

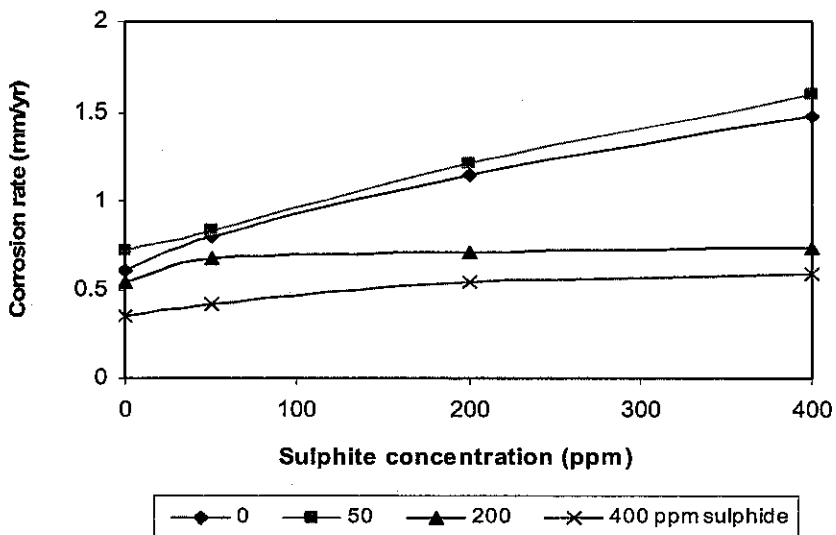


Figure 4.10 The effect of sulphite concentration on the corrosion rate of X52 steel in various sulphide concentrations with the presence of 400 ppm lactate in the simulated solution.

The effects of sulphite concentrations on the X52 corrosion rate in various sulphide concentrations with the addition of 400 ppm lactate in the simulated solution is shown in Figure 4.10. It is observed that the addition of 400 ppm lactate did not change the trend of sulphite concentrations on the X52 corrosion rate.

Generally, it is observed that the corrosion rate of X52 steel increased with the increase of sulphite concentration. It is also seen that the significant effect of sulphite concentration was observed at 0 ppm and 50 ppm sulphide concentrations. This trend is true in all lactate concentrations.

4.1.2.2 Electrochemical Impedance Spectroscopy

EIS tests were conducted under various conditions similar to the LPR tests. EIS test could give information not only limited to the corrosion rate, but also it can give other information such as the corrosion mechanism.

In this sub chapter, the results of EIS tests divided in terms of effect of sulphide and sulphite studied in various lactate concentrations.

a. Effect of Sulphide

The effect of sulphide concentration studied in various lactate and sulphite concentrations are presented in subchapters below (a-d).

a.1. Effect of Sulphide without the Presence Lactate in Various Sulphite Concentrations in the Simulated Solution

Figure 4.11 to Figure 4.14 show impedance spectra of sulphide concentration effect on the corrosion behaviour of X52 steel under various sulphite concentrations without the presence of lactate in the solution.

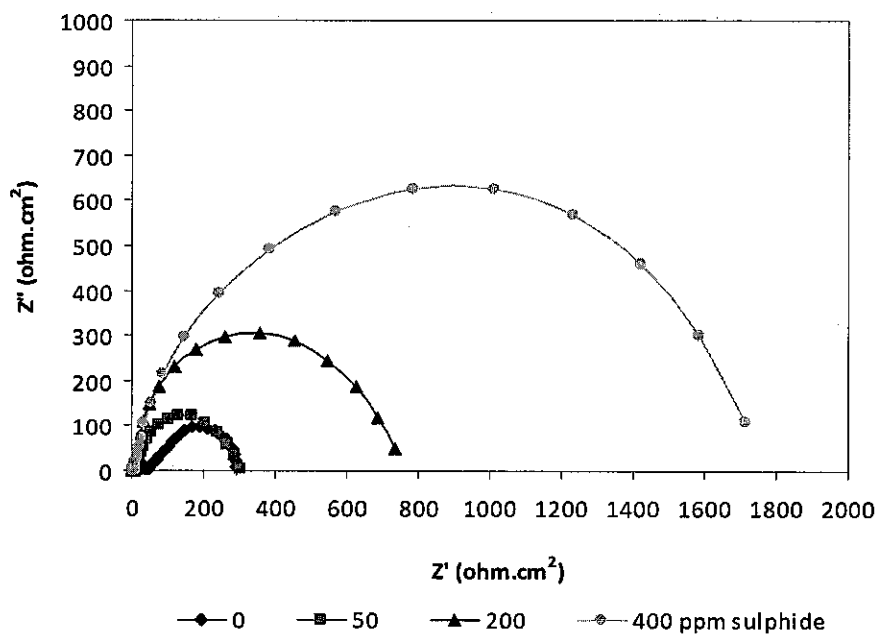


Figure 4.11 Impedance spectra, presented as Nyquist plot, showed the effect of sulphide concentration without the presence of sulphite in the simulated solution.

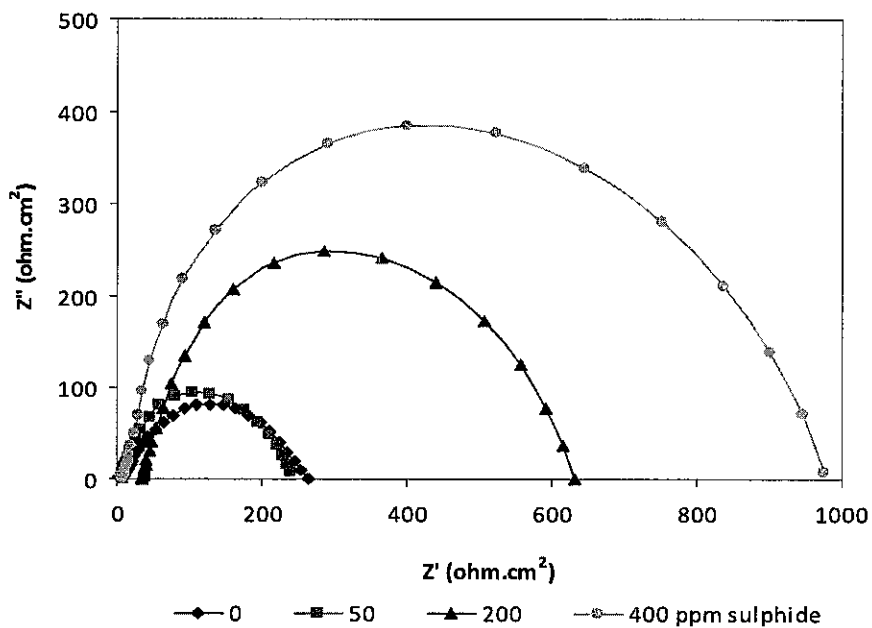


Figure 4.12 Impedance spectra, presented as Nyquist plot, showed the effect of sulphide concentration with the presence of 50 ppm sulphite in the simulated solution.

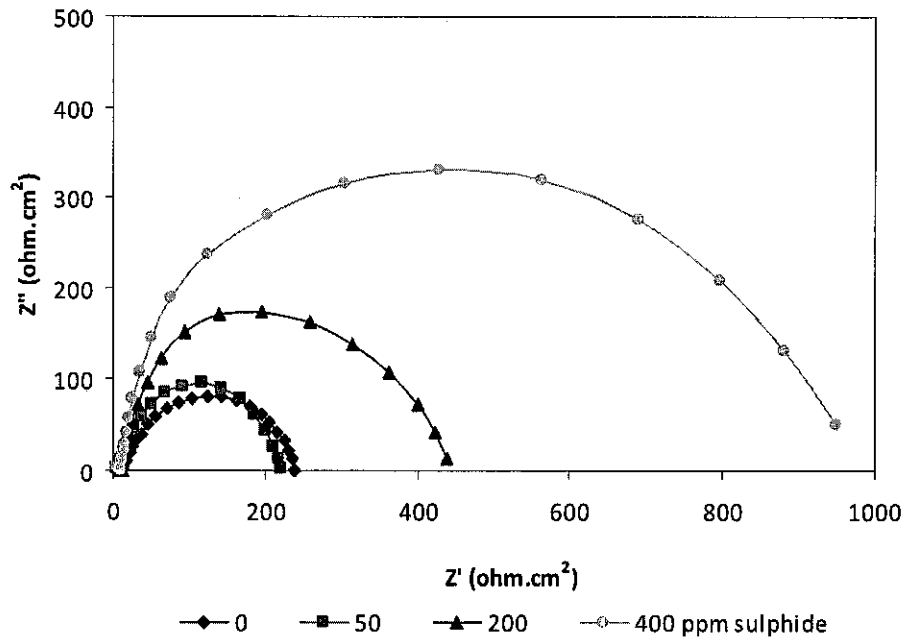


Figure 4.13 Impedance spectra, presented as Nyquist plot, showed the effect of sulphide concentration with the presence of 200 ppm sulphite in the simulated solution.

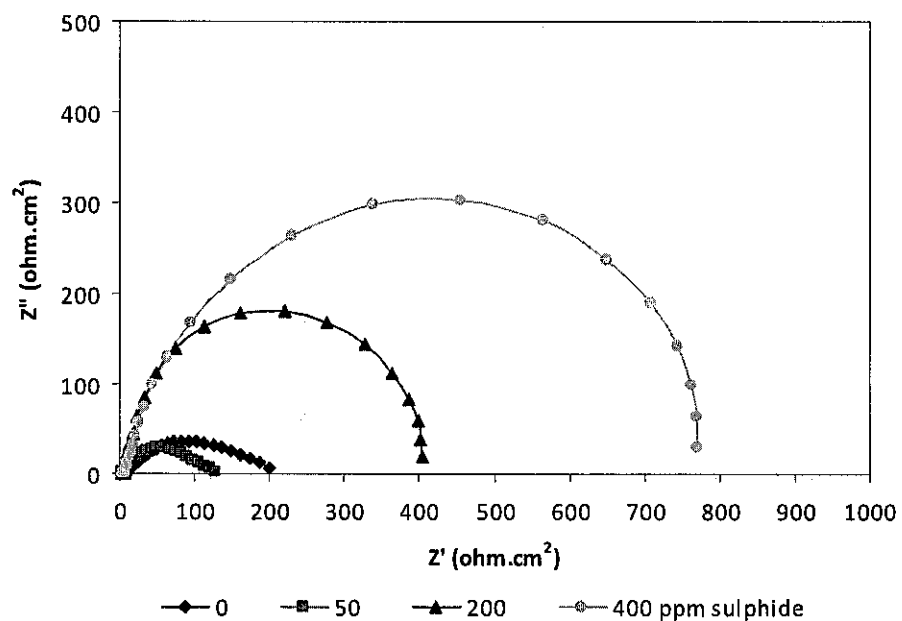


Figure 4.14 Impedance spectra, presented as Nyquist plot, showed the effect of sulphide concentration with the presence of 400 ppm sulphite in the simulated solution.

Table 4.2 shows the impedance parameters obtained by circuit fitting. It is observed, the R_t value of 50 ppm sulphide smaller than 0 ppm sulphide. However, with the presence of 200 and 400 ppm sulphide concentration, the R_t increased. Since the value of R_t is inversely proportional to the value of corrosion rate, therefore the corrosion rate of X52 steel increased with the presence of 50 ppm, and then decreased with the presence of 200 and 400 ppm sulphide. This trend was also observed in 50, 200 and 400 ppm sulphite introduce to the solution.

Table 4.2 Electrochemical impedance parameters fitted from the measured EIS data

$C_{SO_3^{2-}}$ (ppm)	C_S^{2-} (ppm)	R_s ($\Omega.cm^2$)	R_t ($\Omega.cm^2$)	Parameter of CPE (P)	Coefficient of P (n)
0	0	30.24	267	0.00052	0.63
	50	5.5	320	0.0035	0.9
	200	4.5	720	0.0026	0.85
	400	6.5	1700	0.002	0.8
50	0	3	237	0.002	0.4
	50	7.9	225	0.0049	0.9
	200	18.5	630	0.0025	0.82
	400	8.42	990	0.0023	0.88
200	0	10.19	236	0.0003	0.74
	50	7.9	216	0.0032	0.9
	200	11.3	450	0.0048	0.85
	400	4	960	0.0036	0.9
400	0	5	210	0.0053	0.5
	50	8.5	120	0.0057	0.63
	200	5	418	0.0058	0.88
	400	3.7	784	0.0037	0.89

a.2. Effect of Sulphide with the Presence of 50 ppm Lactate and Various Sulphite Concentrations in the Simulated Solution

Figure 4.15 to Figure 4.18 show Nyquist plot of the effect of sulphide concentration on the corrosion behaviour of X52 steel under various sulphite concentrations with the presence of 50 ppm lactate in the solution.

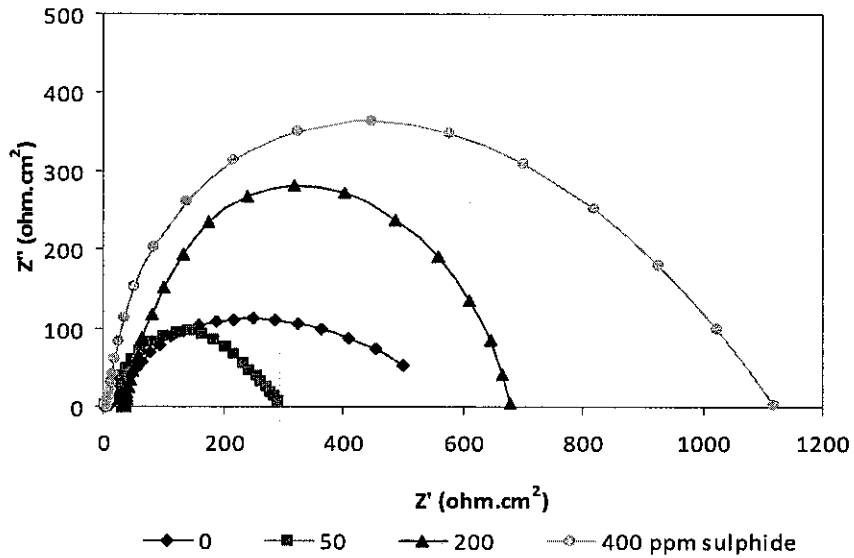


Figure 4.15 Impedance spectra, presented as Nyquist plot, showed the effect of sulphide concentration without the presence of sulphite in the simulated solution.

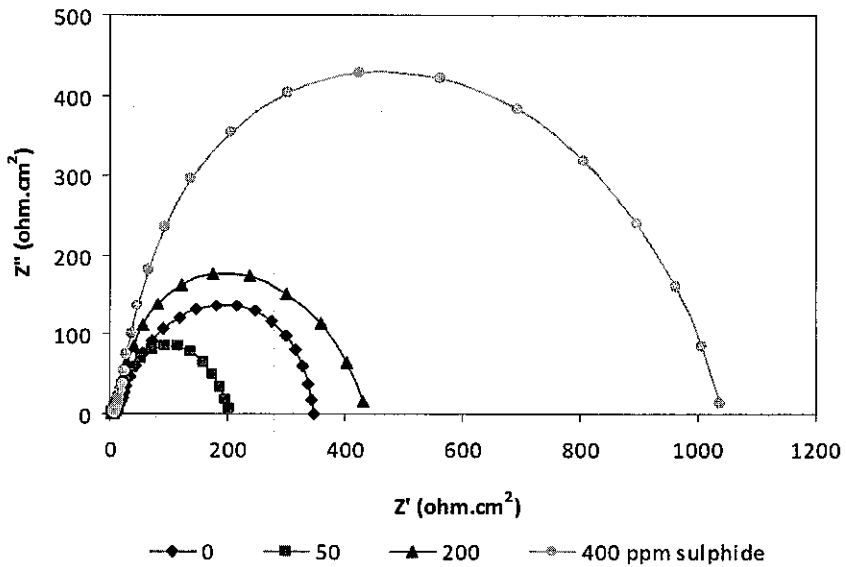


Figure 4.16 Impedance spectra, presented as Nyquist plot, showed the effect of sulphide concentration with the presence of 50 ppm sulphite in the simulated solution.

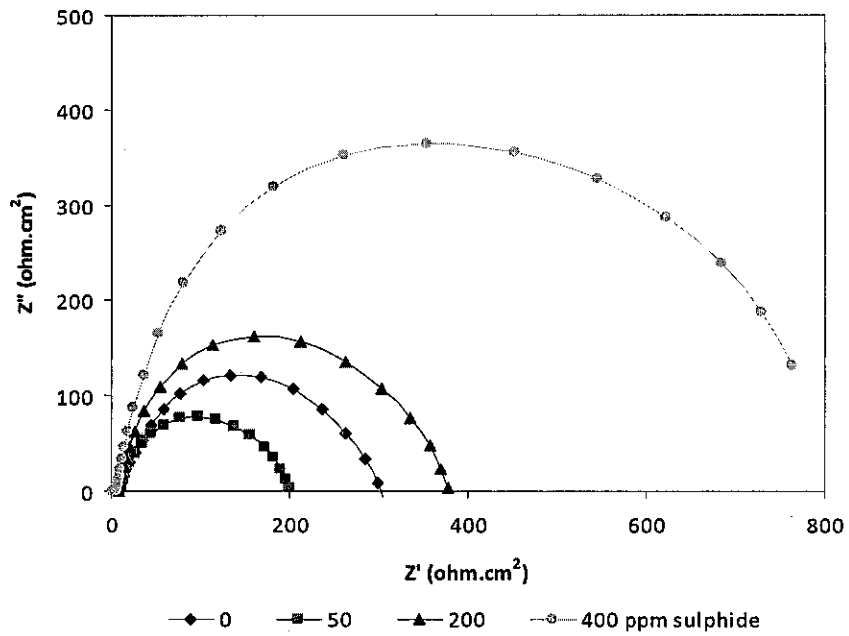


Figure 4.17 Impedance spectra, presented as Nyquist plot, showed the effect of sulphide concentration with the presence of 200 ppm sulphite in the simulated solution.

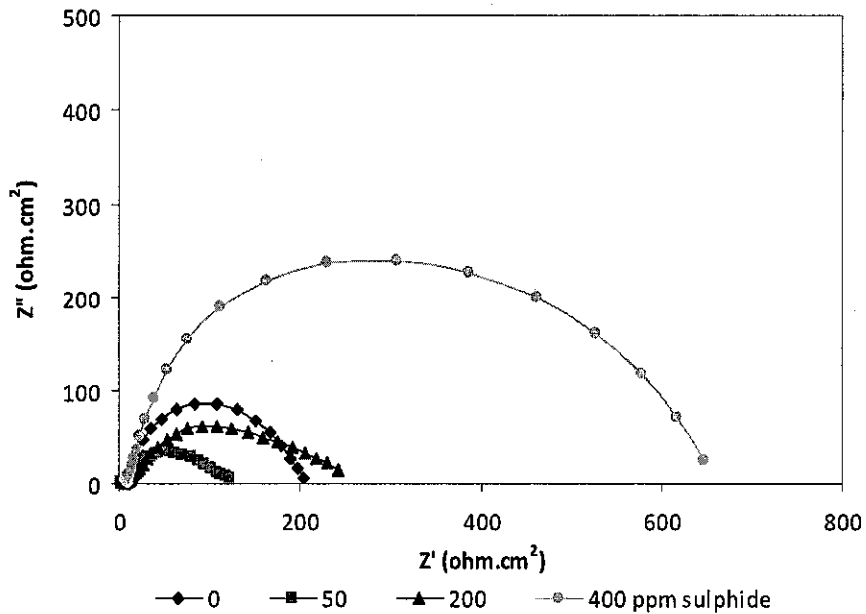


Figure 4.18 Impedance spectra, presented as Nyquist plot, showed the effect of sulphide concentration with the presence of 400 ppm sulphite in the simulated solution.

Table 4.3 shows the impedance parameters obtained by circuit fitting. Similar behaviour was observed between solution with 50 ppm lactate and 0 ppm lactate. The R_t value of 50 ppm sulphide was smaller than 0 ppm sulphide. However, with addition of 200 and 400 ppm sulphide, the R_t increased.

Table 4.3 Electrochemical impedance parameters fitted from the measured EIS data

$C_{SO_3^{2-}}$ (ppm)	C_S^{2-} (ppm)	R_s ($\Omega.cm^2$)	R_t ($\Omega.cm^2$)	Parameter of CPE (P)	Coefficient of P (n)
0	0	4.4	510	0.0034	0.62
	50	6.9	285	0.002	0.74
	200	25	693	0.0025	0.86
	400	4.9	1300	0.0037	0.79
50	0	9.4	350	0.00046	0.86
	50	7.3	205	0.0032	0.86
	200	9.9	420	0.0025	0.88
	400	5.02	1080	0.0025	0.88
200	0	3.2	318	0.003	0.87
	50	8.2	195	0.006	0.88
	200	5	365	0.004	0.92
	400	5.02	800	0.0025	0.94
400	0	5.5	240	0.005	0.63
	50	8	125	0.01	0.7
	200	5	205	0.0048	0.93
	400	5.02	680	0.0034	0.81

a.3. Effect of Sulphide with the Presence of 200 ppm Lactate and Various Sulphite Concentrations in the Simulated Solution

Figure 4.19 to Figure 4.22 show Nyquist plot of the effect of sulphide concentration on the corrosion behaviour of X52 steel under various sulphite concentrations with the presence of 200 ppm lactate in the solution.

As shown in Table 4.4, it is observed that the presence of 200 ppm lactate in the solution did not change the behaviour of R_t value. The behaviour was similar with 0 and 50 ppm lactate solution.

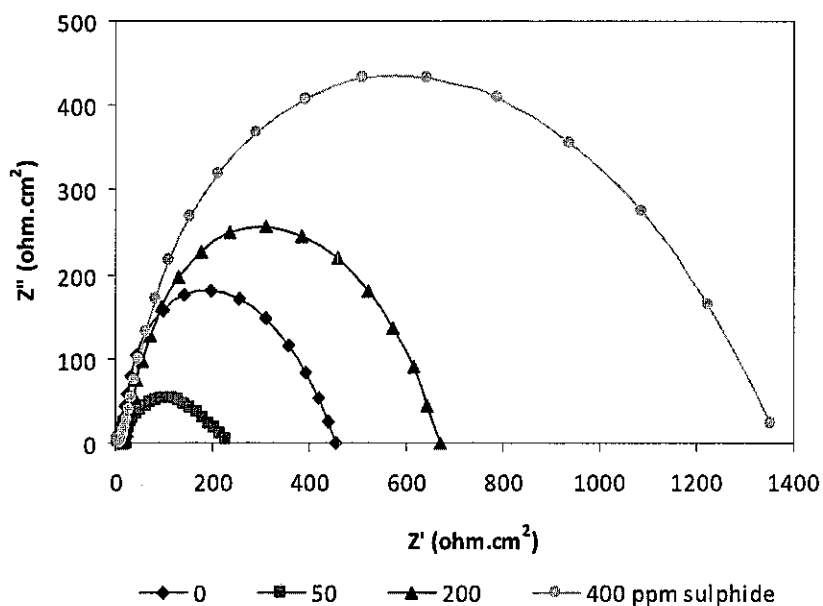


Figure 4.19 Impedance spectra, presented as Nyquist plot, showed the effect of sulphide concentration without the presence of sulphite in the simulated solution.

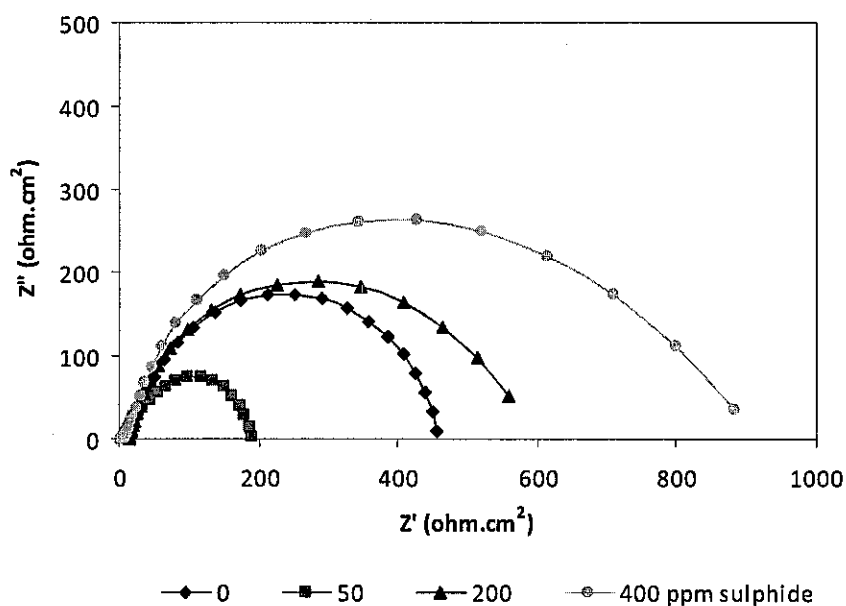


Figure 4.20 Impedance spectra, presented as Nyquist plot, showed the effect of sulphide concentration with the presence of 50 ppm sulphite in the simulated solution.

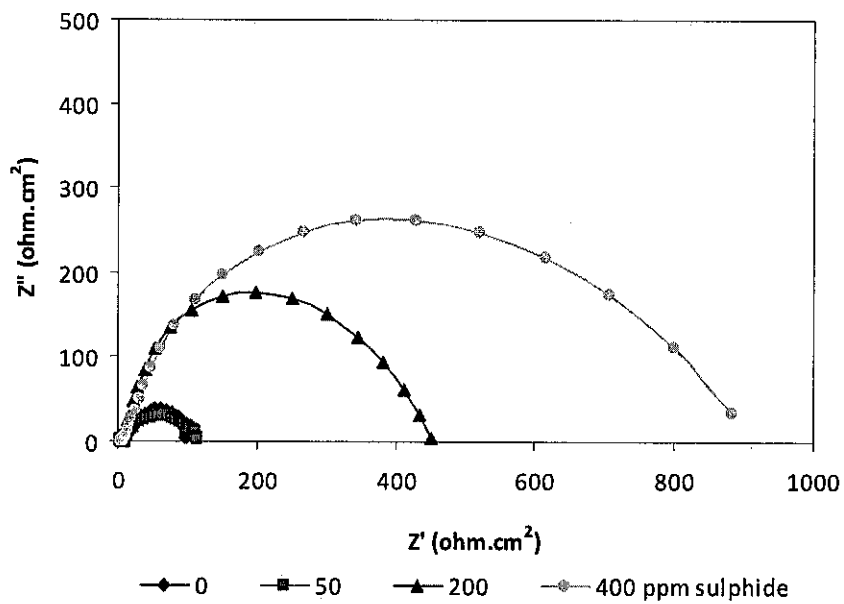


Figure 4.21 Impedance spectra, presented as Nyquist plot, showed the effect of sulphide concentration with the presence of 200 ppm sulphite in the simulated solution.

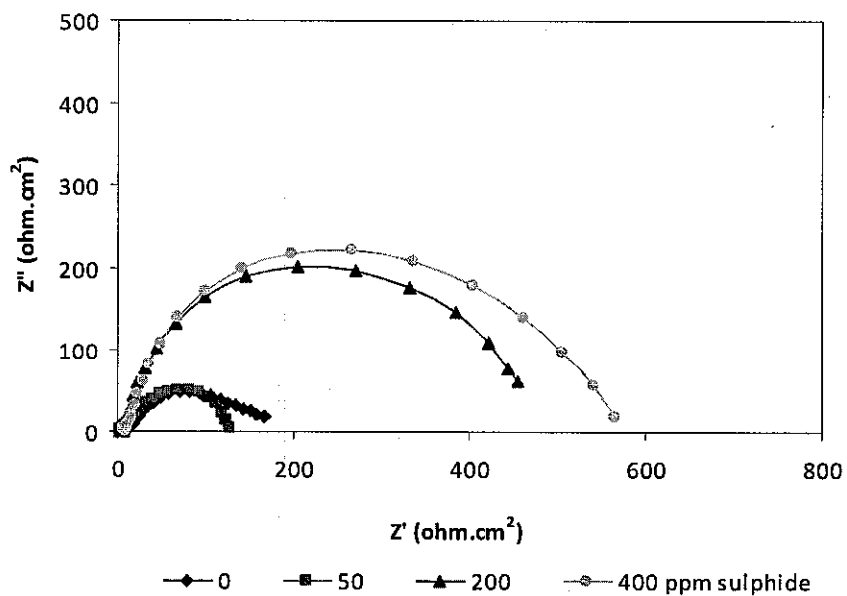


Figure 4.22 Impedance spectra, presented as Nyquist plot, showed the effect of sulphide concentration with the presence of 400 ppm sulphite in the solution.

Table 4.4 Electrochemical impedance parameters fitted from the measured EIS data

$C_{SO_3^{2-}}$ (ppm)	$C_{S^{2-}}$ (ppm)	R_s ($\Omega.cm^2$)	R_t ($\Omega.cm^2$)	Parameter of CPE (P)	Coefficient of P (n)
0	0	3	439	0.003	0.82
	50	8	230	0.0035	0.6
	200	6	640	0.003	0.88
	400	6	1350	0.0037	0.76
50	0	10.1	434	0.00022	0.87
	50	8	190	0.00075	0.83
	200	6	640	0.0036	0.96
	400	6	1400	0.0035	0.75
200	0	8	350	0.0053	0.6
	50	8	112	0.0042	0.65
	200	6	440	0.0037	0.96
	400	6	880	0.0035	880
400	0	8	220	0.0078	0.6
	50	5.2	120	0.0008	0.95
	200	6	455	0.0042	0.96
	400	6	600	0.0035	0.83

a.4. Effect of Sulphide with the Presence of 400 ppm Lactate and Various Sulphite Concentrations in the Simulated Solution

Figure 4.23 to Figure 4.26 show Nyquist plot of the effect of sulphide concentration on the corrosion behaviour of X52 steel under various sulphite concentrations with the presence of 400 ppm lactate in the simulated solution.

As shown in Table 4.5, in the presence of 400 ppm lactate in the solution, the R_t value has similar behaviour with 0, 50 and 200 ppm lactate.

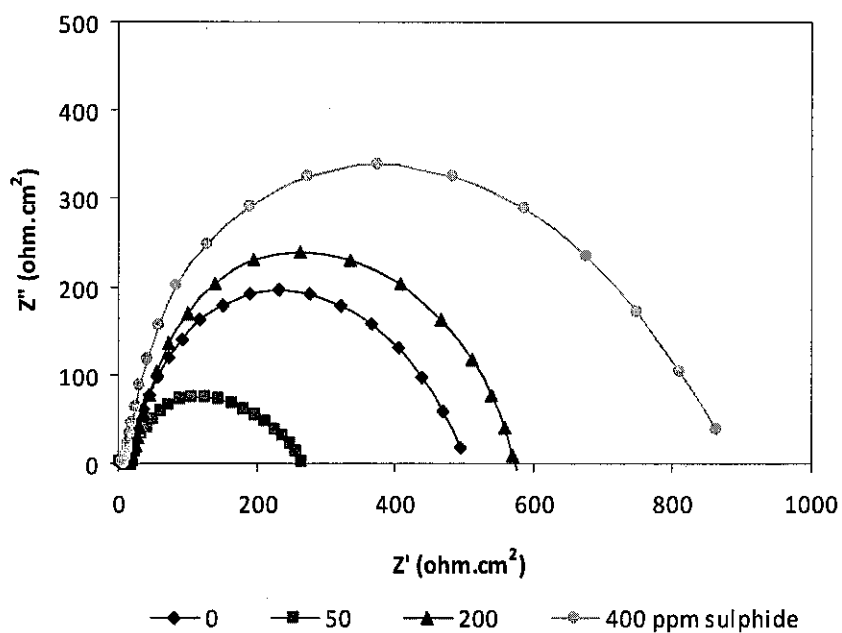


Figure 4.23 Impedance spectra, presented as Nyquist plot, showed the effect of sulphide concentration without the presence of sulphite in the simulated solution.

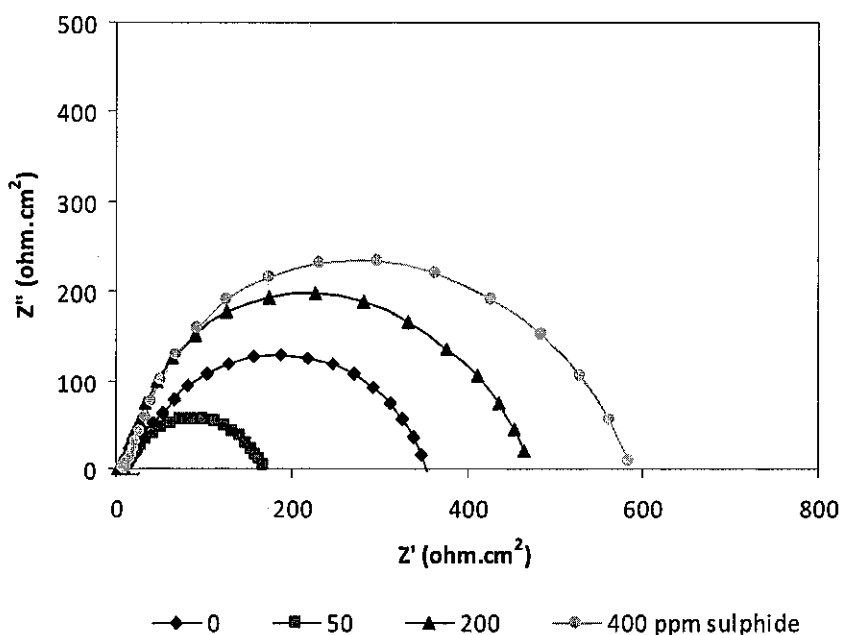


Figure 4.24 Impedance spectra, presented as Nyquist plot, showed the effect of sulphide concentration with the presence of 50 ppm sulphite in the simulated solution.

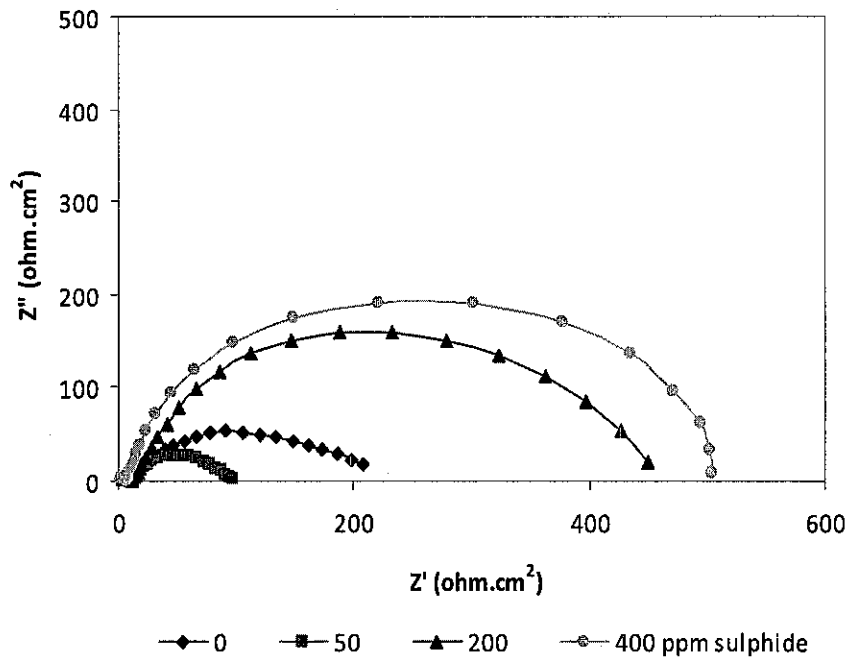


Figure 4.25 Impedance spectra, presented as Nyquist plot, showed the effect of sulphide concentration with the presence of 200 ppm sulphite in the simulated solution.

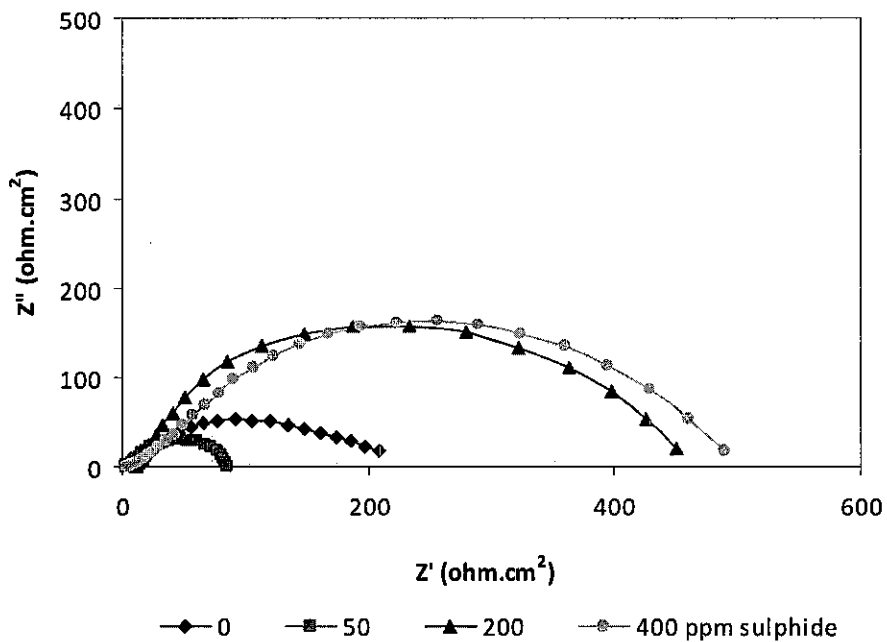


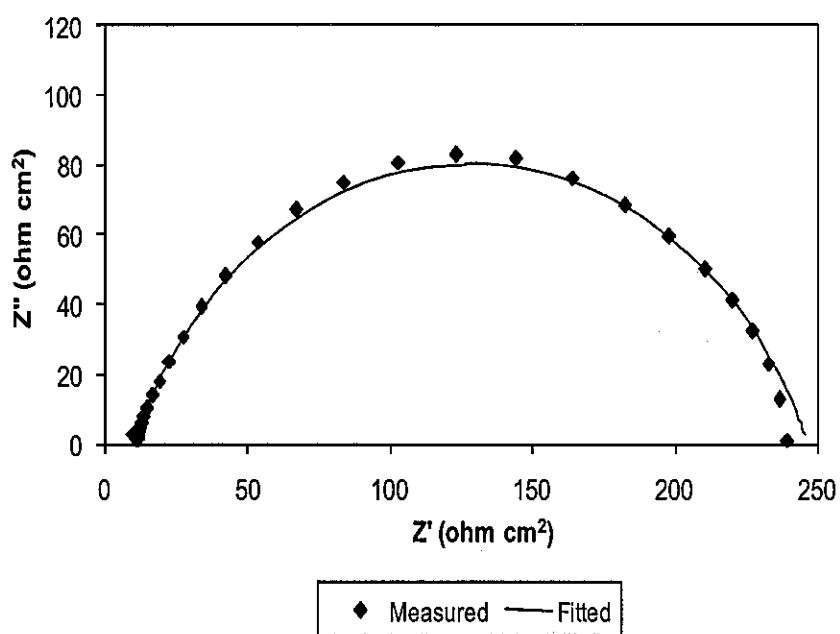
Figure 4.26 Impedance spectra, presented as Nyquist plot, showed the effect of sulphide concentration with the presence of 400 ppm sulphite in the simulated solution.

Table 4.5 Electrochemical impedance parameters fitted from the measured EIS data

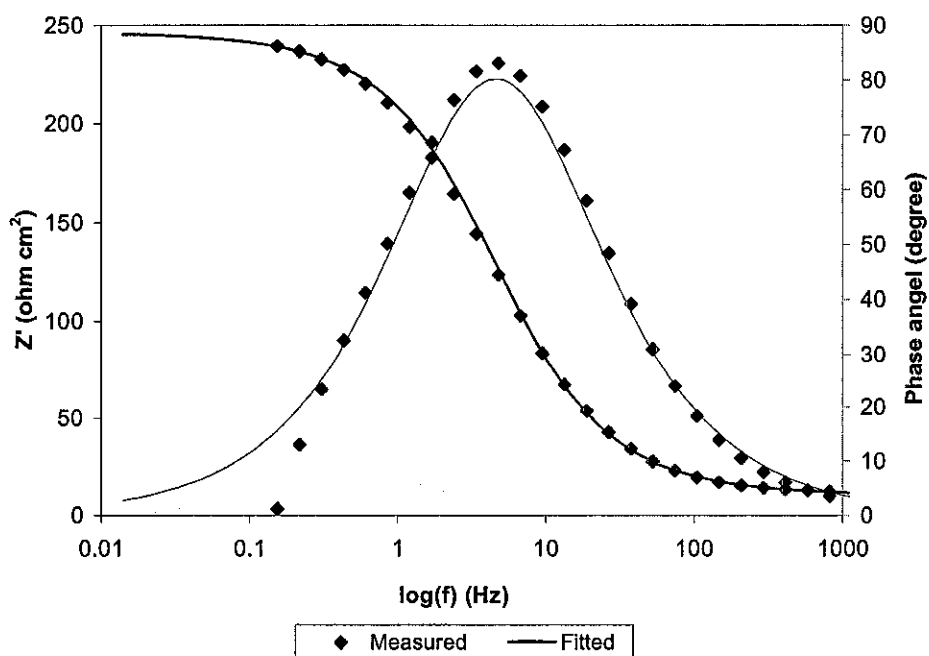
$C_{SO_3^{2-}}$ (ppm)	C_S^{2-} (ppm)	R_s ($\Omega.cm^2$)	R_t ($\Omega.cm^2$)	Parameter of CPE (P)	Coefficient of P (n)
0	0	4	494	0.03	0.73
	50	7	275	0.005	0.68
	200	15	560	0.0025	0.9
	400	8	850	0.0042	0.88
50	0	8	310	0.00082	0.8
	50	10	170	0.0018	0.78
	200	10	460	0.0048	0.9
	400	8	610	0.0039	0.9
200	0	7	230	0.0085	0.63
	50	8	118	0.0043	0.95
	200	8	512	0.0056	0.87
	400	8	580	0.0035	0.9
400	0	7	180	0.0087	0.68
	50	5	80	0.0018	0.83
	200	8	340	0.0047	0.96
	400	4	520	0.004	0.9

In summary, Nyquist plots show that the R_t value of 50 ppm sulphide concentration was smaller than 0 ppm sulphide concentration. However, with the addition of 200 and 400 ppm sulphide, the R_t value increased. It is indicated that with addition of 50 ppm sulphide, the rate of corrosion increased, and then it decreased when the solution was added with 200 and 400 ppm sulphide. These results have good agreement with LPR test. This trend was found in all sulphite and lactate concentration.

A typical fitting result is shown in Figure 4.27, where the EIS plots were measured on X52 steel in the presence of 200 ppm sulphite, 0 ppm lactate and 0 ppm sulphide. It is seen that the measured data and the fitted result matched very well.



(a)



(b)

Figure 4.27 Nyquist diagrams (a) and Bode plot (b) of X52 steel with the addition of 200 ppm sulphite (0 ppm lactate and 0 ppm sulphide) in the simulated solution. Comparison of experimental data with the fitted results.

b. Effect of Sulphite

The effect of sulphite concentration studied in various lactate and sulphide concentrations in the simulated solution are presented in sub chapters below (a-d).

b.1 Effect of Sulphite without the Presence of Lactate in Various Sulphide Concentrations in the Simulated Solution

Figure 4.28 to Figure 4.31 show the effect of sulphite on the corrosion rate of X52 steel under various sulphide concentrations in the simulated solution.

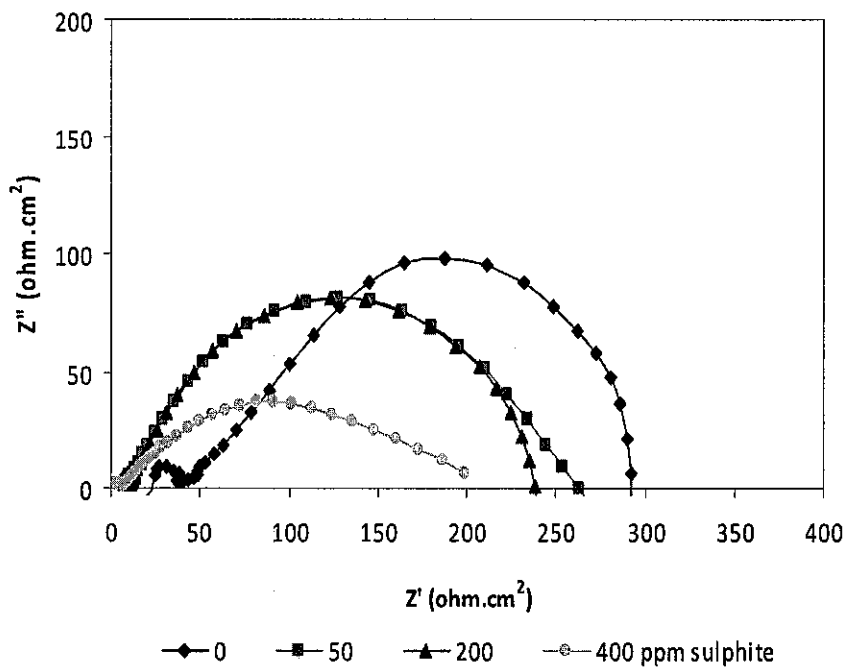


Figure 4.28 Impedance spectra, presented as Nyquist plot, showed the effect of sulphite concentration without the presence of sulphide in the simulated solution.

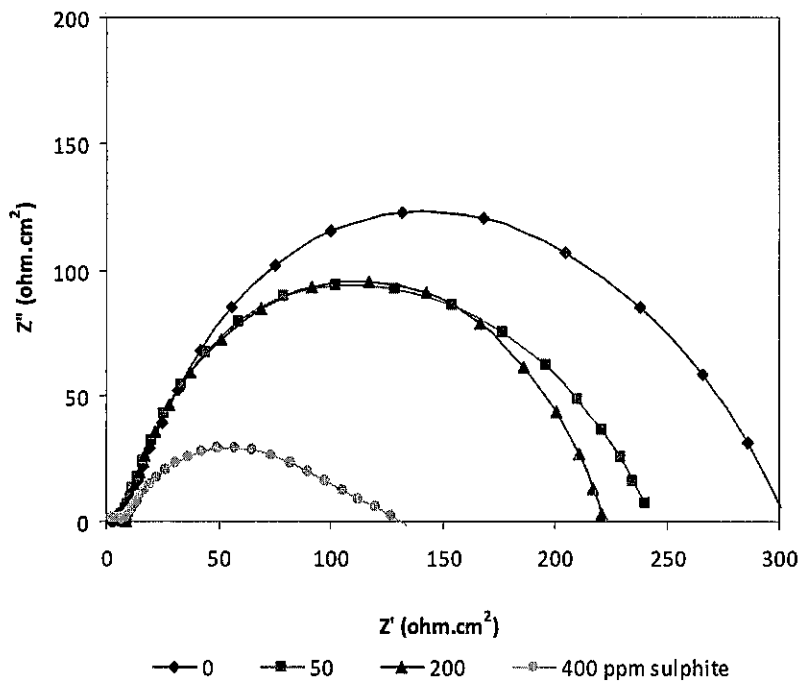


Figure 4.29 Impedance spectra, presented as Nyquist plot, showed the effect of sulphite concentration with the presence of 50 ppm sulphide in the simulated solution.

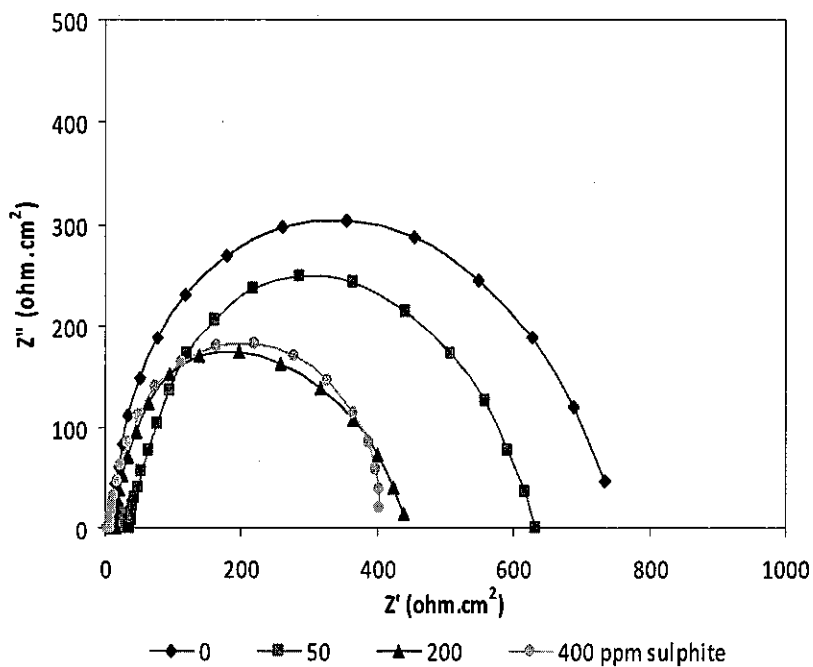


Figure 4.30 Impedance spectra, presented as Nyquist plot, showed the effect of sulphite concentration with the presence of 200 ppm sulphide in the simulated solution.

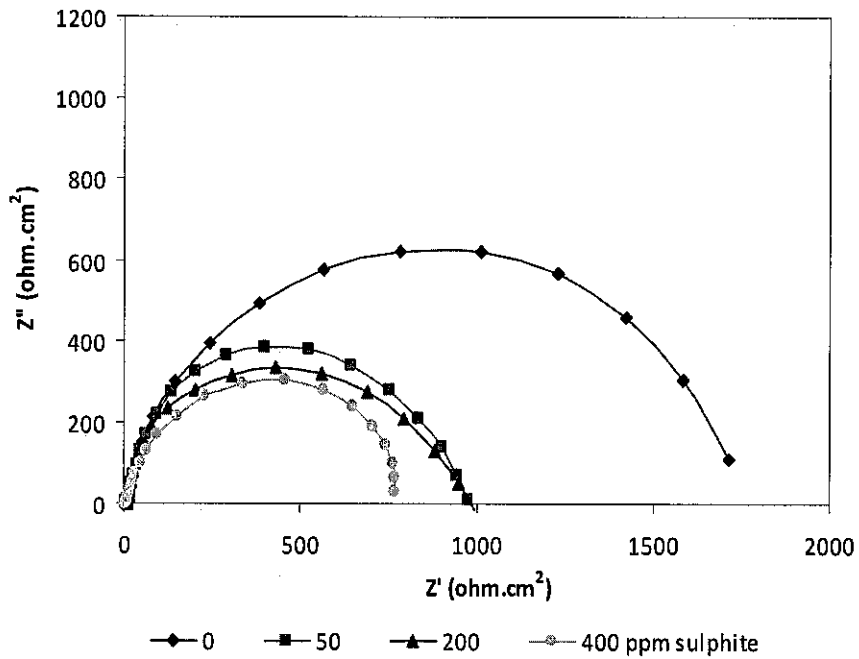


Figure 4.31 Impedance spectra, presented as Nyquist plot, showed the effect of sulphite concentration with the presence of 400 ppm sulphide in the simulated solution.

An equivalent circuit, as shown in Figure 3.4, was used to fit the measured impedance data. Table 4.6 shows the impedance parameters obtained by circuit fitting. It is observed that with the increase of sulphite concentration, the R_t value decreased. It indicated that with the increasing of sulphite concentration, the corrosion rate increased.

Table 4.6 Electrochemical impedance parameters fitted from the measured EIS data

C_S^{2-} (ppm)	$C_{SO_3^{2-}}$ (ppm)	R_s ($\Omega.cm^2$)	R_t ($\Omega.cm^2$)	Parameter of CPE (P)	Coefficient of P (n)
0	0	30.24	267	0.00052	0.63
	50	3	237	0.002	0.4
	200	10.19	236	0.0003	0.74
	400	5	210	0.0053	0.5
50	0	5.5	320	0.0035	0.9
	50	7.9	225	0.0049	0.9
	200	7.9	216	0.0032	0.9
	400	8.5	120	0.0057	0.63
200	0	4.5	720	0.0026	0.85
	50	18.5	630	0.0025	0.82
	200	11.3	450	0.0048	0.85
	400	5	418	0.0058	0.88
400	0	6.5	1700	0.002	0.8
	50	8.42	990	0.0023	0.88
	200	4	960	0.0036	0.9
	400	3.7	784	0.0037	0.89

b.2. Effect of Sulphite with the Presence 50 ppm Lactate and Various Sulphide Concentrations in the Simulated Solution

Figure 4.32 to Figure 4.35 show the effect of sulphite concentration with the presence of 50 ppm lactate under various sulphide concentrations in the simulated solution.

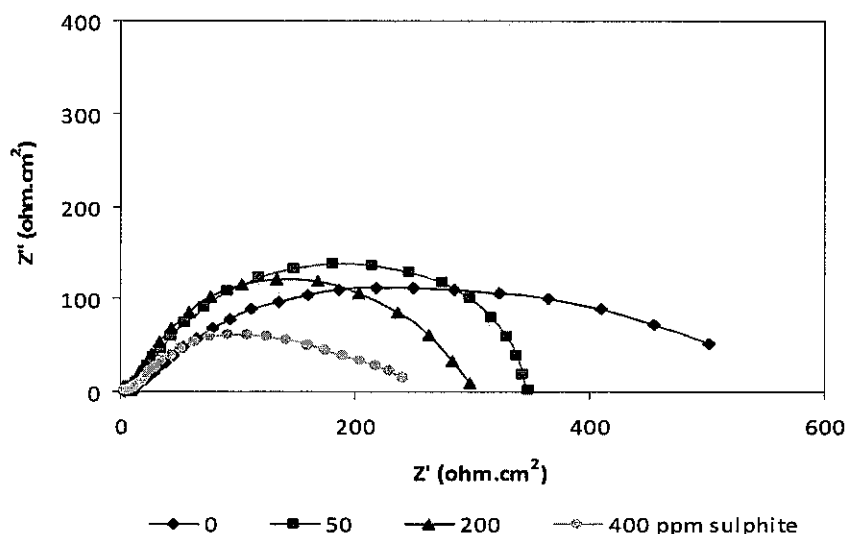


Figure 4.32 Impedance spectra, presented as Nyquist plot, showed the effect of sulphite concentration without the presence of sulphide in the simulated solution.

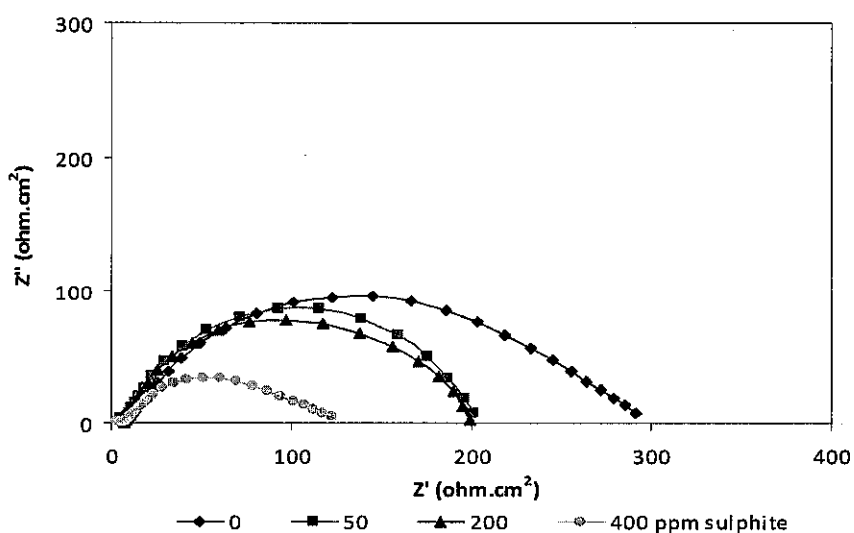


Figure 4.33 Impedance spectra, presented as Nyquist plot, showed the effect of sulphite concentration with the presence of 50 ppm sulphide in the simulated solution.

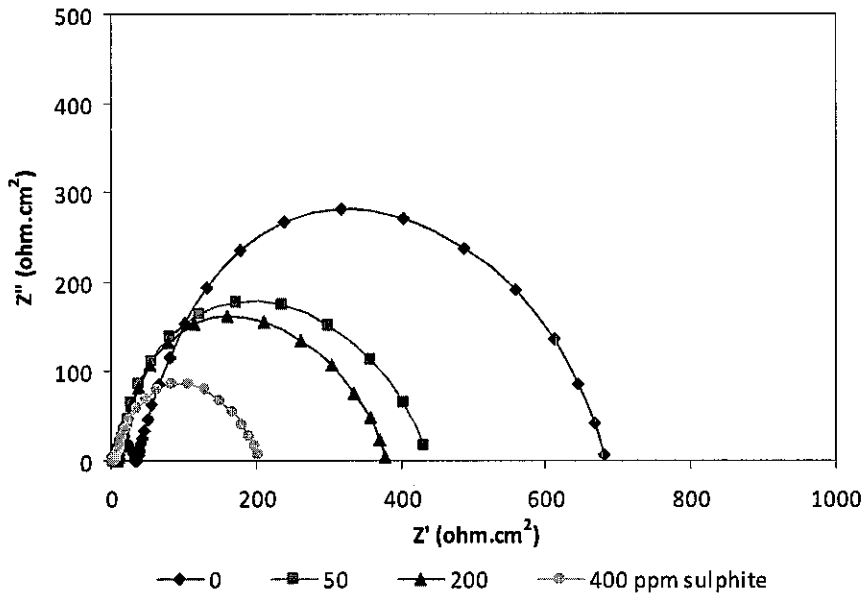


Figure 4.34 Impedance spectra, presented as Nyquist plot, showed the effect of sulphite concentration with the presence of 200 ppm sulphide in the simulated solution.

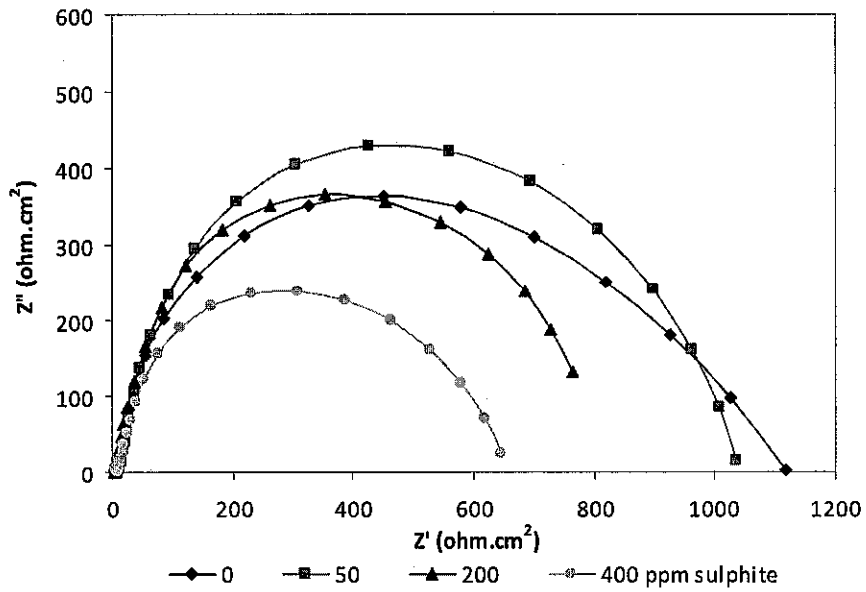


Figure 4.35 Impedance spectra, presented as Nyquist plot, showed the effect of sulphite concentration with the presence of 400 ppm sulphide in the simulated solution.

Table 4.7 shows the impedance parameters obtained by circuit fitting. It is seen that with the increase of sulphite concentration, the R_t value decreased. This behaviour was similar in the simulated solution without the addition of lactate (0 ppm).

Table 4.7 Electrochemical impedance parameters fitted from the measured EIS data

C_S^{2-} (ppm)	$C_{SO_3^{2-}}$ (ppm)	R_s ($\Omega.cm^2$)	R_t ($\Omega.cm^2$)	Parameter of CPE (P)	Coefficient of P (n)
0	0	4.4	510	0.0034	0.62
	50	9.4	350	0.00046	0.86
	200	3.2	318	0.003	0.87
	400	5.5	240	0.005	0.63
50	0	6.9	285	0.002	0.74
	50	7.3	205	0.0032	0.86
	200	8.2	195	0.006	0.88
	400	8	125	0.01	0.7
200	0	25	693	0.0025	0.86
	50	9.9	420	0.0025	0.88
	200	5	365	0.004	0.92
	400	5	205	0.0048	0.93
400	0	4.9	1300	0.0037	0.79
	50	5.02	1080	0.0025	0.88
	200	5.02	800	0.0025	0.94
	400	5.02	680	0.0034	0.81

b.3. Effect of Sulphite with the Presence 200 ppm Lactate and Various Sulphide Concentrations in the Solution

Figure 4.36 to Figure 4.39 showed the effect of sulphite with the presence 400 ppm lactate under various sulphide concentrations in the simulated solution.

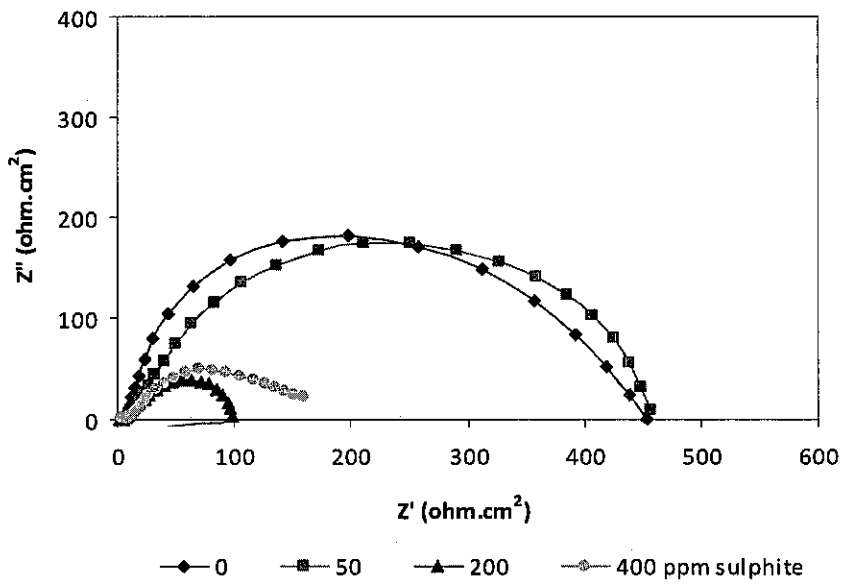


Figure 4.36 Impedance spectra, presented as Nyquist plot, showed the effect of sulphite concentration without the presence of sulphide in the simulated solution.

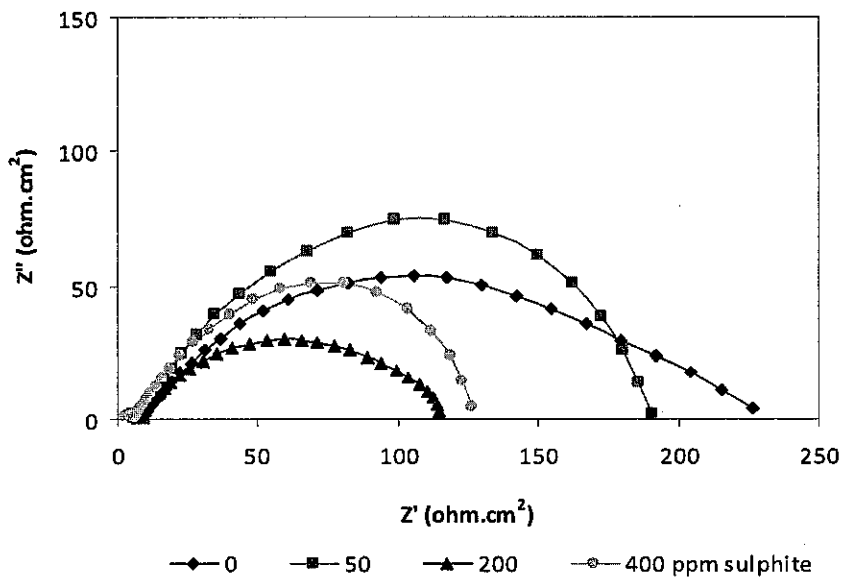


Figure 4.37 Impedance spectra, presented as Nyquist plot, showed the effect of sulphite concentration with the presence of 50 ppm sulphide in the simulated solution.

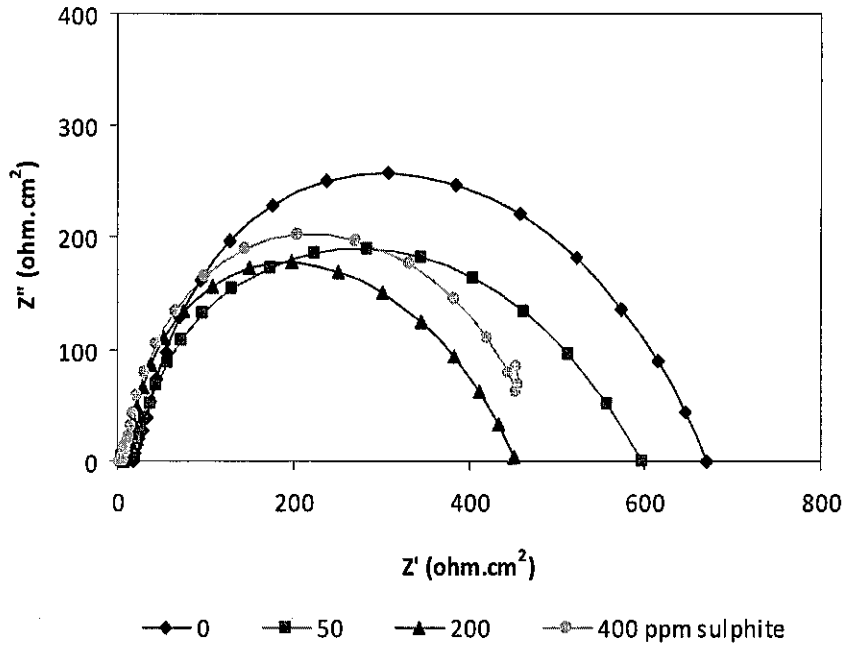


Figure 4.38 Impedance spectra, presented as Nyquist plot, showed the effect of sulphite concentration with the presence of 200 ppm sulphide in the simulated solution.

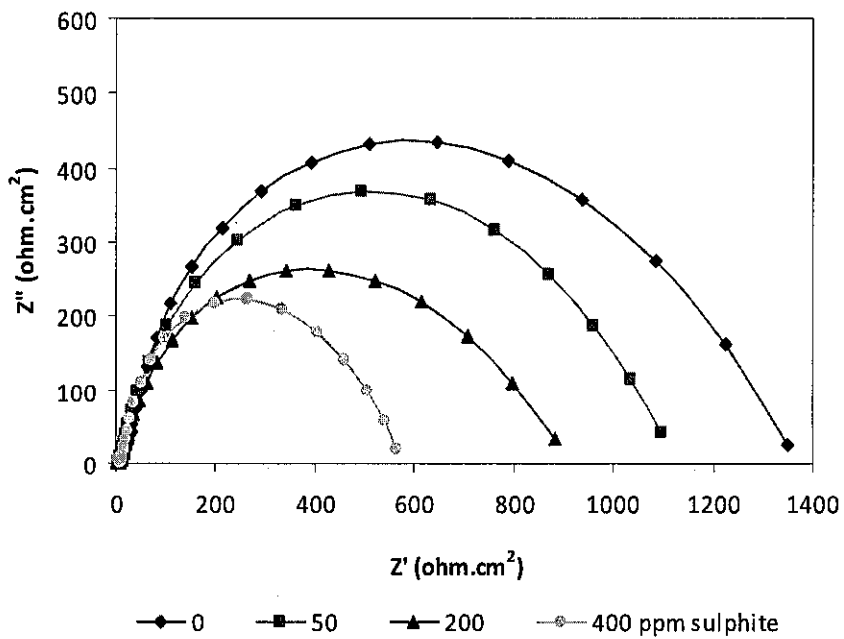


Figure 4.39 Impedance spectra, presented as Nyquist plot, showed the effect of sulphite concentration with the presence of 400 ppm sulphide in the simulated solution.

Table 4.8 shows the impedance parameters obtained by circuit fitting. It is seen that with the increase of sulphite concentration, the R_t value decreased. It indicated that with the increasing of sulphite concentration, the corrosion rate increased. This trend is true in solution with or without the presence of sulphide.

Table 4.8 Electrochemical impedance parameters fitted from the measured EIS data

C_S^{2-} (ppm)	$C_{SO_3^{2-}}$ (ppm)	R_s ($\Omega.cm^2$)	R_t ($\Omega.cm^2$)	Parameter of CPE (P)	Coefficient of P (n)
0	0	3	439	0.003	0.82
	50	10.1	134	0.00022	0.87
	200	8	350	0.0053	0.6
	400	8	220	0.0078	0.6
50	0	8	230	0.0035	0.6
	50	8	190	0.00075	0.83
	200	8	112	0.0042	0.65
	400	5.2	120	0.0008	0.95
200	0	6	640	0.003	0.88
	50	6	640	0.0036	0.96
	200	6	440	0.0037	0.96
	400	6	455	0.0042	0.96
400	0	6	1350	0.0037	0.76
	50	6	1400	0.0035	0.75
	200	6	880	0.0035	880
	400	6	600	0.0035	0.83

b.4. Effect of Sulphite with the Presence 400 ppm Lactate and Various Sulphide Concentrations in the Simulated Solution

Figure 4.40 to Figure 4.43 showed the effect of sulphite with the presence 400 ppm lactate under various sulphide concentrations in the solution.

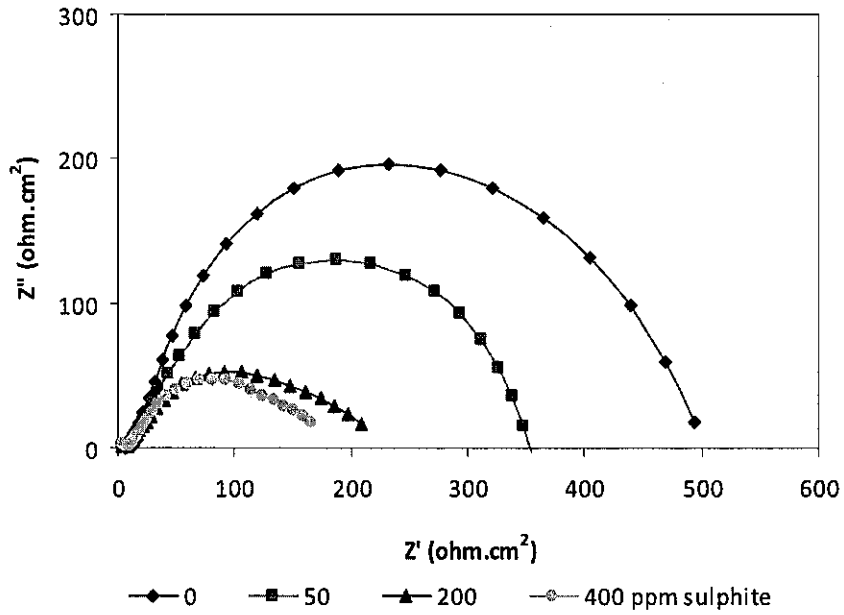


Figure 4.40 Impedance spectra, presented as Nyquist plot, showed the effect of sulphite concentration without the presence of sulphide in the simulated solution.

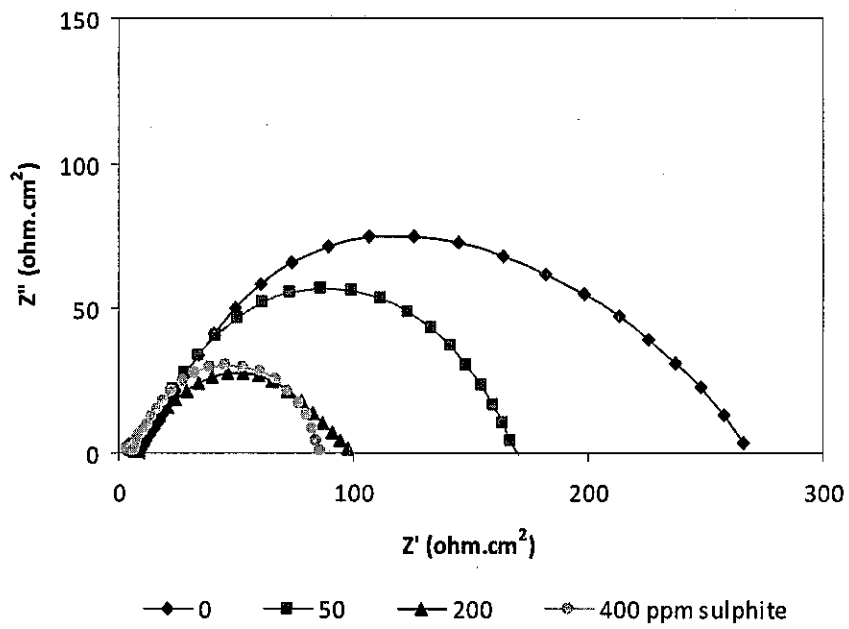


Figure 4.41 Impedance spectra, presented as Nyquist plot, showed the effect of sulphite concentration with the presence of 50 ppm sulphide in the simulated solution.

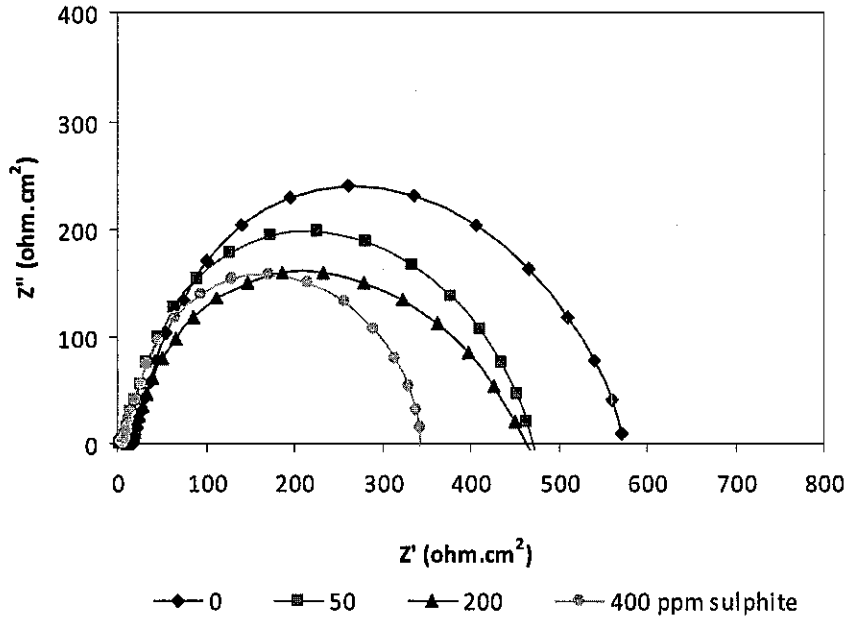


Figure 4.42 Impedance spectra, presented as Nyquist plot, showed the effect of sulphite concentration with the presence of 200 ppm sulphide in the simulated solution.

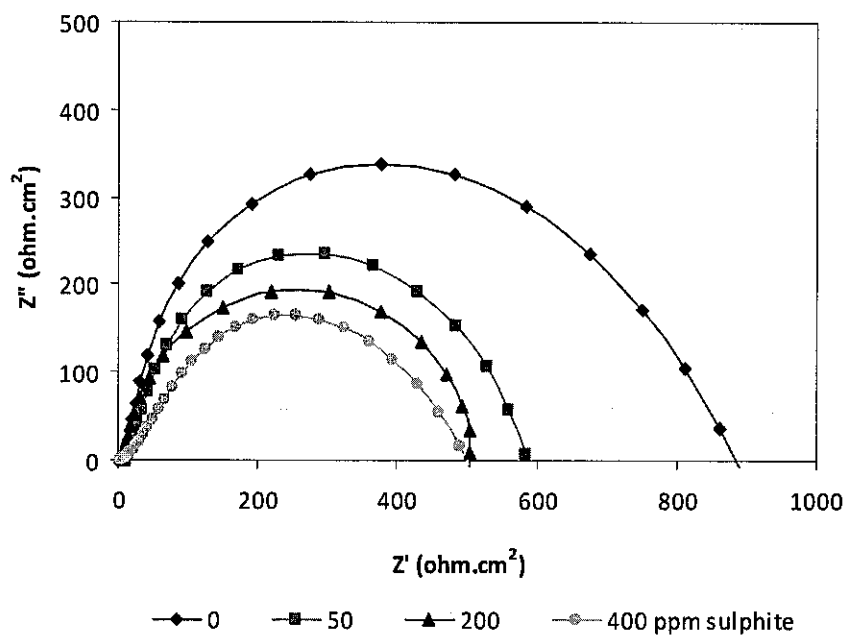


Figure 4.43 Impedance spectra, presented as Nyquist plot, showed the effect of sulphite concentration with the presence of 400 ppm sulphide in the simulated solution.

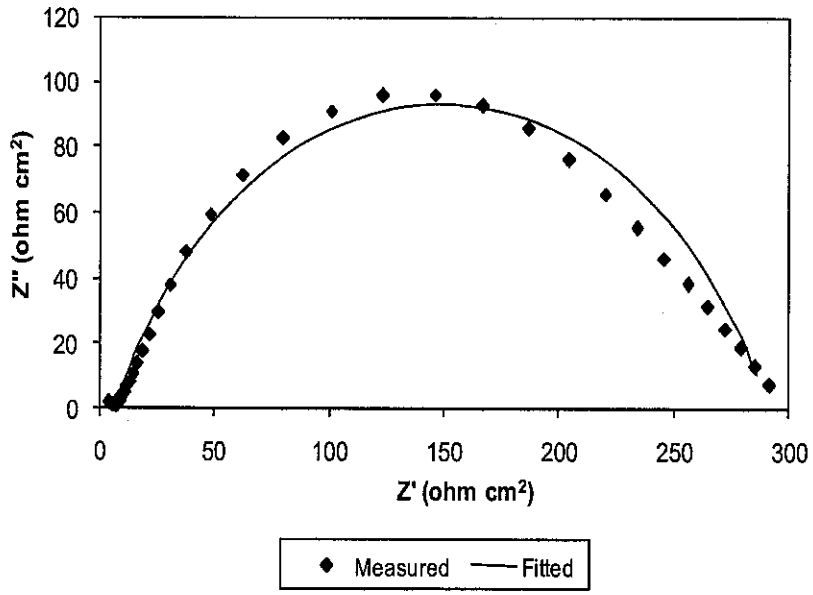
Table 4.9 shows the impedance parameters obtained by circuit fitting. It is seen that the presence of 400 ppm lactate, did not change the behaviour of R_t value. With the increasing of sulphite concentration, the R_t value decreased. This trend is true in solution with or without the presence of sulphide.

Table 4.9 Electrochemical impedance parameters fitted from the measured EIS data

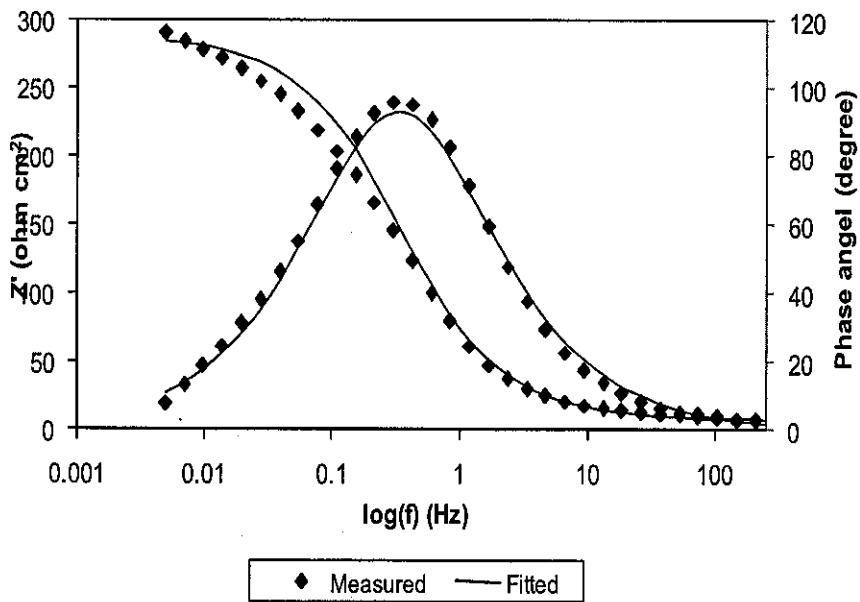
$C_{S^{2-}}$ (ppm)	$C_{SO_3^{2-}}$ (ppm)	R_s ($\Omega.cm^2$)	R_t ($\Omega.cm^2$)	Parameter of CPE (P)	Coefficient of P (n)
0	0	4	494	0.003	0.73
	50	8	310	0.00082	0.8
	200	7	230	0.0085	0.63
	400	7	180	0.0087	0.68
50	0	7	275	0.005	0.68
	50	10	170	0.0018	0.78
	200	8	118	0.0043	0.95
	400	5	80	0.0018	0.83
200	0	15	560	0.0025	0.9
	50	10	460	0.0048	0.9
	200	8	512	0.0056	0.87
	400	8	340	0.0047	0.96
400	0	8	850	0.0042	0.88
	50	8	610	0.0039	0.9
	200	8	580	0.0035	0.9
	400	4	520	0.004	0.9

In summary, under various lactate and sulphide concentrations presence in the solution, the addition of sulphite increased the R_t value. It is indicated that with addition of sulphide, the rate of X52 corrosion increased. These results have a good agreement with LPR tests which also show an increasing of corrosion rate with the increase of sulphite concentration.

A typical fitting result is shown in Figure 4.44, where the EIS plots were measured on X52 steel in the presence of 0 ppm sulphite, 50 ppm lactate and 50 ppm sulphide in the simulated solution. It is seen that the measured data and the fitted result matched very well.



(a)



(b)

Figure 4.44 Nyquist diagrams (a) and Bode plot (b) of X52 steel with the addition of 50 ppm lactate and 50 ppm sulphide (0 ppm sulphite) in the simulated solution. Comparison of experimental data with the fitted results.

4.1.2.3 Tafel Polarization

Because of its destructive characteristic, polarization tests were conducted only in selected environments. Figure 4.45 shows the polarization curves of the effect of sulphide with the presence of 200 ppm sulphite and 50 ppm lactate in the simulated solution.

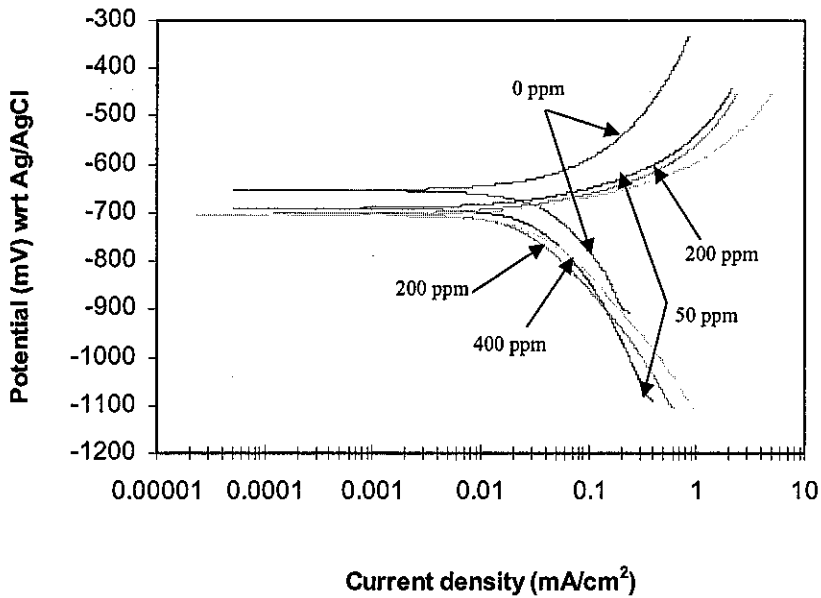


Figure 4.45 Polarization curve of X52 steel with various sulphide concentrations in the presence of 50 ppm lactate and 200 ppm sulphite in the simulated solution.

The electrochemical parameters *e.g.* corrosion potential (E_{corr}); corrosion current density (i_{corr}); and anodic and cathodic Tafel slopes (b_a and b_c), were obtained by performing a least square fit of the measured polarized data, as shown in Table 4.10. It is evident from Table 4.10 that the addition of 50 ppm sulphide increased the corrosion current (i_{corr}). However, with addition of 200 and 400 ppm sulphide, the corrosion current decreased. It indicates that the corrosion rate of X52 steel increased with addition 50 ppm sulphide and decreased with addition of 200 and 400 ppm sulphide. Additionally, it is observed that the increasing of corrosion current (i_{corr}) is followed by the increasing of cathodic Tafel slope (b_c). It indicates that the increasing of corrosion current is due to the increasing of cathodic reaction with the addition of 50 ppm sulphide. Furthermore, with the addition of 200 and 400 ppm sulphide, it is

observed a decreasing of cathodic Tafel slope (b_c). The decreasing of cathodic Tafel slope is related to the decreasing of corrosive species that adsorb on the surface which is influenced by the film thickness.

Table 4.10 Electrochemical parameters fitted from polarization curves.

Sulphide ion concentration (ppm)	E_{corr} (mV, Ag/AgCl)	i_{corr} (mA/cm ²)	b_a (mV/dec)	b_c (mV/dec)
0	-653	0.064	251	401
50	-691	0.074	150	404
200	-703	0.06	136	226
400	-691	0.049	99	189

Figure 4.46 shows the polarization curves of the effect of sulphite with the presence of 200 ppm sulphite and 50 ppm lactate in the simulated solution. The electrochemical parameters *e.g.* corrosion potential (E_{corr}); corrosion current density (i_{corr}); and anodic and cathodic Tafel slopes (b_a and b_c), were obtained by performing a least square fit of the measured polarized data, as shown in Table 4.11. It is evident from Table 4.11 that the addition of sulphite increased the corrosion current (i_{corr}). The extent of increase in i_{corr} is found to be a function of sulphite concentration, the higher sulphite concentration, the larger the increase in i_{corr} values. Additionally, it is observed that the increasing of corrosion current (i_{corr}) is followed by the increasing of cathodic Tafel slope (b_c). It indicates that the increasing of corrosion current is due to the increasing of cathodic reaction with the addition of sulphite concentrations.

Table 4.11 Electrochemical parameters fitted from polarization curves

Sulphite ion concentration (ppm)	E_{corr} (mV, Ag/AgCl)	I_{corr} (mA/cm ²)	b_a (mV/dec)	b_c (mV/dec)
0	-703	0.02	52	193
50	-689	0.05	63	194
200	-698	0.06	136	226
400	-690	0.065	101	263

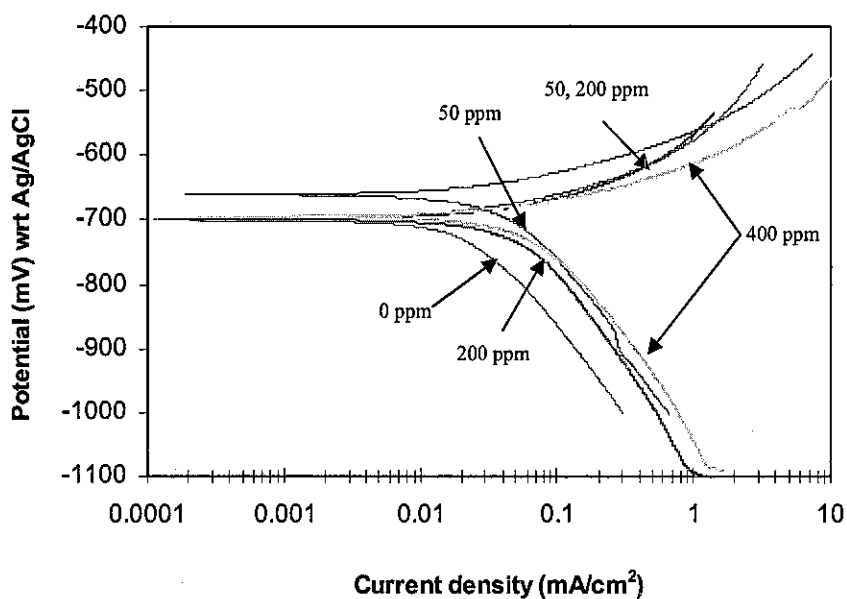


Figure 4.46 Polarization curve of X52 steel with various sulphite concentrations in the presence of 50 ppm lactate and 200 ppm sulphide in the simulated solution.

4.2 Surface morphology and corrosion prediction

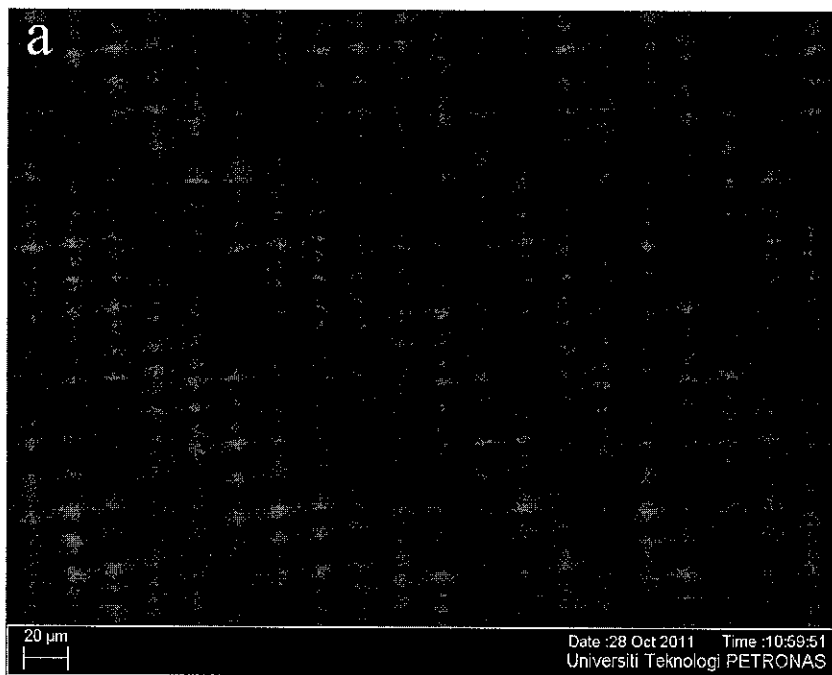
This sub chapter presents the results and discussions of surface morphology and film characterization of X52 steel in the simulated solution containing SRB metabolic products. FESEM, EDAX and XPS techniques were employed to study the surface morphology and to characterize the film on the steel surface. Additionally, this chapter also describes the corrosion mechanism that developed based on LPR, TP, EIS and surface morphology results observation. A development of prediction equation was also described in this sub chapter.

4.2.1 FESEM and EDAX analysis

The corrosion morphology and elemental analysis of X52 steel and the effect of sulphide and sulphite on X52 steel in the simulated solution containing SRB metabolic products are presented below.

4.2.1.1 X52 steel

Surface morphology and elemental analysis of bare X52 steel are shown in Figure 4.47 below. The elemental composition of X52 steel is shown in Table 4.12 which shows comparable results with work by Wang *et al* [95].



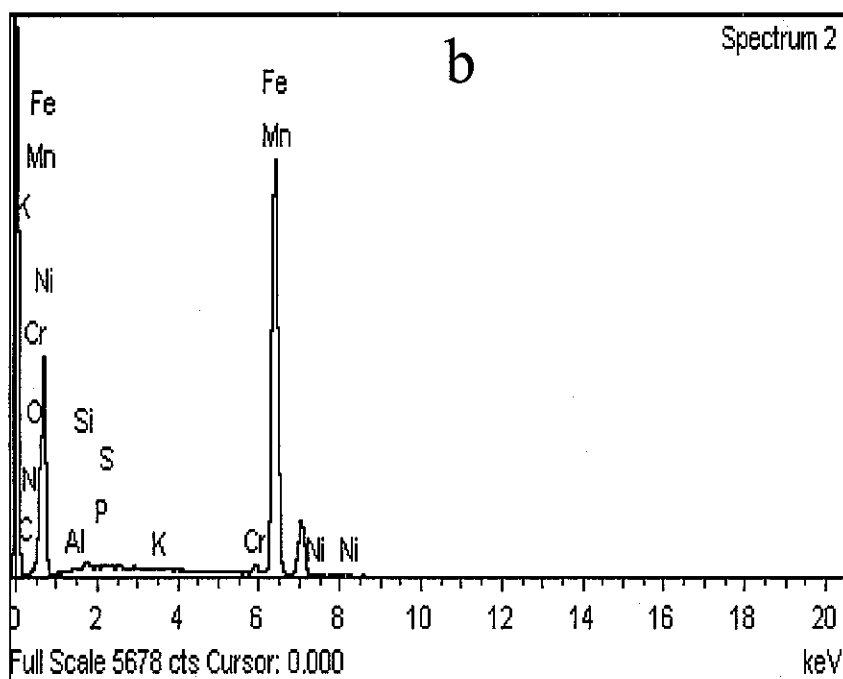


Figure 4.47 (a) Surface morphology of bare X52 steel; (b) EDX results.

Table 4.12 Elemental composition of X52 steel (in wt%)

Elements	Wt%	Elements	Wt%
Carbon (C)	0.16	Nickel (Ni)	0.37
Manganese (Mn)	1.36	Aluminium (Al)	0.07
Phosphorus (P)	0.01	Oxygen (O)	0.48
Silicon (Si)	0.47	Iron (Fe)	Balance
Chromium (Cr)	0.14		

4.2.1.2 Effect of sulphide

Figure 4.48 to Figure 4.52 show surface morphology (face view) and EDAX results of the effect of sulphide on X52 steel with the presence of 200 ppm sulphite and 50 ppm lactate in the simulated solution.

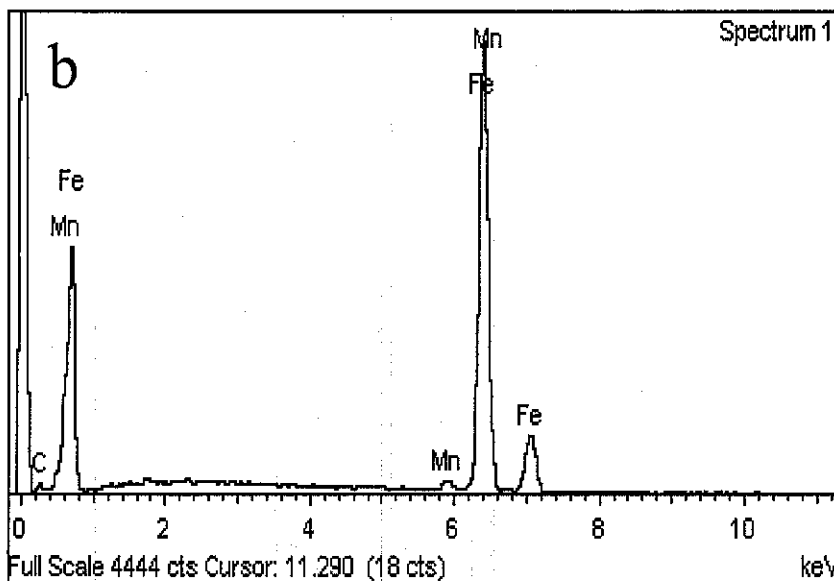


Figure 4.48 (a) Surface morphology (face view) of X52 steel in the simulated solution with the addition of 200 ppm sulphite and 50 ppm lactate without the presence of sulphide (0 ppm); (b) EDAX results.

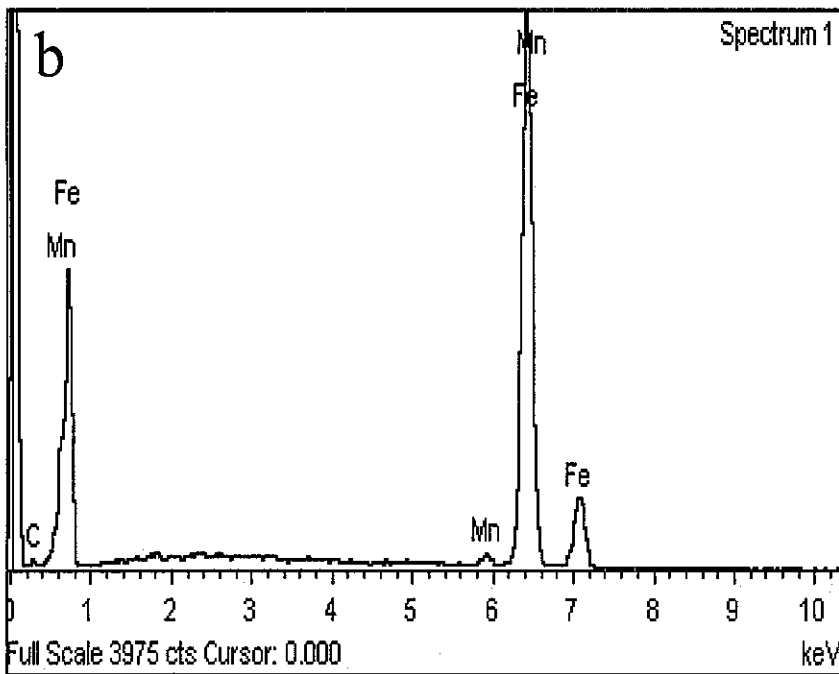
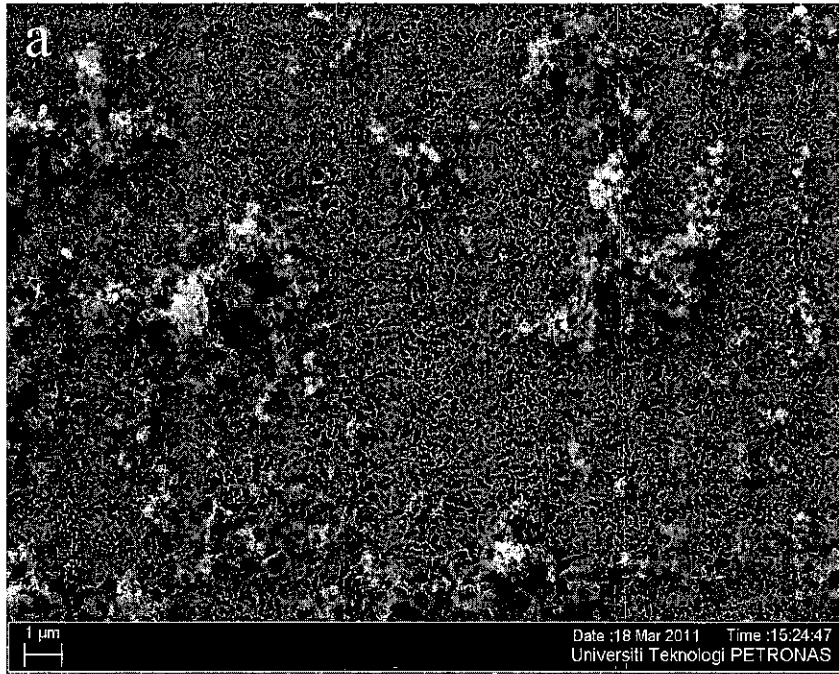


Figure 4.49 (a) Surface morphology (face view) of X52 steel in the simulated solution with the addition of 50 ppm sulphide, 200 ppm sulphite and 50 ppm lactate; (b) EDAX results.

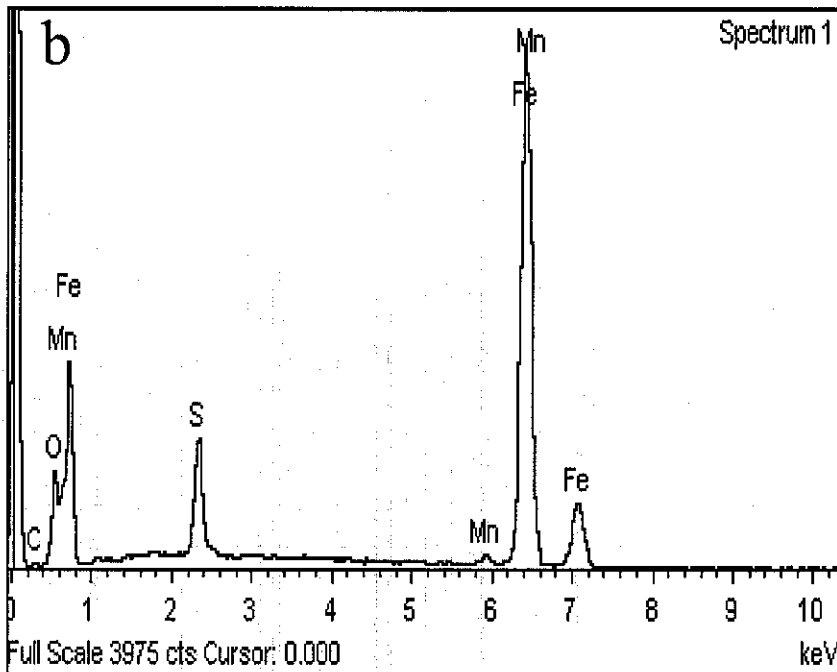
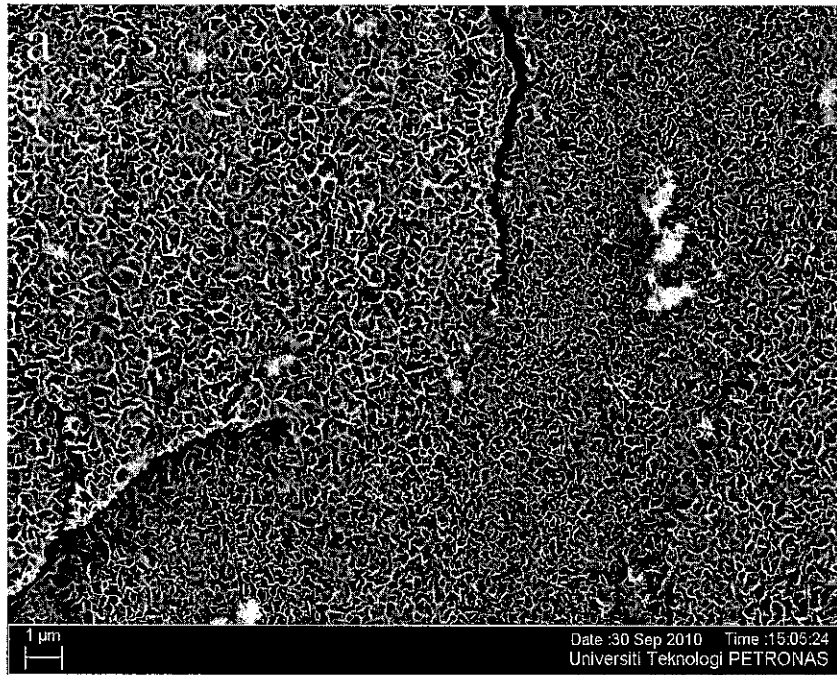
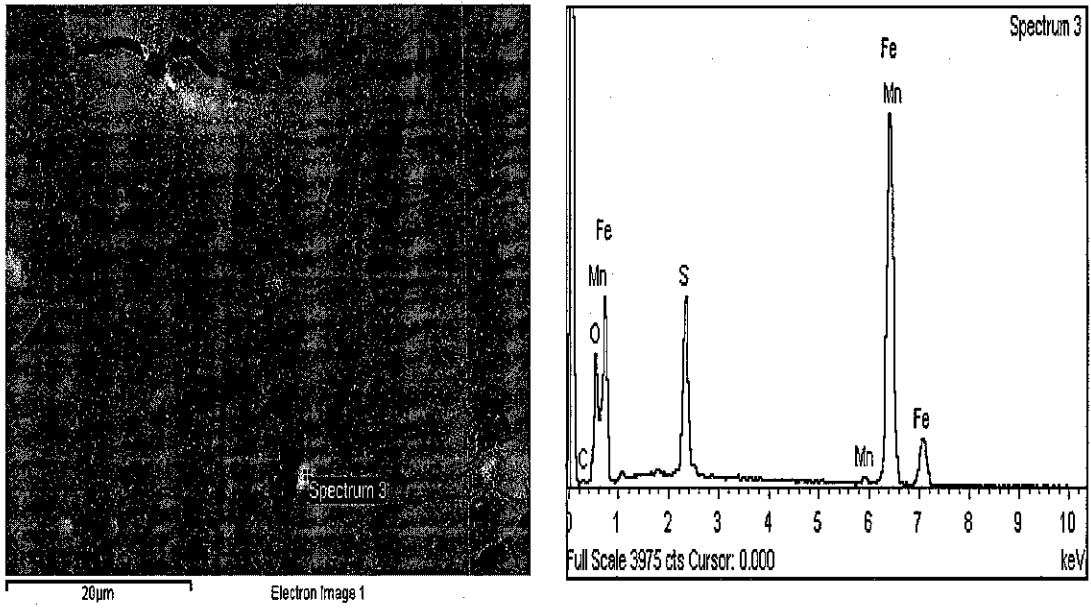
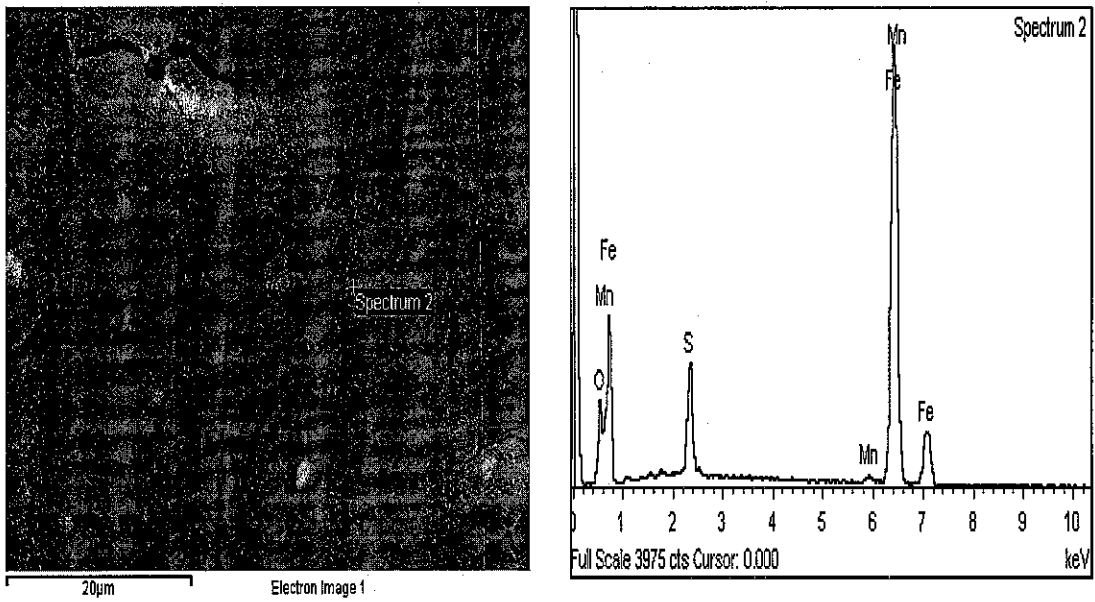


Figure 4.50 (a) Surface morphology (face view) of X52 steel in the simulated solution with the addition of 200 ppm sulphide, 200 ppm sulphite and 50 ppm lactate; (b) EDAX results.



(a)



(b)

Figure 4.51 Elemental film analysis by EDX (a) C element on the grain (b) S element on the film scale.

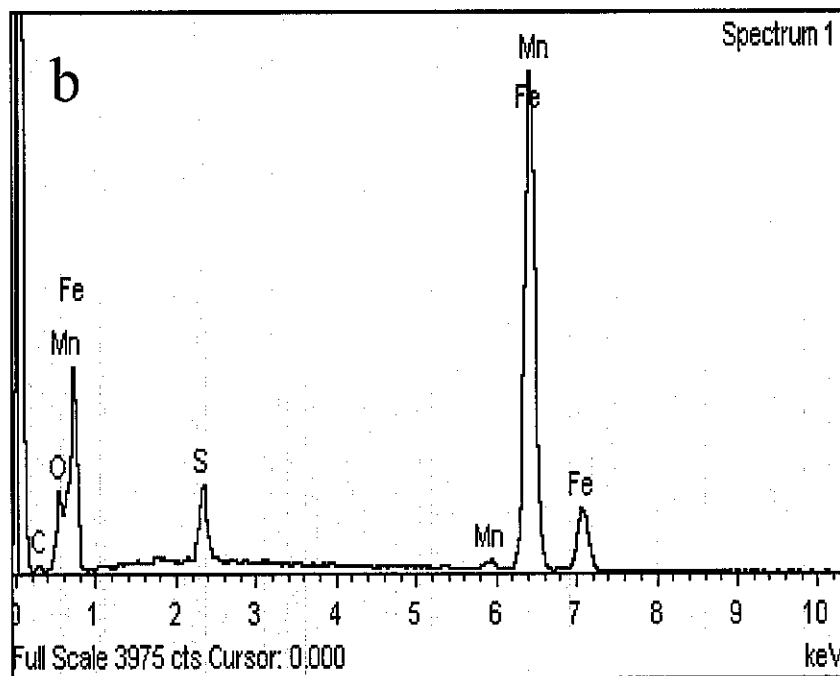
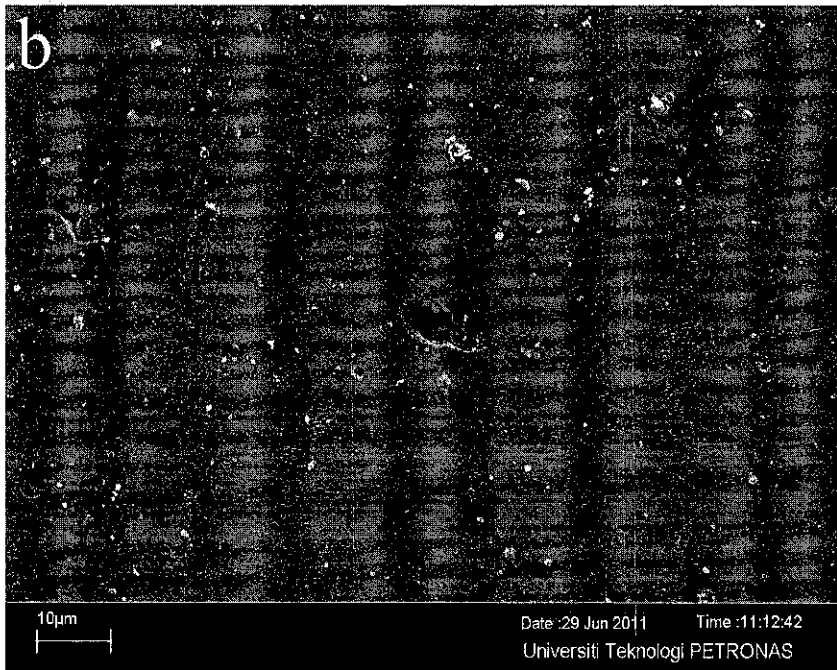
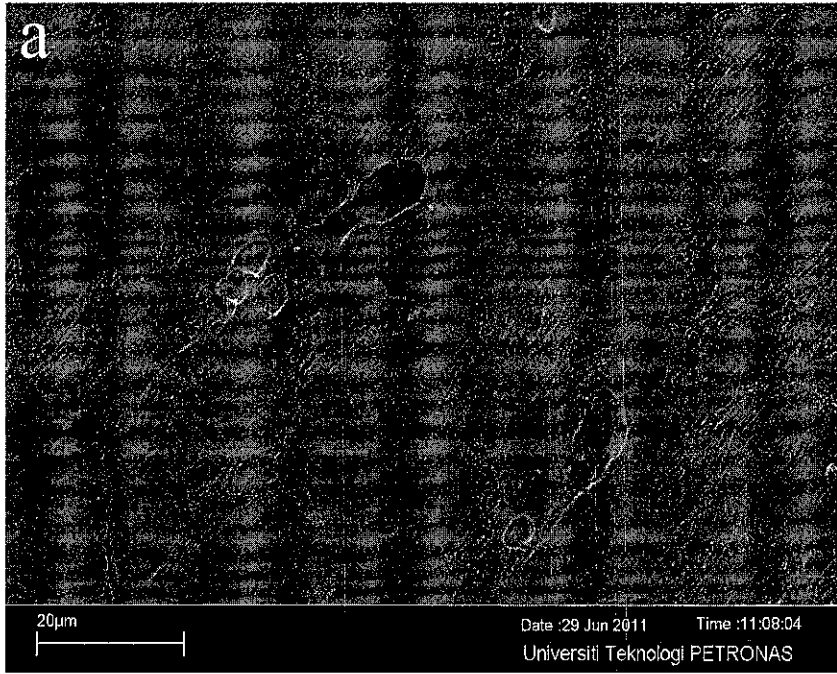


Figure 4.52 (a) Surface morphology (face view) of X52 steel in the simulated solution with the addition of 400 ppm sulphide, 200 ppm sulphite and 50 ppm lactate; (b) EDAX results.



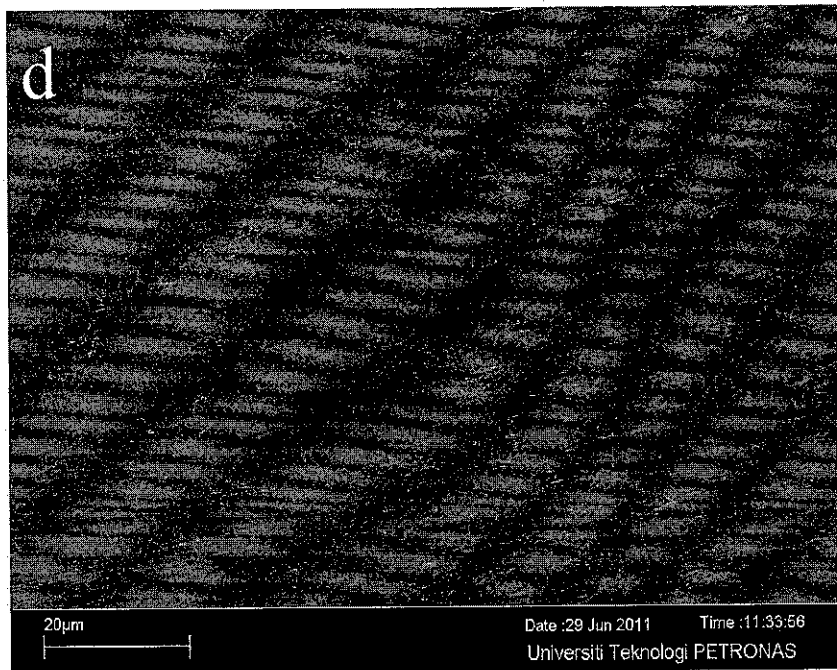
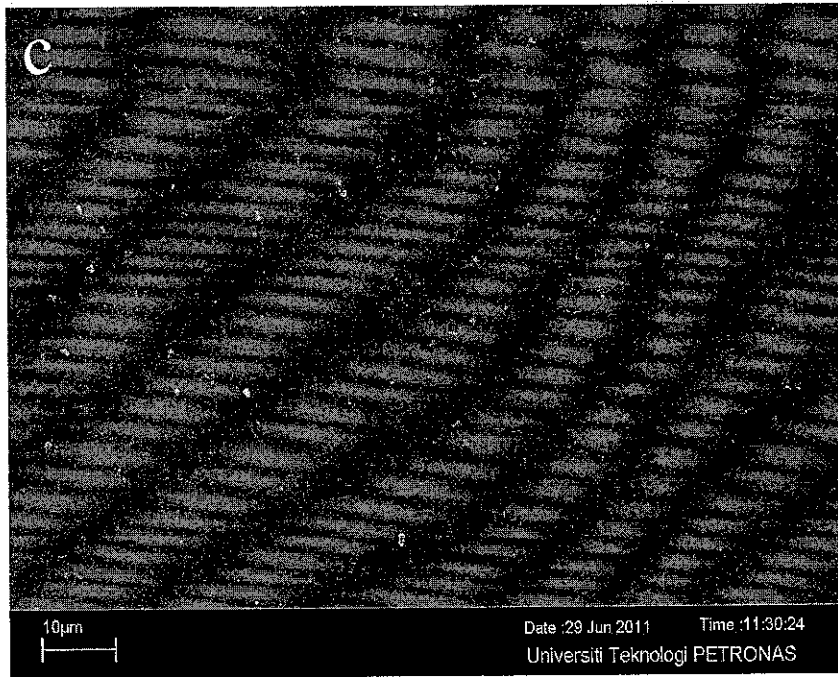


Figure 4.53 Surface morphology of X52 steel after corrosion product removal in the simulated solution with the addition of 200 ppm sulphite and 50 ppm lactate in various sulphide concentrations (a) 0 ppm; (b) 50 ppm; (c) 200 ppm; (d) 400 ppm.

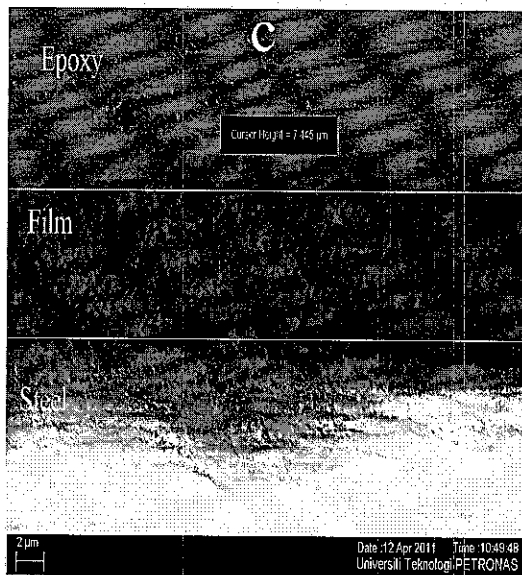
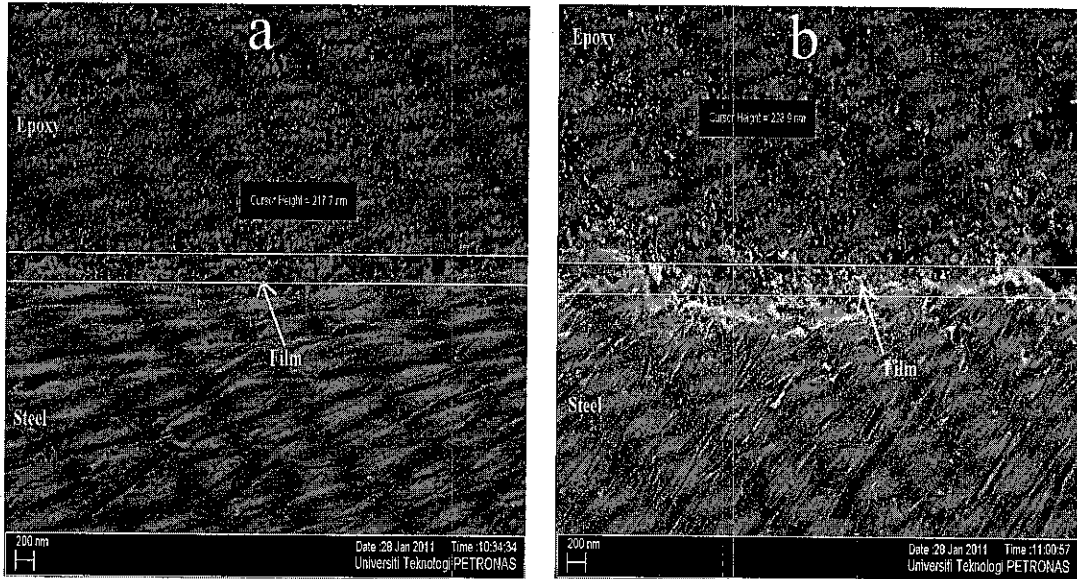


Figure 4.54 Surface morphology (cross view) of X52 steel in the simulated solution with the addition of 200 ppm sulphite and 50 ppm lactate in various sulphide concentrations (a) 0 ppm; (b) 50 ppm; (c) 400 ppm.

As shown in

Figure 4.48, a flat and compact film was observed in sulphide free solution. With the addition of sulphide to the simulated solution, the film formed became more compact. The FeS film (in fragmented form) is appeared to be more visible in high sulphide concentration (200 and 400 ppm) as shown in Figure 4.50 and Figure 4.52. It might be related to the high concentration of sulphide.

In 50 ppm solution containing sulphide, a small crystal grains were observed on the film scale (Figure 4.49). However, its number decreased with increasing sulphide concentrations. It is suspected that the small crystal grain is FeCO₃ film. This assumption is confirmed by EDAX results which detected C element in the crystal grain as shown in Figure 4.51. In high concentration of sulphide (200 and 400 ppm), FeS film is likely to form than FeCO₃ film.

After removing the corrosion products on the X52 steel surface, pitting corrosion were observed in sulphide free solution and 50 ppm sulphide added to the solution (Figure 4.53 a and b). However, with the addition of 200 and 400 ppm sulphide, no pitting was observed on the surface (Figure 4.53 c and d).

As shown in Figure 4.54, cross sectional view results show that there is not much difference in the film thickness with the sulphide concentration range between 0 ppm and 50 ppm sulphide. The film thickness is around 220 nm. However, with addition of 400 ppm sulphide, the film thickness increased significantly to 7.45 μm (Figure 4.54 c). The significant increase of film thickness caused a better protection to the corrosion (general and pitting corrosion). This result is in good agreement with electrochemical studies which showed a decreasing of corrosion rate with the presence of 400 ppm sulphide.

4.2.1.3 *Effect of sulphite*

Figure 4.55 to Figure 4.60 show surface morphology (face view) and EDAX results of X52 steel in the simulated solution with the addition of 200 ppm sulphide and 50 ppm lactate in various sulphite concentrations.

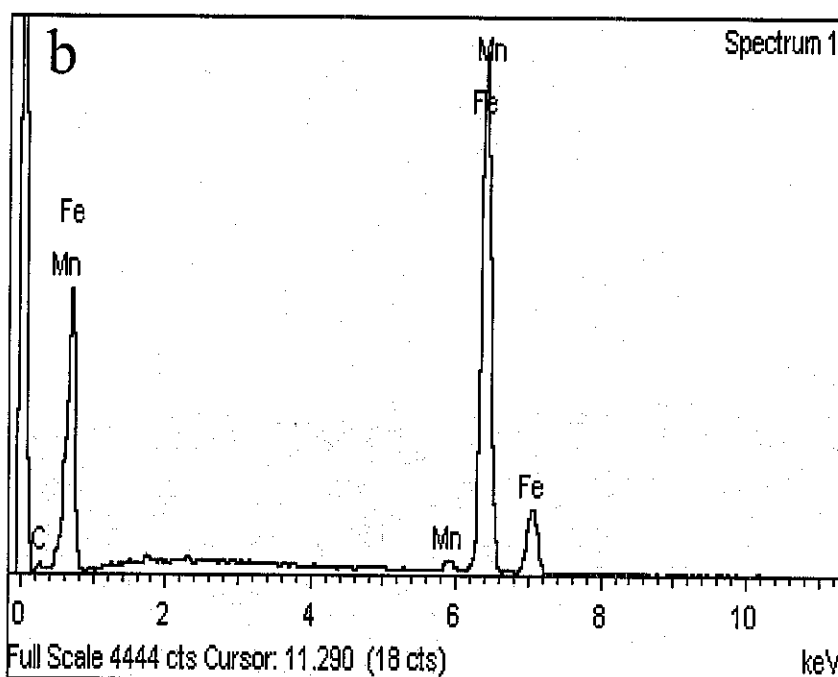
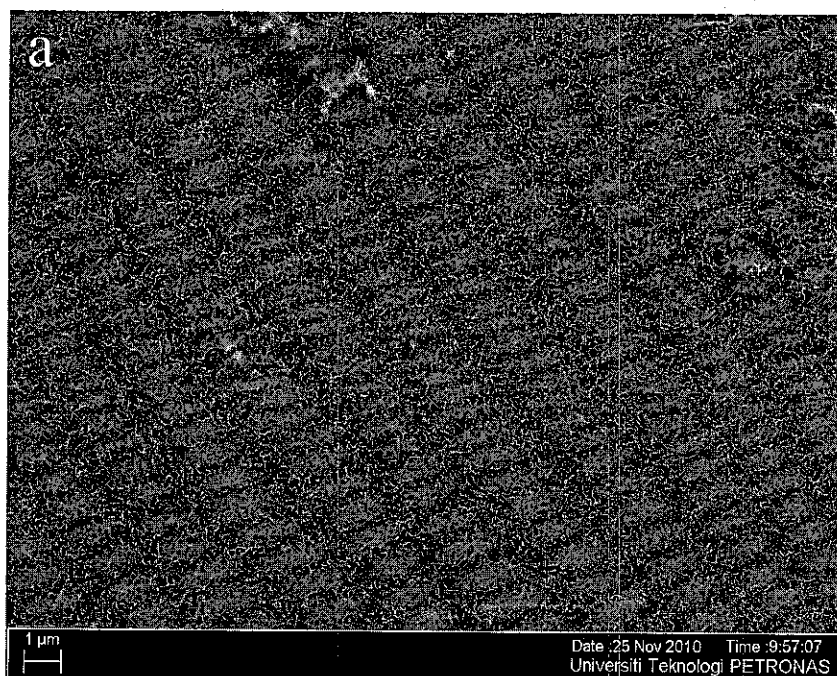


Figure 4.55 (a) Surface morphology (face view) of X52 steel in the simulated solution with the addition of 200 ppm sulphide and 50 ppm lactate without the presence of sulphite (0 ppm); (b) EDAX results.

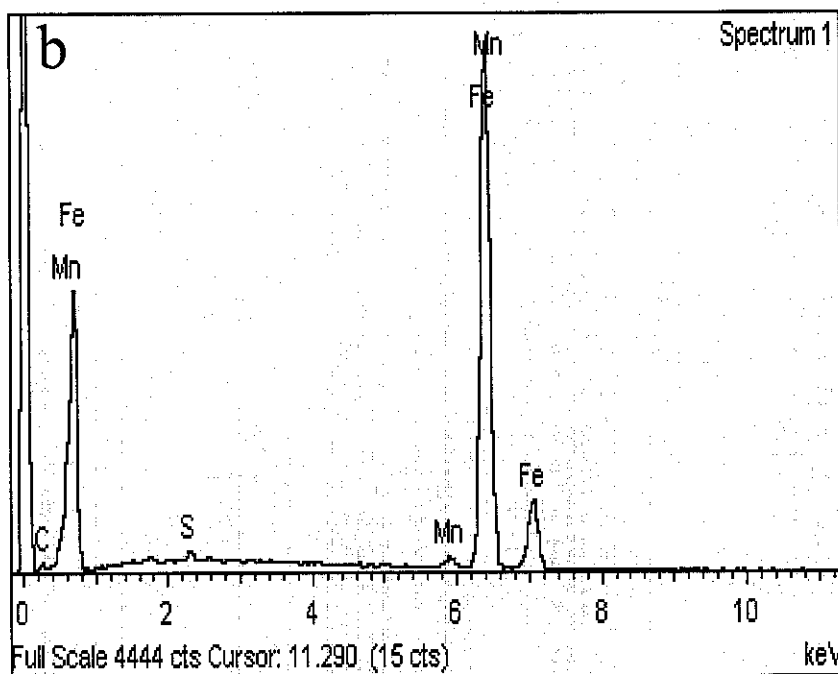


Figure 4.56 (a) Surface morphology (face view) of X52 steel in the simulated solution with the addition of 50 ppm sulphite, 200 ppm sulphide and 50 ppm lactate; (b) EDAX results.

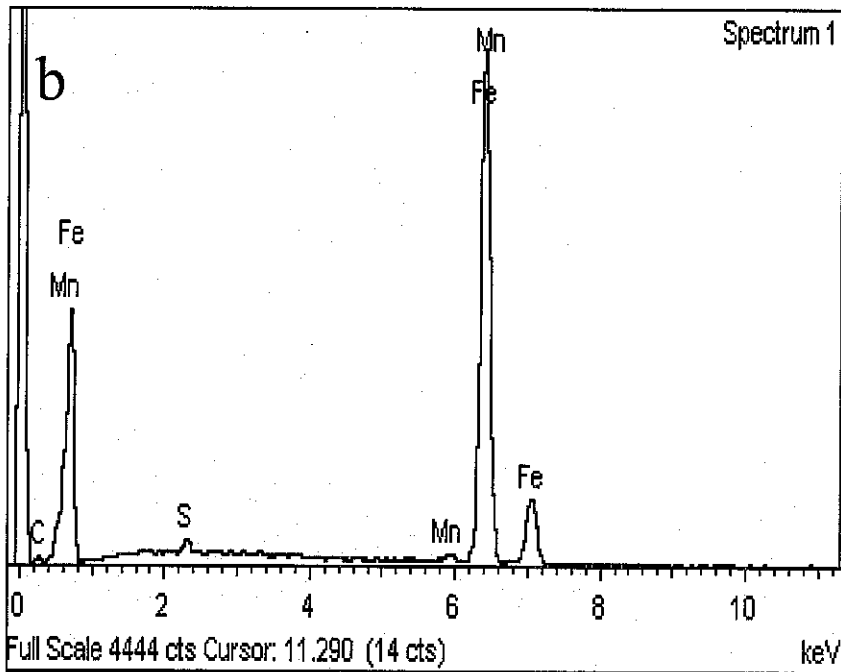


Figure 4.57 (a) Surface morphology (face view) of X52 steel in the simulated solution with the addition of 200 ppm sulphite, 200 ppm sulphide and 50 ppm lactate; (b) EDAX results.

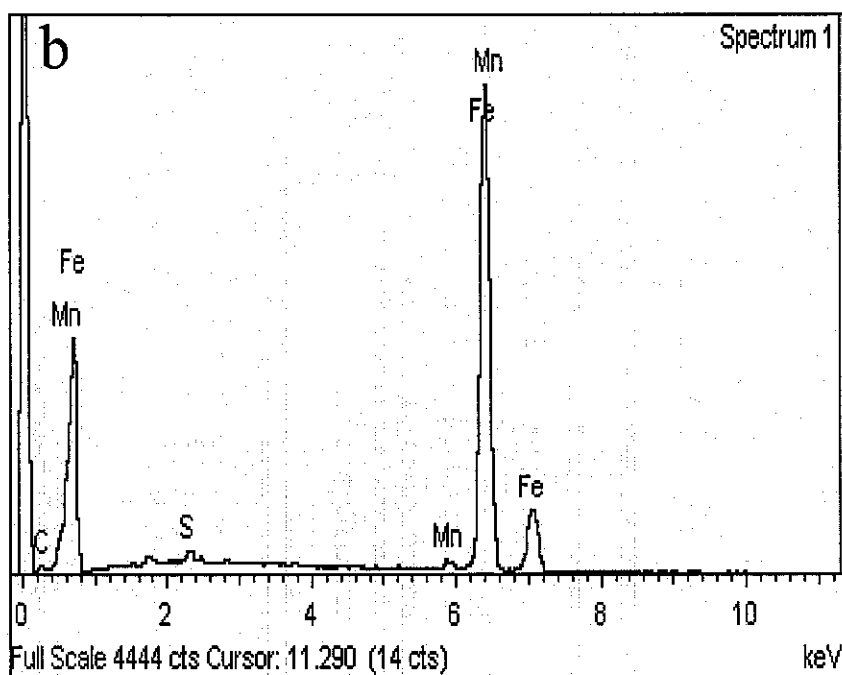
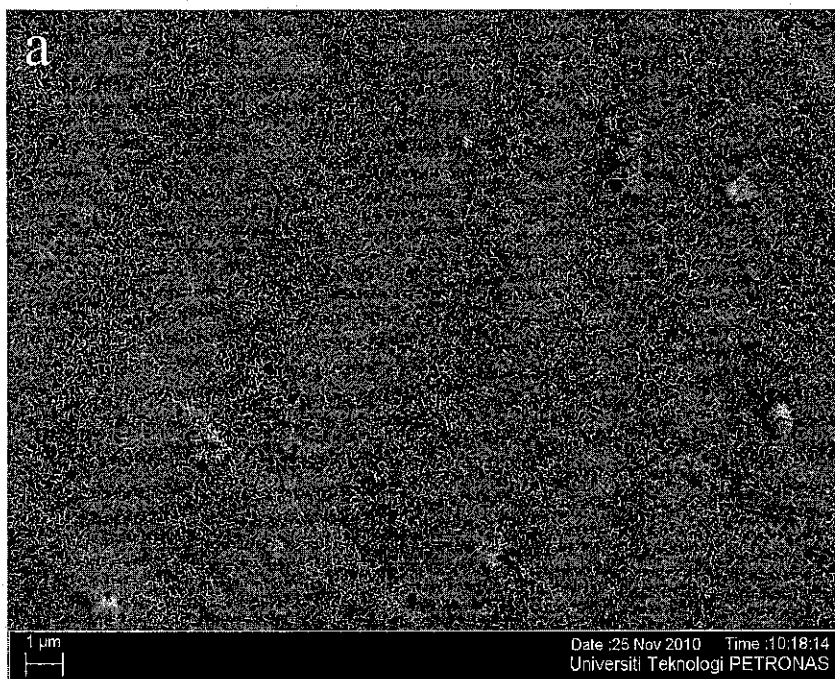
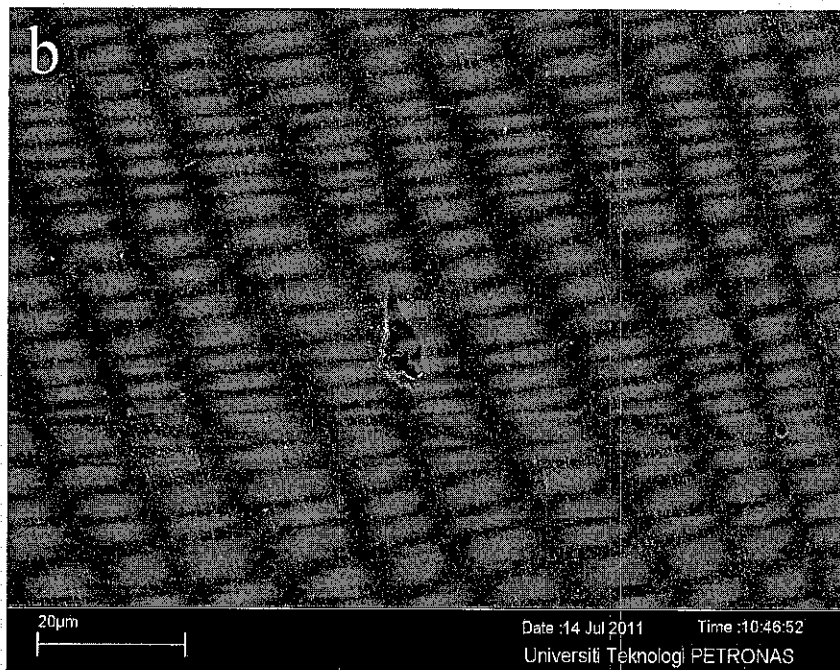
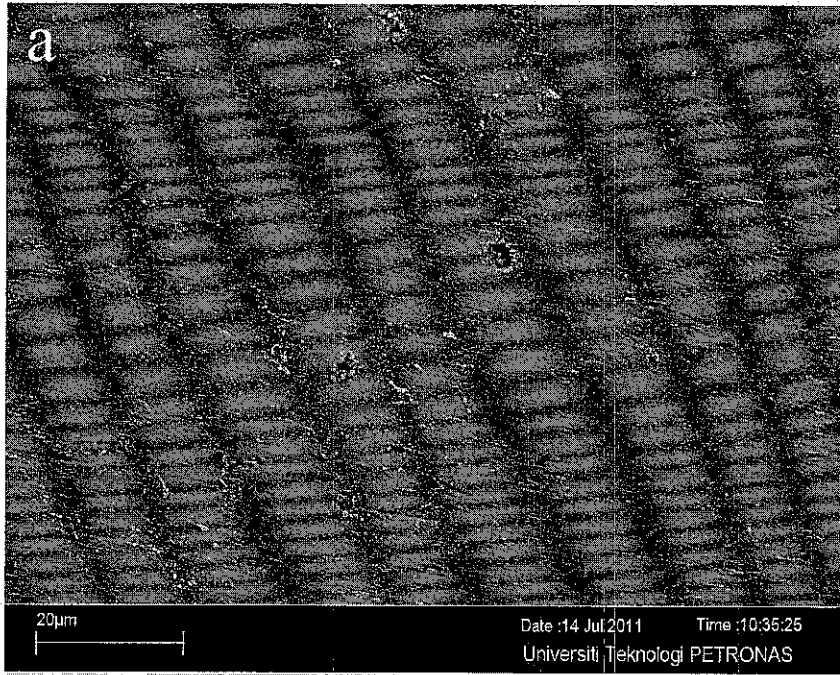


Figure 4.58 (a) Surface morphology (face view) of X52 steel in the simulated solution with the addition of 400 ppm sulphite, 200 ppm sulphide and 50 ppm lactate; (b) EDAX results.



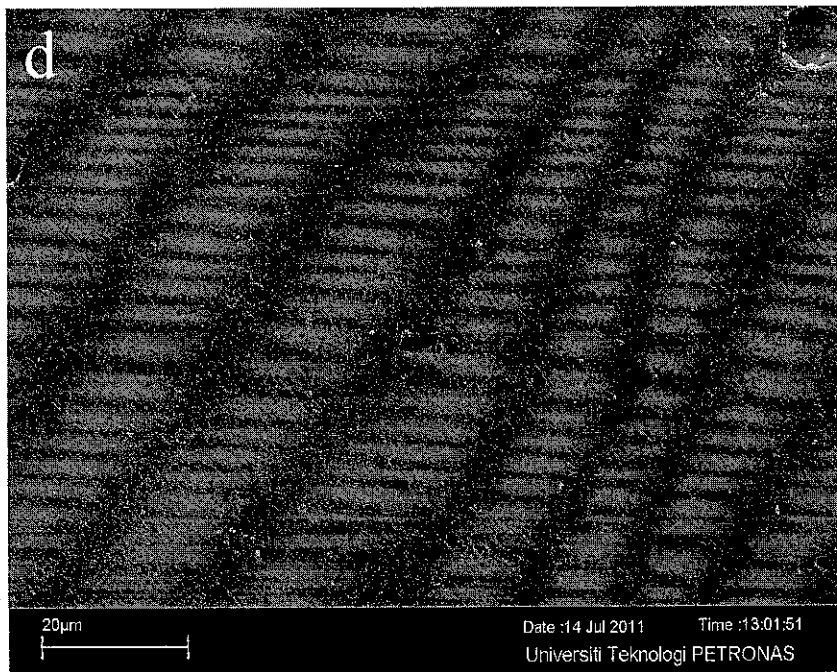
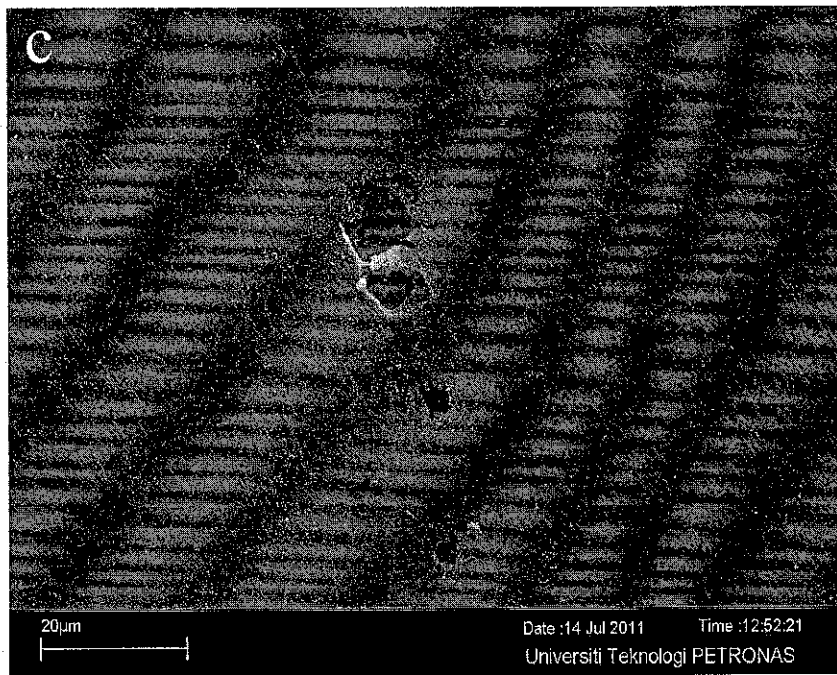


Figure 4.59 Surface morphology of X52 steel after corrosion product removal in the simulated solution with the addition of 200 ppm sulphide and 50 ppm lactate in various sulphite concentrations (a) 0 ppm; (b) 50 ppm; (c) 200 ppm (d) 400 ppm.

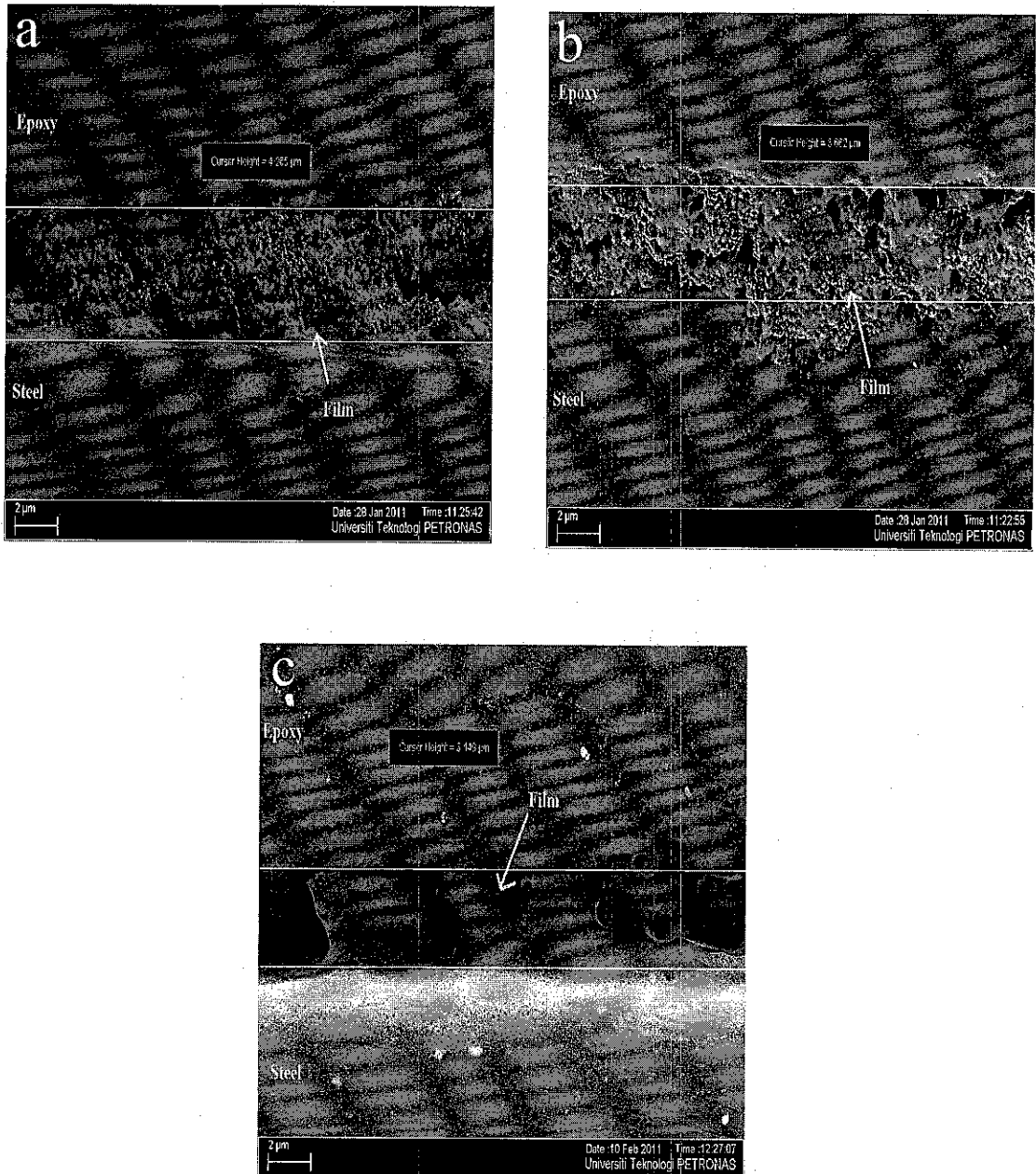


Figure 4.60 Surface morphology (cross view) of X52 steel in the simulated solution with the addition of 200 ppm sulphide and 50 ppm lactate in various sulphite concentrations (a) 0 ppm; (b) 50 ppm; (c) 400 ppm.

As shown in Figure 4.55, without the presence of sulphite, a flat and compact film is observed. EDX results confirmed the presence of C element on the film surface. It is believed that there is only FeCO_3 film formed on that environment. With the addition of sulphite, it is observed that there is no change on the film morphology (Figure 4.55-4.58). EDX results confirmed the presence of S and C elements on the film. It is suspected that the typically film formed are FeS and FeCO_3 film. The existence of both film (FeS and FeCO_3) will be confirmed by the XPS results.

After removing the corrosion products on the X52 steel surface, pitting corrosion were observed on all samples (Figure 4.59). However, with the increase in sulphite concentration, the pitting is more clearly visible on the surface.

Figure 4.60 shows cross sectional view of the film. It is seen that with addition of more sulphite concentration, the film thickness decreased. It is believed that the decreasing of film thickness, caused to the increasing of corrosion rate with the increase of sulphite concentrations.

4.2.2 Effect of immersion time

The effect of immersion time was studied by prolong the immersion time of X52 steel in the solution up to 24 hours. The results are presented below.

4.2.2.1 Effect of Sulphide

The effects of sulphide ion on the corrosion rate of X52 steel for 90 minutes and 24 hours of immersion times in the solution are shown in Figure 4.61 below. The study was conducted with the addition of 200 ppm sulphite and 50 ppm lactate with various sulphide concentrations in the simulated solution.

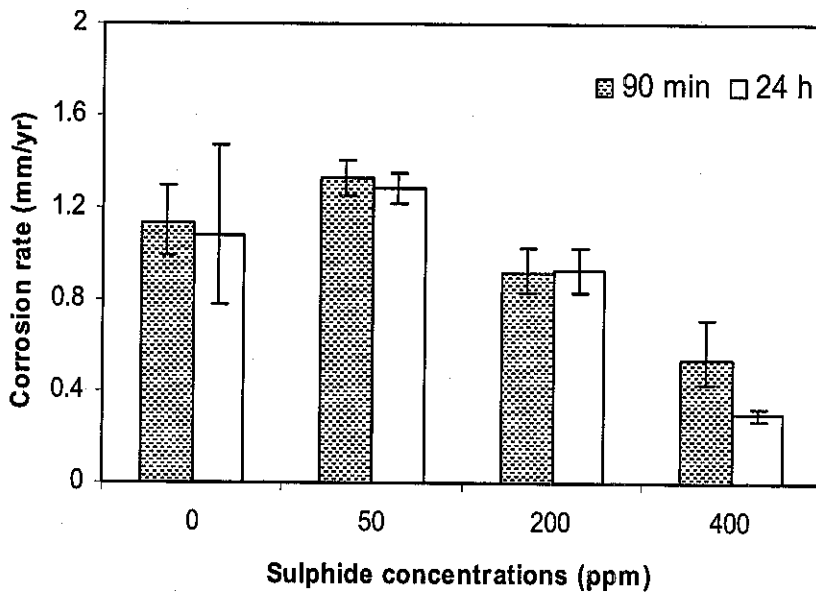


Figure 4.61 Effects of immersion time on the corrosion rate of X52 steel in various sulphide concentrations in the simulated solution.

It is observed that there is not much difference on the corrosion rate of X52 steel between 90 minutes and 24 hours of immersion times. It can be said, the corrosion rate of X52 steel in the solution had been stable within 90 minutes of immersion times.

The corrosion morphology of X52 steel in various sulphide concentrations after 24 hours immersion times are shown in Figure 4.62 to Figure 4.65.

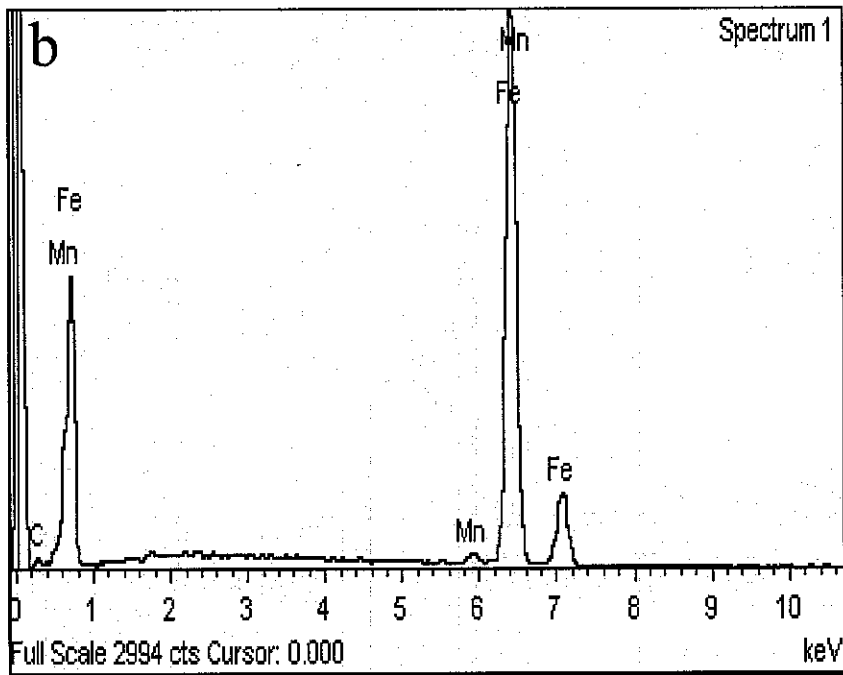
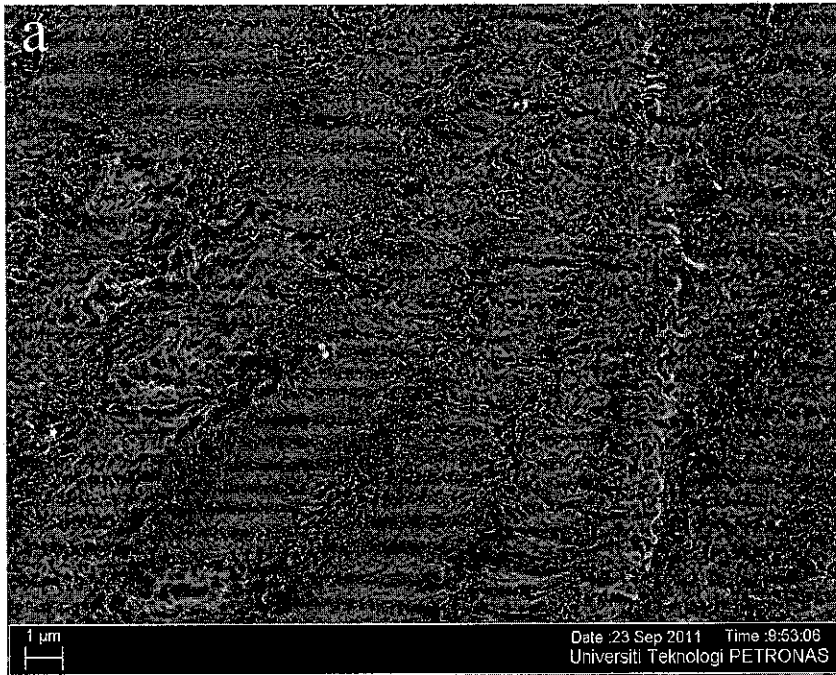


Figure 4.62 (a) Surface morphology (face view) of X52 steel in the simulated solution with the addition of 200 ppm sulphite and 50 ppm lactate without the presence of sulphide (0 ppm); (b) EDAX results.

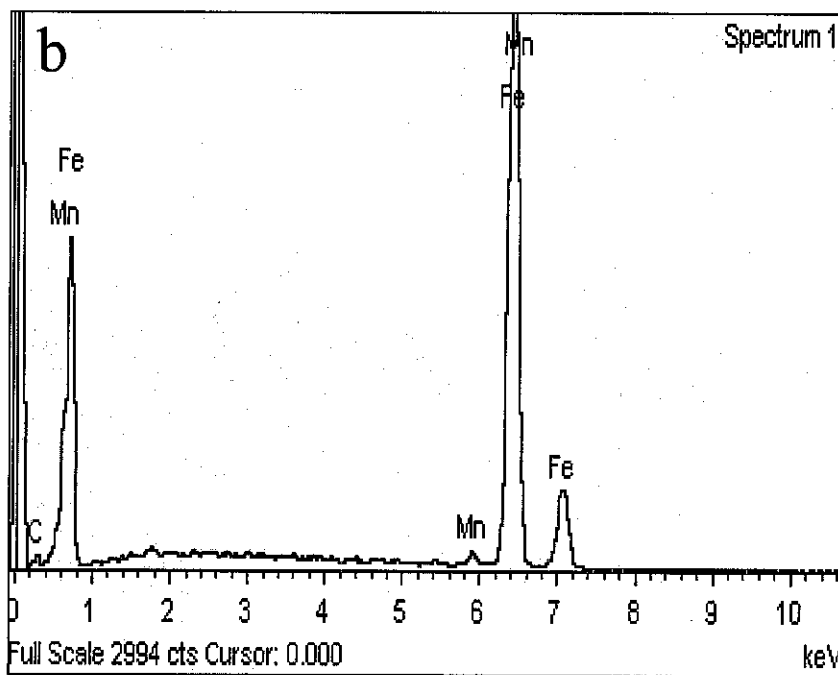
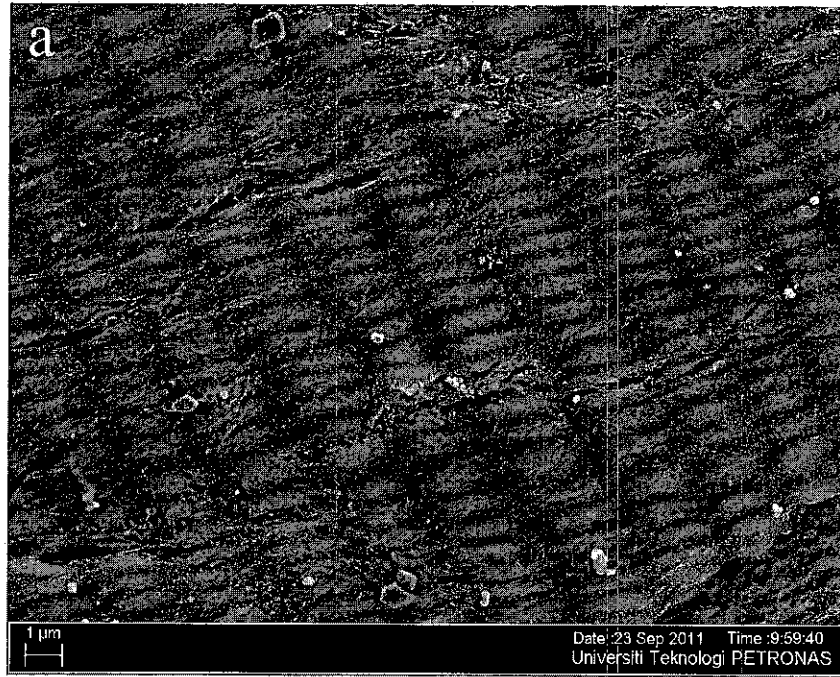


Figure 4.63 (a) Surface morphology (face view) of X52 steel in the simulated solution with the addition of 50 ppm sulphide, 200 ppm sulphite and 50 ppm lactate;
 (b) EDAX results.

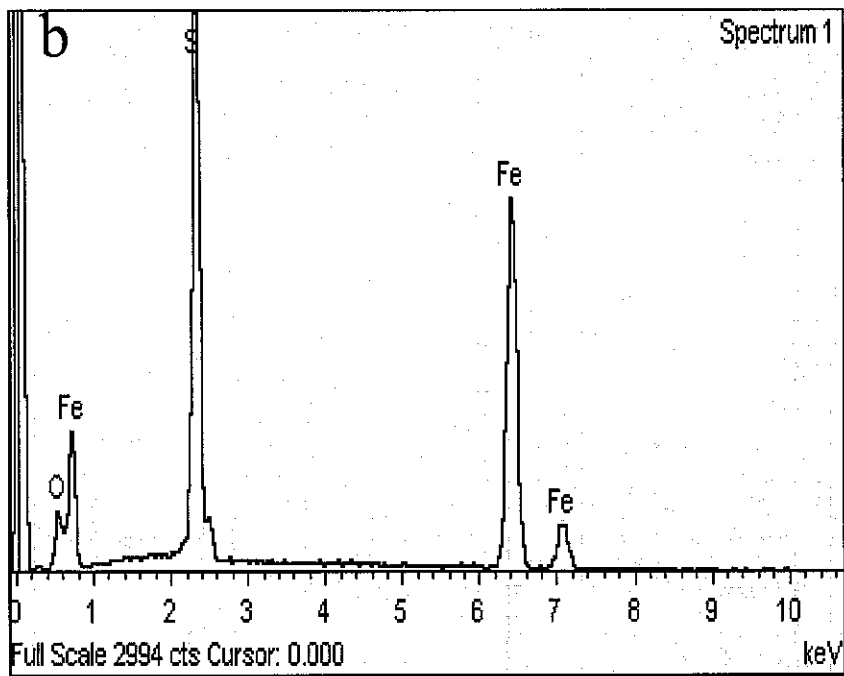
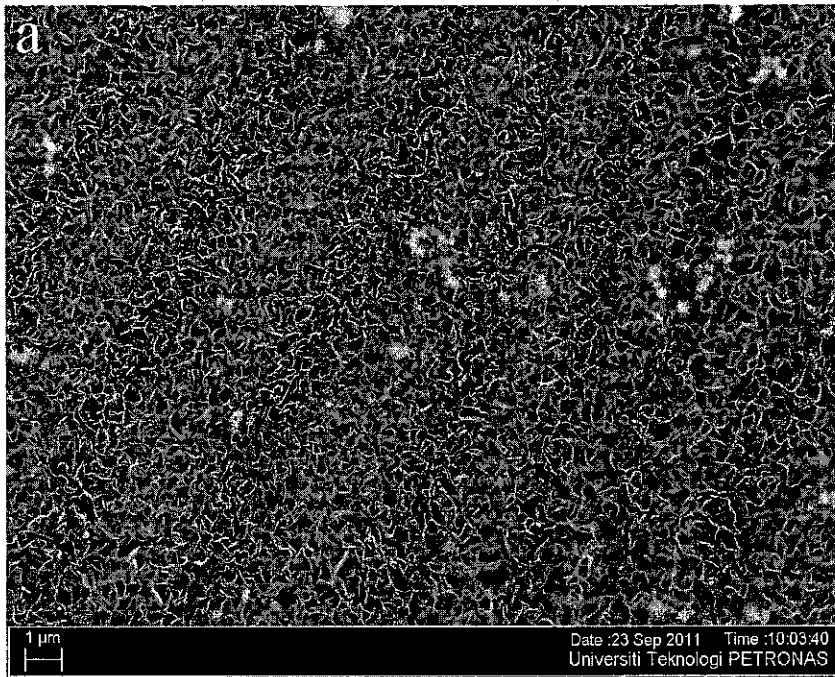


Figure 4.64 (a) Surface morphology (face view) of X52 steel in the simulated solution with the addition of 200 ppm sulphide, 200 ppm sulphite and 50 ppm lactate; (b) EDAX results.

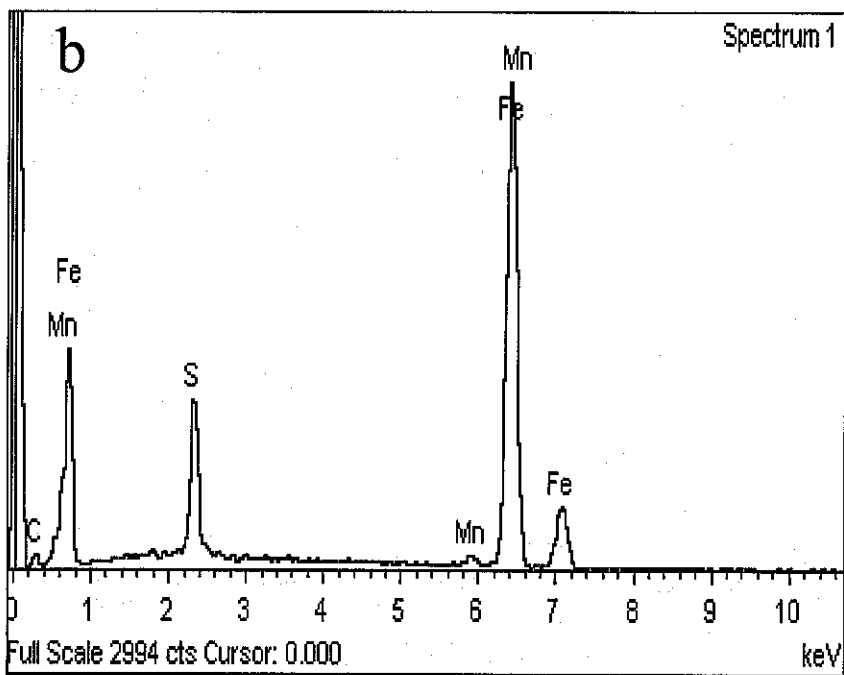
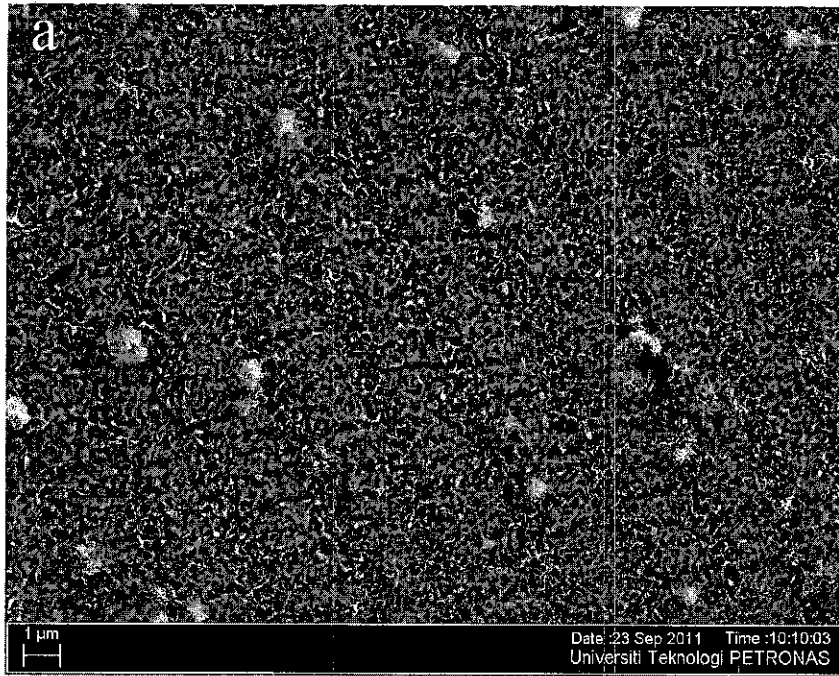
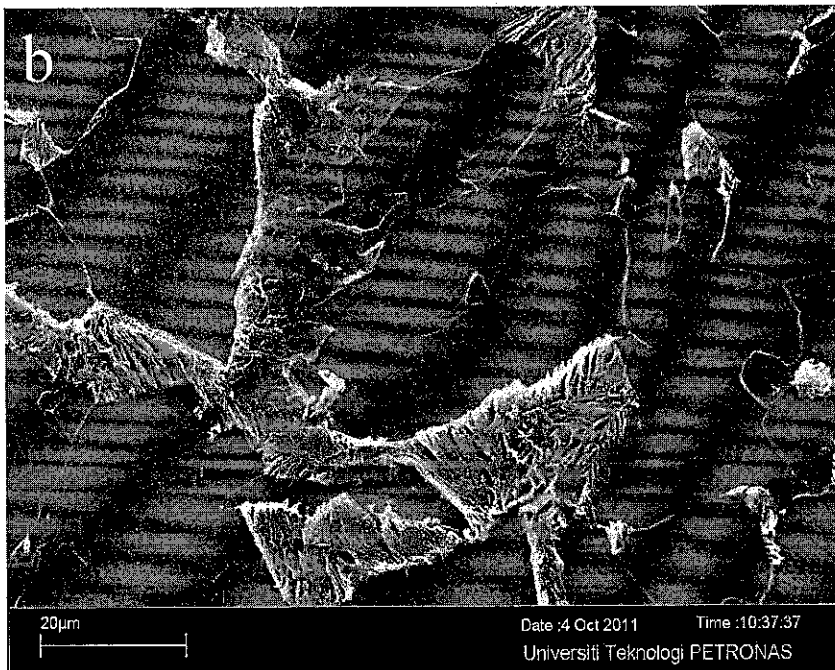
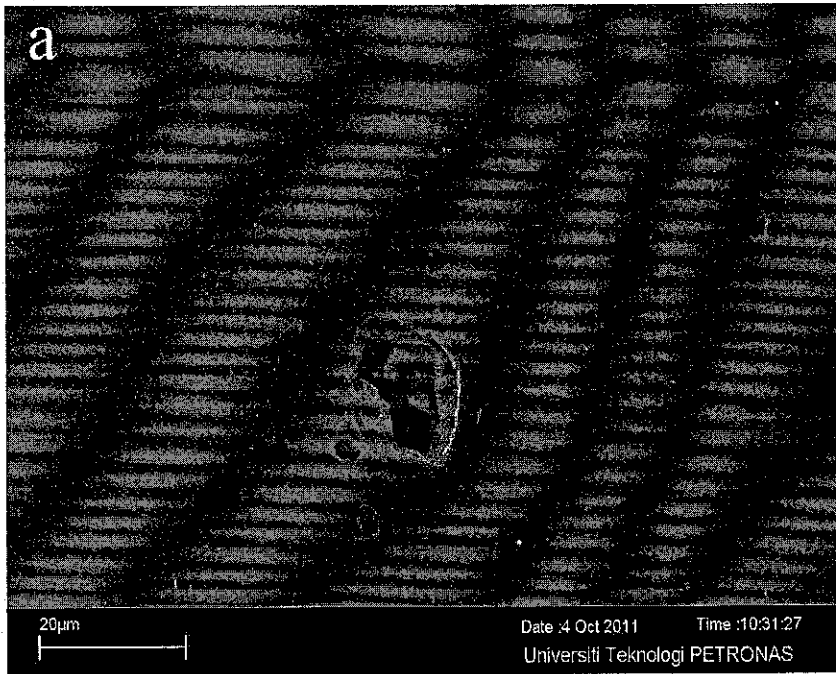


Figure 4.65 (a) Surface morphology (face view) of X52 steel in the simulated solution with the addition of 400 ppm sulphide, 200 ppm sulphite and 50 ppm lactate; (b) EDAX results.



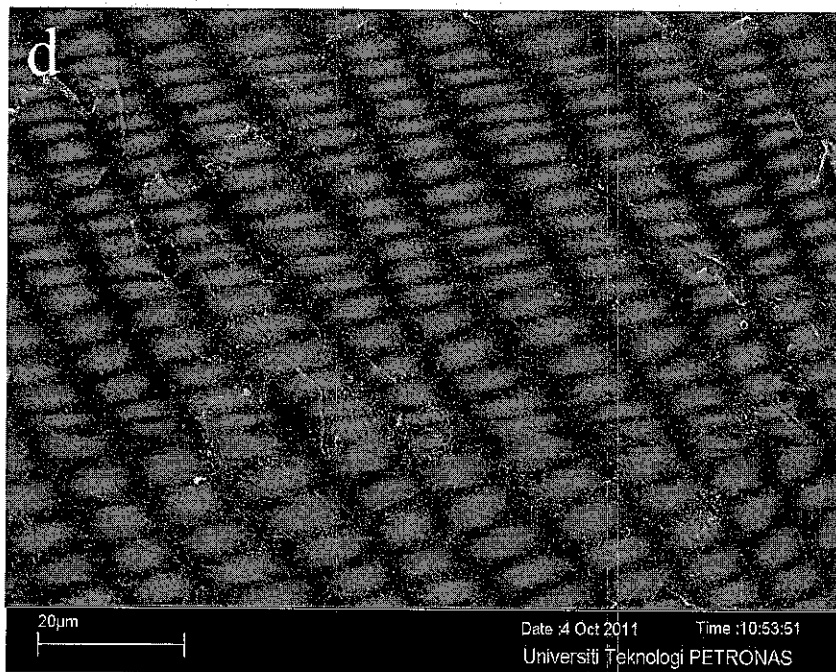
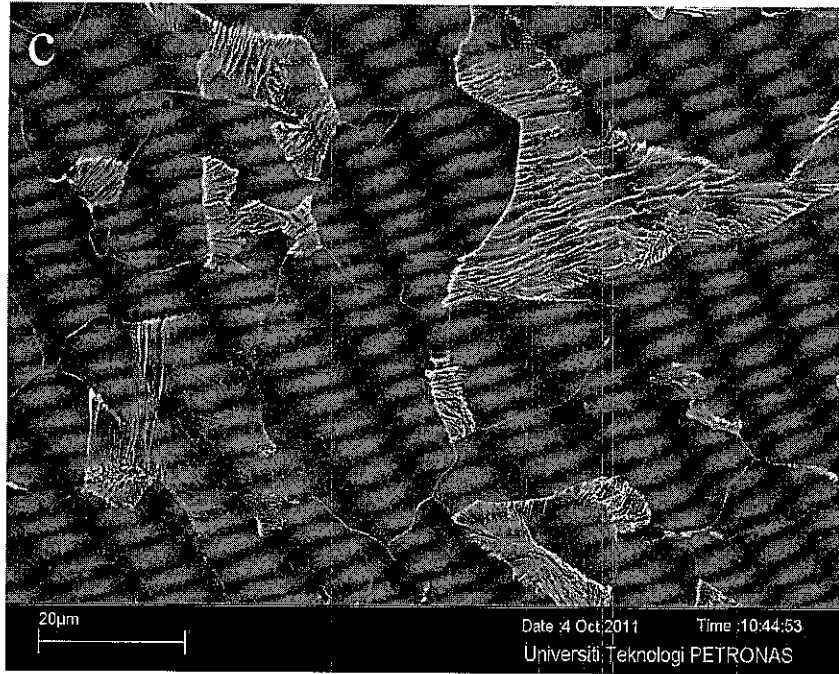


Figure 4.66 Surface morphology of X52 steel after corrosion product removal in the simulated solution with the addition of 200 ppm sulphite and 50 ppm lactate in various sulphide concentrations (a) 0 ppm; (b) 50 ppm; (c) 200 ppm (d) 400 ppm.

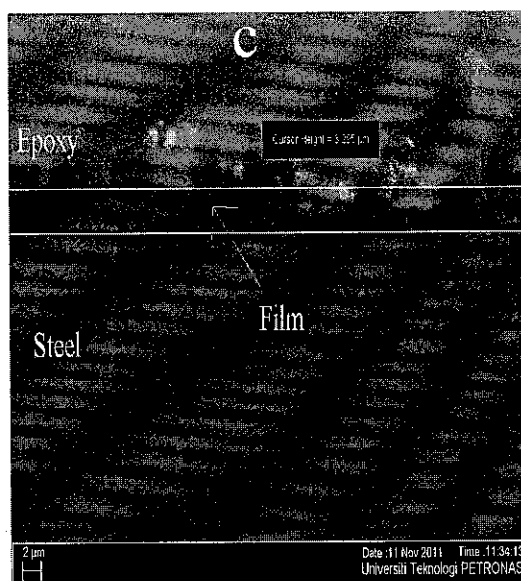
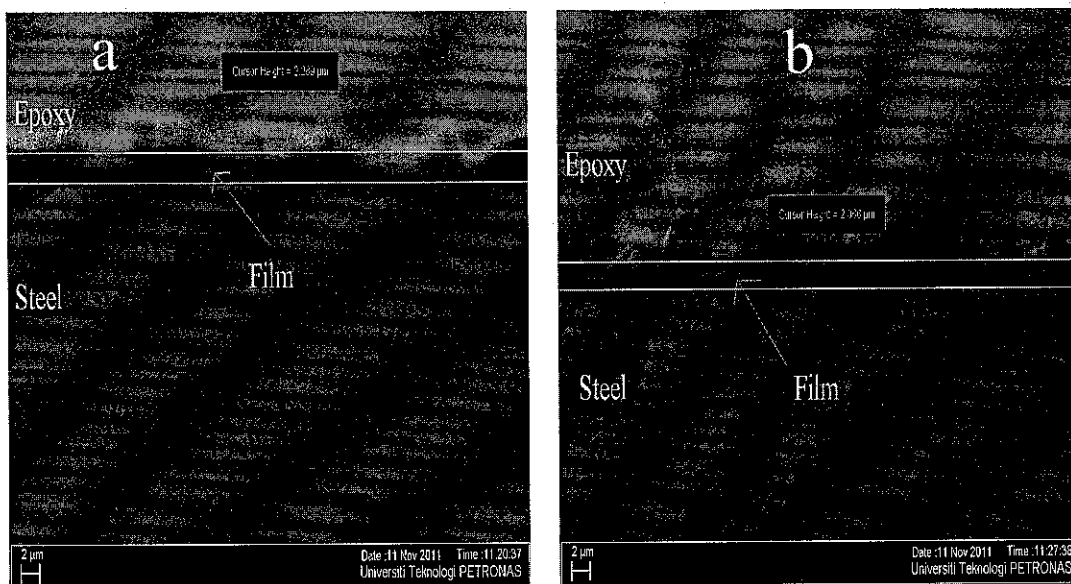


Figure 4.67 Surface morphology (cross view) of X52 steel in the simulated solution with the addition of 200 ppm sulphite and 50 ppm lactate in various sulphide concentrations (a) 0 ppm; (b) 50 ppm; (c) 400 ppm.

As shown in Figure 4.62, a flat and compact film was observed in sulphide free solution. With the addition of sulphide to the simulated solution, the film formed became more compact. However, with the addition of 50 ppm sulphide to the solution, it is observed a crack on the film (Figure 4.63). The crack on the film could cause a diffusion of corrosive species to the metal surface yielding an increasing of corrosion rate. The result is inline with LPR results, which show an increasing of corrosion rate with the addition of 50 ppm sulphide (Figure 4.53). Similar with 90 minutes of immersion times, the FeS film (in fragmented form) is appeared to be more visible in high sulphide concentration (200 and 400 ppm) as shown in Figure 4.64 and Figure 4.65.

After removing the corrosion products on the X52 steel surface, pitting corrosion was apparent only in sulphide free solution as shown in Figure 4.66 (a). With the addition of sulphide, there was no pitting on the steel surface observed (Figure 4.66 b-d). It is believed that the presence of FeS film protects the steel from corroded.

As shown in Figure 4.67 (a-c), cross sectional view results show that there is not much difference in the film thickness with the sulphide concentration range between 0 ppm and 50 ppm sulphide. The film thickness is around 2 μm . However, with addition of 400 ppm sulphide, the film thickness increased to 3.2 μm (Figure 4.67 c). The increase of film thickness caused a better protection to the corrosion. This result is in good agreement with electrochemical studies which showed a decreasing of corrosion rate with the presence of 400 ppm sulphide.

4.2.2.2 *Effect of sulphite*

The effects of sulphite ion on the corrosion rate of X52 steel for 90 minutes and 24 hours of immersion times in the simulated solution are shown in Figure 4.68 below.

The study was conducted with the addition of 200 ppm sulphide and 50 ppm lactate in various sulphite concentrations in the simulated solution.

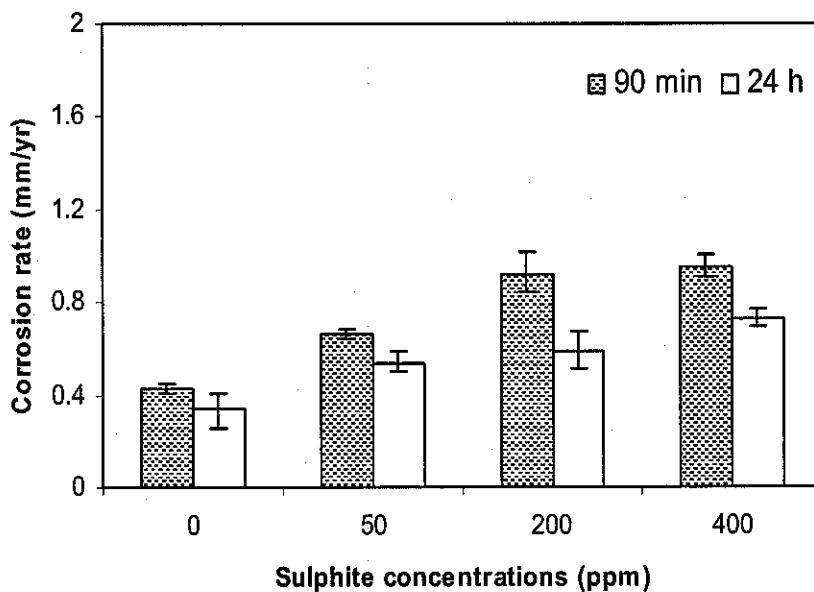


Figure 4.68 Effects of immersion time in various sulphite concentrations in the simulated solution.

It is observed that the corrosion rate in 90 minutes of immersion times slightly larger than 24 hours of immersion time. However, the results are still in good agreement. It is believed that the difference was influenced by the film formed.

The corrosion morphology of X52 steel in the simulated solution with the addition of 200 ppm sulphide and 50 ppm lactate with various sulphite concentrations after 24 hours immersion times are shown in Figure 4.69 to Figure 4.72.

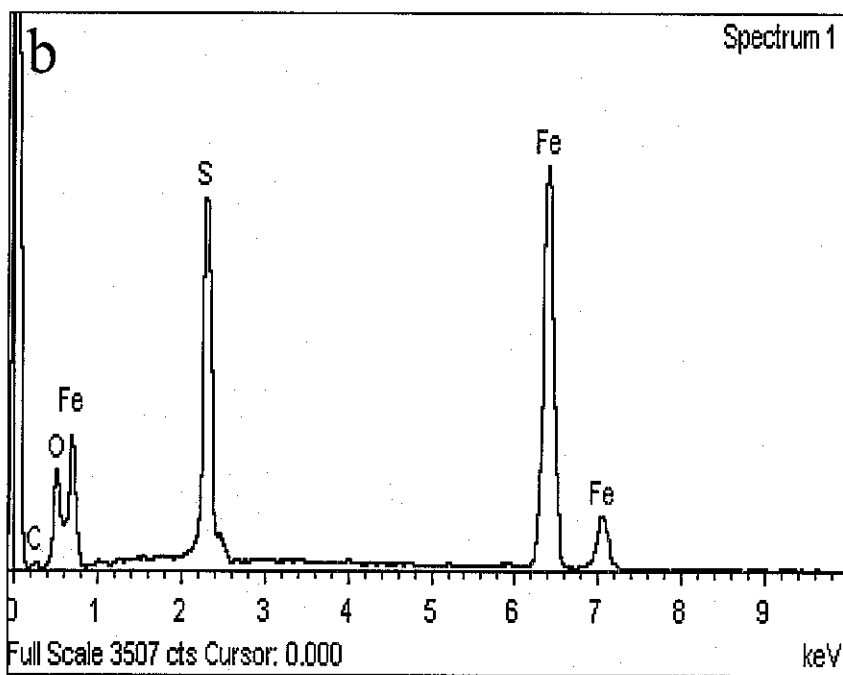
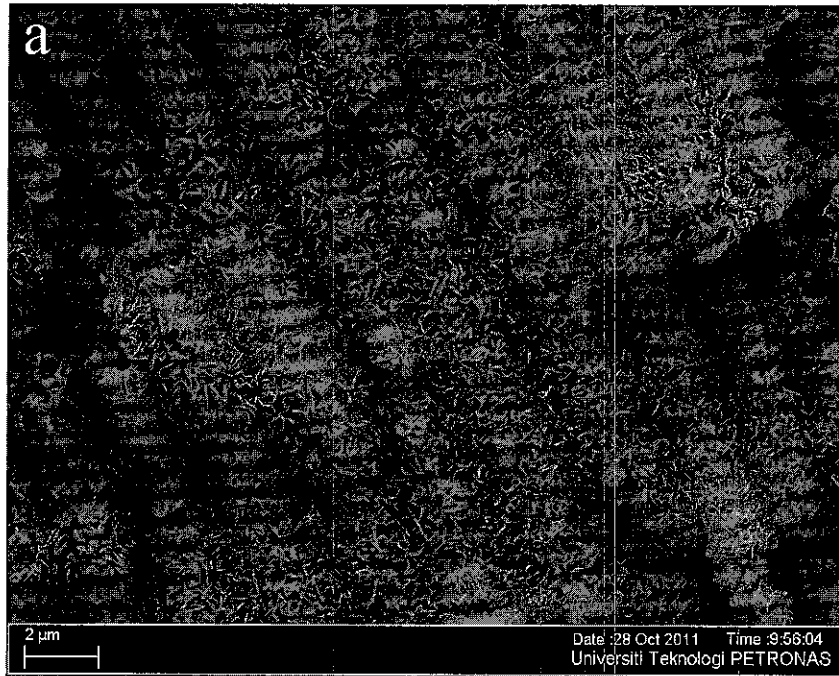


Figure 4.69 (a) Surface morphology (face view) of X52 steel in the simulated solution with the addition of 200 ppm sulphide and 50 ppm lactate without the presence of sulphite (0 ppm); (b) EDAX results.

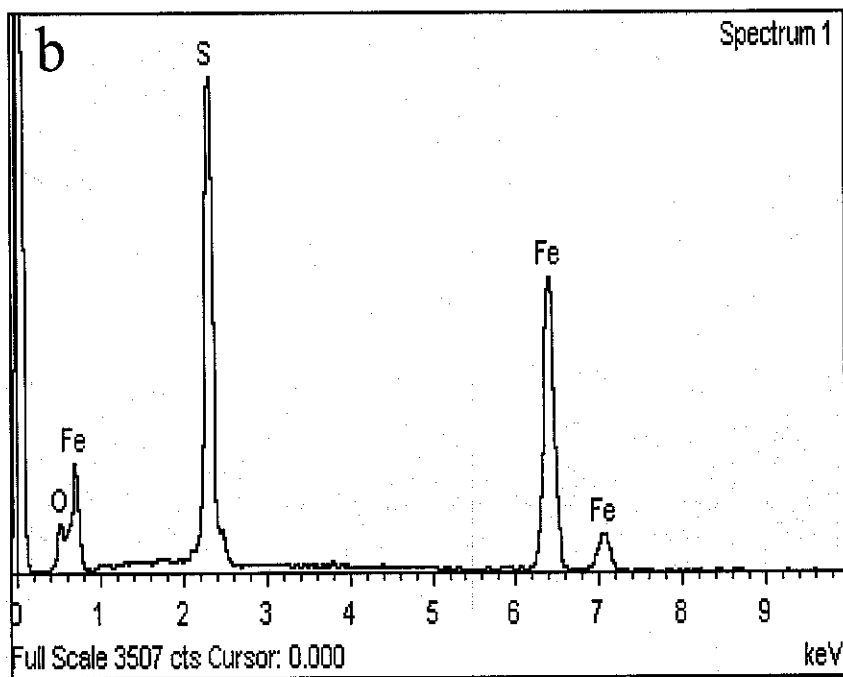
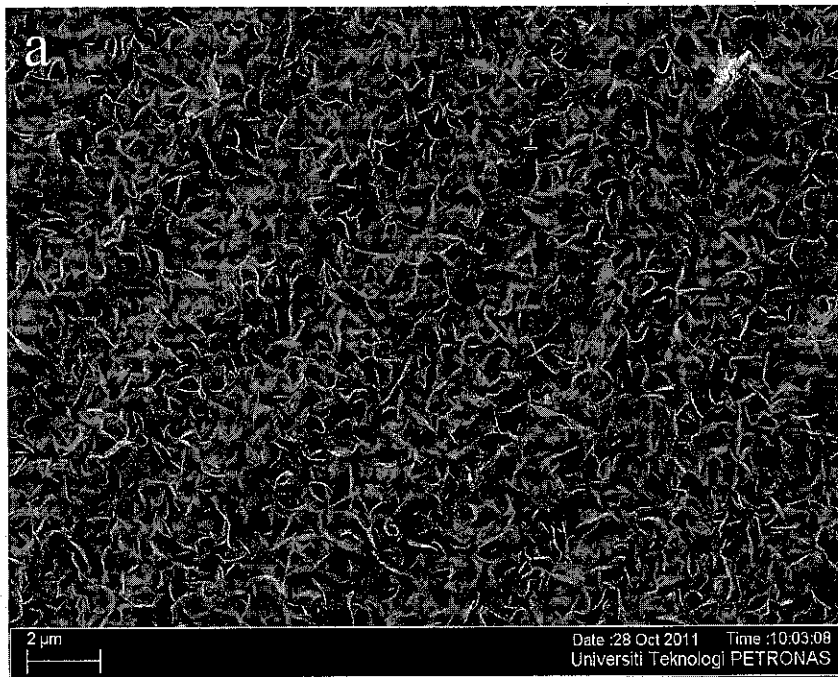


Figure 4.70 (a) Surface morphology (face view) of X52 steel in the simulated solution with the addition of 50 ppm sulphite, 200 ppm sulphide and 50 ppm lactate; (b) EDAX results.

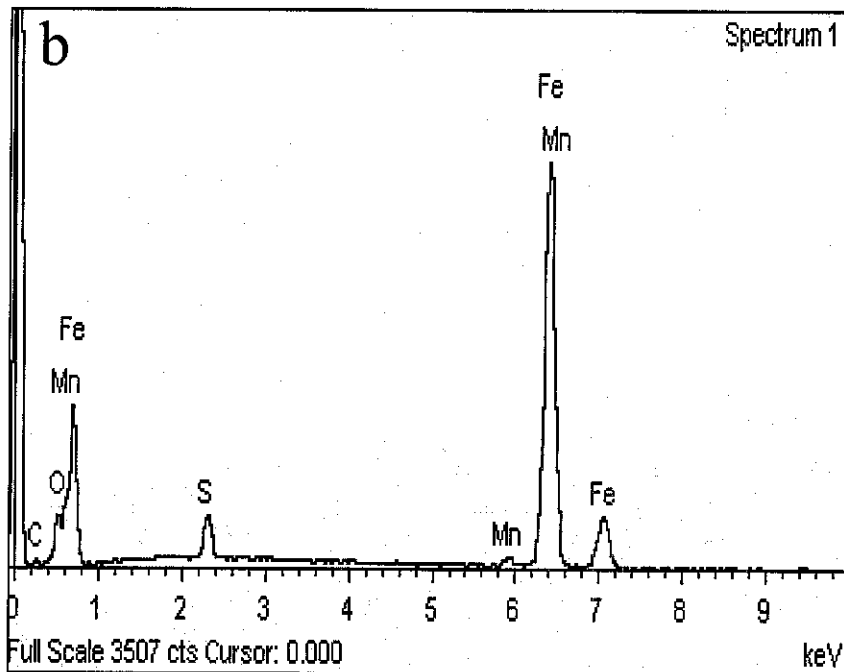
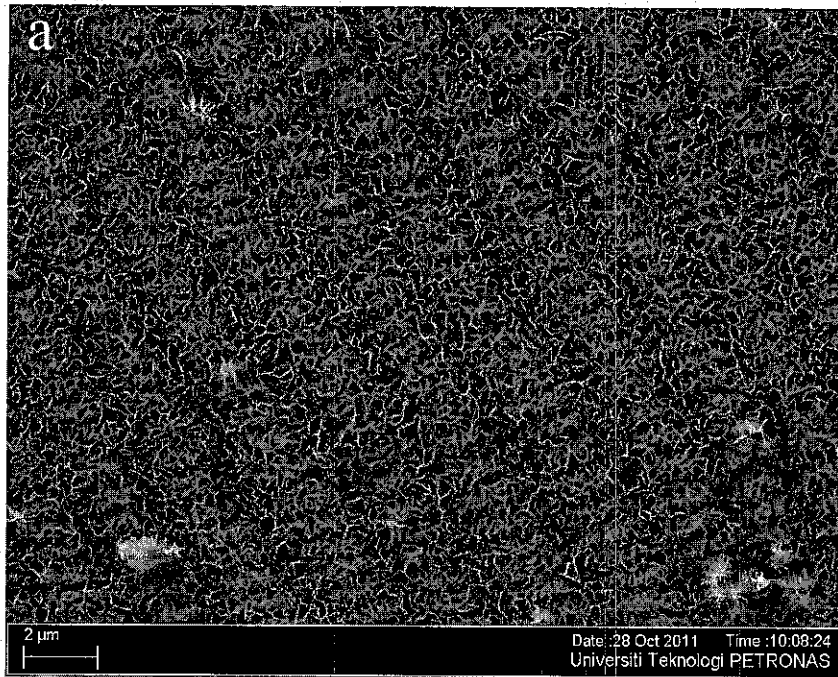


Figure 4.71 (a) Surface morphology (face view) of X52 steel in the simulated solution with the addition of 200 ppm sulphite, 200 ppm sulphide and 50 ppm lactate; (b) EDAX results.

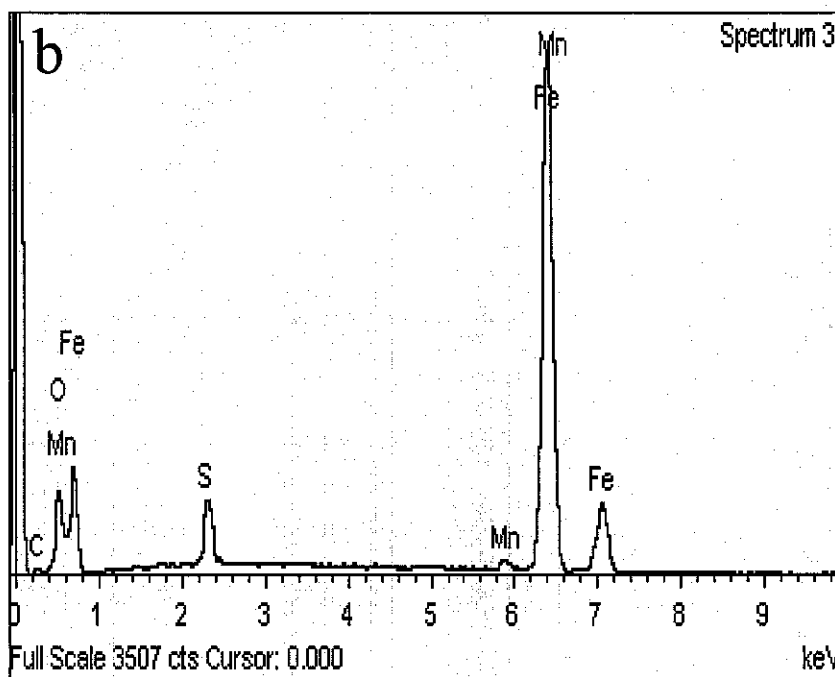
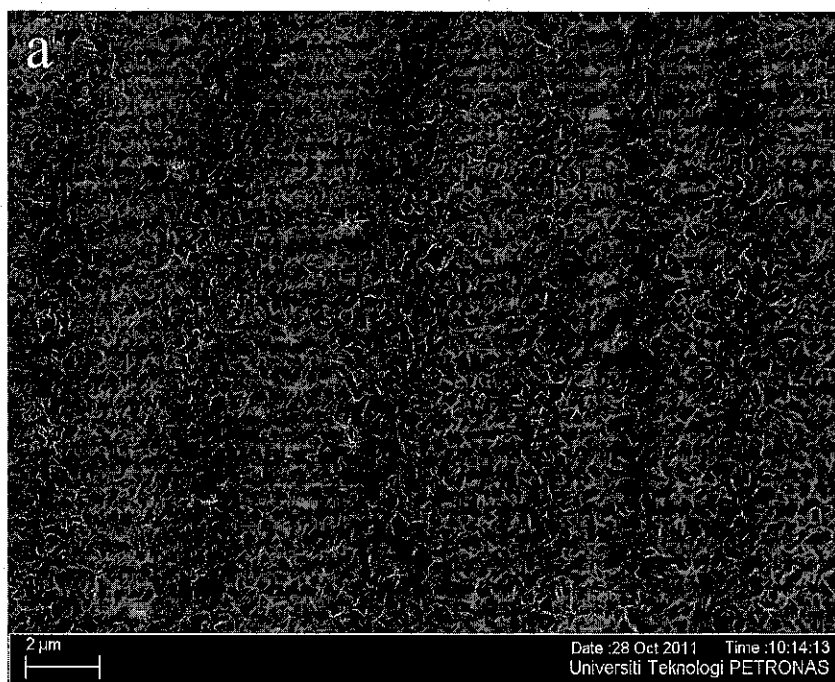
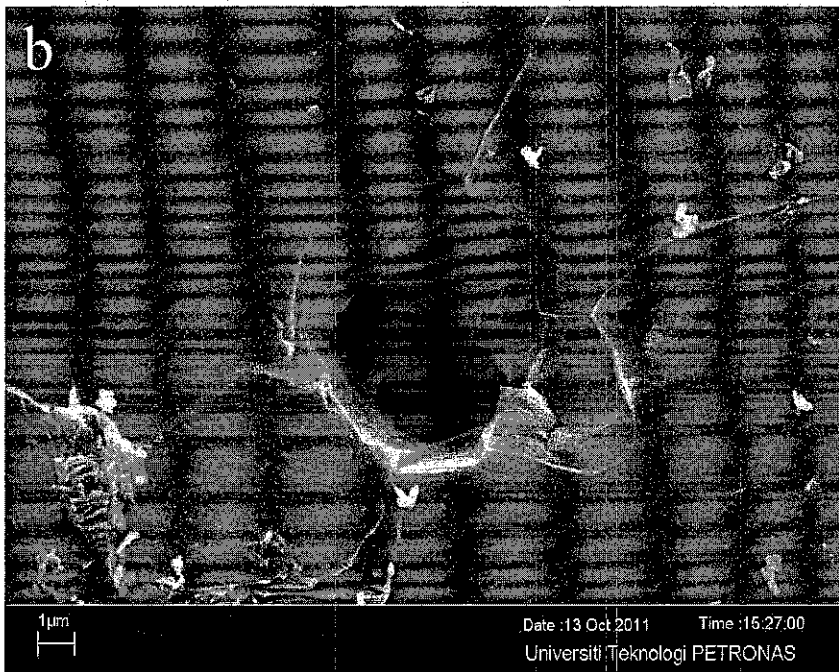
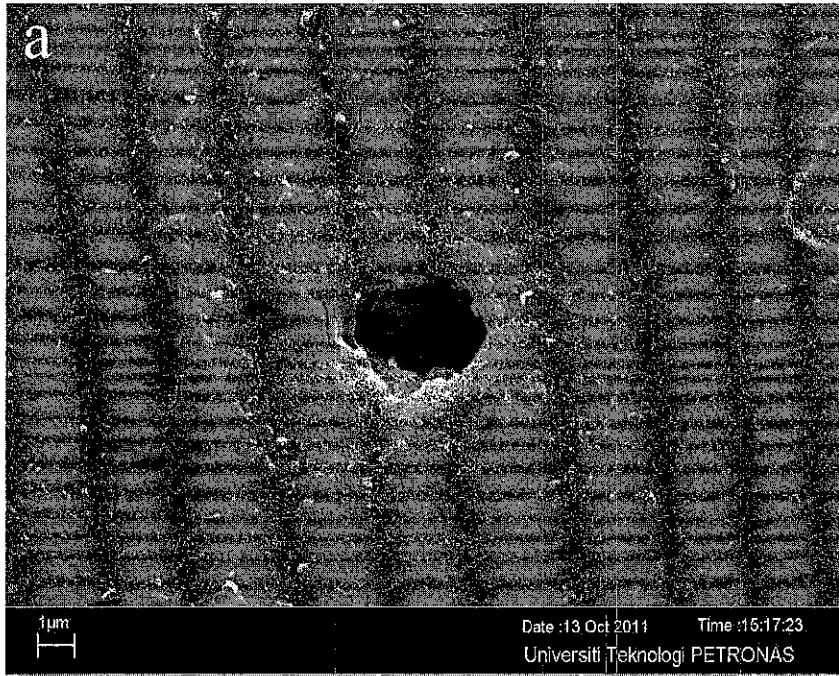


Figure 4.72 (a) Surface morphology (face view) of X52 steel in the simulated solution with the addition of 400 ppm sulphite, 200 ppm sulphide and 50 ppm lactate; (b) EDAX results.



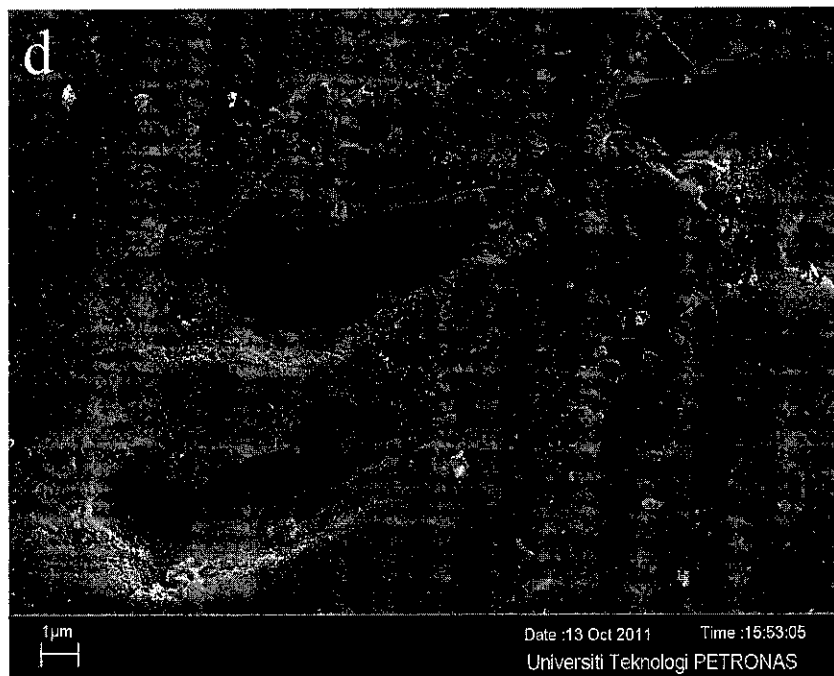


Figure 4.73 Surface morphology of X52 steel after corrosion product removal in the simulated solution with the addition of 200 ppm sulphide and 50 ppm lactate in various sulphite concentrations (a) 0 ppm; (b) 50 ppm; (c) 200 ppm; (d) 400 ppm.

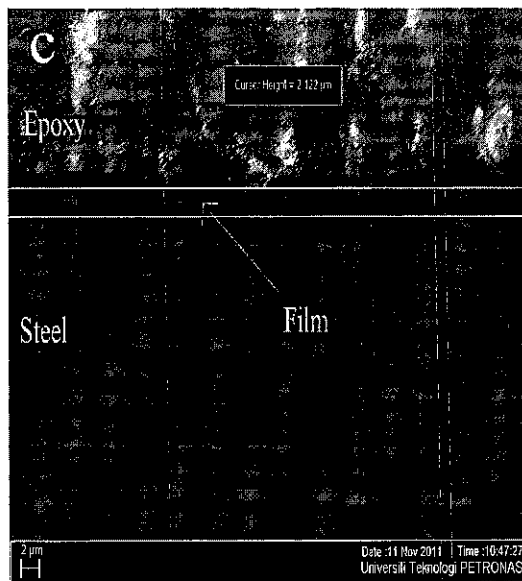
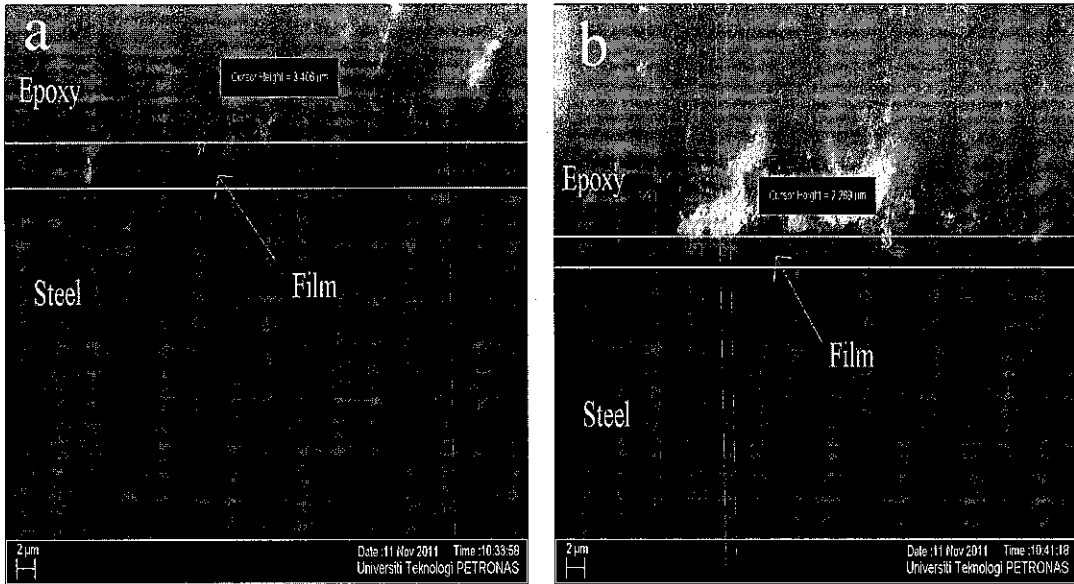


Figure 4.74 Surface morphology (cross view) of X52 steel in the simulated solution with the addition of 200 ppm sulphide and 50 ppm lactate in various sulphite concentrations (a) 0 ppm; (b) 50 ppm; (c) 400 ppm.

As shown in Figure 4.69, without the presence of sulphite, two layers of film were observed on the sample surface (both in fragmented form). With addition 50 ppm sulphite (Figure 4.70), the upper layer was vanished and the morphology of base layer becomes more apparent. However, with addition of 200 and 400 ppm sulphite, the apparent of film morphology tends to reduce as shown in Figure 4.71 and Figure 4.72, respectively.

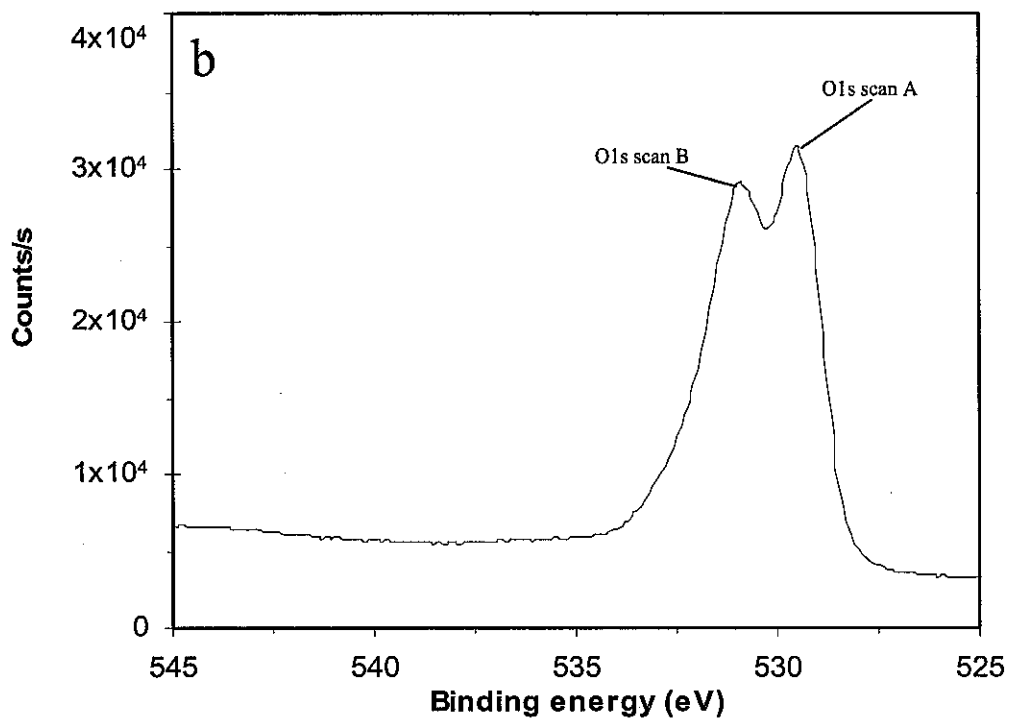
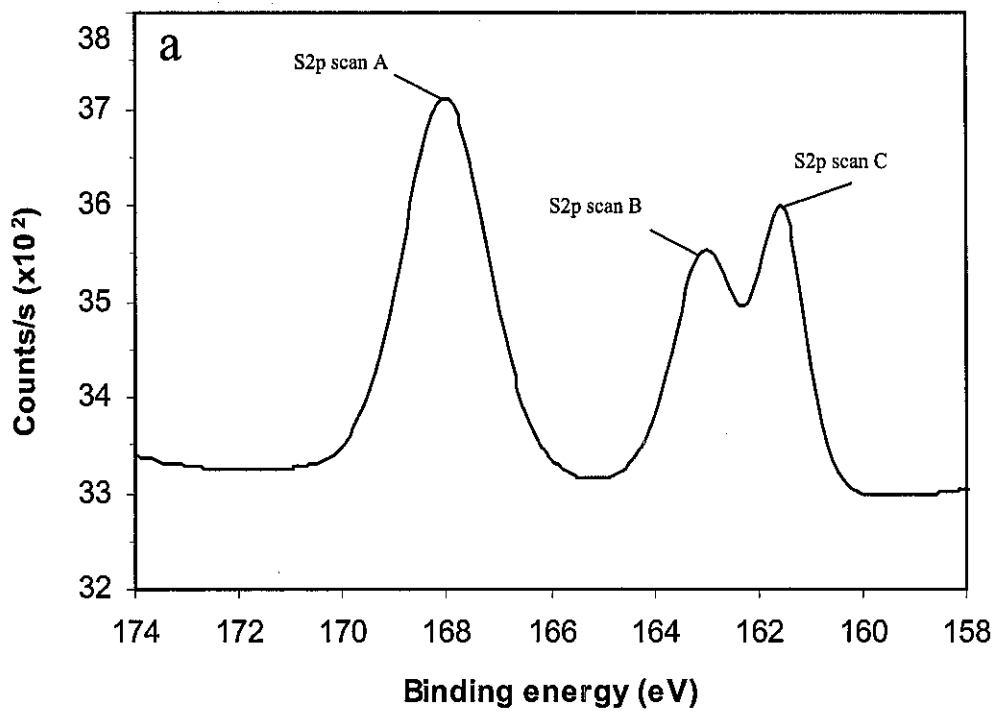
After removing the corrosion products on the X52 steel surface, pitting corrosion were observed on all samples (Figure 4.73 a-d). However, with the addition of sulphite, the increased of pitting's diameter were observed.

Figure 4.74 (a-c) shows cross sectional view of the film. It is seen that with addition of more sulphite concentration, the film thickness decreased. However, there is no significant difference in film thickness between 200 ppm and 400 ppm sulphite. The film thickness is around 2 μm . It is believed that the decreasing of film thickness, contributed to the increasing of corrosion rate with the increase of sulphite concentrations.

4.2.3 XPS analysis

XPS analysis was performed on the corrosion product of the sample surface. The analysis was focused on examining the existence of FeCO_3 and FeS as it had been detected by EDAX. For this purpose, Fe, C, O and S were registered in the XPS examination to get the spectra. XPS analysis in this study was conducted in sulphide free solution, sulphite free solution and solution with 400 ppm sulphide and 200 ppm sulphite.

Figure 4.75 shows XPS spectra for sulphide free solution with the presence of 200 ppm sulphite and 50 ppm lactate in the simulated solution.



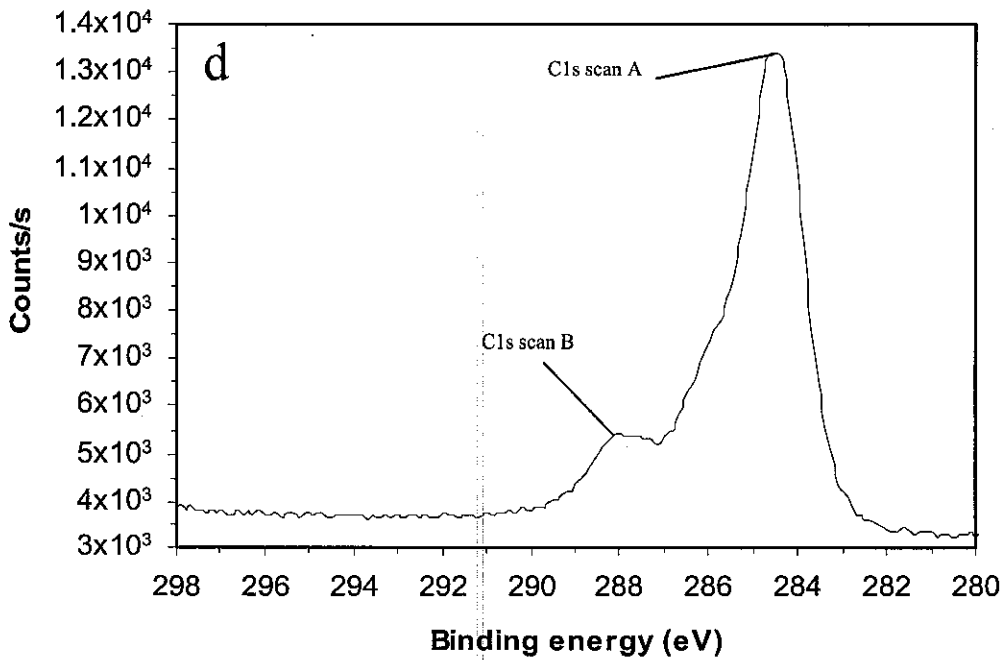
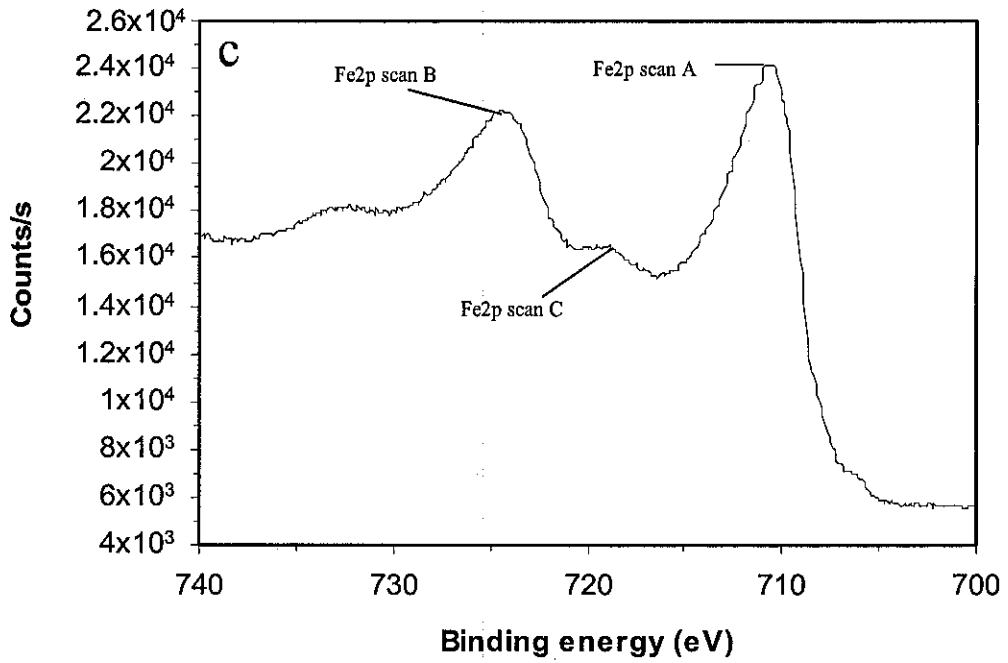


Figure 4.75 XPS spectra of X52 steel in the simulated solution with the addition of 200 ppm sulphite and 50 ppm lactate (no sulphide): (a) S2p, (b) O1s, (c) Fe2p, (d) C1s.

Figure 4.75 (a) shows that three peaks of S2p were observed in the spectra. Those are at: 161.52 eV; 163.01 eV; and 168.2 eV. The peak at 161.52 eV corresponds to *pyrite* [96]. The peak at 163.01 eV near 163.1eV corresponds to *polysulfide* [54, 97]. The peak at 168.2 eV was close to 168.3 corresponds to sulphate (SO_4^{2-}) [98].

Two peaks of O1s were observed in the spectra as shown in Figure 4.75 (b). Those are at: 529.48 eV and 530.98 eV. The peak at 529.48 eV corresponds to Fe_3O_4 [99] and the peak at 530.98 eV corresponds to FeCO_3 [100-102].

In addition, the scan of Fe2p binding energies reveals three peaks as shown by Figure 4.75 (c). Those are at: 710.64 eV; 724.19 eV and 718.88 eV. The peak at 710.64 eV corresponds to the binding energy of Fe_3O_4 [103-104]. The peak at 718.88 near 719.9 eV corresponds to Fe^0 [105-106]. The peak at 724.19 eV was close to 724.3 eV corresponds to Fe_3O_4 [107].

Lastly, Figure 4.75 (d) shows that two peaks of C1s were observed in the spectra. Those are at: 284.5 eV and 288 eV. The peak at 284.5 eV corresponds to hydrocarbon and the peak at 288 eV corresponds to FeCO_3 [80, 100].

In summary, in sulphide free solution with the presence of 200 ppm sulphite and 50 ppm lactate in the simulated solution, it is proven that the FeCO_3 and FeS (typically *pyrite*) film were formed on the X52 steel surface.

For solution with the presence of 400 ppm sulphide, 200 ppm sulphite and 50 ppm lactate, in the simulated solution the XPS spectra is shown in Figure 4.76.

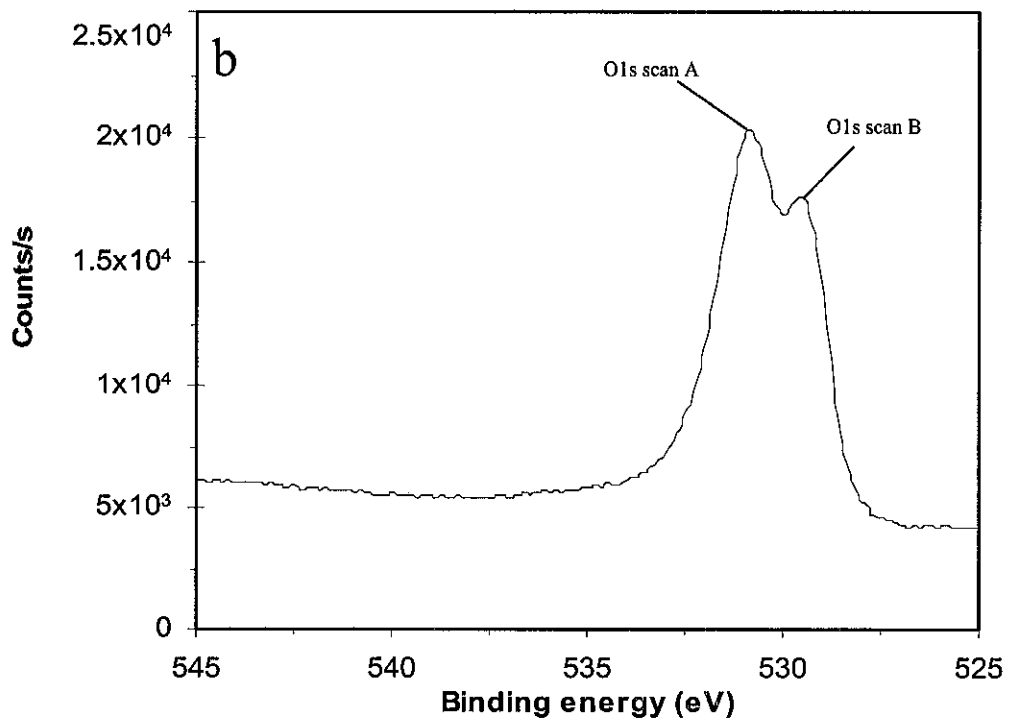
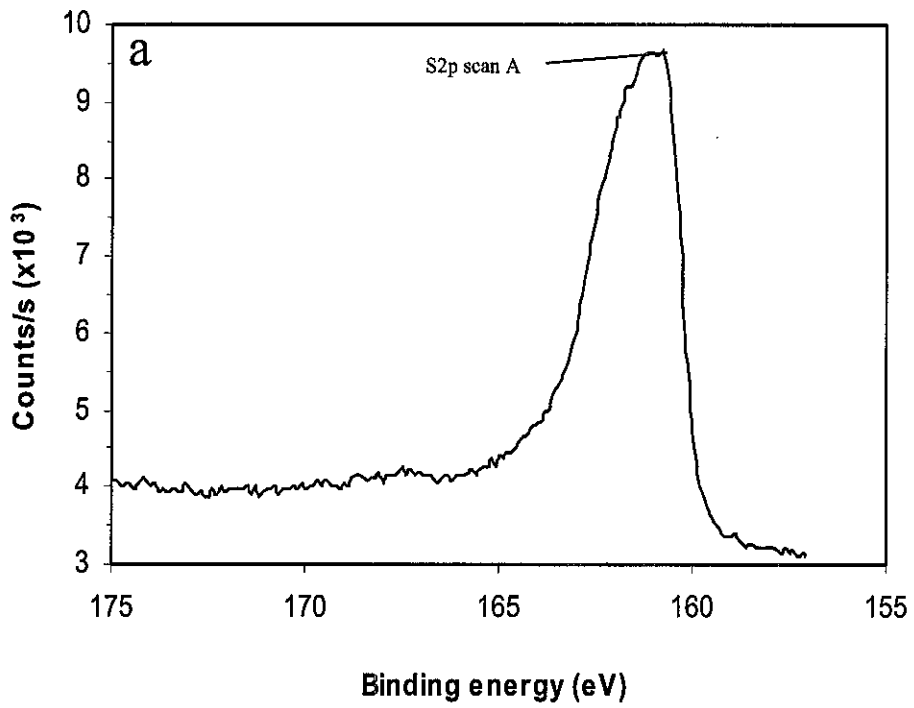
Figure 4.76 (a) shows that one peak of S2p was observed in the spectra at 161.2 eV. The peak at 161.2 eV corresponds to *mackinawite* FeS and more likely to *nanocrystalline mackinawite* (FeS_n) [108].

Two peaks of O1s were observed in the spectra as shown in Figure 4.76 (b). Those are at: 529.5 eV and 530.8 eV. The peak at 529.5 eV corresponds to Fe_3O_4 [99] and the peak at 530.8 eV corresponds to FeCO_3 [100-102].

In addition, Figure 4.76 (c) shows that four peaks of Fe2p were observed in the spectra. Those are at: 707.09 eV; 710.29 eV; 723.7 eV and 720.08 eV. The peak at 707.09 eV was close to 707.3 corresponds to *pyrite* [54, 98, 108-109]. The peak at 710.64 eV was close to 710.8 eV, corresponds to Fe₂O₃ [103-104]. The peak at 720.08 near 719.9 eV corresponds to Fe⁰ (clean iron). The peak at 723.7 eV was close to 724.3 eV, corresponds to Fe₂O₃ [107].

Lastly, Figure 4.76 (d) shows that two peaks of C1s were observed in the spectra. Those are at: 284.7 eV and 288 eV. The peak at 284.7 eV corresponds to hydrocarbon [54] and the peak at 288 eV was attributed to FeCO₃ [80, 100].

In summary, in the presence of sulphide and sulphite, it is observed that FeCO₃ and FeS film were formed on the electrode surface. However, it is noted that the typically FeS film formed were *pyrite* and *mackinawite*.



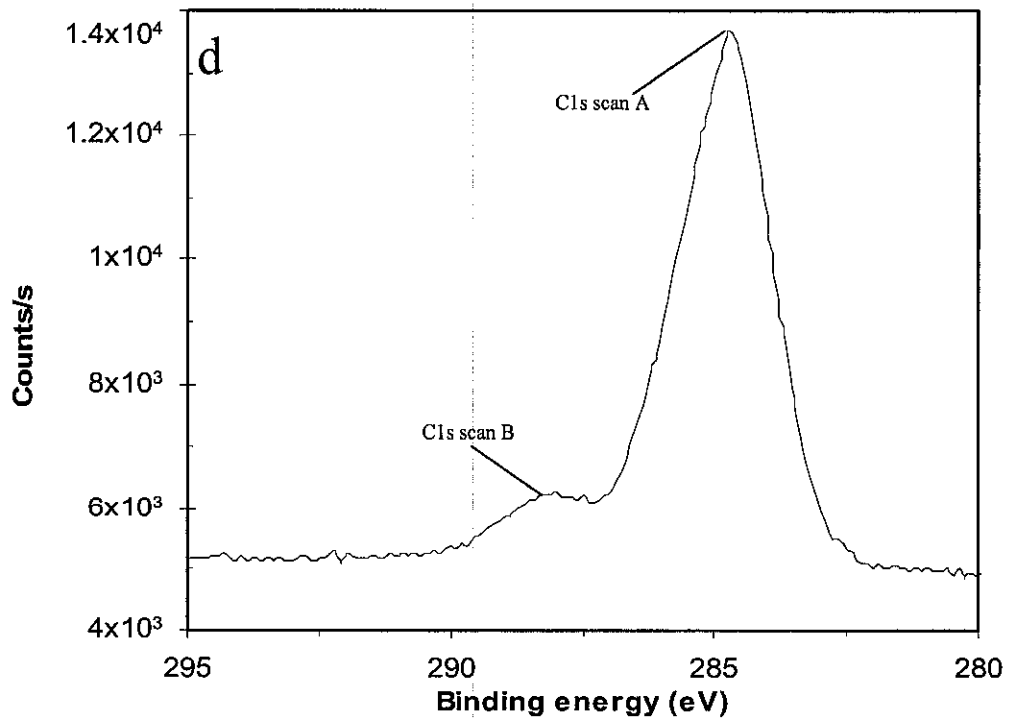
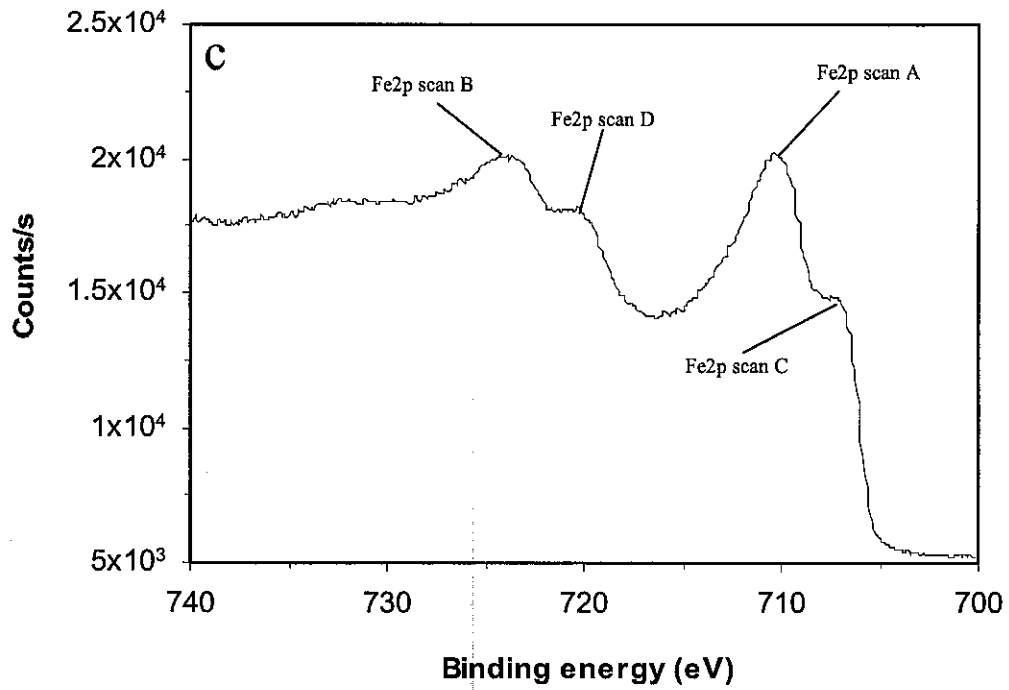
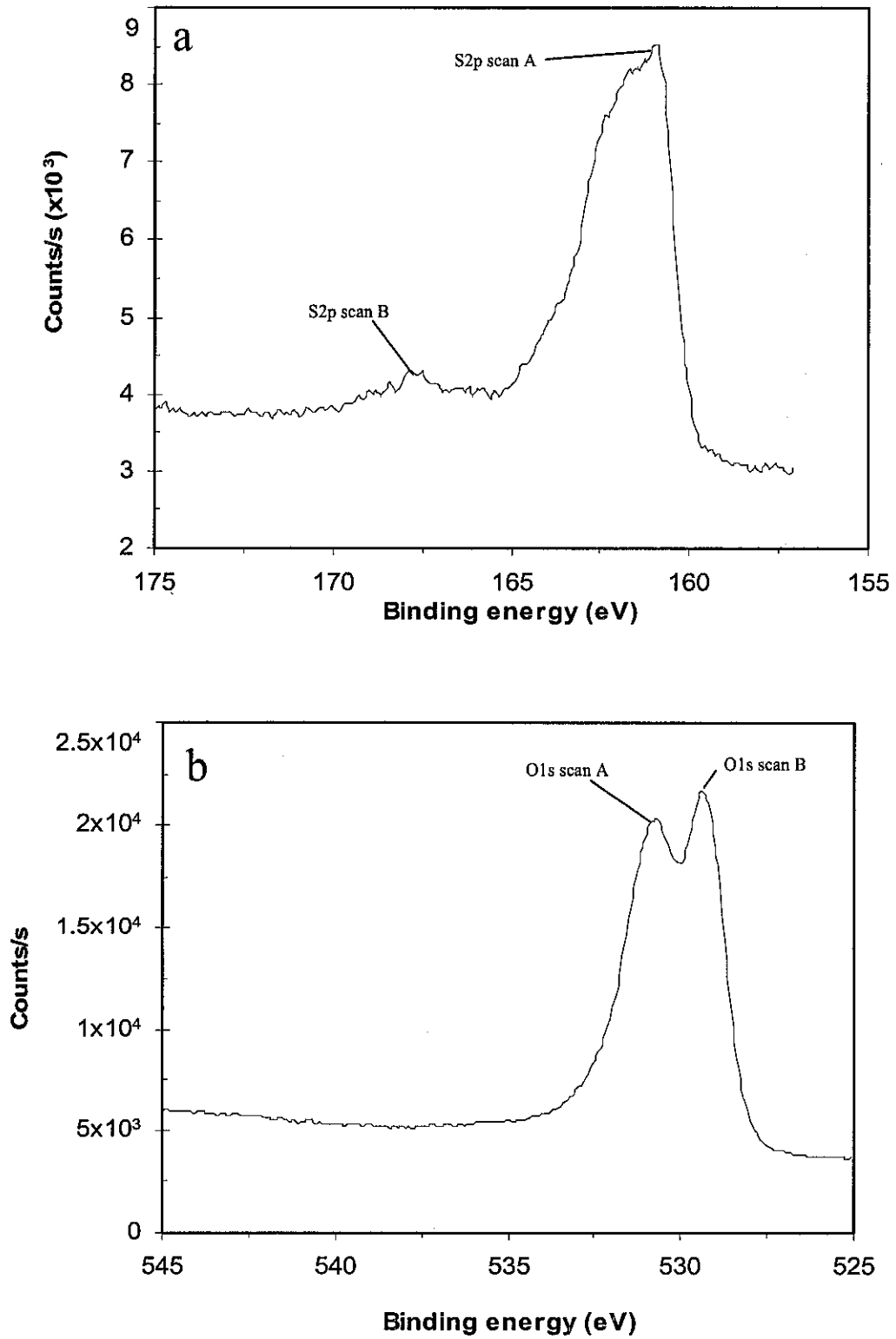


Figure 4.76 XPS spectra of X2 steel in the presence of 400 ppm sulphide, 200 ppm sulphite and 50 ppm lactate in the simulated solution: (a) S2p, (b) O1s, (c) Fe2p, (d) C1s.

Figure 4.77 shows XPS spectra for sulphite free solution with the presence of 200 ppm sulphide and 50 ppm lactate in the solution.



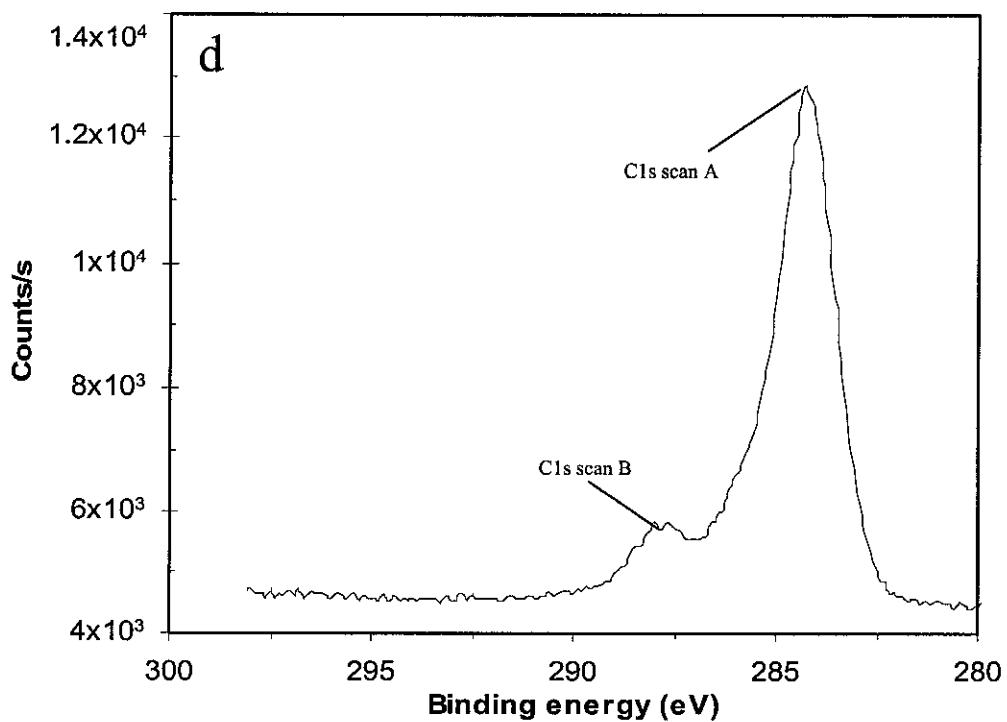
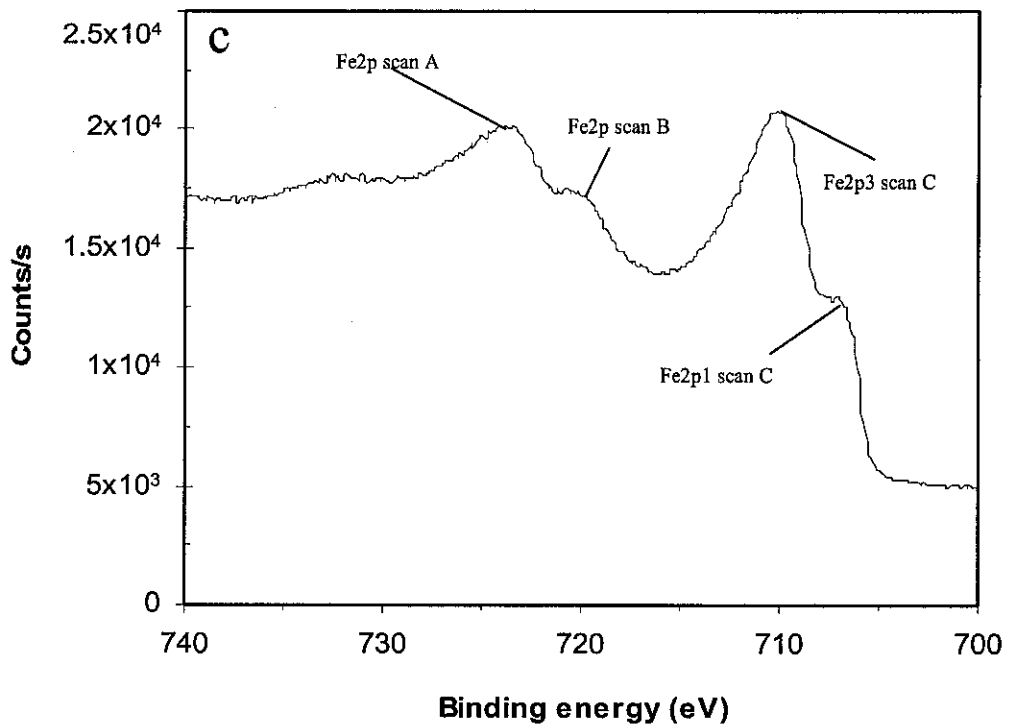


Figure 4.77 XPS spectra of X2 steel in the presence of 200 ppm sulphide and 50 ppm lactate in the simulated solution (no sulphite): (a) S2p, (b) O1s, (c) Fe2p, (d) C1s.

Figure 4.77 (a) shows that two peaks of S2p were observed in the spectra at 161.05 eV and 167.65 eV. The peak at 161.05 eV is corresponded to *mackinawite* FeS and more likely to *nanocrystalline mackinawite* (FeSn).[108] The peak at 167.65 eV is close to 168.3 corresponds to (SO₄²⁻) [98].

Moreover, two peaks of O1s were observed in the spectra as shown in Figure 4.77 (b). Those are at: 529.3 eV and 530.8 eV. The peak at 529.3 eV is corresponded to from Fe₃O₄ [99] and the peak at 530.8 eV is corresponded to FeCO₃ [100-102].

In addition, Figure 4.77 (c) shows that four peaks of Fe were observed in the spectra. Those are at: 706.88 eV; 709.88 eV; 719.78 eV and 723.5 eV. The peak at 706.88 eV is attributed to the peak of Fe2p1 from FeS₂ [54, 98]. The peak at 709.88 eV is attributed to the peak of Fe2p3 and close to the binding energy of FeO and Fe(III)-S (*greigite*) which are 709.5 and 709.2, respectively [97]. The peak at 719.98 is attributed to the peak of Fe2p from Fe⁰ (clean iron). The peak at 723.5 eV is attributed to the peak of Fe2p from FeO [106].

Lastly, Figure 4.77 (d) shows that two peaks of C1s were observed in the spectra. Those are at: 284.3 eV and 287.8 eV. The peak at 284.3 eV is corresponded to hydrocarbon [54] and the peak at 287.8 eV is corresponded to FeCO₃ [80, 100].

In summary, in sulphite free solution with the presence of 200 ppm sulphide and 50 ppm lactate in the simulated solution, it is observed that FeCO₃ and FeS film were formed on the electrode surface. However, it is noted that the typically FeS film formed were *mackinawite*, *greigite* and FeS₂.

4.3 Discussion

LPR, TP and EIS show that the addition of 50 ppm sulphide increased the corrosion rate of X52 steel. However, with the addition of 200 and 400 ppm sulphide, the corrosion rate was decreased.

In water, the sulphide ion (S^{2-}) reacts with available hydrogen forming H_2S . The amount of H_2S in the system could increase or decrease the rate of corrosion depending on the environment conditions *e.g.* pH, Fe^{2+} concentration, etc [64, 69, 110].

As shown by polarization curves, the increasing or decreasing of corrosion rate was affected by the cathodic site. It is seen from Table 4.10 that the slope of cathodic side (b_c) increased with addition of 50 ppm sulphide and decreased with addition of 200 and 400 ppm sulphide. In addition, it is also observed changes in the slope of anodic side (b_a). However, the changes of anodic side b_a are not significant as in cathodic side (b_c).

It is believed that the increased of cathodic reaction in both Tafel slope and redox potential is due to the change in the nature of cathode reaction in the presence of sulphide ions as shown in the following reactions [111-113].



In addition, with the presence of 200 and 400 ppm sulphide, a decreased of corrosion rate was observed which indicated the inhibitive characteristic of H_2S . Its inhibitive characteristic is related to the ferrous sulphide film, which is typically a thin *mackinawite* film [114-115]. The *mackinawite* film could further transform into a more stable film, *e.g.* *troilite*, *pyrhotite*, *greigite* and *pyrite* [116]. The XPS results confirmed the presence of FeS film in this study *i.e.* *pyrite*, *greigite* and *mackinawite*.

According to Ma *et al.* [68, 117], a probable mechanism of the inhibitive effect of H_2S could be described as follows:





The species FeSH^+ may be incorporated directly into a growing layer of *mackinawite* via Eq. (5.6)



Or it may be hydrolyzed to yield Fe^{2+} via Eq. (5.7)



Ma *et al.* [68] stated, if reaction (4.6) dominated the electrode surface, then the nucleation and growth of one or more of the iron sulphides, *i.e.* *mackinawite*, *cubic ferrous sulphide* or *troilite* could occur. However, the role of H_2S , accelerates or inhibits the rate of corrosion, also depending on the pH value. At lower pH values (<2), ferrous ion dissolve through reaction (4.7). As a result, less iron sulphide film is formed due to its high solubility at low pH. Meanwhile, at the pH values of 3-5, a *mackinawite* film is formed through reaction (4.6). The *mackinawite* could convert into *pyrrhotite*, *pyrite* and *troilite* which are a typicalall more stable and protective FeS film. At a pH of more than 5, *mackinawite* is the only observed product of corrosion.

Compare to the effect of sole sulphide (without the presence of other species), this study showed that the presence of other species change the behaviour of sulphide corrosion. Both studies showed inhibitive characteristic of FeS film. However, without the presence of other species, the typical FeS film formed is *mackinawite* [11], while with the presence of other species the typical FeS film formed are *pyrite*, *greigite* and *mackinawite*.

Moreover, LPR and EIS showed that the addition of sulphite to the solution increased the rate of X52 corrosion. Polarization curve showed that the addition of sulphite increased the cathodic side of the Tafel slope. Therefore, it can be concluded that the addition of sulphite increased the corrosion rate by increasing the cathodic reaction.

According to Hemmingsen and Valand [118], sulphite ion can be oxidized to sulphate ions or reduced to hydrogen sulphide with the first partial reaction to form dithionite ion ($S_2O_4^{2-}$). The reactions are shown below [118-119]:



In the SRB metabolism process, it is found that *Desulfovibrio* (*Desulfovibrio species*) reduced sulfite to sulphide as its partial end-product [120].

In addition, it is evidenced by EDAX results which shown S element in the solution containing sulphite. The detected S element might indicate that there is sulphide corrosion related product on the steel surface. XPS results confirmed the presence of *mackinawite* and *pyrite* on the steel surface in the solution containing sulphite. However, eventhough those stable FeS film formed (*mackinawite* and *pyrite*), the addition of sulphite caused the film became less compact and thinner. This caused the corrosive species easily adsorb on the metal surface yielding an increase in corrosion rate.

In the sulphite free solution (0 ppm sulphite, 200 ppm sulphide, 50 lactate), XPS results confirmed the presence of *mackinawite*, *gregite* and FeS_2 . In this case, the presence of *mackinawite*, *gregite* and FeS_2 might come from the sulphide in the simulated solution.

4.3.1 A possible physical mechanism of corrosion by SRB produced metabolism

Based on the results of electrochemical and surface morphology studies, a physical mechanism for corrosion caused by SRB metabolic products is proposed as shown in Figure 4.78.

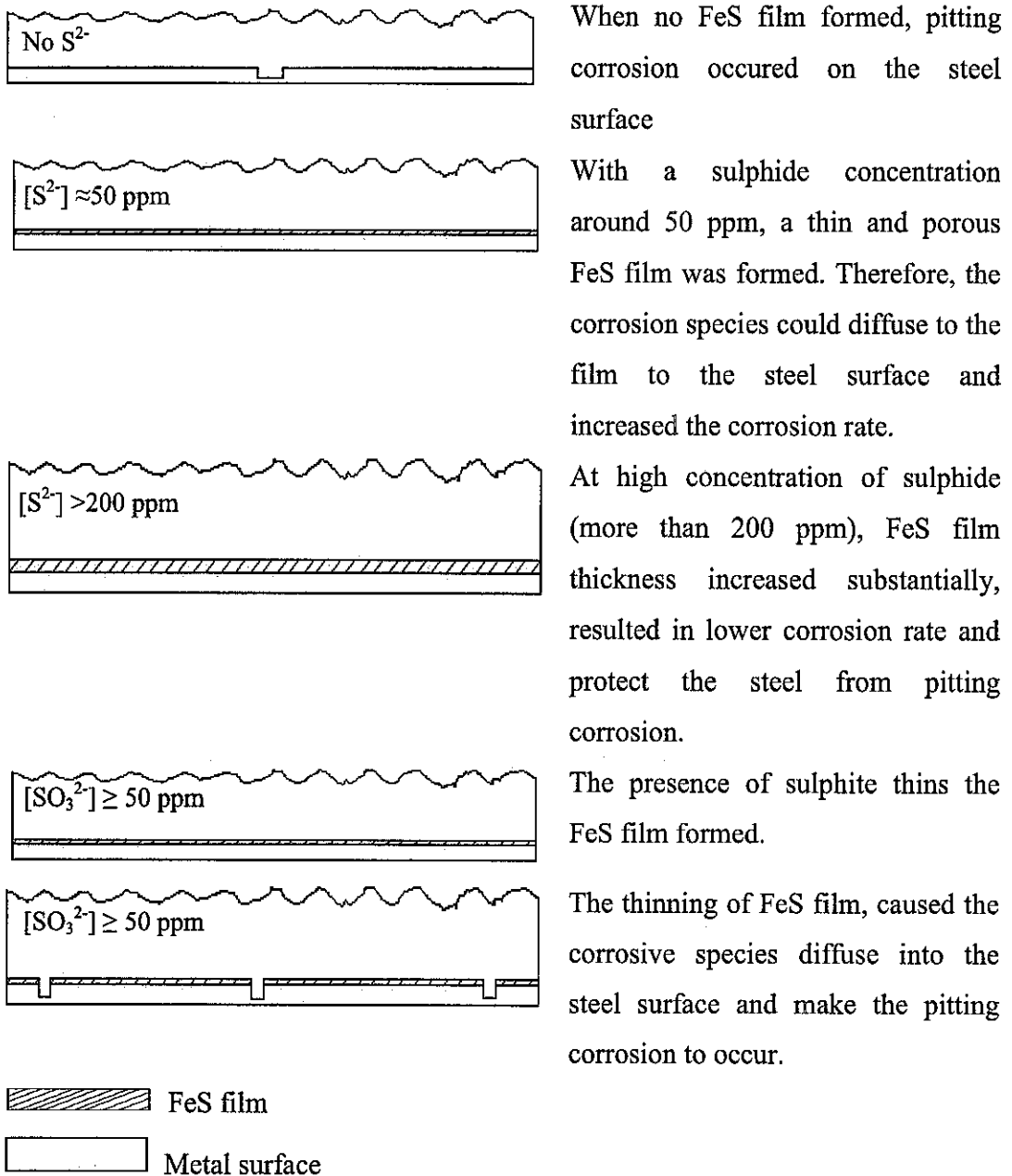


Figure 4.78 Sequence of possible physical mechanism that might occur in SRB corrosion.

In summary, our study shows that the FeS film formed is adherent on the steel surface. However, with the presence of sulphite, the FeS film becomes thinning and cause the corrosive species diffuse to the steel surface yielding localized corrosion.

4.3.2 Comparison with SRB experiment

As the corrosion geometry caused by SRB is in the form of uniform or localized corrosion (pitting), the corrosion comparison in this study were conducted in the uniform and pitting corrosion form.

For the comparison purposes, data from open source were used in this study. The data collected were based on SRB corrosion on carbon steel.

4.3.2.1 Uniform corrosion

Table 4.13 shows summary of carbon steel corrosion caused by SRB. It is seen that the corrosion rate caused by SRB on carbon steel is ranging from 0.3 – 0.5 mm/yr with the typically film formed is *mackinawite*. Unfortunately, not much work was conducted to measure the number of sulphide generated by SRB and its effect on carbon steel corrosion rate.

Kuang *et al.* [10] stated that the corrosion rate of carbon steel caused by SRB is highly related to the biotic sulphide produced. He observed that the presence of 50 ppm biotic sulphide during the bacteria death phase, caused corrosion rate around 0.34 mm/yr. Our experimental work showed that 50 ppm of abiotic sulphide (depending on the sulphite and lactate concentration), caused corrosion rate ranging from 0.67 to 2.5 mm/yr. This is inline with Thomas *et al.* [121] observation that the abiotic sulphide should result in higher corrosion rate than the biotic one. It is due to the fact that there is a difference between the measurable and the effective biotic sulphide involved on the corrosion process. Bacteria are known to produce copious slimes. Such a slime layer could provide a barrier to the transport of corrosive species

to the metal surface. An interspecies transfer of ions between bacteria could also render much of the measured sulphide unavailable to the steel. In contrast, all the abiotic sulphide added is able to contribute in the corrosion process.

Table 4.13 Summary of carbon steel corrosion caused by SRB

No	Author	E_{corr} (mV) (vs SCE)	Corrosion rate (mm/yr)	Film type
1.	Kuang <i>et al.</i> [10]	-726	0.34	-
2.	Sherar <i>et al.</i> [11]	-	-	FeS (<i>mackinawite</i>)
3.	Rainha and Fonseca [42]	-766	0.35	-
4.	Miranda <i>et al.</i> [45]	-	0.21 - 1.18	FeS
5.	Duan <i>et al.</i> [46]	-	0.3	-
6.	Gayosso <i>et al.</i> [49]	-	0.35 – 0.5	FeS
7.	Rao <i>et al.</i> [122]			FeS
8.	Jack <i>et al.</i> [123]	-	0.2	-
9.	Fonseca <i>et al.</i> [124]	-899	0.48	

In addition, the biotic FeS film formed is not limited to the *mackinawite*. The FeS film, typically *greigite*, was also characterized in the sample containing SRB [53-54]. Videla *et al.* [59] also found the presence of *greigite* in the SRB biofilm. Little and Lee concluded that on continued exposure to SRB, *mackinawite* alters to *greigite* [125].

In summary, it is observed that the abiotic studies conducted show reasonable corrosion rate with the SRB experiment. Additionally, the typical FeS film form in abiotic studies is similar with that found in SRB experiment *i.e.* *mackinawite* and *greigite*. Therefore, we believed that abiotic chemistry could be used to predict the corrosion caused by SRB.

4.3.2.2 Pitting corrosion

In order to compare the results of corrosion rate with the pitting depth found in the real SRB experiment/field, a pitting equivalent calculation was developed based on the corrosion rate obtained by LPR tests. The following assumptions were made for the pitting equivalent development:

1. The pit form is assumed in cylindrical and hemispherical form [126-127].
2. For cylindrical form, the pitting diameter is assumed equal to 160 μm . The diameter assumption was based on pitting diameter found in the SRB experiments [128] .

The pitting depth equivalent is derived from the following equation [129]:

$$Cr(\text{mm. / yr}) = \frac{87.6xW}{DxAxT} \quad 4.12$$

For the mass loss

$$W(\text{mg}) = \frac{CrxDxAxT}{87.6} \quad 4.13$$

$$W(\text{g}) = \frac{CrxDxAxT}{87600} \quad 4.14$$

Where,

W = weight loss (mg)

D = metal density (g/cm^3)

A = area of sample (cm^2)

T = exposure time (hours)

Cr = corrosion rate (mm/yr)

The total metal loss is equal to the volume of pit, therefore:

$$D(\text{g} / \text{cm}^3) = \frac{W}{V} \quad 4.15$$

$$V(\text{cm}^3) = \frac{W}{D} = \frac{1}{87600} CrxAxT \quad 4.16$$

For cylindrical geometry, the volume is $V = \frac{1}{4} \pi d^2 h$

Thus, the pit depth is

$$h(\text{cm}) = \frac{4xCrxAxT}{87600x\pi d^2} \quad 4.17$$

where d is pitting diameter in cm.

$$h(\mu\text{m}) = \frac{4xCrxAxT}{8.76x\pi d^2} \quad 4.18$$

For hemispherical geometry, the volume is $V = \frac{2}{3} \pi r^3$

Since the hemisphere depth is equal to its radius, therefore, the pitting depth is

$$r = \sqrt[3]{\frac{3V}{2\pi}} \quad 4.19$$

For the comparison purpose, a minimum value of 75 (μm) and a maximum value of 790 (μm) pitting depth is used. These data is taken based on the pitting depth found in the real SRB experiment [37] and in waste ater environment [130].

Figure 4.79 shows the comparison of calculated pitting depth equivalent results with SRB experiment in the cylindrical geometry. For hemispherical geometry, the comparison is shown in Figure 4.80.

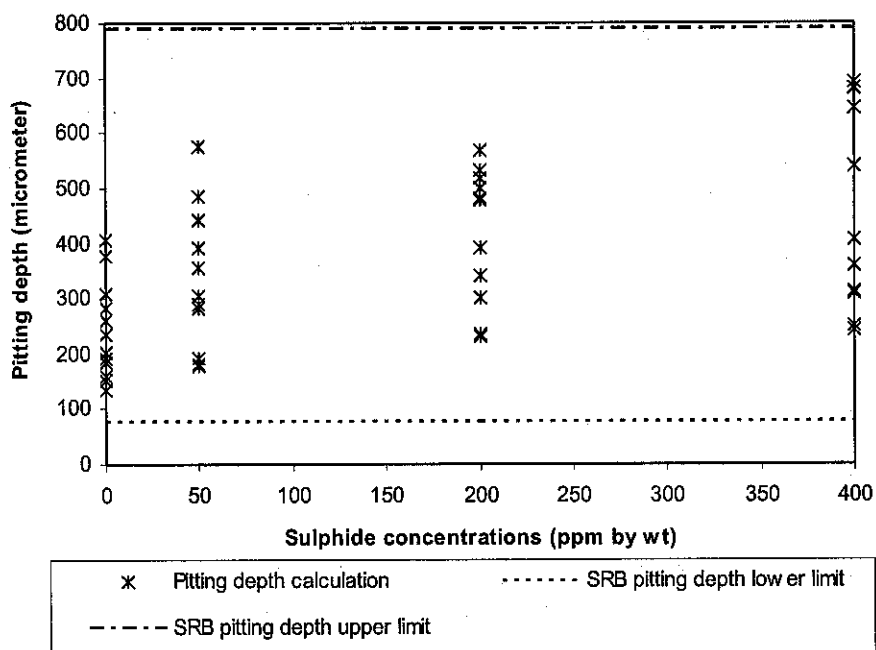


Figure 4.79 Comparison of pitting depth equivalent calculation with SRB experiments/field in cylindrical geometry.

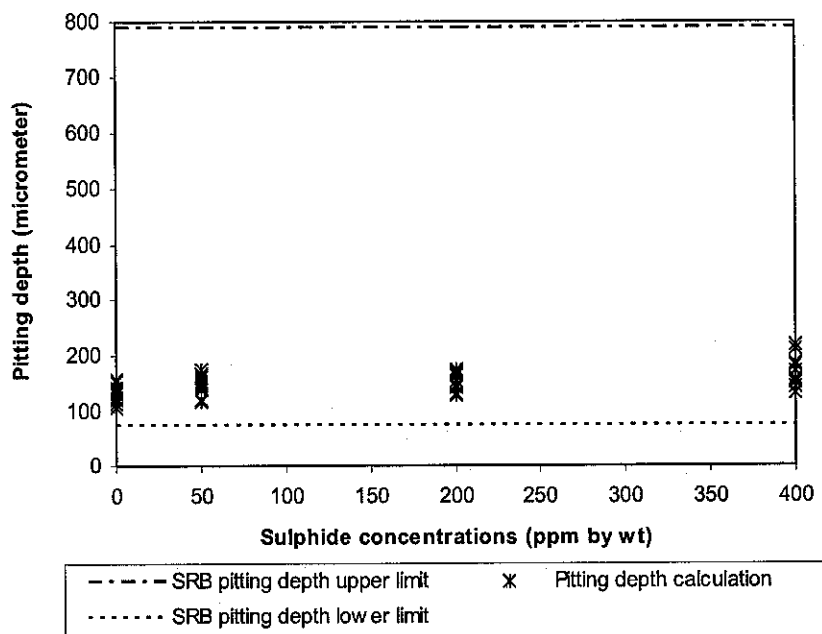


Figure 4.80 Comparison of pitting depth equivalent calculation with SRB experiments/field in hemispherical geometry.

Both results (in cylindrical and hemispherical geometry) show that the pitting depth equivalent calculation is in the range of minimum and maximum pitting depth of SRB experiment/environment. However, it is observed that the pitting equivalent in cylindrical geometry show more reasonable results than that of hemispherical geometry.

4.3.3 An empirical equation to predict SRB corrosion rate in temperature 25°C

Based on the LPR results obtained, an empirical equation was developed with three independent variables (sulphide, sulphite and lactate concentrations) and one dependent variable (corrosion rate). The curve fitting was conducted using Minitab 15[®] software.

Using multiple non-linear regression model, the regression equation obtained is

$$\log CR = 0.685 + 0.163 \log [\text{sulphite}] - 0.444 \log [\text{sulphide}] - 0.0711 \log [\text{lactate}] \quad 4.20$$

Where, *CR* is corrosion rate (mm/yr), [*Sulphite*] is sulphite concentration (ppm by weight), [*Sulphide*] is sulphide concentration (ppm by weight) and [*Lactate*] is lactate concentration (ppm by weight).

The statistical analyses of the regression model are given in Table 4.14-4.16 below:

Table 4.14 Analysis of variance

Source	DF	SS	MS	F	P
Regression	3	0.87138	0.29046	62.62	0.000
Residual error	23	0.10668	0.00464		
Total	26	0.97806			

Table 4.15 Analysis of coefficients results

Predictor	Coef	SE Coef	T	P
Constant	0.6849	0.1337	5.12	0.000
Log sulphite	0.16294	0.03491	4.67	0.000
Log sulphide	-0.44423	0.03491	-12.73	0.000
Log lactate	-0.07109	0.03491	-2.04	0.053

$S = 0.0681060$ $R^2 = 89.1\%$ R^2 (adj) = 87.7%

R^2 (pred) = 83.76%

Table 4.16 Sum of square

Source	DF	Seq SS
Log sulphite	1	0.10105
Log sulphide	1	0.75109
Log lactate	1	0.01923

Table 4.14 shows the analysis of variance of the regression. The analysis of variance described the confidence level of predicted parameters involved in the regression model. According to Table 4.14, the regression P-value is equal to 0.000 (lower than α value = 0.05) which means that the model estimated by the regression procedure has a level confidence of 95%. This also indicates that at least one independent variable are significant to dependent variable.

Table 4.15 shows that the p-values for the estimated coefficients of log sulphite and log sulphide are both 0.000, indicating that they are significantly related to log CR. The P-value for log lactate is 0.053, indicating that it is not related to log CR at an α -level of 0.05. Additionally, the sequential sum of squares (Table 4.16) indicates that the predictor log lactate doesn't explain a substantial amount of unique variance. This suggests that a model with log sulphide and log sulphite might be more appropriate.

The R^2 value indicates that the predictors explain 89.1% of the variance in log CR. The adjusted R^2 is 87.7%, which accounts for the number of predictors in the model. Both values indicate that the model fits the data well.

The predicted R^2 value is 83.76%. Because the predicted R^2 value is close to the R^2 and adjusted R^2 values, the model does not appear to be overfit and has adequate predictive ability.

The plot of residuals versus the fitted values is shown in Figure 4.81. It shows that the residuals distribution tends to be similar among smaller and higher fitted values, which may indicate the residuals have a constant variance. Figure 4.82 shows the normal probability plot has a consistent linear pattern consistent with a normal distribution.

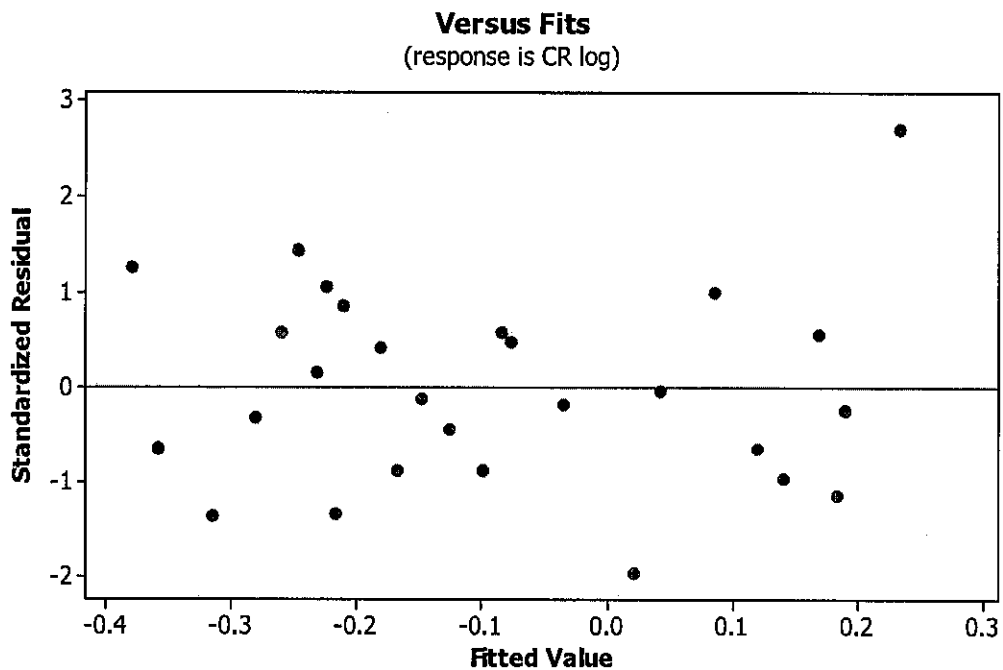


Figure 4.81 Plot of residuals vs fitted value

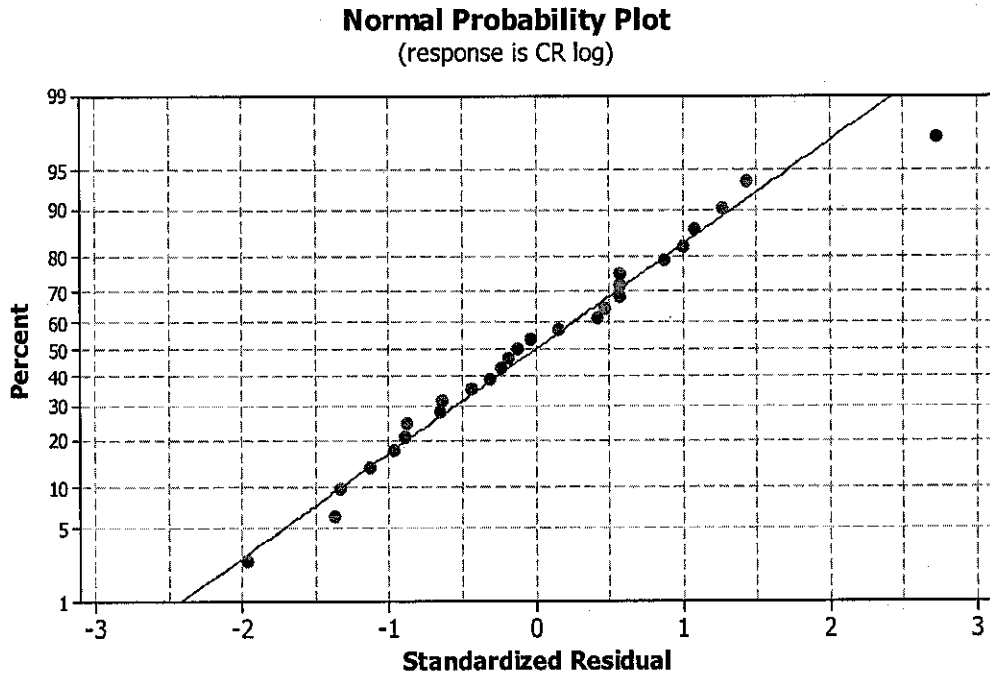


Figure 4.82 Normal plot of residuals

4.3.3.1 Equation validation with the data of SRB experiment

The empirical equation (Eq. 4.20) was validated with the corrosion rate data from SRB experiment. The summarized data in Table 4.13 shows that the corrosion rate of carbon steel caused by SRB is ranging from 0.2 to 1.18 mm/yr. Due to the limitation of information that consider the correlation of SRB metabolic species (sulphide and sulphite concentrations) and corrosion rate, the minimum and maximum value of SRB corrosion rate was taken regardless of the species concentrations.

Comparison of the empirical equation with SRB experimental data is shown in Figure. 4.83. It is seen that most of empirical calculation at various sulphide and sulphite concentrations are in the range of minimum and maximum value of SRB experiment. It can be concluded that the empirical equation developed has a good ability to predict the corrosion rate by SRB. However, it should be noted that the

calculation results are strongly related to the value of sulphide and sulphite concentrations.

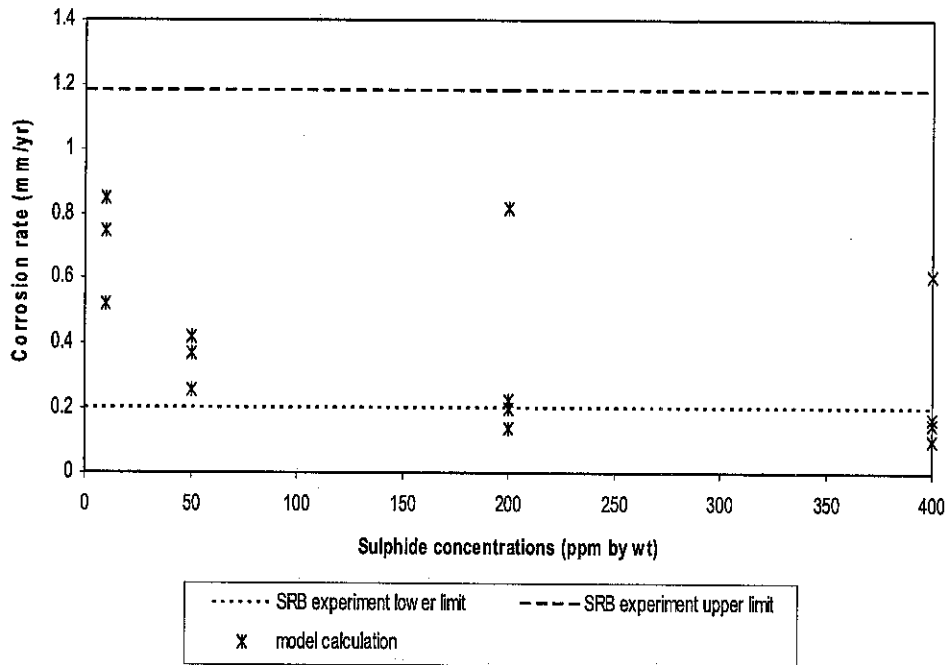


Figure 4.83 Comparison of the empirical equation with SRB experimental data

CHAPTER 5

CONCLUSIONS AND RECOMMENDATIONS

5.1 Conclusions

The main conclusions of the research are based on the new understanding in the area of corrosion mechanism, corrosion kinetics and corrosion prediction of SRB metabolic species.

1. The corrosiveness of system changes with the presence of various SRB metabolic species. It is observed that, sulphide, sulphite and lactate have more significant effects in increasing X52 steel corrosion rate compared to acetate, thiosulphate, pyruvate and lactate.
2. In the presence of 50 ppm sulphide, the corrosion rate of X52 steel increased. However, with the addition of 200 and 400 ppm sulphide, the corrosion rate of X52 steel decreased. The increasing of corrosion rate is due to the increasing of cathodic reaction in the presence of sulphide, whilst the decreasing of corrosion rate is due to the protectiveness of FeS film form *i.e.* *pyrite* and *mackinawite*. Additionally, it is observed that the corrosion rate of X52 steel increased with the addition of sulphite to the simulated solution. Sulphite increased the corrosion rate by increasing the cathodic reaction through its reduction to hydrogen sulphide.
3. The possible corrosion mechanism caused by dominant SRB metabolic species is summarized below:
 - When no FeS film formed, pitting corrosion occurred on the steel surface.

- The formation of FeS film is due to the presence of sulphide. With sulphide concentration around 50 ppm, a thin and porous FeS film was formed. Therefore, the corrosion species could diffuse to the steel surface and increased the corrosion rate.
 - At high concentration of sulphide (more than 200 ppm), FeS film thickness increased substantially, resulted in lower corrosion rate and protect the steel from pitting corrosion.
 - The FeS film formation was observed to be influenced by the presence of other metabolic species, particularly sulphite. The presence of sulphite thins the FeS film formed.
 - The thinning of FeS film allowed the corrosive species to diffuse to the steel surface which resulted in pitting corrosion.
4. Empirical relationships of corrosion rate with sulphide, sulphite and lactate ions concentrations at temperature 25°C is given by:

$$\log CR = 0.685 + 0.163 \log [\text{sulphite}] - 0.444 \log [\text{sulphide}] - 0.0711 \log [\text{lactate}]$$

Where, *CR* is corrosion rate (mm/yr), [*Sulphite*] is sulphite concentration (ppm by weight) and [*Sulphide*] is sulphide concentration (ppm by weight) and [*lactate*] is lactate concentration (ppm by weight).

5.2 Recommendations

The overall activities carried out in this study identify several recommendations for further exploration of the area. Those are as follows:

1. Corrosion type caused by SRB could be formed in general and localized corrosion. This study is limited to investigate the rate of corrosion in general form. In future works, it is suggested to conduct the experiment with patchy, galvanic or crevice geometry to investigate the localized corrosion.

2. SRB could grow well within the temperature range between 5°C and 50°C. However, this study was conducted only at the room temperature ($\pm 25^\circ \text{C}$). Investigation on the effect of temperature is suggested for further study.
3. In this study, comparisons of the results were conducted with the data from open literature. Most of the data available, only limited to the rate of corrosion and type of film formed. In future works, the actual biotic SRB experiments could be conducted to investigate the whole range of its metabolic products and its actual concentrations on the corrosion behaviour of X52 steel.
4. The prediction equation built could be used at temperature of 25°C only. Effect of temperature could be included in the future work.

References

- [1] H. C. Flemming, "Economical and technical overview," in *Microbiologically Influenced Corrosion of Materials*, E. Heitz, H. C. Flemming, and W. Sand, Eds., ed Berlin: Springer-verlag, 1996, pp. 6-14.
- [2] S. Maxwell, C. Devine, F. Rooney, and I. Spark, "Monitoring and control of bacterial biofilms in oilfield water handling systems," presented at the CORROSION/04, New Orleans, 2004.
- [3] K. Zhao, "Investigation of microbiologically influenced corrosion (MIC) and biocide treatment in anaerobic salt water and development of a mechanistic MIC model," PhD, Chemical Engineering, Ohio University, 2008.
- [4] W. S. Borenstein and P. B. Lindsay, "MIC failure of 304 stainless steel piping left stagnant after hydrotesting," *Materials performance*, vol. 41, pp. 70-73, 2002.
- [5] S. S. Abedi, A. Abdolmaleki, and N. Adibi, "Failure analysis of SCC and SRB induced cracking of a transmission oil products pipeline," *Engineering Failure Analysis*, vol. 14, pp. 250-261, 2007.
- [6] A. K. Tiller, "Some case histories of corrosion failures induced by bacteria," *International Biodeterioration*, vol. 24, pp. 231-237, 1988.
- [7] C. A. H. V. W. Kuhr and L. S. v. d. Vlught, "The graphitization of cast iron as an electrobiochemical process in anaerobic soils," *Water*, vol. 18, pp. 147-165, 1934.
- [8] T. Dominique and S. Wolfgang, "Microbially influenced corrosion," in *Corrosion mechanism in theory and practice*, P. Marcus, Ed., ed New York: Marcel Dekker, 2002, pp. 563-603.

- [9] R. C. Newman, K. Rumash, and B. J. Webster, "The effect of pre-corrosion on the corrosion rate of steel in neutral solutions containing sulphide: relevance to microbially influenced corrosion," *Corrosion Science*, vol. 33, pp. 1877-1884, 1992.
- [10] F. Kuang, J. Wang, L. Yan, and D. Zhang, "Effects of sulfate-reducing bacteria on the corrosion behavior of carbon steel," *Electrochimica Acta*, vol. 52, pp. 6084-6088, 2007.
- [11] B. W. A. Sherar, I. M. Power, P. G. Keech, S. Mitlin, G. Southam, and D. W. Shoesmith, "Characterizing the effect of carbon steel exposure in sulfide containing solutions to microbially induced corrosion," *Corrosion Science*, vol. 53, pp. 955-960, 2011.
- [12] R. Javaherdashti, "A review of some characteristics of MIC caused by Sulfate reducing bacteria: past, present and future," *Anti-corrosion methods and materials*, vol. 46, pp. 173-180, 1999.
- [13] "Hydrogen Transportation Pipelines," European Industrial Gases association 2004.
- [14] B. Vargas-Arista, J. S. Romero, C. A. Chavez, A. Albiter, and J. M. Hallen, "Deterioration of the Corrosion Resistance of Welded Joints in API5L X52 Steel Isothermally Aged," *International Journal of Electrochemical Science*, vol. 6, pp. 367-378, 2011.
- [15] M. d. Romero, L. U. d. Zulia, S. C. Urdaneta, M. Barrientos, G. Romero, and U. L. Olivias, "Correlation between desulfovibrio sessile growth and OCP, hydrogen permeation, corrosion products and morphological attack of iron," presented at the CORROSION/04, New Orleans, 2004.

- [16] Z. Lewandoski, T. E. Cloete, S. C. Dexter, W. H. Dickinson, Y. Kikuchi, B. Little, F. Mansfeld, H. Rossmore, W. Sand, and H. A. Videla, "MIC issues: commentary from the corrosion 2002 MIC panel discussion," presented at the CORROSION/03, San Diego, 2003.
- [17] C. M. Jobalia, A. Hu, T. Gu, and S. Nestic, "Biochemical Engineering Approaches to MIC," presented at the CORROSION/05, Houston, 2005.
- [18] B. J. Little, R. I. ray, and R. K. Pope, "The relationship between corrosion and the biological sulfur cycle," presented at the CORROSION/00, Houston, 2000.
- [19] D. R. Lovley and E. J. P. Philips, "Novel process for anaerobic sulfate production from elemental sulfur by sulfate reducing bacteria," *Applied Environmental Microbiology*, vol. 60, pp. 2394-2399, 1994.
- [20] R. Javaherdasty, "A review of some characteristic of MIC caused by sulfate reducing bacteria: past, present and future," *Anti Corrosion Methods and Materials*, vol. 46, pp. 173-180, 1999.
- [21] S. W. Borenstein, *Microbiologically influenced corrosion handbook*. Cambridge: Woodhead Publishing Limited, 1994.
- [22] W. P. Iverson and G. J. Olson, "Problems related to sulfate reducing bacteria in the petroleum industry," in *Petroleum Microbiology Atllass*, R. M, Ed., ed New York: Macmilan publishing company, 1984.
- [23] G. J. Tortora, B. R. Funke, and C. L. Case, *Microbiology: An Introduction*, Eight ed. San Fransisco: Pearson, 2004.
- [24] E. C. S. Chan, "Microbial nutrition and basic metabolism," in *The Handbook of Water and Wastewater Microbiology*, D. Mara and N. Horan, Eds., ed London: Academic Press, 2003.

- [25] J. Starosvetsky, D. Starosvetsky, and R. Armon, "Identification of microbiologically influenced corrosion (MIC) in industrial equipment failures," *Engineering Failure Analysis*, vol. 14, pp. 1500-1511, 2007.
- [26] G. Gobbi, G. Zappia, and C. Sabbioni, "Sulphite quantification on damaged stones and mortars," *Asmoperic Environment*, vol. 32, pp. 783-789, 1998.
- [27] L. L. Barton and R. M. Plunkett, "Sulfate-reducing-bacteria: environmental and technology aspects," in *Encyclopedia of environmental microbiology*, G. Bitton, Ed., ed New York: Wiley-Interscience, 2002, pp. 3087-3096.
- [28] R. D. Bryant, W. Jansen, J. Bovin, e. J. Laishley, and J. W. Costerton, "Effect of hydrogenase and mixed sulfate reducing bacteria populations on the corrosion of steel," *Applied Environmental Microbiology*, vol. 57, pp. 2804-2809, 1991.
- [29] A. S. Traore, C. E. Hatchikian, J. P. Belaich, and J. L. Gall, "Microcalorimetric studies of the growth of sulfate-reducing bacteria: energetics of *Desulfovibrio vulgaris* growth," *Journal of Bacteriology*, vol. 145, pp. 191-199, 1981.
- [30] T. Wind and R. Conrad, "Sulfur compounds, potential turnover of sulfate and thiosulfate, and numbers of SRB in planted and unplanted paddy soil," *Fens Microbiology Ecology*, vol. 18, pp. 257-266, 1995.
- [31] W. Lee, "Corrosion of mild steel under an anaerobic biofilm," PhD, Chemistry, Montana State University, 1990.
- [32] R. H. King, J. D. A. Miller, and J. S. smith, "Corrosion of mild steel by iron sulphide," *British corrosion Journal*, vol. 8, p. 137, 1973.

- [33] J. A. Costello, "Cathodic depolarization by sulphate reducing bacteria," *South African Journal of Science*, vol. 70, p. 202, 1969.
- [34] S. D. Silva, R. Basseguy, and A. Bergel, "A new definition of cathodic depolarization in anaerobic microbially influenced corrosion," presented at the CORROSION/02, Denver, 2002.
- [35] M. F. d. Romero, "The mechanism of SRB action in MIC based on sulphide corrosion and iron sulphide corrosion product," presented at the CORROSION/05, Houston, 2005.
- [36] L. Ocando, M. F. d. Romero, O. Perez, O. T. d. Rincon, and R. Ortiz, "Evaluation of pH and H₂S on biofilms generated by sulphate reducing bacteria: influence of ferrous ions," presented at the CORROSION/07, Nashville, 2007.
- [37] T. Gu and D. Xu, "Demistifying MIC mechanism," presented at the CORROSION/10, Texas, 2010.
- [38] T. Gu, K. Zhao, and S. Nescic, "A new mechanistic model for MIC based on biocatalytic cathodic sulphate reduction theory," presented at the CORROSION/09, Atlanta, 2009.
- [39] A. Darwin, K. Annadorai, and K. Heidesbach, "Prevention of corrosion in carbon steel pipelines containing hydrotest water-an overview " presented at the CORROSION/10, San Antonio, Texas, 2010.
- [40] R. Heidersbach, *Metallurgy and corrosion control in oil and gas production*: John Wiley & Sons, 2011.

- [41] S. Al-Sulaiman, A. Al-Mithin, A. Al-Shamari, and M. Islam, "Microbiologically influenced corrosion of a crude oil pipeline," presented at the CORROSION/10, San Antonio, Texas, 2010.
- [42] V. L. Rainha and I. T. E. Fonseca, "Kinetic studies on the SRB influenced corrosion of steel: A first approach," *Corrosion Science*, vol. 39, pp. 807-813, 1997.
- [43] M. Amaya and R. Perez, "Bacterial influence on the corrosion of API-XL70 steel," presented at the CORROSION/02, Denver, 2002.
- [44] X. D. Benetton and H. Castaneda, "SRB biofilm growth and influence in corrosion monitoring by electrochemical impedance spectroscopy," presented at the CORROSION/05, Houston, 2005.
- [45] E. Miranda, M. Bethencourt, F. J. Botana, M. J. Cano, J. M. Sánchez-Amaya, A. Corzo, J. G. de Lomas, M. L. Fardeau, and B. Ollivier, "Biocorrosion of carbon steel alloys by an hydrogenotrophic sulfate-reducing bacterium *Desulfovibrio capillatus* isolated from a Mexican oil field separator," *Corrosion Science*, vol. 48, pp. 2417-2431, 2006.
- [46] J. Duan, S. Wu, X. Zhang, G. Huang, M. Du, and B. Hou, "Corrosion of carbon steel influenced by anaerobic biofilm in natural seawater," *Electrochimica Acta*, vol. 54, pp. 22-28, 2008.
- [47] Z. Dzierzewicz, B. Cwalina, E. Chodurek, and T. Wilczok, "The relationship between microbial metabolic activity and biocorrosion of carbon steel," *Research in Microbiology*, vol. 148, pp. 785-793, 1997.
- [48] M. J. H. Gayosso, G. Z. Olivares, R. G. Esquivel, J. L. M. Mendoza, and A. A. Padilla, "Evaluation of corrosion rate on API XL 52 steel, induced by a

- microbial consortium, isolated from a gas pipeline," presented at the CORROSION/04, New Orleans, 2004.
- [49] M. J. H. Gayosso, G. Z. Olivares, N. R. Ordaz, C. J. Ramirez, R. G. Esquivel, and A. P. Viveros, "Microbial consortium influence upon steel corrosion rate, using polarisation resistance and electrochemical noise techniques," *Electrochimica Acta*, vol. 49, pp. 4295-4301, 2004.
- [50] F. P. d. Frank, D. S. B. Bias, and I. R. d. Melo, "Effect of introduction of CO₂ on the formation of biofilms/biocorrosion on AISI 1018 carbon steel surfaces exposed in a dynamic system," presented at the CORROSION/09, Atlanta, 2009.
- [51] J. L. M. Mendoza, R. G. Esquivel, A. A. P. Viveros, L. Martinez, M. M. B. C. A. Ch, and O. Flores, "Study of internal MIC in pipelines of sour gas, mixed with formation waters," presented at the CORROSION/01, Houston, 2001.
- [52] S. Y. Li, Y. G. Kim, and Y. T. Kho, "Corrosion behaviour of carbon steel influenced by sulphate reducing bacteria in soil environments," presented at the CORROSION/03, San Diego, 2003.
- [53] J. P. Gramp, J. M. Bigham, F. S. Jones, and O. H. Tuovinen, "Formation of Fe-sulfides in cultures of sulfate reducing bacteria," *Journal of Hazardous Materials*, vol. 174, pp. 1062-1067, 2010.
- [54] R. B. Herbert Jr, S. G. Benner, A. R. Pratt, and D. W. Blowes, "Surface chemistry and morphology of poorly crystalline iron sulfides precipitated in media containing sulfate-reducing bacteria," *Chemical Geology*, vol. 144, pp. 87-97, 1998.

- [55] X. Zhao, J. Duan, B. Hou, and S. Wu, "Effect of sulfate reducing bacteria on corrosion behaviour of mild steel in sea mud," *Journal of Material Sciences and Technology*, vol. 23, pp. 323-328, 2007.
- [56] A. Hu, "Investigation of sulfate reducing bacteria growth behaviour for the mitigation of microbiologically influenced corrosion (MIC)," MSc, Chemical Engineering, Ohio University, 2004.
- [57] C. M. Jobalia, "The role of a biofilm and its characteristics in microbiologically influenced corrosion of steel," MSc, Chemical Engineering Ohio University, 2004.
- [58] H. A. Videla, R. G. Edyvean, C. Swords, and M. F. L. d. Mele, "Comparative study of the product films formed in biotic and abiotic media," presented at the CORROSION/99, Texas, 1999.
- [59] H. A. Videla, C. L. Swords, and G. J. Edyvean, "Corrosion products and biofilm interactions in the SRB influenced corrosion of steel," presented at the CORROSION/02, Colorado, 2002.
- [60] B. Brown, K. Lee, and S. Nesic, "Corrosion in multiphase flow containing small amount of H₂S," presented at the CORROSION/03, San Diego, 2003.
- [61] S. N. Smith and M. W. Joosten, "Corrosion of carbon steel by H₂S in CO₂ containing oilfield environments," presented at the CORROSION/06, San Diego, 2006.
- [62] M. L. Fransson, "Understanding corrosion inhibition: A surface science study of thiophene derivatives on iron surfaces in gaseous and liquid system," PhD, Department of Chemistry, Princeton University, 2005.

- [63] D. W. shoesmith, P. Taylor, M. G. Bailey, and d. G. Owen, "The formation of ferrous monosulfide polymorphs during the corrosion of iron by aqueous hydrogen sulphide at 21°C," *Journal electrochemical Society*, vol. 125, pp. 1007-1015, 1980.
- [64] W. Sun, "Kinetics of iron carbonate and iron sulphide scale formation in CO₂/H₂S corrosion," PhD, Chemical Engineering Department, Ohio University, 2006.
- [65] S. N. Smith and J. L. Pacheco, "Prediction of corrosion in slightly sour environments," presented at the CORROSION/02, New Orleans, 2002.
- [66] S. N. Smith and E. J. Wright, "Prediction of minimum H₂S level required for slightly sour corrosion," presented at the CORROSION/94, Houston, 1994.
- [67] T. Hemmingsen, F. Fusek, and E. Skavås, "Monitoring of the corrosion process on sulphide film formation with electrochemical and optical measurements," *Electrochimica Acta*, vol. 51, pp. 2919-2925, 2006.
- [68] H. Ma, X. Cheng, G. Li, S. Chen, Z. Quan, S. Zhao, and L. Niu, "The influence of hydrogen sulfide on corrosion of iron under different conditions," *Corrosion Science*, vol. 42, pp. 1669-1683, 2000.
- [69] J. Tang, Y. Shao, J. Guo, T. Zhang, G. Meng, and F. Wang, "The effect of H₂S concentration on the corrosion behavior of carbon steel at 90°C," *Corrosion Science*, vol. 52, pp. 2050-2058, 2010.
- [70] Multicorp, ed: Institute for Corrosion and Multiphase Technology, Ohio University.
- [71] K. Lee, "A mechanistic modelling of CO₂ corrosion of mild steel in the presence of H₂S," PhD, Chemical Engineering Ohio University, 2004.

- [72] A. K. Agrawal, C. Durr, and G. H. Koch, "Films and corrosion rates of AISI 1018 carbon steel in saline solutions in the presence of H₂S and CO₂ at temperature up to 175°F," presented at the CORROSION/04, New Orleans, 2004.
- [73] J. Kvarekval, R. Nyborg, and M. Seirsten, "Corrosion product films on carbon steel in semi sour CO₂/H₂S environments," presented at the CORROSION/02, Denver, 2002.
- [74] M. Singer, B. Brown, A. Camacho, and S. Nestic, "Combined effect of CO₂, H₂S and acetic acid on bottom of the line corrosion," presented at the CORROSION/07, Colorado, 2007.
- [75] C. J. Carew, "CO₂ corrosion of L-80 steel in simulated oil well conditions," presented at the CORROSION/02, Denver, 2002.
- [76] G. Schmitt and M. Papenfuss, "Understanding localized CO₂ corrosion of carbon steel from physical properties of iron carbonate scales fracture to mechanical properties of iron carbonate scale," presented at the CORROSION/99, Texas, 1999.
- [77] K. S. George and S. Nestic, "Electrochemical investigation and modelling of carbon dioxide corrosion of carbon steel in the presence acetic acid," presented at the CORROSION/04, New Orleans, 2004.
- [78] L. zhang, J. Yang, Jianbo, Sun, Minxu, and Lu, "Effect of pressure on wet CO₂/H₂S corrosion of pipeline steel," presented at the CORROSION/09, Atlanta, 2009.
- [79] M. V.D, S. P. Shatilo, K. K. Gumerskii, and V. A. Belyaev, "Effect of oxygen and hydrogen sulphide on carbon dioxide corrosion of welded structures of oil

- and gas installations," *Chemical and Petroleum Engineering*, vol. 36, pp. 125-130, 2000.
- [80] Y.-S. Choi, S. Nesic, and S. Ling, "Effect of H₂S on the CO₂ corrosion of carbon steel in acidic solutions," *Electrochimica Acta*, vol. 56, pp. 1752-1760, 2011.
- [81] E. Abelev, J. Sellberg, T. A. Ramanarayanan, and S. L. Bernasek, "Effect of H₂S on Fe corrosion in CO₂ saturated brine," *Journal of Material Sciences and Technology*, vol. 44, pp. 6167-6181, 2009.
- [82] M. C. Ismail, "Prediction of CO₂ corrosion with the presence acetic acid," PhD, School of Corrosion and Protection Centre, University of Manchester Institute of Science and Technology, 2006.
- [83] S. Nesic, J. Postlethwaite, and M. Vrhovac, "CO₂ corrosion of carbon steel- from mechanistic to empirical modeling," presented at the CORROSION/97, Houston, 1997.
- [84] C. G. Peng, S. Y. Suen, and J. K. Park, "Modeling of anerobic corrosion influenced by sulfate-reducing bacteria," *Water Environment Research*, vol. 66, pp. 707-715, 1994.
- [85] M. M. Al-Darbi, K. Agha, and M. R. Islam, "Modeling and simulation of the pitting microbiologically influenced corrosion in different industrial system," presented at the CORROSION/05, Houston, 2005.
- [86] J. D. Garber, K. Knierim, J. Acuna, and K. C. Deokar, "Modeling pitting corrosion in a CO₂ system containing bacteria," presented at the CORROSION/08, Houston, 2008.

- [87] G. H. Jeffery, J. Basset, J. Mendham, and R. C. Denney, *Vogel's textbook of quantitative chemical analysis*, fifth ed.: Longman scientific and technical, 1989.
- [88] B. S. Furniss, A. J. Hannaford, P. W. G. Smith, and A. R. Tatchell, *Vogel's textbook of practical organic chemistry*: Longman scientific and technical, 1989.
- [89] ASTM, "Standard practice for calculation of corrosion rates and related information from electrochemical measurements," ed, 2010.
- [90] M. Stern and A. L. Geary, "Theoretical analysis of the shape of polarization curves," *Journal Electro Chemical Society*, vol. 104, pp. 56-63, 1957.
- [91] Available: www.abc.chemistry.bsu.by/vi/analyser/program/program.htm
- [92] F. Esaka, H. Yamamoto, N. Matsubayashi, Y. Yamada, M. Sasase, K. Yamaguchi, S. Shamoto, M. Magara, and T. Kimura, "X-ray photoelectron and X-ray absorption spectroscopic study on β -FeSi₂ thin films fabricated by ion beam sputter deposition," *Applied Surface Science*, vol. 256, pp. 3155-3159, 2010.
- [93] T. J. Finnegan and R. C. Corey, "Removal of Corrosion Products from Iron," *Industrial & Engineering Chemistry Research*, vol. 5, pp. 89-90, 1933.
- [94] H. Firmanto, "Reaction layers in diffusion bonded of sialon to ferritic steel," PhD, Mechanical Engineering Universiti Teknologi PETRONAS, 2011.
- [95] J. Q. Wang, A. Atrens, D. R. Cousens, P. M. Kelly, C. Nockolds, and S. Bulcock, "Microstructure of X52 and X65 pipelines steel," *Journal of Materials Science*, vol. 34, pp. 1721-1728, 1999.

- [96] S. W. Knipe, J. R. Myroft, A. R. Pratt, H. W. Nesbitt, and G. M. Bancroft, "X-ray photoelectron spectroscopy study of water adsorption on iron sulphide minerals," *Geochimica et Cosmochimica Acta*, vol. 59, pp. 1079-1090, 1995.
- [97] M. Mullet, S. Boursiquot, M. Abdelmoula, J.-M. Génin, and J.-J. Ehrhardt, "Surface chemistry and structural properties of mackinawite prepared by reaction of sulfide ions with metallic iron," *Geochimica et Cosmochimica Acta*, vol. 66, pp. 829-836, 2002.
- [98] A. L. Neal, S. Techkarnjanaruk, A. Dohnalkova, D. McCready, B. M. Peyton, and G. G. Geesey, "Iron sulfides and sulfur species produced at hematite surfaces in the presence of sulfate-reducing bacteria," *Geochimica et Cosmochimica Acta*, vol. 65, pp. 223-235, 2001.
- [99] S. r. chowdhury, e. K. Yanful, and A. R. Pratt, "Arsenic removal from aqueous solutions by mixed magnetite-maghemite nanoparticles," *Environmental earth sciences*, 2010.
- [100] J. K. Heuer and J. F. Stubbins, "An XPS characterization of FeCO₃ films from CO₂ corrosion," *Corrosion Science*, vol. 41, pp. 1231-1243, 1999.
- [101] D. A. López, W. H. Schreiner, S. R. de Sánchez, and S. N. Simison, "The influence of inhibitors molecular structure and steel microstructure on corrosion layers in CO₂ corrosion: An XPS and SEM characterization," *Applied Surface Science*, vol. 236, pp. 77-97, 2004.
- [102] S. L. Wu, Z. D. Cui, F. He, Z. Q. Bai, S. L. Zhu, and X. J. Yang, "Characterization of the surface film formed from carbon dioxide corrosion on N80 steel," *Materials Letters*, vol. 58, pp. 1076-1081, 2004.
- [103] T. Fujii, F. M. F. d. Groot, G. A. Sawatzky, F. C. Vooght, T. Hibma, and K. Okada, "In situ XPS analysis of various iron oxide films grown by NO₂-

- assisted molecular-beam epitaxy," *Physical review B*, vol. 59, pp. 3195-3202, 1999.
- [104] A. Goordarzi, Y. Sahoo, M. T. Swihart, and P. N. Prasad, "Aqueous ferrofluid of citric acid coated magnetite particles," *Materials research society symposium proceeding*, vol. 789, pp. N6.6.1-N6.6.6, 2004.
- [105] P. C. J. Graat and M. A. J. Somers, "Simultaneous determination of composition and thickness of thin iron-oxide films from XPS Fe 2p spectra," *Applied Surface Science*, vol. 100–101, pp. 36-40, 1995.
- [106] S. J. Roosendaal, B. van Asselen, J. W. Elsenaar, A. M. Vredenberg, and F. H. P. M. Habraken, "The oxidation state of Fe(100) after initial oxidation in O₂," *Surface Science*, vol. 442, pp. 329-337, 1999.
- [107] G. Zou, K. Xiong, C. Jiang, H. Li, T. Li, J. Du, and Y. Qian, "Fe₃O₄ Nanocrystals with Novel Fractal," *The Journal of Physical Chemistry B*, pp. 18356-18360, 2005.
- [108] M. Langumier, R. Sabot, R. Obame-Ndong, M. Jeannin, S. Sable, and P. Refait, "Formation of Fe (III)-containing mackinawite from hydroxysulphate green rust by sulphate reducing bacteria," *Corrosion science*, vol. 51, pp. 2694-2702, 2009.
- [109] J.-A. Bourdoiseau, M. Jeannin, C. Remazeilles, R. Sabot, and P. Refait, "The transformation of mackinawite into greigite studied by Raman spectroscopy," *Journal of Raman spectroscopy*, vol. 42, pp. 496-504, 2010.
- [110] Z. F. Yin, W. Z. Zhao, Z. Q. Bai, Y. R. Feng, and W. J. Zhou, "Corrosion behavior of SM 80SS tube steel in stimulant solution containing H₂S and CO₂," *Electrochimica Acta*, vol. 53, pp. 3690-3700, 2008.

- [111] I. Betova, M. Bojinov, O. Hyökyvirta, and T. Saario, "Effect of sulphide on the corrosion behaviour of AISI 316L stainless steel and its constituent elements in simulated Kraft digester conditions," *Corrosion Science*, vol. 52, pp. 1499-1507, 2010.
- [112] M. C. Fatah, M. C. Ismail, B. Ari-Wahjoedi, and K. A. Kurnia, "Effects of sulphide ion on the corrosion behaviour of X52 steel in a carbon dioxide environment at temperature 40°C," *Materials Chemistry and Physics*, vol. 127, pp. 347-352, 2011.
- [113] K. Rahmouni, M. Keddou, A. Srhiri, and H. Takenouti, "Corrosion of copper in 3% NaCl solution polluted by sulphide ions," *Corrosion Science*, vol. 47, pp. 3249-3266, 2005.
- [114] J. L. Kun-Lin and S. Nescic, "EIS investigation of CO₂/H₂S corrosion," presented at the CORROSION/04, New Orleans, 2004.
- [115] W. Sun and S. Nescic, "A mechanistic model of H₂S corrosion of mild steel," presented at the CORROSION/07, Colorado, 2007.
- [116] M. A. Veloz and I. González, "Electrochemical study of carbon steel corrosion in buffered acetic acid solutions with chlorides and H₂S," *Electrochimica Acta*, vol. 48, pp. 135-144, 2002.
- [117] H. Ma, X. Cheng, S. Chen, C. Wang, J. Zhang, and H. Yang, "An ac impedance study of the anodic dissolution of iron in sulfuric acid solutions containing hydrogen sulfide," *Journal of Electroanalytical Chemistry*, vol. 451, pp. 11-17, 1998.
- [118] T. Hemmingsen and T. Vøland, "The reaction of the sulphite/bisulphite couple on SMO steel under anaerobic conditions," *Electrochimica Acta*, vol. 36, pp. 1367-1375, 1991.

- [119] E. J. Kim, J. H. Kim, A. M. Azad, and S. Chang, "Facile synthesis and characterization of Fe/FeS nanoparticles for environmental applications," *Applied Materials & Interfaces*, vol. 3, pp. 1457-1462, 2011.
- [120] L. L. Barton, *Sulfate-reducing bacteria*: Plenum press, 1995.
- [121] C. J. Thomas, R. G. J. Edyvean, R. Brook, and I. M. Austen, "The effects of microbially produced hydrogen sulphide on the corrosion fatigue of offshore structural steels," *Corrosion Science*, vol. 27, pp. 1197-1204, 1987.
- [122] T. S. Rao, T. N. Sairam, B. Viswanathan, and K. V. K. Nair, "Carbon steel corrosion by iron oxidising and sulphate reducing bacteria in a freshwater cooling system," *Corrosion Science*, vol. 42, pp. 1417-1431, 2000.
- [123] T. R. Jack, M. J. Wilmott, R. L. Sutherby, and R. G. Worthingham, "External corrosion of line pipe: A summary of research activities," *Materials Performance*, vol. 35, pp. 18-24, 1996.
- [124] I. T. E. Fonseca, M. J. Feio, A. R. Lino, M. A. Reis, and V. L. Rainha, "The influence of the media on the corrosion of mild steel by *Desulfovibrio desulfuricans* bacteria: an electrochemical study," *Electrochimica Acta*, vol. 43, pp. 213-222, 1998.
- [125] B. J. Little and J. S. Lee, *Microbiology Influenced Corrosion*: John Willey & Sons, 2007.
- [126] S. Y. Li, Y. G. Kim, K. S. Jeon, and Y. T. Kho, "Microbiologically influenced corrosion of underground pipelines under the disbonded coatings," *Metals and Materials*, vol. 6, pp. 281-286, 2000.

- [127] S. E. Werner, C. A. Johnshon, N. J. Laycock, P. T. Wilson, and B. J. Webster, "Pitting of type 304 stainless steel in the presence of a biofilm containing sulphate reducing bacteria," *Corrosion Science*, vol. 40, pp. 465-480, 1998.
- [128] A. A. Padilla-Viveros, G. Zavala-Olivares, R. G.-E. M.J. Hernandez-Gayosso, J. Galindez, and J. L. Mora-Mendoza, "Electrochemical kinetics of sulfate reducing bacteria isolated from a gas pipeline," presented at the CORROSION/03, San Diego, 2003.
- [129] V. S. Sastri, E. Ghali, and M.Elboujdaini, *Corrosion prevention and protection: practical solution*: John Wiley & Sons, 2007.
- [130] M. M. Al-Darbi, K. Agha, and R. Islam, "Modeling and simulation of the pitting microbiologically influenced corrosion (MIC) in different industrial system," presented at the CORROSION/05, Houston, 2005.